Carbon Black Dispersion using Polymeric Dispersants Prepared *via* RAFT Polymerisation

Majda Akrach

A thesis submitted in partial fulfilment of the requirements for the degree of

Doctor of Philosophy in Chemistry

Department of Chemistry

University of Warwick

April 2018

“It’s lack of faith that makes people afraid of meeting challenges.

I hated every minute of training but I said, don’t quit. Suffer now and live the rest of your life as a champion.

Impossible is potential. Impossible is temporary. Impossible is nothing”

Mohammed Ali.

“A winner is a dreamer who never gives up.

I never lose. I either win or learn.”

Nelson Mandela

Scars show us where we’ve been, they did not dictate where we are going.

Contents

List of Figures

List of Tables

List of Schemes

Abbreviations

Abbreviation	Name
AIBN	2,2'-Azobis(2-methylpropionitrile)
AM	Acrylamide
ATRP	Atom Transfer Radical Polymerisation
AVE	Alkyl Vinyl Ether
BET	Brunauer Emmet and Teller
BHT	Butylated hydroxytoluene
BMA	Butyl methacrylate
BMDPT	Butyl-2-methyl-2-[(dodecylsulfanylthiocarbonyl) sulfanyl] propionate
BuAc	Butyl acetate
^{13}C NMR	Carbon Nuclear Magnetic Resonance
˚C	Degree
CB	Carbon Black
$CHCl_3$	Chloroform
CTA	Chain Transfer Agent
C_{tr}	Chain transfer constant
DEGMA	Diethylene glycol methacrylate
DLS	Dynamic Light Scattering
DMAc	Dimethyl acetamide
DMAEA	2-(Dimethylamino)propyl acrylate
DMAEMA	2-(Dimethylamino)propyl methacrylate
DMAPAA	3-(Dimethylamino)-1-propyl amine
DMF	N-N-Dimethylformamide
DMSO	Dimethylamino sulfoxide
DOSY	Diffusion-Ordered Spectroscopy
DP	Degree of Polymerisation
Đ	Dispersity
Eq	Equation

FRP	Free Radical Polymerisation
FT-IR	Fourier transform InfraRed
HRTEM	High Resolution Transmission Electronic Microscopy
I	Initiator
IGC	Inverse Gas Chromatography
IV	Intrinsic Viscosity
kDa	Kilo Dalton
L	Livingness
LRP	Living Radical Polymerisation
LS	Light Scattering
M	Molar
MA	Maleic anhydride
MADIX	Macromolecular Design *via* the Interchange of Xanthates
MALDI	Matrix Assisted Laser Desorption/Ionization
MCTP	1,1'-Methyl-4-cyano-4-(dodecylthiocarbonothioylthio)pentanoate
MMA	Methyl Methacrylate
$M_{n.SEC}$	Molar mass determined by SEC
$M_{n.TH}$	Molar mass theoretical
MPA	Methoxypropyl acetate
MS	Mass spectroscopy
NaOH	Sodium hydroxide
***n*BA**	*n*Butyl acrylate
NMP	Nitroxide mediated Polymerisation
NMR	Nuclear Magnetic Resonance
PABTC	2-((butylthio)-carbonothioyl)propanoic acid
PAN	Poly Acrylonitrile
PE	Poly Ethylene
PMMA	Poly Methyl Methacrylate
PP	Poly Propylene
PS	Poly Styrene
PVDF	Polyvinylidene fluoride

RAFT	Reversible Addition-Fragmentation chain Transfer
RI	Refractive Index
S	Styrene
SEC	Size Exclusion Chromatography
SMA	Styrene Maleic Anhydride
SMAD	Styrene Maleic acid
SMI	Styrene Maleimide
stat	Statistical
TEM	Transmission Electronic Microscopy
Tg	Glass transition temperature
TGA	Thermogravimetric analysis
THF	Tetrahydrofurane
UV	Ultraviolet
Vazo-88	Azobis(cyclohexanecarbonitrile)
V-601	Dimethyl 2,2'-azobis(2-methylpropionate)
VAc	Vinyl acetate
XPS	X-ray Photoelectron Spectroscopy
XRD	X-ray Diffraction

Acknowledgements

I would like to take this opportunity to thank all the people who supported me during my PhD at Warwick University.

Firstly, I would like to thank my academic supervisor Professor Sébastien Perrier for giving me the opportunity to carry out my work in his team and also for his support throughout these last 3 years. Many thanks for your patience, the (very) long discussions in your office and all the useful advice you have given for my career.

Secondly, I could not have completed this thesis without the support of Lubrizol. It was a great pleasure to be supervised by Dr. Andrew Shooter and Dr. Stuart Richards, and I really appreciate the opportunity to learn about coating scale up in Blackley (Manchester), and also to interact with all the wonderful workers there, including Robert Jennings, Shabana, Elliot, Sasa and everyone else who kindly took care of me.

A specific and enormous thanks to Dr. Edward Mansfield and Dr. Daniel Lester for correcting my manuscripts during these last few weeks and over the Christmas holidays, and also for your patience and help.

The research and life at Warwick University would not have been easy without all the scientists; Ivan (NMR), Dan (GPC), Marc Walker (XPS), Houari (TEM), Jason Noone (IT) Nishi, Monika, Sukhi, Olvi and Sukhjit. I cannot forget to mention Nick Barker, one of the most wonderful, amazing and comprehensive human that I have ever met in my life. Thank you very much for all your support, your positive vibes and your humanity!!

I cannot skip-my colleagues, for those of you who have supported me during the hard times of my PhD. The French team: Caroline Bray, with whom I spent many hours complaining about life Guillaume Moriceau for his help, advice and for being the best driver!, Agnes Kuroki for her 24/7 smile (I am pretty sure you smile when you sleep) and Dr. Sophie Larnaudie for her amazing cakes. To my friend, Dr. Junliang Zhang, with whom I spent all my weekends in the lab and staying late in the office. Thank you so much for your support, your smile, positivity and vegetarian dumplings! To my (best and favourite) enemy, Dr. Liam Martin with whom I had daily arguments Finally, the rest of the (massive) crew, Dr. Carlos Sanchez-Cano, Pratik Gurnani, Fannie Burgevin, Andy Lunn, Joji Tanaka, Thomas Floyd, Dr. Jie Yang, Dr. Qiao Song, and Dr. Ming; thank you very much for your advice, help and support these last few years. I was also pleased to meet students in Dave Haddleton's group such as Rachel, George, Attau, Evelina, Glen, Vasiliki, Sam, and Richard, who created a nice ambiance in the corridor. I have also to mention my sisters Nurul'ain, Nursakinah, Faeza and Amina who make my life at Warwick University so peaceful and bright! God bless you.

The best part for me is to mention my best friend Guillaume Magigue who was there for me literally every single day for the last 4 years. All my pain, stress, success and happiness was with you. I do not have words strong enough to describe how much I value and appreciate your help and presence. My others best friends Nelly De Oliveira (little sister), Bewinda Taurand and the amazing Dr. Alice Gimat for being the same person after 14 years now!! Bethan Davies (future Doctor in life sciences), a wonderful woman, an angel who supported and believed in me since day one, when I met her at a Warwick open day in 2014!

Finally, to my family, Hamza, Samira, Khadija, and my mum, who drive me crazy but also reminds me why I am going through all of these sacrifices. I will conclude my acknowledgements with my host family in Barry (Wales): Elisabeth, Russel, Robert and of course Ruby (my love)!! Elisabeth, you are such an inspiring, strong and lovely woman. The 3 months spent in your house have been the best part of my life so far. Without this experience, I would not have had the power to carry out my PhD!! A thousand thanks for everything you have done for me. I wish, one day, that I reward you in the same way.

Declaration

Experimental work contained in this thesis is original research carried out by the author, unless otherwise stated, in the Department of Chemistry at the University of Warwick, January 2015 and January 2018. No material contained herein has been submitted for any other degree, or at any other institution.

Results from other authors are referenced in the usual manner throughout the text.

Date:

_____

Majda Akrach

Abstract

The aim of this thesis is the investigation of the use of a RAFT agent developed by the company Lubrizol, BMDPT (Butyl-2-methyl-2-[(dodecylsulfanylthiocarbonyl) sulfanyl] propionate) produced in tonnes scale to make amphiphilic block copolymers in ester solvent (butyl acetate and methoxypropyl acetate). For this purpose, a broad range of monomers including acrylate, methacrylate and styrenic containing tertiary amine were polymerised and used as pigment dispersants.

As the starting point, the reactivity of *n*-butyl acrylate (*n*-BA) and di(methyl)aminopropyl acrylate (DMAEA) monomer followed by the synthesis of acrylate diblock copolymers in acetate solvents (butyl acetate and methoxypropyl acetate) are investigated.

The second chapter is focused on the methacrylate polymerisation which is a large body of work of this thesis. The poor reactivity of the trithiocarbonate RAFT agent towards methacrylate monomer was already published few times. Consequently, the kinetic studies of butyl methacrylate (BMA) and di(methyl)amino ethyl methacrylate (DMAEMA) was investigated in batch mode. Subsequently, a new synthetic route is explored to reach a well-controlled diblock copolymers.

In the third chapter, a novel class of amphiphilic diblock copolymer containing acrylate and a mixture of styrene and maleic anhydride is explored. Then, the functionalisation of polymer backbone is carried out by using an amine in order to insert an anchoring group for pigment affinity.

Finally, the efficiency of all the diblock copolymers on carbon black pigment dispersion is reported. A combination of different techniques such as dynamic light scattering (DLS), transmission electronic microscopy (TEM) and thermogravimetric analysis (TGA) are used to investigate the interaction between the polymer and the pigment

Chapter 1: Introduction

Chapter 1 : Introduction

1.1. Free Radical Polymerisation

One of the most popular methods to synthesise commercial polymers is free radical polymerisation (FRP), first reported in the literature by Flory in the 1930's.[1] This process is insensitive to impurities and less demanding in terms of reaction conditions, which is the main criteria from an industrial point of view. Polymerisations can be carried out in presence of stabilizers (such as hydroquinone) which are commonly present in commercial monomers or in purified solvents. Nowadays, the production of commercial polymers in bulk uses free radical polymerisation. The polymerisation mechanism involves initiation, propagation and termination steps.[2] Initiation involves the decomposition of an initiator (I) in which the primary radicals ($I^{\bullet}$) are formed by thermolysis, redox reactions, or photolysis. Then, the free radicals react with the vinyl monomer (M) in order to initiate the propagation step and allowing the polymer to grow ($I\text{-}M^{\bullet}$) (**Scheme 1.1**). The primary radical can also react with another free radical by combination or disproportionation, reducing the initiation step efficiency. The propagation step consists of the growing polymeric chain by sequential addition of monomer molecules to the polymeric radical ($P_n^{\bullet}$), leading the formation of a new polymeric radical (P_{n+1}). The "head-to-tail" addition is the main propagation mechanism, in which the radical reacts to the least-substituted-end of the monomer double bond. This step is characterised by a propagation constant (k_p) of 10^2-10^4 $L.mol^{-1}.s^{-1}$ for most monomers. Finally, the irreversible destruction of the radicals leads the formation of "dead" polymers (inactive chains) either by a combination or disproportionation process.

Consequently, the radical concentration is reduced leading chain end termination. The combination of two radicals will provide a polymer chain with a specific length, depending on the sum of the two radicals. In a disproportionation mechanism, a transfer of the hydrogen atom from one radical to another will form an unsaturated end-group on the polymer chain.

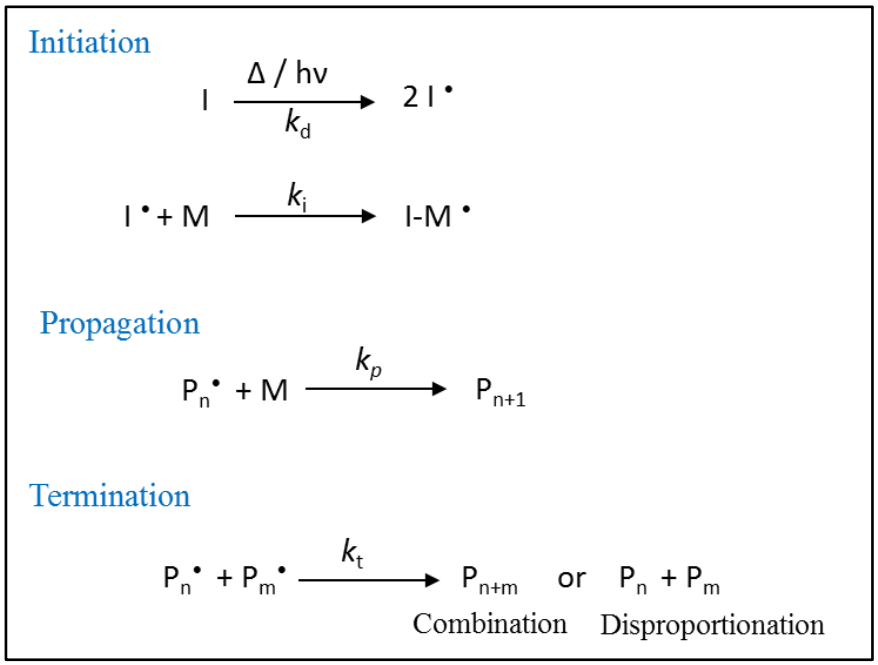

Scheme 1.1: General scheme of free radical polymerisation[2]

All the steps of conventional radical polymerisation described here occur in a few seconds, while the rate of monomer consumption can be relatively slow (from minutes to days).

Thus, the formation of high molecular weight polymers is obtained in the early stages of the reaction, giving a chains with different degrees of polymerisation ($Đ$ > 1.2) and high dispersity as a result.

Flory was the first to introduce the chain transfer term in 1936 **Scheme 1.2** shows the reaction between the propagating radical with a chain transfer agent (CTA), which terminates one chain and leaves a free radical, $CT^{\bullet}$, available to reinitiate a new monomer in order to produce another propagating radical ($P_m^{\bullet}$).[3] Nowadays, transfer agents are widely used to control a polymerisation by decreasing the molecular weight.

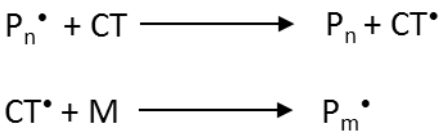

Scheme 1.2: Chain transfer of radical from propagating radical chain to another monomer.[3]

Here, the **Scheme 1.2** shows a transfer mechanism involving the transfer of an atom to the monomer but the chain-transfer can also occurs with another component such a solvent, intiator, a polymer chain or a chain transfer agent.

1.2. Living radical polymerisation

Szwarc was the first to report living polymerisations in 1956, where the presence of carbanion decreased significantly the amount of termination.[4] However, the presence of unavoidable chain termination affects the control over the polymerisation, giving a high dispersity values. The disadvantages of the FRP are overcome with the appearance of the living radical polymerisation which is less sensitive towards the reagent purity and can provides a similar control as the anionic polymerisations.[5]

The introduction of the dynamic equilibrium in radical polymerisation is the key to give a predictable molecular weight polymer with a narrow dispersity and high end-chain functionality (**Figure 1.1**).

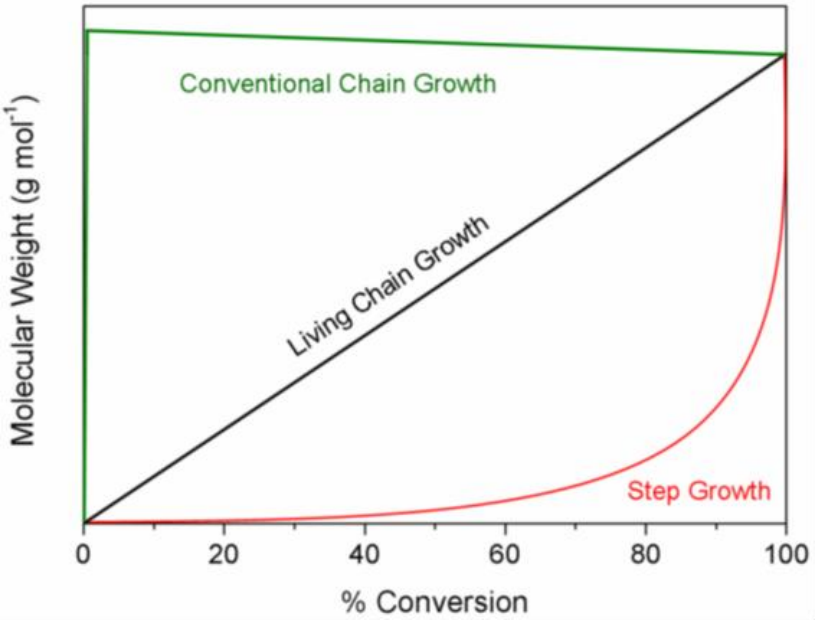

Figure 1.1: Evolution of molecular weight with conversion using different polymerisation techniques

Controlled living radical polymerisation (CLRP) is based on the activation/deactivation of the propagating macro-radicals which allows the polymeric chains grow simultaneously as the monomer is consumed. Similarly to free radical polymerisation, the termination step cannot be avoided, meaning that the CLRP is not a "pure" living system. However having similar conditions to LRP, as reported by Quirk and Lee, use of the term "living" for the nitroxide mediated polymerisation (NMP)[6,7] atom transfer radical polymerisation (ATRP)[8,9] or reversible addition-fragmentation chain transfer polymerisation (RAFT)[10,11] can be justified.

Since the aim of this thesis is to focus on the synthesis of block and multiblock copolymers using RAFT polymerisation, a study of the kinetic for polymerisations of a wide range of monomers in organic solvents using an industrial specific RAFT agent is reported.

1.2.1. Reversible-addition Fragmentation Chain Transfer

RAFT polymerisation was first reported in 1998 by the Commonwealth Scientific and Industrial Research Organisation (CSIRO), and at the same time by Rhodia in France (called MADIX for Macromolecular Design *via* the Interchange of Xanthates). The RAFT process is based on a degenerative mechanism corresponding to the transfer of a radical from one polymeric chain to another keeping the radical concentration constant.[12,13] The polymerisation involves the use of monomers, conventional radical initiators (*e.g.* AIBN, V601 or Vazo-88), a chain transfer agent (CTA or RAFT agent) and can be performed in suspension, emulsion, solution or bulk. Trithiocarbonylthio compounds (RSC(Z)=S) are the main CTA used in RAFT polymerisation. The design and the choice of RAFT agent must be appropriate for the monomer and reaction conditions in order to achieve good control over the molecular weight distribution.

The efficiency of the chain transfer agent leading a narrow molecular weight distributions is illustrated by Moad *et al*. which compard the polymerisation of styrene in free radical polymerisation and in presence of the cumyl dithiobenzoate chain transfert agent (**Figure 1.2**).[11]

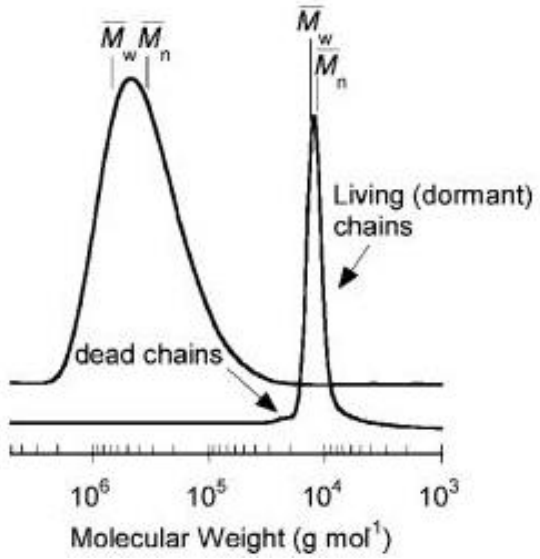

Figure 1.2: Molecular-weight distributions for a conventional and RAFT polymerisation of styrene under similar experimental conditions. The SEC chromatograms show a polystyrene prepared by thermal polymerisation of styrene at 100 ˚C for 16 h (M_n = 324 000 g/mol), $Đ$ = 1.74 and 72 % of conversion) and a similar polymerisation in a presence of cumyl dithiobenzoate (M_n = 14 400 g/mol, $Đ$ = 1.04, 55 % of conversion).[11]

1.2.2. RAFT polymerisation mechanism

The mechanism of RAFT polymerisation is relatively similar to the that of free radical polymerisation, with the presence of an additional step involving the CTA, as depicted in a **scheme 1.3**.[11, 14,15] The initiation and termination steps are similar to conventional free radical polymerisation. The second step is the addition of the propagating radical ($P_n^{\bullet}$) to the initial RAFT agent (**1**) to form an intermediate species (**2**) which can undergo fragmentation towards either the starting species (k_{-add}) or release the radical $R^{\bullet}$ and form a new propagating radical (k_{β}) (**3**). The reinitation step then occurs where the $R^{\bullet}$ species will add another monomer to produce a new propagating polymeric chain ($P_m^{\bullet}$).

Upon consumption of the chain transfer agent, an equilibrium is established allowing all chains to grow at a uniform rate. When the polymerisation is complete or stopped a number of polymeric chain retain the thiocarbonyl-thio end group. Finally, termination will occur leading the formation of dead chains by bimolecular reactions.

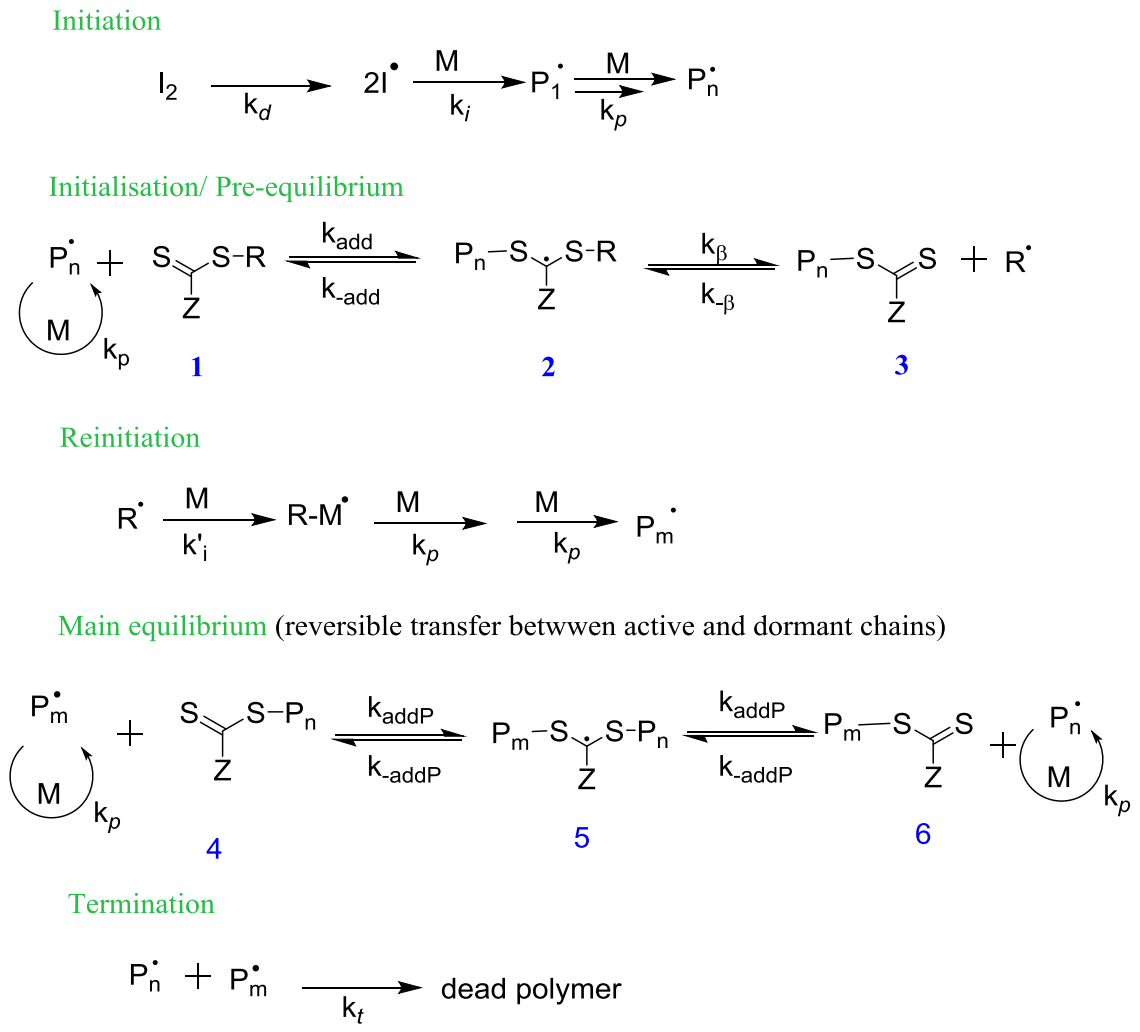

Scheme 1.3: Reversible Addition chain transfer polymerisation mechanism[14]

The high tolerance to impurities in the reaction mixture and the possibility to use a wide range of monomers and solvents confirms the robust and versatile nature of the RAFT process.[16] Different classes of monomers from more activated monomers (styrene, acrylic and methacrylic) to the less activated monomers (*N*-vinyl pyrrolidone, vinyl acetate) have been established and reported in the literature.[17,18] Also, the effect of the temperature[19] and solvents (organic[20] and aqueous[21]) have been widely studied.

1.2.3. The chain transfer agent

Control of the molecular weight and the dispersity (*Đ*) is controlled mainly by the choice of the chain transfer agent. The efficiency of the chain transfer constant (C_{tr}) can be evaluated by using different methods as described by Destarac.[22,23] The C_{tr} value for a given CTA is calculated according to **Equation 1**:

$$C_{tr} = \frac{k_t}{k_p} \quad \textbf{Equation 1}$$

The chain transfer constant is directly linked to the transfer and propagation constants (k_{tr} and k_p respectively). A higher value of C_{tr} (> 1) means that the transfer rate constant (k_{tr}) is significantly higher than the propagation constant (k_p). In contrary, a low value of a chain transfer constant suggests a slow consumption of the CTA, inducing a higher experimental M_n than the calculated, and a broad dispersity.

Different methods can be used to measure C_{tr}. The conventional approach is to use a Mayo plot method which can be determined by size-exclusion chromatography and **Equation 2**.[12,24]

$$\frac{1}{DP} = \frac{1}{DP^0} + C_{tr}\frac{[CTA]}{[Monomer]}$$ **Equation 2**

DP is the number average degree of polymerization obtained in the presence of the CTA. DP^0 is the number averaged degree of polymerization obtained in the absence of chain transfer agent. [CTA] and [M] are the concentration of chain transfer agent and monomer respectively.

1.2.4. Choice and design of the RAFT agent

A wide range of RAFT agents have been designed over last decade, allowing for a wide range of compatibility for different monomers and polymerisation conditions. For thiocarbonylthio RAFT agents, dithioesters[25] were initially developed followed by dithiocarbonates, dithiocarbamates[26] and trithiocarbonates[27,28]. Design of the RAFT agent influences the effectiveness of the polymerisation and also the thermal stability. A typical RAFT agent composed of R and Z groups which will directly affect the value of the chain transfer constant is depicted in **Scheme 1.4**.

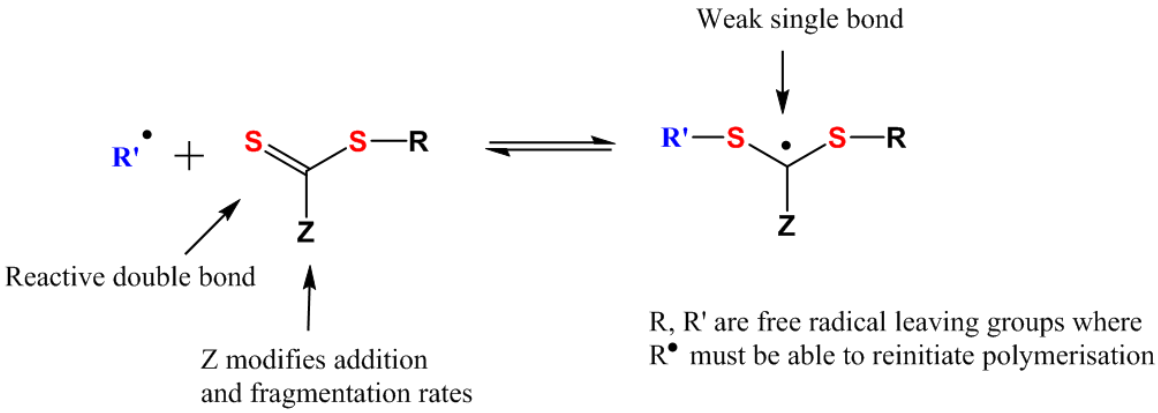

Scheme 1.4: Structural features required for an optimal RAFT agent

The presence of the highly reactive C=S bond allows for fast radical attack and release of the radical leaving group (R•) in order to reinitiate the polymerisation to generate a new polymeric chain. The intermediate radical (**2 and 5** in **Scheme 1.3**) should fragment rapidly and must partition in favour of the products (3 and 6 in **Scheme 1.3**). As such, choice of R and Z group can have drastic impacts on the efficiency of the reaction.

- Effect of the R group

Different substituents have been designed to understand their impact on the control over the polymerisation. The main role of the R group is to be a good radical leaving group but also to efficiently reinitiate the reaction in order to start the formation of a new polymeric chain. Consequently, an efficient homolytic group is required to release the radical (R•), and the stability of the expelled radical (R•), based on the polarity or steric hindrance of the substituent, for each class of RAFT agent has been broadly reported in the literature.[20,29,30,31]

For instance, a sterically bulky R group (styrene) or those containing an electron withdrawing groups (-CN, -COOR…) increase the rate of fragmentation, which form excellent leaving groups. Chong *et al*. have explored the effect of different substituents on several monomers and they established good guidelines for the choice of CTA (**Figure 1.3**).[32]

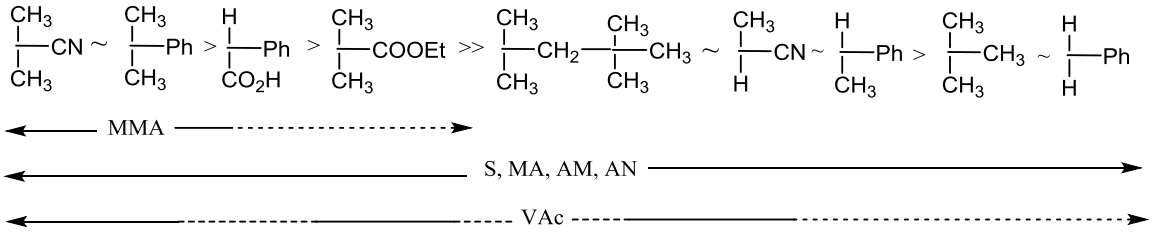

Figure 1.3: Selection of the R group for a RAFT agent with a decrease of fragmentation rates from left to right for methyl methacrylate (MMA), styrene (S), methyl acrylate (MA), acrylamide (AM), acrylonitrile (AN) and vinyl acetate (VAc).[32]

❖ Effect of the Z group

The Z group relates the relative stability and reactivity of the C = S bond throughout the activation/deactivation process. The Z substituents will directly influence the rate of radical addition onto the double bond. Similarly to the R group, studies have been reported on how the electron withdrawing groups enhance the reactivity of the RAFT group, and how the presence of substituents bearing an oxygen or nitrogen with a lone pair deactivate the radical leading to poor control of the polymerisation.[33] Similarly to the previous R group study, guidelines for the choice of Z group substituents have also been reported (**Figure 1.4**).[34]

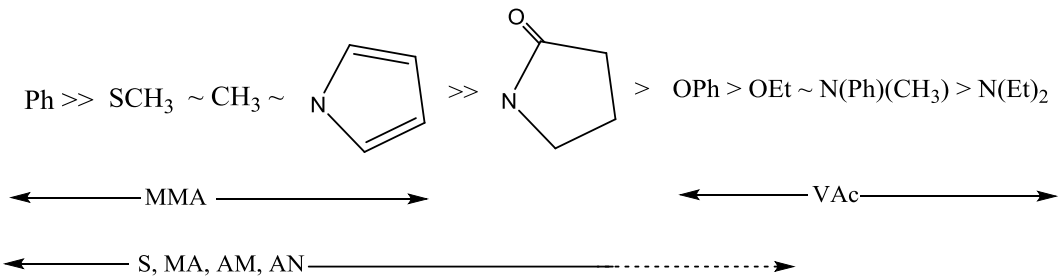

Figure 1.4: Selection of the Z group for a RAFT agent with a decrease of fragmentation rates from left to right for methyl methacrylate (MMA), styrene (S), methyl acrylate (MA), acrylamide (AM), acrylonitrile (AN) and vinyl acetate (VAc).[34]

As discussed, RAFT is a highly versatile method to polymerise a wide range of materials. As such it can be easily manipulated to synthesise a wide range of polymer architectures such as linear, star, brush and multiblock. The design of amphiphilic diblock copolymers is the main purpose of this thesis project.

1.3. Synthesis of block and multiblock copolymers by RAFT process

1.3.1. Block copolymer synthesis

Block copolymers include a range of architectures such as linear, comb, star copolymers (**Figure 1.5**), leading to specific properties and allowing to target a diverse range of applications.[35] It is well established that block copolymer composed of a hydrophobic and hydrophilic segments can self-assemble based on hydrophobic inetractions. Typically, the morphology of the nano-scale structure is directly dependent of the ratio between the two blocks, but also the composition, the block chain length and the dispersity.[36,37]

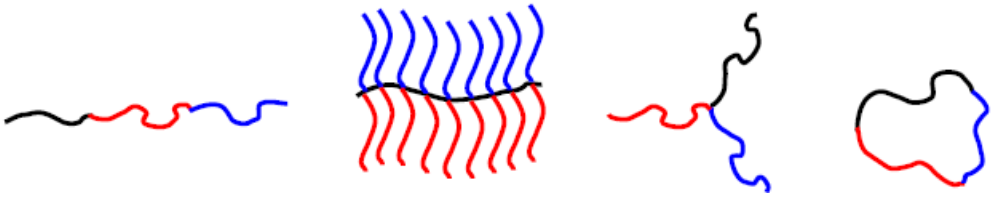

Figure 1.5: Representative architecture of linear block copolymer terpolymers, "comb" graft polymers, miktoarm star terpolymers and cyclic block terpolymers.[36]

For many years, the synthesis of block copolymer was performed *via* anionic polymerisation, providing polymers with narrow molecular weight distribution.[38]

However this technique suffers from a few disadvantages such as monomer purity and stringent requirements on reaction conditions. To address some of these shortcomings, group transfer polymerisation (GTP) was developed, and provide a good control of methacrylates polymerisation over a wide range of temperatures and initiators (cyanide, azide, fluoride) is reported.

For instance, Sogah and Owen W.Webster have reported the synthesis of a broad range of methacrylates (MMA, LMA, BMA, HEMA…) but also acrylates and acrylonitrile monomers using nucleophilic anions (KHF_2, Bu_4NF...) or Lewis acids ($ZnBr_2$, ZnI_2, $ZnCl_2$…) leading a well-defined homopolymers and copolymers ($Đ \leq 1.2$).[39,40] However, the technique si still limited by the need to remove water and is still sensitive to certain functionalities.

Free radical polymerisation (FRP) on the other hand is a versatile polymerisation technique that require simple setup, non stringent conditions and is tolertant to a wide variety of functional groups. On the othe hand, it is prone to many side rerecatiosn such as termination and irreversible chain transfer and therefore give poor control over molecular weight, thus making the synthesis of block copolymers impossible. However, Solomon et al. have patented in 1985 the synthesis of block and graft copolymers with short chein legth in free radical polymerisation.[41] This concept has also been used by Krstina and co-workers to show the possibility to achieve a high-purity block copolymers by FRP using a macromonomers as chain transfer agent. A successful p(butyl methacrylate-*block*-phenyl methacrylate) is synthesised *via* an addition-fragmentation chain-transfer where BMA propagating species reacts with the phenyl methacrylate macromonomer ($Đ \approx 1.3$).[42,43]

More recently, Haddleton and coworkers have further developed this approach to synthesise sequence-controlled methacrylic multiblock copolymers using macrochain transfer agents in dispersed media.[44,45] Thus, the RDRP (Reversible Deactivation Radical Polymerisation) is more attractive than ionic polymerisation for its tolerance to reactive groups and reaction conditions.

To date, the most common RDRP techniques are NMP, ATRP and RAFT polymerisations. The process relies on the formation of dormant dormant ("living") chains, end-capped with a dithioester, allowing chain extension to generate well-defined block copolymers. One of the main parameter to consider is the proportion of the "living" chains (ω-chain ends) which must be as high as possible for a successful block synthesis. As already discussed, this system is not fully living due to the presence of dead chains (α-chain end derived from initiator) generated by the radical termination. Nevertheless, a high fraction of dormant chains can be achieved by optimising the ratio $[\text{monomer}]_0$ / $[\text{RAFT agent}]_0$, which determine the theroretical degree of polymerisation and the number average molar mass (M_n). The ratio $[\text{RAFT agent}]_0$ / $[\text{Initiator}]_0$ determine the number of α and ω chain-end, and must be kept as high as possible in order to form a maximum of "living" chains. Considering kinetic parameters, the proportion of living chains is linked to the amount of radicals present in the reaction, and the fraction of living chains (L) can be quantified as shown in **Equation 3**:

$$L\ (\%) = \frac{[\text{CTA}]_0}{[\text{CTA}]_0 + 2.f.[\text{I}]_0.\left(1-e^{-kdt}\right).\left(1-\frac{fc}{2}\right)} \quad \textbf{Equation 3}$$

The initial concentrations of chain transfer agent (CTA) and initiator are represented by $[CTA]_0$ and $[I]_0$ respectively, while the number "2" is attributed to the formation of two primary radicals after thermal decomposition of the azo initiator. The value "*f*" is set at 0.5 for the calculation of livingness in this thesis and k_d is the rate coefficient of initiator decomposition. Finally, the term (1-*f*c/2) describes the production of radical-radical termination by combination or disproportionation.

In RAFT polymerisation, the most common method for block copolymer synthesis is sequential addition of two or more monomers (**Figure 1.6**).

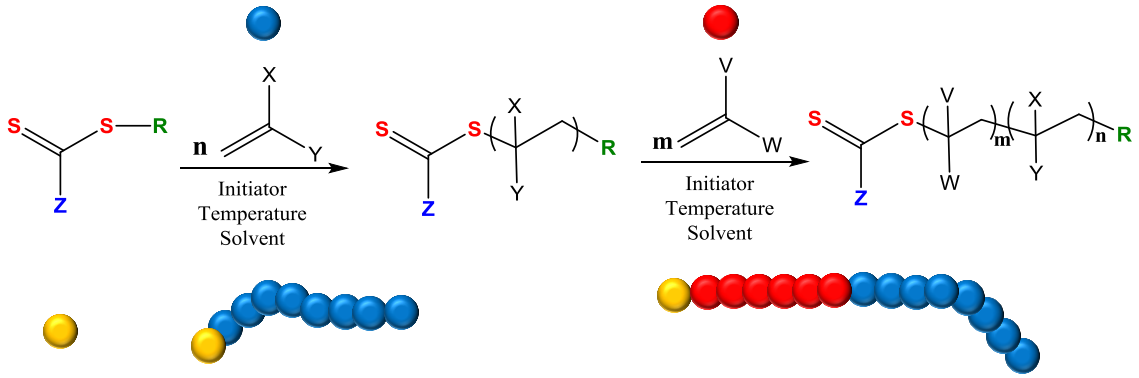

Figure 1.6: General scheme of block copolymer synthesis *via* RAFT polymerisation process

The composition and the control of the block copolymer structure is achieved by selecting compatible monomers and RAFT agent. As stated in **part 1.2.4**, the RAFT agent must possess a Z and R group functionality suitable to the monomer selected. The Z-group of the RAFT agent must give a good control for the both monomers as it is affect the efficiency of the thiocarbonyl group reactivity towards the rate of addition and fragmentation of the RAFT intermediate radical. For instance, if the polymerisation of the first monomer (A) is not controlled the addition of the second monomer (B) will leads a broader dispersity.

In another case, if the chain transfer constant of the RAFT agent is high ($C_{tr} > 1$) towards the monomer (A) and not the monomer (B), the macro-RAFT agent (A) will be well-controlled, but will generate a block copolymer (AB) with a high dispersity and some residual homopolymer (B). It is also important to consider the order of monomer addition. The first block being used as macroCTA, the propagating radical must be highly stable to reinitiate efficiently the polymerisation of the second monomer.

As such, monomers inducing a tertiary radicals (methacrylates or methacrylamides) are polymerised in a first step. General guidelines for the requirements to synthesis block copolymers by RAFT have been described by Keddie.[17]

In the sequential monomer addition approach, the monomers must have the same chemical and physical properties (*i.e*. radical reactivity). This approached using a commercially available monomer is broadly reported in the literature, especially to design amphiphilic block copolymers by RAFT polymerisation[46,47], NMP[48] and ATRP[49,50] Alternatively, the post-polymerisatiom coupling combining two polymerisations techniques is investigated in order to overcome the disavantages of the LRP and to allow the insertion of the desire functionalities.[51,52] For instance Nasrullah *et al*. have combined ATRP and RAFT polymerisations by using a RAFT agent terminated with a propargyl group to make p(*t*BA)$_{ATRP}$-*b*-p(BA)$_{RAFT}$. The homopolymer (tBA) is prepared in presence of CuBr/PMDETA, then the bromine group is substituted by NaN_3. Separetly, the second homopolymer is prepared using a PTTC bearing a propargyl group which then is reacted with the azide group *via* a 'click' reaction. Each homopolymers being well-controlled ($Đ \leq 1.2$), the combination of both blocks leads the formation of well-defined block copolymer.[53]

This orthogonal approach has also been reported by Stenzel and coworkers who have used a "clickable" RAFT agent to polymerise vinyl acetate and styrene in presence of xanthate (bearing an azide) and dithiobenzoate RAFT agent, respectively. A 'click' reaction between both controlled homopolymers provides a range of PS-b-PVAc with a narrow molecular weight distribution.[54]

1.3.2. Multiblock copolymer synthesis

Similar to block copolymers, the preparation of multiblock copolymers can be performed by combining different techniques of polymerisations.[55] Nevertheless, the difficulties cited previously for block copolymer synthesis are enhanced for multiblock architectures.

As seen above, an external source of radical is required in order to chain extend the previous block by another. Consequently, few parameters such as the concentration of radicals and the final concentration of polymerisation mixture need to be considered to prevent a large accumulation of dead chains and to avoid a gel effect (Trommsdorff-Norrish) which may lead a broad molar mass and higher molar mass distribution ($Đ$ > 1.2). By using multiblock copolymers (rather than di or triblock copolymers), it is possible to tune the polymers physicochemical properties and thus expand the number of potential applications. The first example of multiblock copolymer synthesis using a one-pot RAFT polymerisation technique was reported by Gody *et al.*[56]. Recently, a few examples of sulfonated multiblock copolymers for coating applications have also been published showing the advantage of this architecture through tuning the nature of each block to modify the chemical and physical properties.[57,58,59]

1.4. Pigment dispersion

Pigments are dry, insoluble chemical substances which can be used in applications such as: paints[60,61], inks[62], printing[63], coatings[64], and cosmetics[65]. As such, upon dispersion in liquid media, they have a tendency to form aggregates or agglomerates, and therefore methods to improve the dispersion of pigment particles are necessary to enhance their performance for a given application. Several ways to disperse a powder pigment (dry-blend, electrostatic or steric process) have been reported in the literature. Dry-blend processing is typically used in industry to modify the product formulation in a blend without solvent.[66,67]. A compound, such as polymer, is mixed with the pigment in a blend chamber at high speed and a given temperature, followed by addition of a lubricant or other modifier to improve the batch-to-batch consistency and reduce the presence of electrostatic charges. However, this process is inefficient and poorly developed, as opposed to the melt shear process or liquid dispersion. In the polymer melts method, polymers are used as compatibilisers to disperse fillers or pigments; however, the choice of polymer used must be a low molecular weight (typically less than 10 kDa).[68,69,70] The last and most developed process is the pigment dispersion process. Here, block copolymers are used as dispersants in a given solvent system by adsorption onto the pigment surface. As this is the most commonly used method, it will be used in this thesis. Chemisorption and physisorption are the two main adsorption methods, and show efficient adhesion between the polymer and the pigment surface.

The process of coating is widely used in industry. It is defined as the addition of an organic, inorganic or hybrid continuous layer, typically based on polymeric materials, onto a specific surface, forming a 3-dimentional structure.[71]

Coating additives such as thickening agents, surface active agents or surface modifiers, to name few, are substances added in small quantity to a material, to improving their physicochemical properties. Different types of coatings have been established, and depending on the dispersant media, can be either waterborne, organic solvent-based or dry (solventless, in bulk).

1.4.1. Pigment dispersant methods

1.4.1.1. Chemisorption method

The first method to be investigated was the chemisorption method, in which the pigment surface is modified prior to the *in situ* synthesis of a polymer *via* the emulsion polymerisation process, forming a shell.[72,73,74,75]

Alternatively, the polymer chain can be grafted by direct polymerisation from the pigment surface if the functional group present can be initiated. Papirer and Donnet have combined both techniques to study the reactivity of five different carbon black pigments.[76] Treatment of the surface of the carbon black was performed by halogenation (bromination and chlorination) and oxidation followed by evaluation of the surface properties by inverse gas chromatography (IGC). Reactivity of the surface after modification was also studied, after grafting short alkyne chains *via* an anionic method and long alkyne chains using a free radical process.

Chemisorption has expanded on the use of polymers as dispersing agents, and makes it possible to use carbon black pigments in waterborne applications.

However, the difficulty and complexity of these processes, requiring many steps, can reduce the potential applications and increase the cost of production, which may be inappropriate for an industrial perspective.

1.4.1.2. Physisorption method

Alternatively, physisorption was developed and is now a well-known technique used to improve the interactions between a pigment surface and the polymer used as a dispersing agent. Adsorption of a surfactant onto a solid surface influences the quality of the dispersion, and has led to a new range of dispersants being developed over the last few years. Indeed, complex oligomers/polymers, which are typically block copolymers or branched polymers, have been synthesised to achieve a fine dispersion, allowing for high pigment loading whilst maintaining a low viscosity.

Many complex polymeric architectures such as star[77,78], graft[79,80,81] , hyperbranched[82] or dendritic[83] have been widely described. However, amphiphilic diblock copolymers show a similar or even better efficiency as a stabiliser for various colloidal dispersions in aqueous and organic[84] media.[85,86,87,88] Two types of pigment dispersion techniques are used; electrostatic stabilisation, mainly used in waterborne systems, and steric stabilisation, suitable for solventborne media.

By the 1990s, automotive industries began to look at new polymeric dispersants to increase the colour quality of aqueous pigment dispersions. They investigated acrylic and methacrylic acid moieties, which bear a strong polar anchoring group that can be readily synthesised by free radical polymerisation, and easily combined with a conventional

surfactants. A few years later, the synthesis of copolymers was optimised using controlled free radical polymerisation techniques and were shown to exhibit a better efficiency.[89, 90]

In the new method, design of the polymer is crucial to prevent flocculation and bridging between polymer chains. Auschra *et al*. investigated the synthesis of acrylic diblock copolymers *via* ATRP methods and studied the effect of chemical composition, molecular weight, and block length on the dispersant performance.[91] A similar composition of triblock copolymer was reported, showing the presence of bridging flocculation due to the interpenetration of long polymer chains.[92,93]

Although electrostatic stabilisation plays a key role in the development of novel dispersing agents, this project focuses mainly on the use of steric stabilisation as it is the most suitable technique to disperse organic pigment in organic media.

1.5. Dispersion of pigment using polymeric surfactant

The dispersion process can be described by a sequence of processes; wetting, separation and stabilisation (**Figure 1.7**).[94]

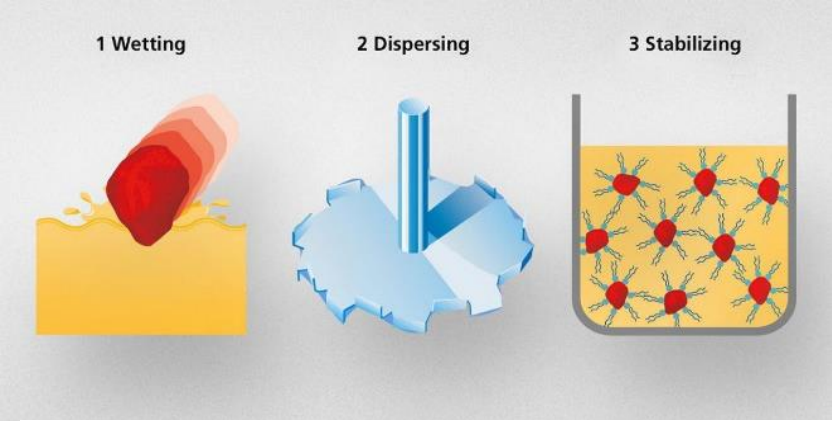

Figure 1.7: Pigment dispersion process.[94]

The *wetting* step is characterised by a displacement of any air present on the surface of a pigment (or between the agglomerates) by the coating vehicle (solvent or resin).

The main parameter to consider here is the surface tension of the media, which must be lower than the surface tension of the pigment to allow for fast penetration of the solvent through the clusters. Optimal wetting leads to a low viscosity mixture.

The *separation* process is achieved by using a suitable mechanical process (such as grinding or milling) to separate pigment aggregates into smaller particles. The choice of equipment is pivotal to reach a fast rate of separation, which is directly driven by the magnitude of the shear stress and the particle-particle interaction.

The last step is *stabilization* and is highly important to ensure the long term stability of the pigment.

Inefficient stabilization will lead to reversible flocculation, leading to a decrease in colour intensity by reduction of light absorption caused by the presence of large particles. To avoid or minimize the pigment flocculation, a surfactant is usually added during the stabilisation process. The two main mechanisms for stabilisation are electrostatic stabilisation and steric stabilisation.

1.5.1. Electrostatic stabilization

Electrostatic stabilization (or charge repulsion) is based on charge repulsion and is widely used in aqueous media.

Here, additive molecules must bear functional groups able to strongly adsorb onto the pigment surface by hydrogen bonding, dipole interactions or ionic bonding.

As mentioned previously, the surface tension must be low to reach a good wettability, however, water has a high surface tension (72.6 mN/m at 20 ˚C) meaning that the additive moieties must have an extremely strong affinity for the pigment in order to overcome this.[95,96]

Derjaguin, Landau, Verwey and Overbeek developed a theory which states that the stabilization of colloid is defined by strong coulombic (repulsive) forces that occur when two charged particles approach each other.[97,98] As such, a stable colloidal system is governed by two major forces; electrostatic repulsion and van der Waal's attractive forces where the combination of both forces form a double layer of counterions (**Figure 1.8**).[99]

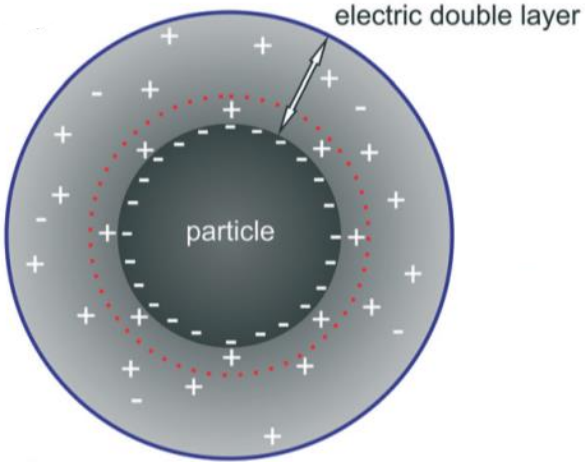

Figure 1.8: Schematic representation of the charged double from DLVO theory.[99]

Figure 1.9 summarises the interaction energies involved between two particles as a function of their distance. A short distance between the particles increases the magnitude of repulsive electrostatic and attractive Van der Waals forces. Consequently, the repulsive barrier named "Vmax" defines the stability of the dispersed colloids and must be large in order to prevent flocculation. In the other words, electrostatic repulsion must overcome the attraction forces in order to achieve a stable dispersion.[100]

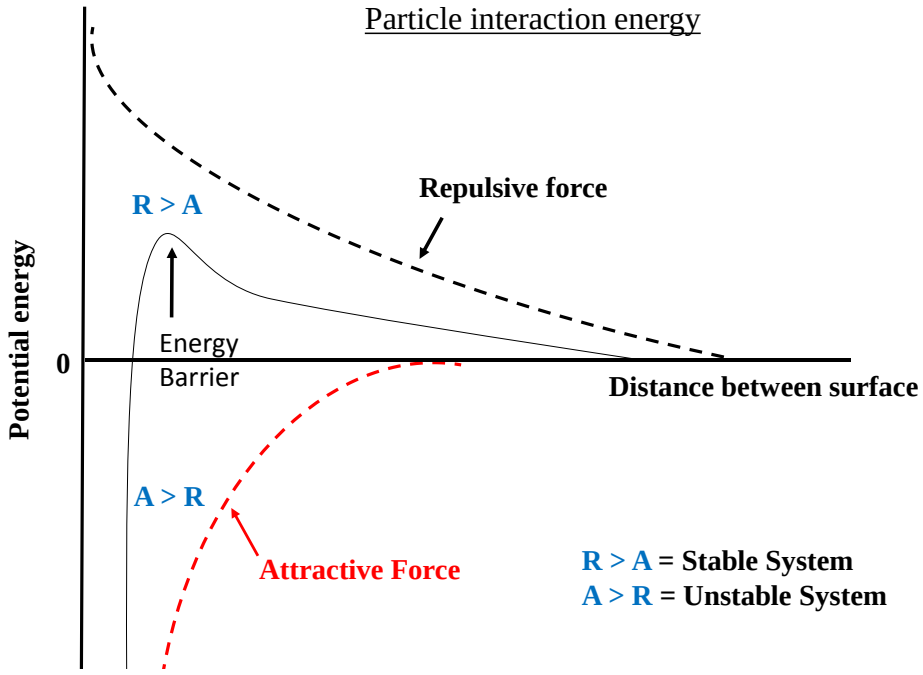

Figure 1.9: Evolution of potential energy for charged particles of potential energy for charged particles.[100]

In media with high dielectric constants only the electrostatic stabilisation will dominate, leading to a strong attraction between the positive counter-ions and a negative surface *via* the electric field, forming an electrical double layer.

However, this method is very sensitive to multivalent ion contamination and ion concentration, which can drastically alter the attractive forces between the two species (**Figure 1.10**).[101,102]

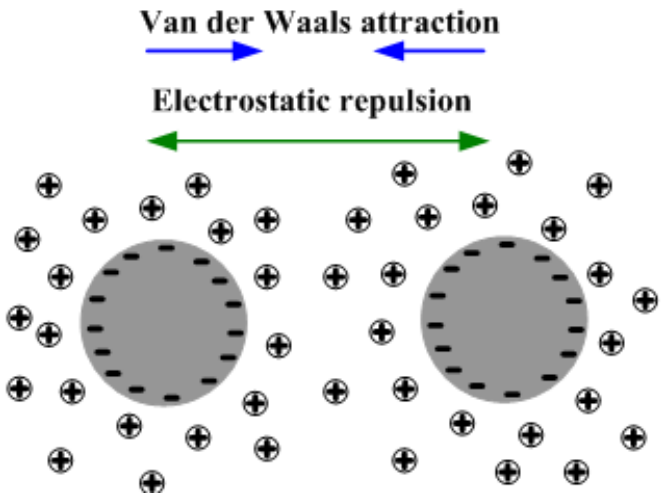

Figure 1.10: Electrostatic repulsion and attractive forces in water media[101]

Several factors, such as ion concentration, ionic strength and pH of the solution can alter or disrupt the double layer. The Schulze-Hardy law explains the influence of the salts on the electrical layer by studying the effect of electrolyte addition on the electrostatic potential around the particle. The increased ionic strength caused by the presence of electrolytes decreases the electrostatic potential. As such, flocculation will increase in the presence of the following cationic charges in negatively charged media; $Na^{+} < Ca^{2+} < Al^{3+}$ or Fe^{3+}. In positively charged media, the flocculation increase with the power of anions: $Cl^{-} < SO_4^{2-} < PO_4^{3-}$. A study of colloidal stabilisation with an excess of four polyelectrolytes (amidine latex, poly(styrene sulfonate), sulfate latex and poly(ethylene imine) at different pH values to confirm the DLVO theory was investigated by Hierrezuelo.

The charged colloidal particle stabilization mechanism was studied by using electrophoretic mobility and dynamic light scattering techniques which highlighted the link between the ionic strength and the repulsive electrostatic double-layer forces.

1.5.2. Steric stabilization

Steric stabilisation (or entropic repulsion) is defined as a repulsion of layers adsorbed onto a material's surface present in solution. This process requires the use of a functional surfactant with a low molecular weight (up to 10 kDa). This surfactant can be a polymeric compound with two segments; a buoy block that will be miscible in the solvent and an anchor block which will interact with the pigment surface *via* a chemical covalent or physical bond. The anchor group must bear one or more adsorbing groups which are commonly amines, hydroxyls, carboxylic acids or esters depending on the pigment surface. Oppositely, the buoy block is usually a long alkyne chain, which takes a loop or tails conformation in solution, and forms a thick layer around the pigment. **Figure 1.11** shows the role of the buoy and anchor chains in the steric stabilisation mechanism. The circular red spots on the surface represents the anchor groups, and the long orange segments correspond to the hydrophobic segments, providing the steric stabilization.[103]

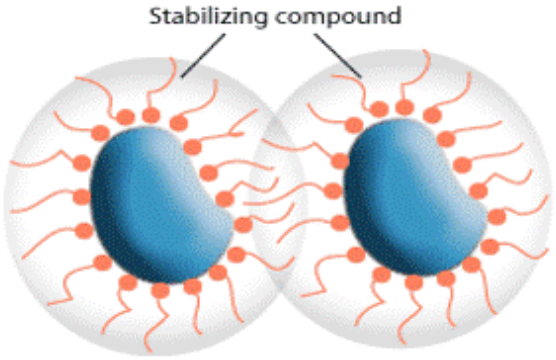

Figure 1.11: Steric repulsion of pigment particles coated by polymer.[103]

The repulsion mechanism occurs owing to the particles mobility under Brownian motion. The interaction between two particles is related to the thickness of the layers coated at the surface pigment. Several theories describing steric stabilisation have been described, and the ideas presented by Napper are generally accepted.[104] In Napper's theory, the schematic of which can be found in **Figure 1.12**, the potential configuration of a polymer layer in solution, where, "L" is the layer thickness and "D" the distance between two particles is described. The configuration (a) named "*non-interactional domain*" corresponds to the distance between two particles when they are far away from each other (D > 2L).

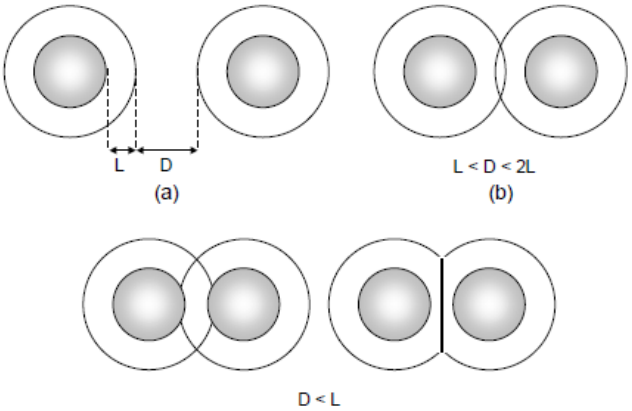

Figure 1.12: Representation of adsorbed layers overlapping by three approaches. (a) non-interactional domain; (b) interpenetrational domain; (c) compression mechanism

In solution, the particles get close to each other due to Brownian motion. Consequently, the "*interpenetrational domain* "is reducing the distance between two particles (D = 2L) leading to an overlapping of polymeric layers (b). At this stage, the enthalpy (ΔH) increases while the entropy (ΔS) decreases, suggesting a change in the configuration of the initial polymer chain. The last state (c) is total interpenetration of the polymers chains leading to a compression effect.

This phenomenon can occur depending on the elastic modulus of the adsorbed layer. The energy change occurring due to these interactions can be quantified, making it possible to determine the degree of stabilization. The overlapping layers is expressed by the change of Gibbs free energy. Given that $\Delta G = \Delta H - T\Delta S$, a positive ΔG corresponds to a stable system while a negative ΔG suggests flocculation or coagulation. By being aware of the mechanism, it is possible to design a polymer with the specific properties to overcome these disadvantages. Factors such as the molecular weight of the polymer (1), the thickness of the layers coated (2), the surface nature (neutral, acidic or basic) of the particle (3), and the solvent used (4) are the main targets to consider for optimal dispersion.

In the first case, the size of the polymer is crucial regarding the possibility of bridging flocculation to occur in solution. When two particles approach each other, the long buoy chains can interpenetrate leading to the formation of aggregates, while an optimal size will only have a steric effect, as was already discussed. Furthermore, the choice of anchor group needs be designed based on the pigment surface properties. For instance, carbon black FW200, as was used for this project, has a strongly acidic surface composed mainly of lactone, carbonyl and ester moieties.

Consequently, as the physical interaction process was chosen to disperse this pigment, a specific anchor block bearing a tertiary amine was selected to form strong hydrogen bonds with the pigment surface. Finally, the conformation of the polymer in solution is important, as it can affect how stabilization takes place. Depending on the polymer solvability, the non-adsorbing segment (buoy) will either form a tail or a loop, impacting the repulsion effect.

Hence, whatever the adsorption method (coulombic, hydrogen bond, dipole interaction, or Van der Waals forces), the size of the polymer will define how strongly the segments interact with the particle surface, resulting in a polymer that is adsorbed more at one point than another. The first representation of interactions between soluble polymers and colloidal particles was reported by Jenckel and Rumbach in 1951. They found that the adsorption of a single point can be easily desorbed under shear stress, whereas multipoint attachment makes the desorption mechanism much more difficult, or even irreversible.

The main advantage of steric stabilisation over charge stabilisation is the decreased sensitivity to the presence of ions in solution, or changes in the dielectric constant of solvents. Also, the thickness of the layer is less sensitive in steric stabilisation mechanism, however, in aqueous media an excess of charge at the pigment surface can lead to the formation of a gel, induced by interactions between the layers.

Finally, the addition of an electrolyte in waterborne media causes irreversible coagulation, while flocculated particles formed in organic media can be disrupted under dilute conditions. These advantages give steric stabilization more attention and, as such, is widely used in solvent-based or waterborne coatings.

1.6. References

1. Flory, P. J. *Journal of the American Chemical Society* **1936,** *58* (10), 1877-1885.

2. Dube, M. A.; Rilling, K.; Penlidis, A. *Journal of Applied Polymer Science* **1991,** *43* (11), 2137-2145.

3. Flory, P. J. *Journal of the American Chemical Society* **1937,** *59* (2), 241-253.

4. Szwarc, M. *Journal of Polymer Science Part A: Polymer Chemistry* **1998,** *36* (1), IX-XV.

5. Baskaran, D.; Müller, A. H. E. *Progress in Polymer Science* **2007,** *32* (2), 173-219.

6. Quirk, R. P.; Lee, B. *Polymer International* **1992,** *27* (4), 359-367.

7. Moad, G.; Rizzardo, E. *Macromolecules* **1995,** *28* (26), 8722-8728.

8. Kato, M.; Kamigaito, M.; Sawamoto, M.; Higashimura, T. *Macromolecules* **1995,** *28* (5), 1721-1723.

9. Wang, J.-S.; Matyjaszewski, K. *Journal of the American Chemical Society* **1995,** *117* (20), 5614-5615.

10. Chiefari, J.; Chong, Y. K.; Ercole, F.; Krstina, J.; Jeffery, J.; Le, T. P. T.; Mayadunne, R. T. A.; Meijs, G. F.; Moad, C. L.; Moad, G.; Rizzardo, E.; Thang, S. H. *Macromolecules* **1998,** *31* (16), 5559-5562.

11. Moad, G.; Rizzardo, E.; Thang, S. H. *Australian Journal of Chemistry* **2005,** *58* (6), 379-410.

12. Destarac, M.; Bzducha, W.; Taton, D.; Gauthier-Gillaizeau, I.; Zard, S. Z. *Macromolecular Rapid Communications* **2002,** *23* (17), 1049-1054.

13. Chong, B. Y. K.; Le, T. P. T.; Moad, G.; Rizzardo, E.; Thang, S. H. *Macromolecules* **1999,** *32*, 2071.

14. Chong, Y. K.; Le, T. P. T.; Moad, G.; Rizzardo, E.; Thang, S. H. *Macromolecules* **1999,** *32* (6), 2071-2074.

15. Barner-Kowollik, C.; Davis, T. P.; Heuts, J. P. A.; Stenzel, M. H.; Vana, P.; Whittaker, M. *Journal of Polymer Science Part A: Polymer Chemistry* **2003,** *41* (3), 365-375.

16. Moad, G.; Rizzardo, E.; Thang, S. H. *Australian Journal of Chemistry* **2009,** *62* (11), 1402-1472.

17. Keddie, D. J. *Chemical Society Reviews* **2014,** *43* (2), 496-505.

18. Sun, X.-L.; He, W.-D.; Li, J.; Li, L.-Y.; Zhang, B.-Y.; Pan, T.-T. *Journal of Polymer Science Part A: Polymer Chemistry* **2009,** *47* (24), 6863-6872.

19. Paulus, R. M.; Becer, C. R.; Hoogenboom, R.; Schubert, U. S. *Australian Journal of Chemistry* **2009,** *62* (3), 254-259.

20. Benaglia, M.; Rizzardo, E.; Alberti, A.; Guerra, M. *Macromolecules* **2005,** *38* (8), 3129-3140.

21. Hoff, E. A.; Abel, B. A.; Tretbar, C. A.; McCormick, C. L.; Patton, D. L. *Polymer Chemistry* **2017,** *8* (34), 4978-4982.

22. Destarac, M. *Polymer Reviews* **2011,** *51* (2), 163-187.

23. Adamy, M.; van Herk, A. M.; Destarac, M.; Monteiro, M. J. *Macromolecules* **2003,** *36* (7), 2293-2301.

24. Chiefari, J.; Chong, Y. K.; Ercole, F.; Krstina, J.; Jeffery, J.; Le, T. P. T.; Mayadunne, R. T. A.; Meijs, G. F.; Moad, C. L.; Moad, G.; Rizzardo, E.; Thang, S. H. *Macromolecules* **1998,** *31* (null), 5559.

25. Thang, S. H.; Chong, Y. K.; Mayadunne, R. T. A.; Moad, G.; Rizzardo, E. *Tetrahedron Lett.* **1999,** *40*, 2435.

26. Destarac, M.; Charmot, D.; Franck, X.; Zard, S. Z. *Macromolecular Rapid Communications* **2000,** *21* (15), 1035-1039.

27. Moad, G.; Chiefari, J.; Krstina, J.; Postma, A.; Mayadunne, R. T. A.; Rizzardo, E.; Thang, S. H. *Polym. Int.* **2000,** *49*, 933.

28. Lambrinos, P.; Tardi, M.; Polton, A.; Sigwalt, P. *European Polymer Journal* **1990,** *26* (10), 1125-1135.

29. Chong, Y. K.; Krstina, J.; Le, T. P. T.; Moad, G.; Postma, A.; Rizzardo, E.; Thang, S. H. *Macromolecules* **2003,** *36* (7), 2256-2272.

30. Donovan, M. S.; Lowe, A. B.; Sumerlin, B. S.; McCormick, C. L. *Macromolecules* **2002,** *35*, 4123.

31. Schilli, C.; Lanzendörfer, M. G.; Müller, A. H. E. *Macromolecules* **2002,** *35* (18), 6819-6827.

32. Chong, Y. K.; Krstina, J.; Le, T. P. T.; Moad, G.; Postma, A.; Rizzardo, E.; Thang, S. H. *Macromolecules* **2003,** *36* (7), 2256-2272.

33. Quinn, J. F.; Rizzardo, E.; Davis, T. P. *Chemical Communications* **2001,** (11), 1044-1045.

34. Chiefari, J.; Mayadunne, R. T. A.; Moad, C. L.; Moad, G.; Rizzardo, E.; Postma, A.; Thang, S. H. *Macromolecules* **2003,** *36* (7), 2273-2283.

35. Feng, H.; Lu, X.; Wang, W.; Kang, N.-G.; Mays, J. *Polymers* **2017,** *9* (10), 494.

36. Blanazs, A.; Armes, S. P.; Ryan, A. J. *Macromolecular Rapid Communications* **2009,** *30* (4-5), 267-277.

37. Otsuka, H.; Nagasaki, Y.; Kataoka, K. *Materials Today* **2001,** *4* (3), 30-36.

38. Szwarc, M.; Levy, M.; Milkovich, R. *Journal of the American Chemical Society* **1956,** *78* (11), 2656-2657.

39. Sogah, D. Y.; Hertler, W. R.; Webster, O. W.; Cohen, G. M. *Macromolecules* **1987,** *20* (7), 1473-1488.

40. Patrickios, C. S.; Hertler, W. R.; Abbott, N. L.; Hatton, T. A. *Macromolecules* **1994,** *27* (4), 930-937.

41. Solomon, D. H. R., E.; Cacioli, . Polymerization process and polymers produced thereby.1986.

42. Krstina, J.; Moad, G.; Rizzardo, E.; Winzor, C. L.; Berge, C. T.; Fryd, M. *Macromolecules* **1995,** *28*, 5381.

43. Jiang, S.; Deng, J.; Yang, W. *Polymer Journal* **2008,** *40*, 543.

44. Engelis, N. G.; Anastasaki, A.; Nurumbetov, G.; Truong, N. P.; Nikolaou, V.; Shegiwal, A.; Whittaker, M. R.; Davis, T. P.; Haddleton, D. M. *Nature Chemistry* **2016,** *9*, 171.

45. Engelis, N. G.; Anastasaki, A.; Whitfield, R.; Jones, G. R.; Liarou, E.; Nikolaou, V.; Nurumbetov, G.; Haddleton, D. M. *Macromolecules* **2018,** *51* (2), 336-342.

46. Bian, F.; Xiang, M.; Yu, W.; Liu, M. *Journal of Applied Polymer Science* **2008,** *110* (2), 900-907.

47. York, A. W.; Kirkland, S. E.; McCormick, C. L. *Advanced Drug Delivery Reviews* **2008,** *60* (9), 1018-1036.

48. Bian, K.; Cunningham, M. F. *Macromolecules* **2005,** *38* (3), 695-701.

49. Jankova, K.; Chen, X.; Kops, J.; Batsberg, W. *Macromolecules* **1998,** *31* (2), 538-541.

50. Lee, S. B.; Russell, A. J.; Matyjaszewski, K. *Biomacromolecules* **2003,** *4* (5), 1386-1393.

51. Inglis, A. J.; Sinnwell, S.; Davis, T. P.; Barner-Kowollik, C.; Stenzel, M. H. *Macromolecules* **2008,** *41* (12), 4120-4126.

52. Wu, Y.; Wang, Q. *Journal of Polymer Science Part A: Polymer Chemistry* **2010,** *48* (11), 2425-2429.

53. Nasrullah, M. J.; Vora, A.; Webster, D. C. *Macromolecular Chemistry and Physics* **2011,** *212* (6), 539-549.

54. Quemener, D.; Davis, T. P.; Barner-Kowollik, C.; Stenzel, M. H. *Chemical Communications* **2006,** (48), 5051-5053.

55. Gody, G.; Maschmeyer, T.; Zetterlund, P. B.; Perrier, S. *Macromolecules* **2014,** *47* (10), 3451-3460.

56. Gody, G.; Barbey, R.; Danial, M.; Perrier, S. *Polymer Chemistry* **2015,** *6* (9), 1502-1511.

57. Berlowitz-Tarrant, L.; Tangredi, T. N.; Wnek, G. E.; Nicolosi, R. J. Sulfonated multiblock copolymer and uses therefor.US19960661111, 1998.

58. Baeten, E.; Haven, J. J.; Junkers, T. *Polymer Chemistry* **2017,** *8* (25), 3815-3824.

59. Xu, F.; Wang, T.; Chen, H.; Bohling, J.; Maurice, A. M.; Wu, L.; Zhou, S. *Progress in Organic Coatings* **2017,** *113* (Supplement C), 15-24.

60. Valdesueiro, D.; Hettinga, H.; Drijfhout, J. P.; Lips, P.; Meesters, G. M. H.; Kreutzer, M. T.; Ruud van Ommen, J. *Powder Technology* **2017,** *318* (Supplement C), 401-410.

61. Yossif, N. A.; Kandile, N. G.; Abdelaziz, M. A.; Negm, N. A. *Progress in Organic Coatings* **2017,** *111* (Supplement C), 354-360.

62. Jiang, S.; Wang, Y.; Sheng, D.; Xu, W.; Cao, G. *Carbohydrate Polymers* **2016,** *153* (Supplement C), 364-370.

63. Chen, Y.; Yu, H.; Yi, L.; Liu, Y.; Cao, L.; Cao, K.; Liu, Y.; Zhao, W.; Qi, T. *Powder Technology* **2018,** *325* (Supplement C), 568-575.

64. Díez-Pascual, A. M. In *Handbook of Antimicrobial Coatings*, Elsevier: 2018; pp 411-434.

65. Jean, M. N. B. I. M. Cosmetic composition including a polymeric particle dispersion.US5945095, 1999.

66. Duivenvoorde, F. L.; van Nostrum, C. F.; Laven, J.; van der Linde, R. *Journal of Coatings Technology* **2000,** *72* (909), 145-152.

67. Koning, C.; Van Duin, M.; Pagnoulle, C.; Jerome, R. *Progress in Polymer Science* **1998,** *23* (4), 707-757.

68. Cigana, P.; Favis, B. D.; Jerome, R. *Journal of Polymer Science Part B: Polymer Physics* **1996,** *34* (9), 1691-1700.

69. Gay, C. *Macromolecules* **1997,** *30* (19), 5939-5943.

70. Buttignol, V.; Gerhart, H. L. *Industrial & Engineering Chemistry* **1968,** *60* (8), 68-79.

71. Steiert, N.; Landfester, K. *Macromolecular Materials and Engineering* **2007,** *292* (10-11), 1111-1125.

72. Tiarks, F.; Landfester, K.; Antonietti, M. *Macromol. Chem. Phys.* **2001,** *202*, 51.

73. Yazdimamaghani, M.; Pourvala, T.; Motamedi, E.; Fathi, B.; Vashaee, D.; Tayebi, L. *Materials* **2013,** *6* (9), 3727.

74. Bourgeat-Lami, E.; Lang, J. *Journal of Colloid and Interface Science* **1998,** *197* (2), 293-308.

75. Taniguchi, Y.; Ogawa, M.; Gang, W.; Saitoh, H.; Fujiki, K.; Yamauchi, T.; Tsubokawa, N. *Materials Chemistry and Physics* **2008,** *108* (2), 397-402.

76. Papirer, E.; Lacroix, R.; Donnet, J. B. *Carbon* **1996,** *34* (12), 1521-1529.

77. Coca, S.; O'Dwyer, J. B. Pigment dispersions containing dispersants having core and arm star architecture prepared by controlled radical polymerization.US6336966, 2002.

78. Growney, D. J.; Fowler, P. W.; Mykhaylyk, O. O.; Fielding, L. A.; Derry, M. J.; Aragrag, N.; Lamb, G. D.; Armes, S. P. *Langmuir* **2015,** *31* (32), 8764-8773.

79. Huybrechets, J. Graft copolymer with a urea or imid functional group as a pigment dispersant.US5852123A, 2000.

80. Chu, I. C.; Fryd, M.; Lynch, L. E. Aqueous graft copolymer pigment dispersants.US5231131A, 1993.

81. Ma, S.-H. Graft copolymer pigment dispersants.US6472463B1, 2003.

82. André, X.; Bernaerts, K. Hyperbranched polymeric dispersants and non-aqueous pigment dispersions.US8567935B2, 2013.

83. Abuelyaman, A. S.; Rao, P. S.; Gaddam, B. N. Dendritic polymer dispersants for hydrophobic particles in water-based systems.US6258896B1, 2001.

84. Topham, A. *Progress in Organic Coatings* **1977,** *5* (3), 237-243.

85. Farrokhpay, S. *Advances in Colloid and Interface Science* **2009,** *151* (1), 24-32.

86. Leemans, L.; Fayt, R.; Teyssié, P.; Uytterhoeven, H. *Polymer* **1990,** *31* (1), 106-109.

87. Chen, Y.-M.; Hsu, R.-S.; Lin, H.-C.; Chang, S.-J.; Chen, S.-C.; Lin, J.-J. *Journal of Colloid and Interface Science* **2009,** *334* (1), 42-49.

88. Zhang, L.; Fang, K.; Fu, S.; Zhang, X.; Tian, A. *Journal of Applied Polymer Science* **2012,** *125* (2), 915-921.

89. Creutz, S.; Jérôme, R.; Kaptijn, G. M. P.; van der Werf, A. W.; Akkerman, J. M. *Journal of Coatings Technology* **1998,** *70* (883), 41-46.

90. Ortalano, D. M.; Vissing, C. J. Dye based aqueous pigment dispersions.US6503317B1, 1999.

91. Auschra, C.; Eckstein, E.; Mühlebach, A.; Zink, M.-O.; Rime, F. *Progress in Organic Coatings* **2002,** *45* (2), 83-93.

92. Dicker, I. B.; Hertler, W. R.; Ma, S. H. ABC triblock methacrylate polymers.US5219945A, 1993.

93. Ma, S. H.; Dicker, I. B.; Hertler, W. R. Aqueous dispersions containing ABC triblock polymer dispersants.US5519085A, 1993.

94. BYK. **https://ebooks.byk.com/1/wetting-and-dispersing/the-dispersion-process/**.

95. Hrubý, J.; Vinš, V.; Mareš, R.; Hykl, J.; Kalová, J. *The Journal of Physical Chemistry Letters* **2014,** *5* (3), 425-428.

96. Behrens, S. H.; Christl, D. I.; Emmerzael, R.; Schurtenberger, P.; Borkovec, M. *Langmuir* **2000,** *16* (6), 2566-2575.

97. Kosmulski, M.; Matijević, E. *Colloid and Polymer Science* **1992,** *270* (10), 1046-1048.

98. Hierrezuelo, J.; Sadeghpour, A.; Szilagyi, I.; Vaccaro, A.; Borkovec, M. *Langmuir* **2010,** *26* (19), 15109-15111.

99. Al-Gebory, L.; Mengüç, M. P.; Koşar, A.; Şendur, K. *Renewable Energy* **2018,** *119*, 625-640.

100. Spinelli, H. J. *Advanced Materials* **1998,** *10* (15), 1215-1218.

101. Alsharef, J.; Taha, M.; Khan, T. 2017; Vol. 79.

102. Dhar, N. R.; Ghosh, S. *The Journal of Physical Chemistry* **1925,** *30* (5), 628-642.

103. Xu, M.; Huang, Q.; Chen, Q.; Guo, P.; Sun, Z. *Chem. Phys. Lett.* **2003,** *375*, 598.

104. Napper, D. H. *Journal of Colloid and Interface Science* **1977,** *58* (2), 390-407.

Chapter 2: Synthesis of amphiphilic acrylate and methacrylate diblock copolymers *via* RAFT polymerisation in acetate solvents

In this chapter, the polymerisation acrylate and methacrylate monomers using RAFT polymerisation is reported. Optimisation of n-butyl acrylate and DMAEA monomers using BMDPT RAFT agent (scaled up by Lubrizol) is reported and compared with other RAFT agents (PABTC and MCTP) well-known to control acrylate polymerisation. Under carefully optimised conditions, a well-defined amphiphilic diblock copolymer was obtained (Đ = 1.12) with a high monomer conversion (> 95 %). Moreover, a hybrid amphiphilic diblock copolymer composed of methacrylate and acrylate monomers was also attempted with BMDPT RAFT agent. A poor control is obtained with an increase of dispersity (Đ = 2.3) with a bimodal molar mass distribution. A UV trace recorded by SEC-THF triple detection shown the presence of some unconsumed RAFT agent. Alternatively, the use of MCTP RAFT agent was investigated in methoxypropyl acetate and dioxane solvent to understand and optimised the synthesis of diblock copolymer.

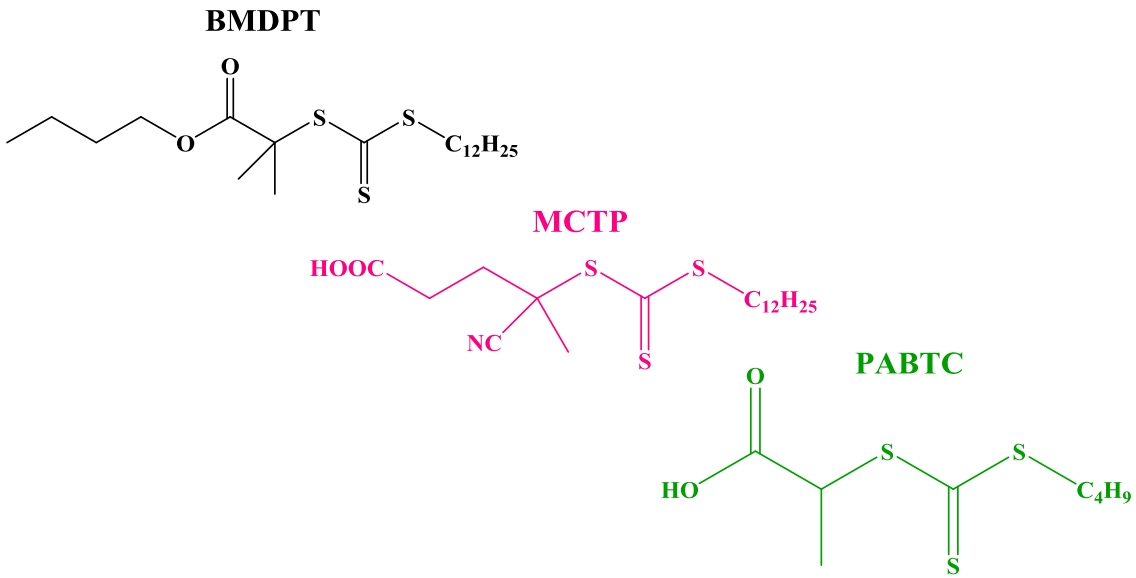

2.1. Introduction

Acrylic and methacrylic polymers are obtained from the polymerisation of acrylic esters or methacrylic acid monomers to yield materials with, for example, strong mechanical properties, adhesion, optical clarity and chemical stability, allowing for their use in a wide range of applications.[1,2] Poly (*n*-butyl acrylate) has a huge importance in industry due to specific properties such as its low glass transition temperature (T_g). As such, it is widely used in thermoplastic elastomers and latex paint formulations, providing water, sunlight and weathering resistance. Acrylates or acrylic acid polymers can be obtained by free radical polymerisation at high temperatures (120 ˚C - 200 ˚C)[3,4], which can lead to many side reactions such as branching, chain transfer or high chain termination; impacting the overall control of the reaction, and resulting polymer properties. The polymerisation can be improved by using anionic and group transfer polymerisation techniques leading the formation of well-defined polymers, however, a large amount of side reactions can occur.[5,6,7] To overcome this problem, several controlled radical polymerisation techniques, such as NMP[8,9] ATRP[10] or RAFT have been developed.[11,12] Reversible Addition-Fragmentation chain Transfer (RAFT) polymerisation relies on a fast equilibrium between the active and dormant growing polymeric chains, and results in the formation of well-defined polymers with a low dispersity. This technique also allows for further polymerisation reactions to occur by chain extending the polymer with a different monomer, resulting in precise block polymers.

The interest in block copolymers has increased significantly over the last few decades, in part due to their potential aggregation in solution and their phase separation behaviour. However, the synthesis of block, or other complex architectures, is challenging and limited by the compatibility of the monomer and reaction conditions. These monomers easily facilitate the propagating radical species to react with the C=S bond, leading to well-defined block co-polymers with a narrow distribution and low dispersity ($Đ \leq 1.2$), at low temperatures using the RAFT agent BMDPT. As discussed, BMDPT RAFT agent is produced in tonne scale by Lubrizol and is used in this thesis to synthesise a range of amphiphilic diblock copolymers composed of *n*butyl acrylate and DMAEA. The application of these polymers will be discussed in Chapter 5.

2.2. Results and Discussion

2.2.1. *n*Butyl acrylate polymerisation

- *Study of nBA polymerisation*

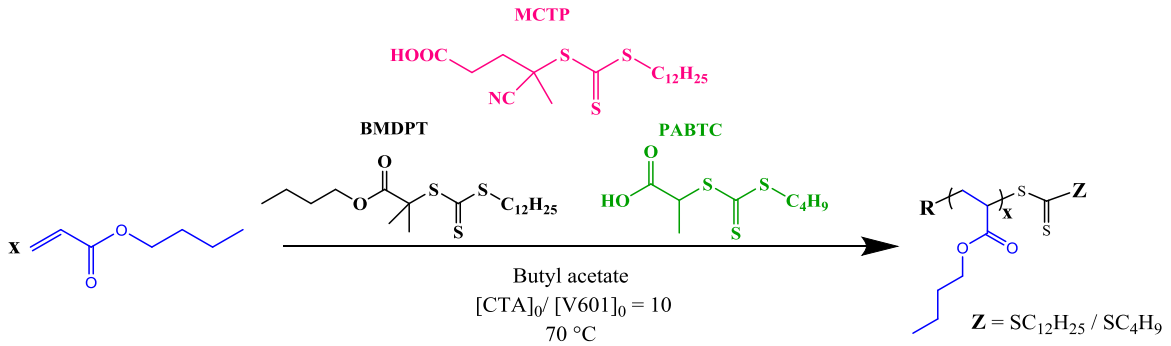

Scheme 2.1: Comparison of *n*-butyl acrylate polymerisation using BMDPT, MCTP and PABTC RAFT agents in butyl acetate solvent with a $[n\text{BA}]_0 = 3$ M and V601 as azoinitator at 70 ˚C

In RAFT polymerisation, design of the RAFT agent is crucial to obtain good control over the polymerisation. As previously discussed, both the R and Z groups play important roles in determining the outcome of polymerisation.[13] The polymerisation of *n*BA is performed in solution which present two main disadvantages in comparison to the bulk polymerisation. The fraction of the dead chains can increased if a chain transfer to the solvent occurs. Additionally, a low monomer concentration favour the mechanism of the intramolecular (backbiting) transfer leading to the formation of tertiary radical which can either undergo a *β*-scission or from a branch points. To this end, control over the polymerisation of *n*-butyl acrylate was compared by using three RAFT agents: the industrially relevant BMDPT, MCTP, which bears a similar "Z" group to BMDPT, and PABTC, well-known to give good control over acrylate polymerisations (**Scheme 2.1**).[14,15]

The rational of using these CTAs was to investigate the impact of radical stability on the molecular weight control of the resulting polymers. Polymerisation of *n*-butyl acrylate were performed under the same conditions ($[n\text{BA}]_0$ = 3 M, $[\text{CTA}]_0/[\text{V601}]_0$ = 10 and T = 70 ˚C) for all the RAFT agents. The **Figure 2.1** shows the overlapping of a symmetrical and narrow THF-SEC chromatograms of p(*n*BA). A high monomer conversion (> 95 %) is reached for each homopolymers. The difference between the experimental and theoretical molar mass can be attributed to the difference of the hydrodynamic volume between the p(*n*BA) and PMMA used for SEC calibration. It is worth nothing that a small shoulder at high molar mass is observed for each polymerisations which correlates to the formation of backbiting as reported in several studies of acrylate polymerisation.

These data correlate with the results published by Lai *et al.* regarding the polymerisation of acrylate and methacrylate using trithiocarbonate ("2-(dodecylthiocarbonothioylthio)-2-methylpropionic acid" similar to BMDPT) as a RAFT agent.[16] However, the shoulder is more significant for p(*n*BA) mediated by BMDPT RAFT agent which can be explained either by the reactivity of the impurities present (≈ 30 %) in the crude Lubrizol RAFT agent or to the underestimated amount of RAFT agent used. In the appendix of this thesis, the MALDI-ToF of the industrial BMDPT RAFT agent is reporter is **Figure A.2**, the experimental and theoretical monoisotopic mass are recorded in **Table A.1** and the structures of the potential impurities in **Figure A.3**. The highest ionization efficiency correspond to the impurities species such as trithiocarbonates or disulphide compounds bearing a "$C_{12}H_{25}$" group (**structures** 1, 6, 5, 7). The small peaks have been attributed to species composed by two trithiocarbonates (**structures** 8, 9, 10). These species can potentially be involved in the polymerisation and compete with the pure RAFT agent. Only few studies have been reported regarding the impact of the RAFT impurities impacting the kinetics of the polymerisation. Plummer and co-workers have studied the effect of the impurities in the cumyl dithiobenzoate (CDB) on RAFT polymerisation. They compared the polymerisation of HEMA (2-hydroxylethyl methacrylate), styrene and methyl acrylate in presence of CDB purified by silica column and CDB-HPLC (purified by HPLC and stored at -20 ˚C for a 1 week). They observed a presence of an inhibition period and retardation effect. Another set of polymerisation was performed by increasing the concentration of CDB showing an increase of the retardation. Based on their kinetic they conclude that the rate of the polymerisation depends on the RAFT agent purity.[17]

The SEC molecular weight distributions show a small shoulder at high molar mass, corresponding to backbiting, which is observed for each RAFT agent. A slightly higher molar mass is observed for BMDPT, as the amount of CTA added in the reaction mixture is underestimated, due to the presence of impurities (see Appendix) in the crude Lubrizol RAFT agent (**Figure 2.1)**.

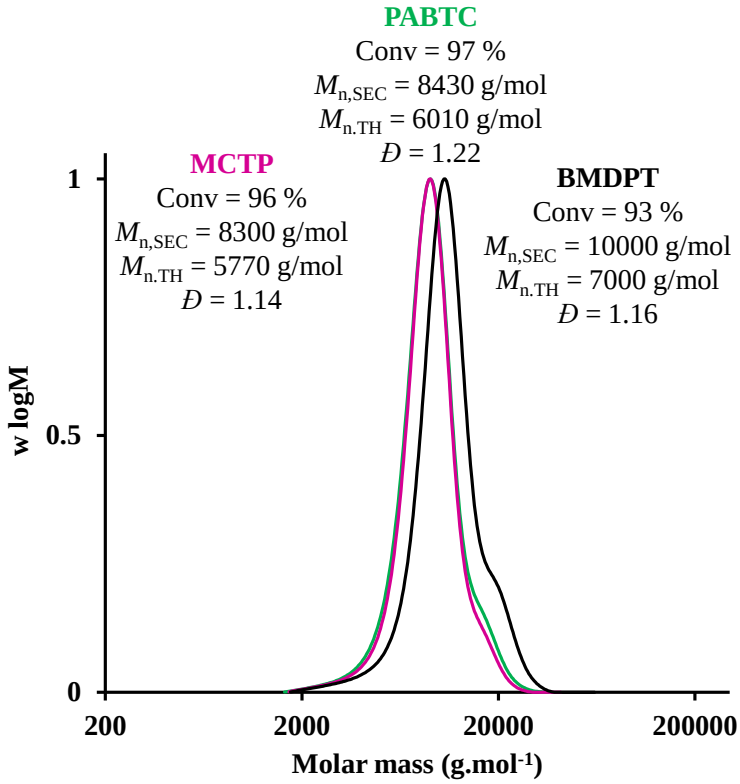

Figure 2.1: Comparison of THF- SEC chromatograms of p(*n*BA)$_{55}$ prepared at 70 ˚C with BMDPT (**black**), MCTP (**pink**) and PABTC (**green**) RAFT agents in butyl acetate solvent with [*n*BA]$_0$ = 3M, [CTA]$_0$/[V601]$_0$ = 10

The similarity of the data obtained in this preliminary study confirm the good control over molecular weight for acrylate monomers. Hence, several parameters such as monomer

concentration and temperature effect were investigated followed by the full kinetics study of acrylate monomers (*n*BA and DMAEA).

- *Monomer concentration study*

Following on from this, changes in the parameters related to the kinetics and the control over the polymerisation, such as monomer concentration and temperature, were varied for *n*-butyl acrylate homopolymerisation, using an acetate solvent and the BMDPT RAFT agent.

Initially, the effect of monomer concentration on *n*-butyl acrylate homopolymerisation at 70 ˚C was carried out. A degree of polymerisation of 55 was targeted at 2 M, 3 M and 4 M concentrations, whilst keeping the ratio $[BMDPT]_0$ / $[V601]_0$ constant at 10 :1.

All reactions were performed in both butyl acetate and methoxy propyl acetate solvents in order to optimise the conditions. The first observation is that the control of *n*-butyl acrylate polymerisation is independent of monomer concentration, however, changes in the concentration impacted the rate of propagation, which was reduced at low monomer volumes, and consequently decreased the overall molecular weight of the polymer. The near quantitative monomer conversion, obtained after 12 hours of polymerisation was determined by ^{1}H NMR analysis in $CDCl_3$ (experimental section:). Additionally, the SEC molecular weight distributions show a monomodal molar mass distribution and narrow dispersity ($Đ \approx 1.10$) for each monomer concentration, indicating good control (**Figure 2.2**). Determination of the molecular weight, relative to the

hydrodynamic volume of PMMA, gives an experimental value for molecular weights lower than the theoretical molecular weight.

Despite good control over the polymerisation, a small shoulder at high molar mass is observed for each monomer concentration. A dilute polymerisation media and a higher monomer conversion increase the probability of mid-chain branching but not a significant difference is observed in these experiments.

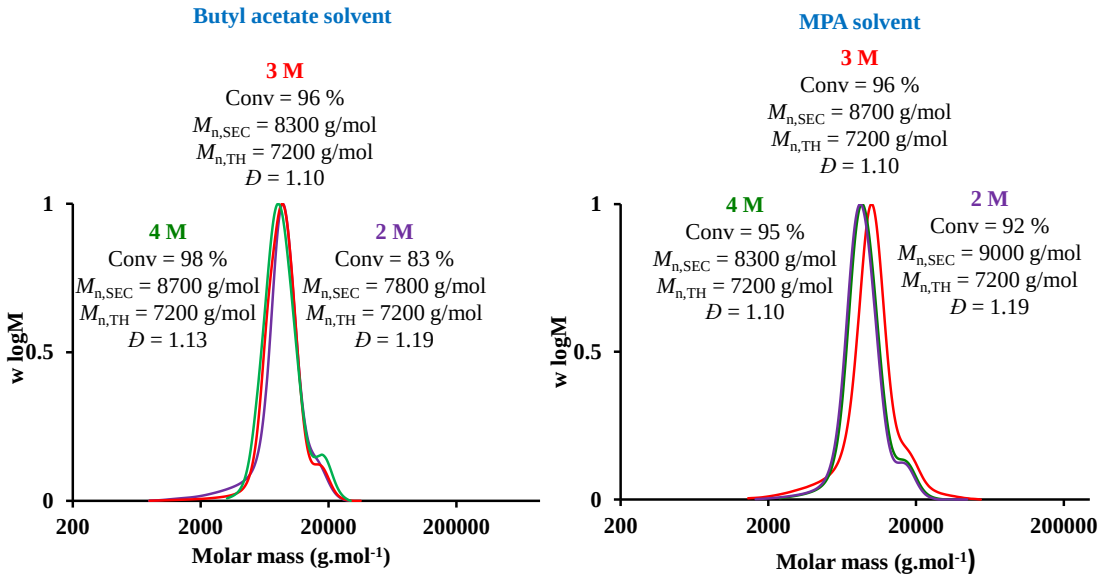

Figure 2.2: Comparison of THF- SEC chromatograms of p(*n*-BA)$_{55}$ at 2 M, 3M and 4M in butyl acetate (**left**) and MPA solvents (**right**) using BMDPT RAFT agent

Based on this study, a monomer concentration of 3 M was chosen for this investigation as a high monomer conversion is reached in a shorter time period. Whilst, a high monomer concentration (*i.e* 4 M) allows for greater monomer conversion it also induces a highly viscous solution. The side reaction of mono-substituted *n*-butyl acrylate sub-units involves the formation of macromonomer chain ends *via* a *β*-scission (or backbiting)

mechanism, and is widely reported in the literature, and some mechanisms have been proposed for acrylate monomers (**Scheme 2.2**).[18,19, 20,21] Chiefari *et al*. have reported two possible paths for the macromonomer formation.[22]

They performed the polymerisation by feeding the azo initiator with a mixture of 10 % w/v *n*-butyl acrylate in butyl acetate solvent at 150 ˚C, yielding a polymer with a narrow dispersity (M_n ~ 100 000 g/mol, $Đ$ ~ 1.1), where no formation of macromonomer was observed. In a second experiment, 10 % w/v of the same polymer was synthesised under the same conditions, however, the monomer was not fed into the reaction. Under these conditions, the homopolymer was unchanged but the formation of macromonomer (M_n ~ 1960 g/mol, $Đ$ ~ 1.75*)* was observed. A polymerisation performed at high monomer concentrations leads to intermolecular hydrogen abstraction, minimising the formation of the macromonomer.[23] Inversely, a higher rate of propagation occurs at high monomer concentration leading to the formation of branched macromonomers. In the same publication, the authors reported a considerable decrease in macromonomer molecular weight when the polymerisation was performed at either 150 ˚C (M_n ~ 2000 g/mol) or 240 ˚C (M_n ~ 1300 g/mol). Such high temperatures cannot be used here as the degradation of the BMDPT RAFT agent occurs at 200 ˚C (**see Appendix A4**).

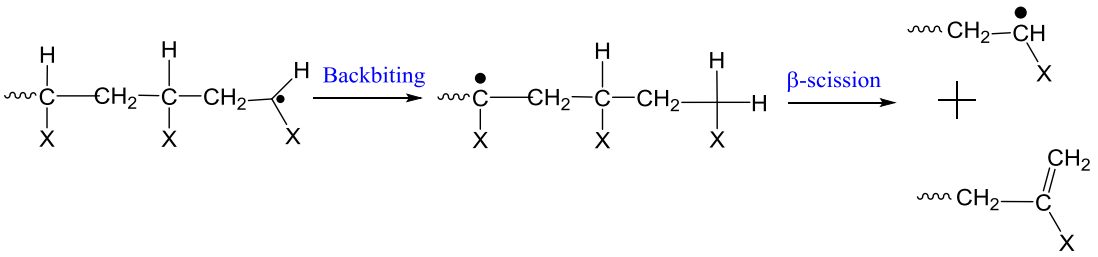

Scheme 2.2: General scheme of backbiting mechanism

- *Effect of temperature study*

In addition to monomer concentration, the effect of the temperature on acrylate polymerisation was also investigated in both butyl acetate and MPA solvents, in order to assess the optimal conditions for *n*-butyl acrylate polymerisation. Based on the previous study, a monomer concentration of 3 M, with a ratio of $[BMDPT]_0$ / $[V601]_0$ = 10, was used to prevent gel formation and to reach a high monomer conversion in a short time. To study temperature effects, a suitable azo-initiator must be chosen based on the desired polymerisation temperature. The temperature effect on acrylate polymerisation was investigated by using two different azoinitators, V601 and Vazo-88, for a polymerisation below 70 ˚C and 90 ˚C respectively. In these conditions, the rate of radicals formed is similar throughout the polymerisation, allowing the comparison between each polymerisation where the theoretical fraction of living chains should be the same. The SEC molecular weight distributions show better polymerisation control at low temperatures. However, full monomer conversion was reached after 20 hours at 60 ˚C, while only 10 hours are required at 70 and 90 ˚C. Poor control of the reaction was obtained at 90 ˚C due to increased chain termination at high temperatures (**Figure 2.3**). Moreover, higher reaction temperatures will favour the abstraction of hydrogen from the polymer backbone and also increase the rate of fragmentation, decreasing the molecular weight of the polymer.[24] As mentioned previously, the presence of the shoulder at high molar mass corresponds to the formation of mid-chain branching which occurs at high monomer conversion.

Finally, the suitable temperature chosen for further polymerisations is 70 ˚C in order retain good control over the molecular weight with a high monomer conversion and livingness.

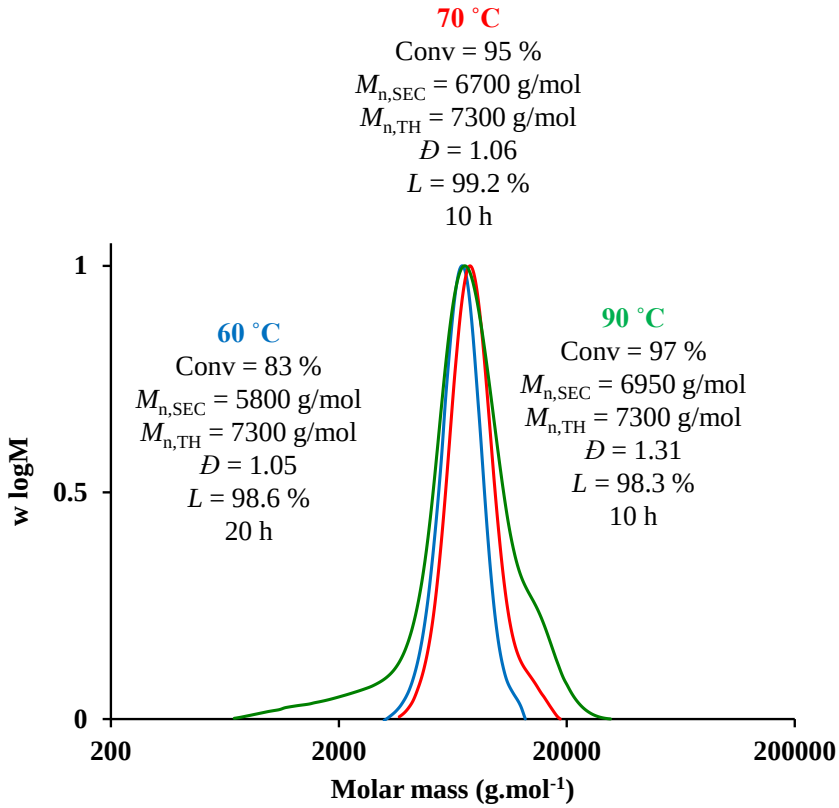

Figure 2.3: Comparison of THF- SEC chromatograms of *n*-butyl acrylate polymerisation using BMDPT RAFT agent at 60 ˚C (**blue**), 70 ˚C (**red**) and 90 ˚C(**green**) with $[n\text{BA}]_0$ = 3 M in butyl acetate solvent

- *Kinetic study on n-butyl acrylate in butyl acetate solvent*

Based on the above investigations, a kinetic study was performed with a ratio of $[\text{BMDPT}]_0$ / $[\text{V601}]_0$ of 10 at 70 ˚C in butyl acetate. The similarity of the theoretical

molecular weight and the experimental values confirms the controlled nature of the polymerisation (**Figure 2.4 A**).

The dispersity remains low over time. **Figure 2.4 B** shows a linear relationship of the first order between $\ln([M]_0/[M]_t)$ and time suggesting a constant radical concentration throughout the reaction.

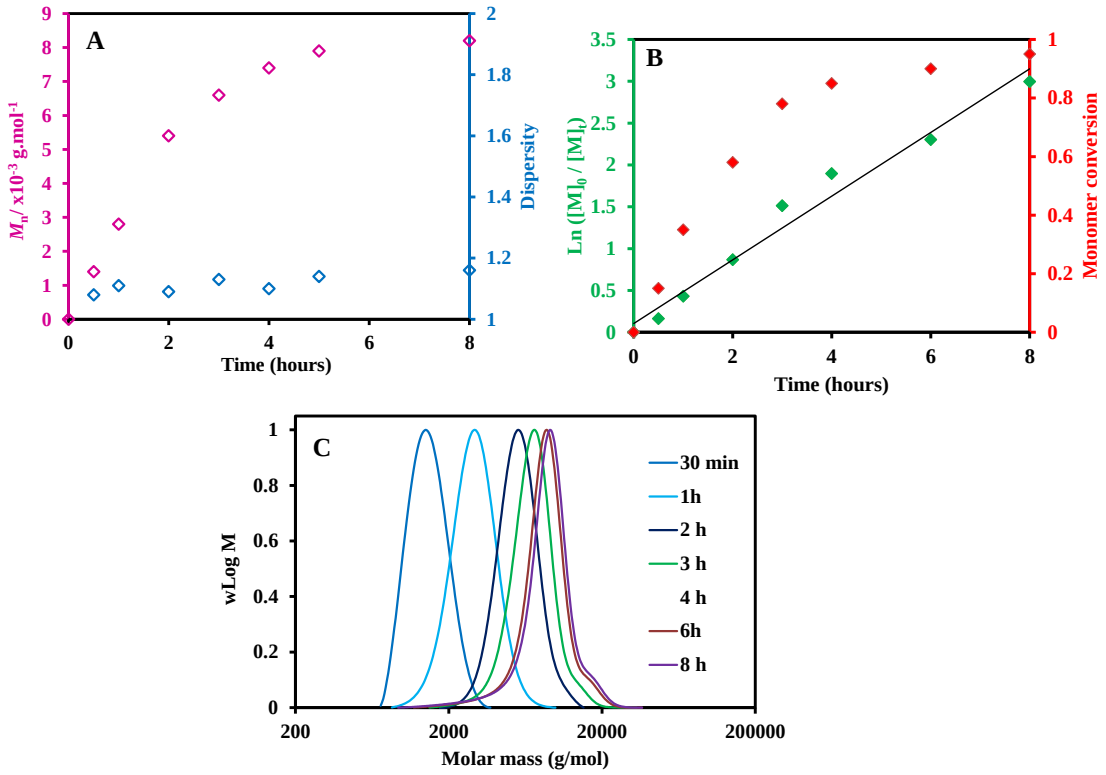

Figure 2.4: (**A**) Molar mass and molar mass distribution evolution *versus* time, (**B**) Kinetic first-order plot and monomer conversion *versus* time; (**C**) SEC-THF chromatograms of *n*BA kinetic performed in butyl acetate solvent at 70 ˚C

➢ *Kinetic study on n-butyl acrylate in methoxypropyl acetate solvent*

In addition, a kinetic study was also performed in methoxypropyl acetate and revealed that the reaction fulfils the criteria of living radical polymerisation with the linearity of the first order plot.

In the **Figure 2.5 B**, a quantitative monomer conversion is reached in 8 hours and no inhibition period is observed. Any significant difference between the polymerisation in butyl acetate and MPA is noticed.

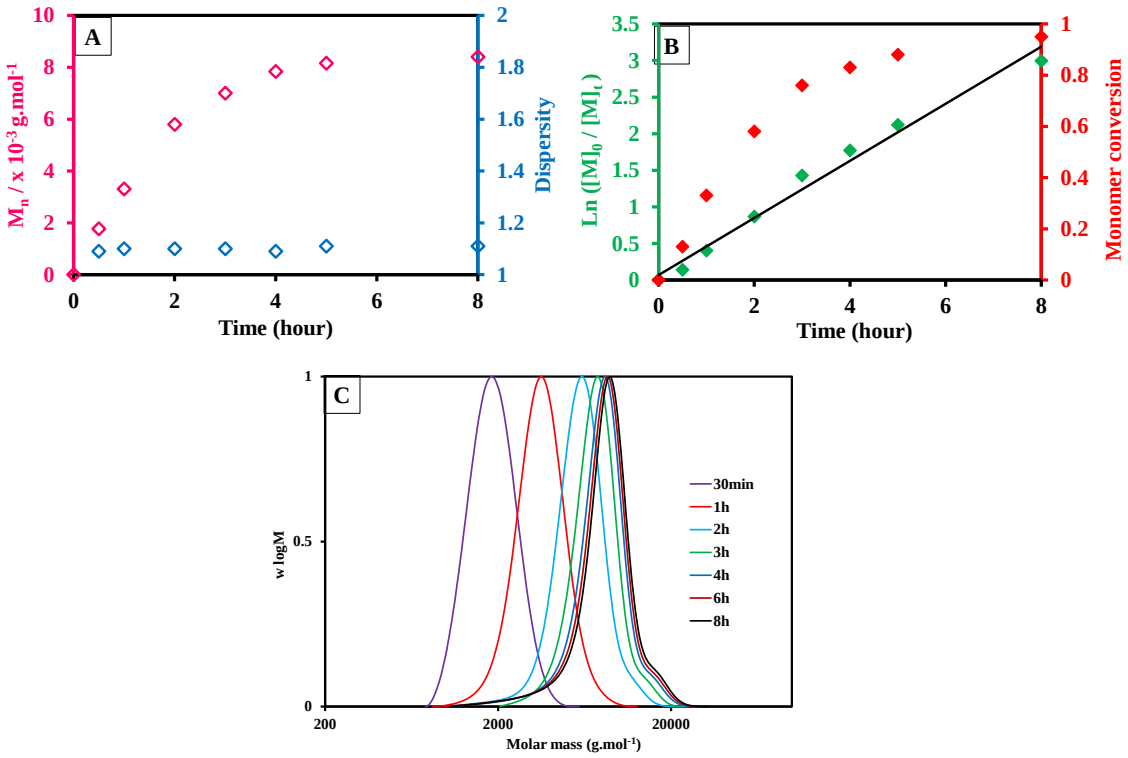

Figure 2.5: (**A**) Molar mass and molar mass distribution evolution *versus* time, (**B**) Kinetic first-order plot and monomer conversion *versus* time; (**C**) SEC-THF chromatograms of p(*n*BA) kinetic performed in MPA solvent at 70 ˚C

The main key parameters such as the monomer concentration, temperature and the structure of the RAFT agent have been investigated for *n*BA polymerisation.

Based on these studies, a monomer concentration of 3 M , a ratio $[CTA]_0$ / $[Initiator]_0$ of 10, a polymerisation temperature of 70 ˚C in methoxypropyl acetate solvent were chosen as optimal conditions for the synthesis of the following diblock copolymer, and for the studies of Chapter 4.

2.2.2. Synthesis of statistical acrylate copolymers

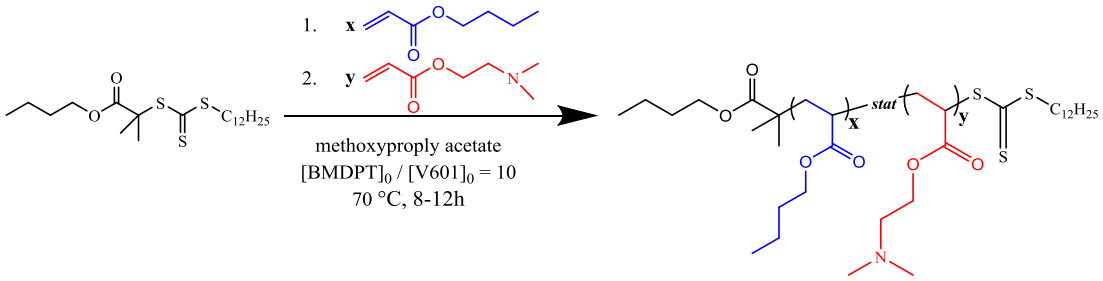

Scheme 2.3: General scheme of poly(*n*BA)-*statistical*-poly(DMAEA) synthesised in MPA solvent at 70 ˚C using BMDPT RAFT agent and V601 as azoinitator

In copolymerisation process, the reactivity of the monomers is guided by the electronic and steric properties of the reactants. The fact that in RAFT polymerisation all chains grow simultaneously throughout the polymerisation leads to the formation of the homogeneous gradient copolymers. One of the common method to determine the monomer sequence distribution of the copolymer is the determination of the reactivity ratio of both monomers. Here, the determination of the *n*BA and DMAEA incorporation is difficult by ^{1}H NMR spectroscopy since the resonance peaks of the protons of the two monomers units overlap.

The kinetic studies of *n*BA and DMAEA polymerisations show a fast polymerisation of *n*BA in comparison to DMAEA which also shows an inhibition period of 30 min.

Additionally, the ratio between *n*BA and DMAEA being 2/3 – 1/3 respectively, *n*BA will be predominant in the final copolymer composition (**Figure 2.6**).

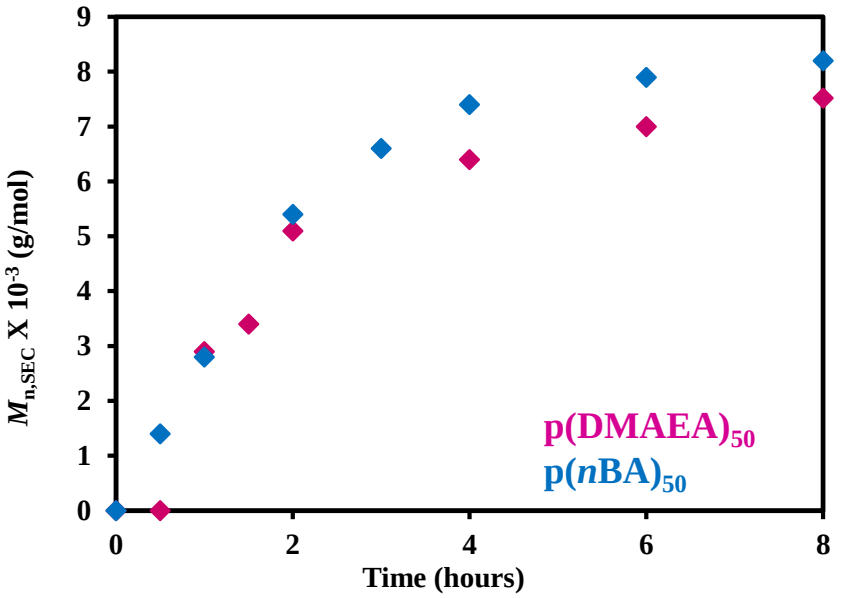

Figure 2.6: Kinetic studies of p(DMAEA)$_{50}$ and p(*n*BA)$_{50}$ evolution *versus* time performed in butyl acetate solvent and mediated by BMDPT RAFT agent. Initial conditions: [monomer]$_0$ =3 M, [BMDPT]$_0$ / [V601]$_0$ = 10, T = 70 ˚C

A series of statistical copolymers of *n*BA and DMAEA with a different range of molecular weights were prepared in batch polymerisation. The SEC-THF chromatograms of the statistical copolymers with the monomers conversion, the experimental and theoretical molar mass distribution are represented in the **Figure 2.7**. A decent monomer conversion is obtained for both blocks, even if the highest monomer conversion for DMAEA seems to be 80 %. That can be explained by the fast hydrolysis of DMAEA which can potentially slow down the polymerisation.[25]

The discrepancy between the $M_{n,SEC}$ and $M_{n,TH}$ is due to the inadequacy of the PMMA standard used to calibrate the SEC column.

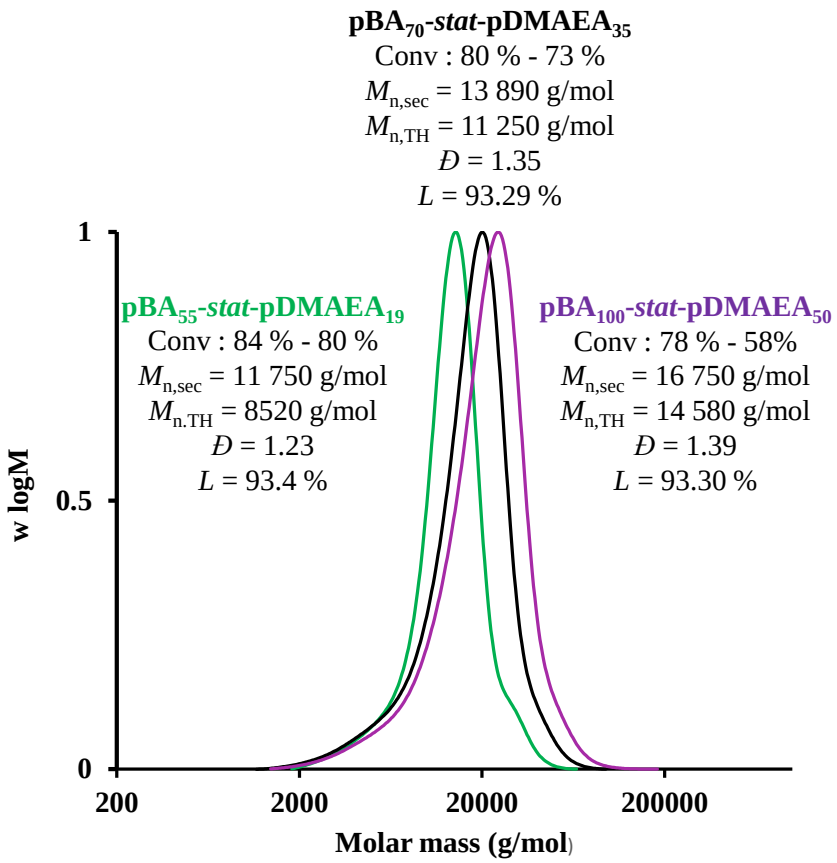

Figure 2.7: Comparison of SEC-THF chromatograms of statistical *n*-BA/DMAEA copolymers with DP of 55/19 (**green**); 70/35 (**black**) and 100/50 (**purple**) respectively synthesised in presence of BMDPT RAFT agent with $[monomer]_0$ = 3 M, $[BMDPT]_0$ / $[V601]_0$ = 10 at 70 ˚C in methoxypropyl acetate solvent

The ^{13}C NMR analysis represented in **Figure 2.8** is used to characterise the incorporation of both monomer. The resonance peak at δ = 174.43 ppm correspond to the carbonyl groups. The CH_2 of (C**H**$_2$-N(CH_3)$_2$) at δ = 62.34 ppm and the CH_3 in (CH_2-N(**CH**$_3$)$_2$) at δ = 42 ppm prove the incorporation of DMAEA monomer in the copolymer. 13C NMR ($CDCl_3$, 400 MHz, δ/ppm): δ = 170 (C=O), 64.41 (C=O-**CH**$_2$-),

62.34 (C=O-CH_2-**CH_2**-N(CH_3)$_2$), 43.25 (-CH_2-N(**CH_3**)$_2$) 35.20 (-CH_2-**CH**-C=O), 30.61 (-**CH_2**-CH-C=O), 29.61 (C=O-CH_2- **CH_2**- CH_2-) 19.1 (C=O-CH_2- CH_2- **CH_2**), 13.73 (-CH_2-N(**CH_3**)$_2$).

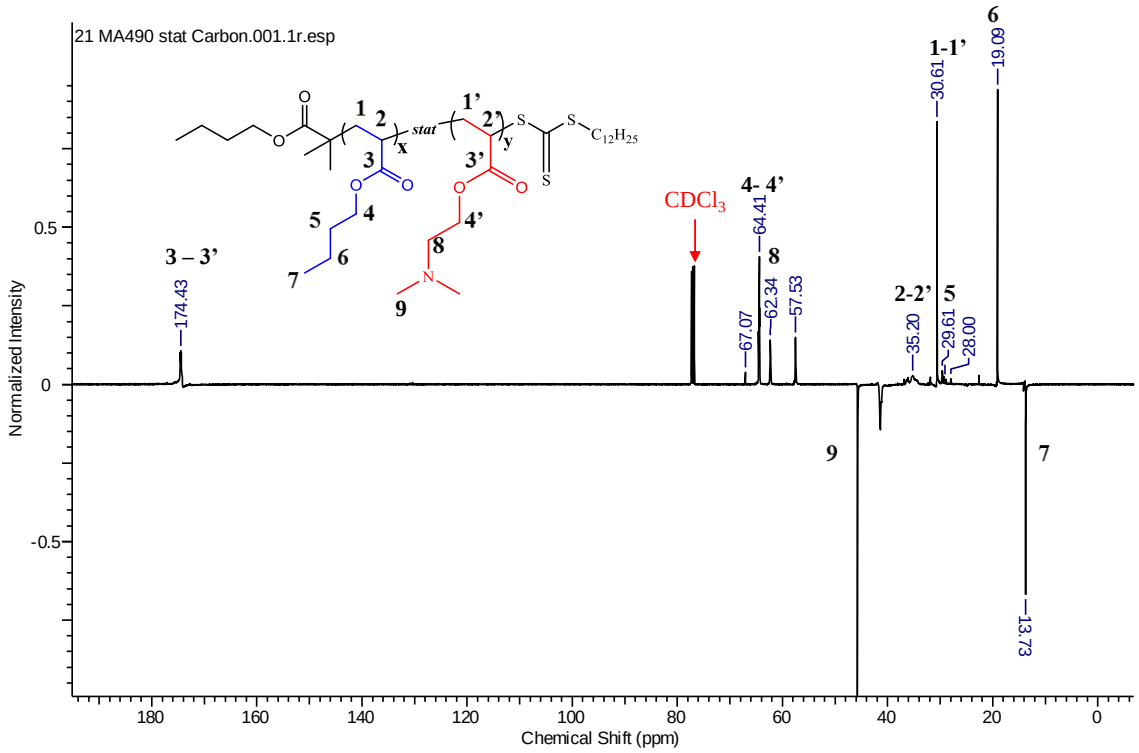

Figure 2.8: ^{13}C NMR analysis of p(*n*BA)$_{19}$-*stat*-p(DMAEA)$_{55}$ synthesised in MPA solvent and run in $CDCl_3$

Based on the previous results, the formation of block copolymers composed by *n*-BA as hydrophobic segment and DMAEA (and DMAEMA) as hydrophilic segment were further investigated, to demonstrate the presence of the ω-chain end in the polymeric chain.

2.2.3. Synthesis of acrylate diblock copolymers

Using the above information, the synthesis of amphiphilic block copolymers composed by a hydrophobic block and hydrophilic block bearing a tertiary amine was investigated to use as dispersants for a carbon black pigment (**Scheme 2.4**).

2.2.3.1. Poly(DMAEA)-*block*- poly(*n*BA)

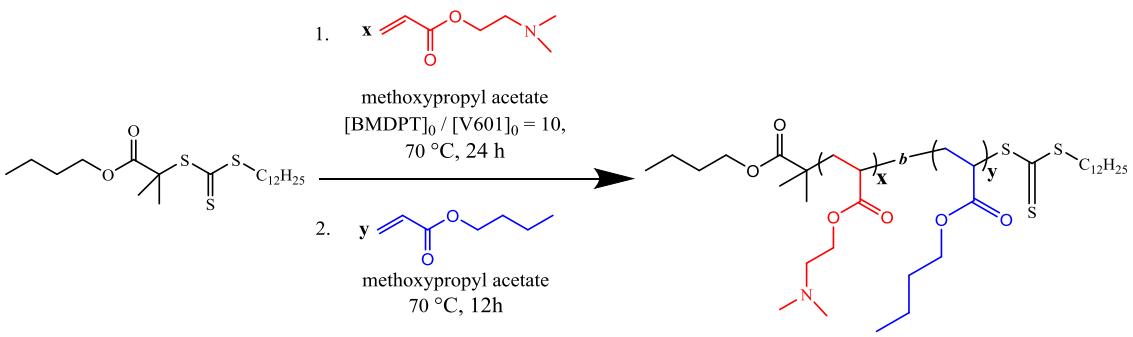

Scheme 2.4: General scheme of poly(DMAEA)-*block*- poly(*n*BA) copolymer synthesised at 70 ˚C using BMDPT RAFT agent and V601 as azoinitator in MPA solvent

Synthesis of amphiphilic block copolymers was performed using the conditions previously established for poly(*n*-butyl acrylate) a sequential monomer addition. Given that the scope of this thesis is pigment stabilisation, controlling the size of each block is of great importance. It was previously established that the average molecular weight for an optimal polymeric stabiliser is around 10 kDa, and the amphiphilic block copolymer must be composed of 70 % hydrophobic (or solvophobic) block for steric stabilisation and 30 % of hydrophilic (solvophilic) block for pigment affinity. As such, a range of diblock copolymers were prepared in order to assess the effect of polymeric chain size on

pigment dispersion efficiency using pBA and pDMAEA. Poly [2-(dimethylamino)ethyl acrylate] is a well-known pH-sensitive polymer in aqueous solutions, due to the presence of a tertiary amine which can easily be quaternized at low pH.

The first attempt to synthesise the diblock copolymer poly(DMAEA)-*block*-poly(*n*-BA) using the previously established conditions yielded poor control over the reaction, as shown in **Figure 2.9**. The homopolymerisation of DMAEA was found to be controlled with a narrow molar mass distribution with a monomer conversion of 84%. After purification of p(DMAEA)$_{19}$ *via* precipitation, however, the chain extension using *n*-BA leads a bimodal distribution suggesting a presence of unconsumed macroCTA or a possible degration of the trithiocarbonate in presence of tertiary amine.

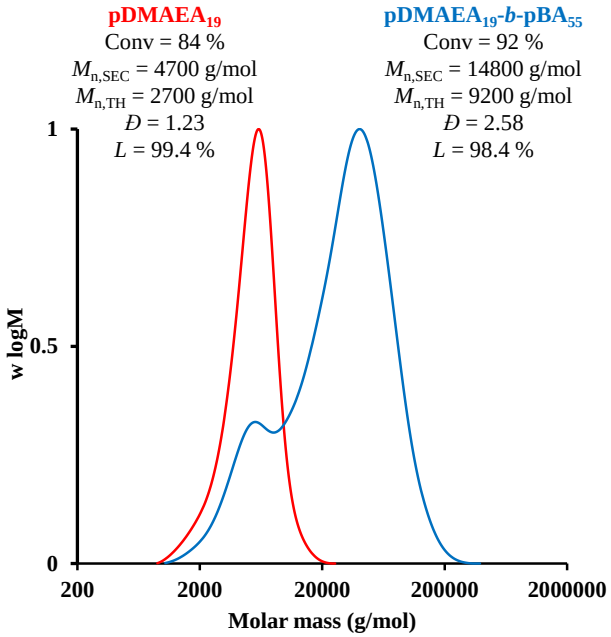

Figure 2.9: Comparison of THF-SEC chromatograms of p(DMAEA)$_{19}$ prepared at 70 ˚C and polymerised to 92% conversion, and subsequent chain extension with p(*n*-BA)$_{55}$ in MPA solvent

Zheng Li and *al.* studied the possible degradation of a trithiocarbonate RAFT agent in DMF using a DMAEA monomer.[26] Degradation of the RAFT agent during the polymerisation was monitored by UV absorbance at 305 nm. Two mechanisms were proposed to explain the decomposition process of the RAFT agent. The first was attributed to direct nucleophilic attack of the amine to the C=S bond, leading to cleavage of the RAFT agent.

In the second mechanism, the amine acts as a base to remove the proton present on the terminal carbon of the ester carbonyl and fragments the RAFT agent. To this end, the synthesis of the diblock was performed in reverse, starting with poly (*n*BA) followed by the chain extension with dimethylaminopropyl acrylate (DMAEA).

An important factor to consider in RAFT polymerisations is the livingness, which is used to quantify the number of living chains (bearing a trithiocarbonate) at the end of the polymerisation. A high livingness is required to target a diblock or other complex architectures in controlled radical polymerisation reactions.

The determination of the number of living chains is given by **Equation 2.1**[27]:

$$L\ (\%) = \frac{[\mathrm{CTA}]_0}{[\mathrm{CTA}]_0 + 2.f.[I]_0.\left(1-e^{-kdt}\right).\left(1-\frac{fc}{2}\right)} \quad \textbf{(Equation 2.1)}$$

Where the initial concentrations of chain transfer agent (CTA) and initiator are represented by $[CTA]_0$ and $[I]_0$ respectively, while the number "2" is attributed to the formation of two primary radicals after thermal decomposition of the azo initiator.

The value "*f*" is set at 0.5 for the calculation of livingness in this thesis and k_d is the rate coefficient of initiator decomposition. Finally, the term (1-*f*c/2) describes the production of radical-radical termination by combination or disproportionation (*f*c = 1 means 100 % bimolecular termination by combination, *f*c = 0 means 100 % bimolecular termination by disproportionation). Using this equation, livingness can be related to the reaction temperature, initiator concentration, and reaction time.

2.2.3.2. poly(*n*BA)-*block*-poly(DMAEA)

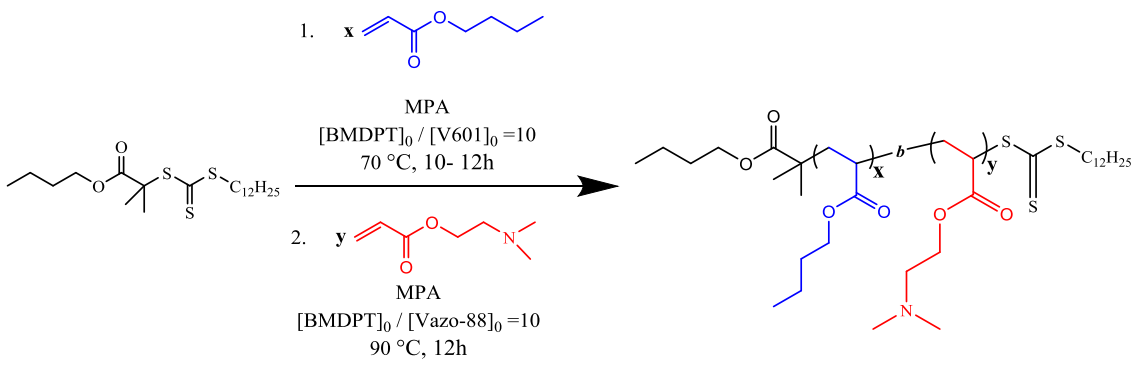

Scheme 2.5: General scheme of poly(*n*BA)-*block*-poly(DMAEA) copolymer synthesised at 70 ˚C using BMDPT RAFT agent and V601 as azoinitator in MPA solvent

The SEC molecular weight distributions reveal a monomodal molecular weight distribution for poly (*n*BA) with a quantitative monomer conversion and a shift to higher molecular weights for all the diblock copolymers, suggesting full consumption of the macroCTA (**Figure 2.10**). The backbiting is only present for the *n*-butyl acrylate homopolymer, noted by the shoulder at higher molecular weight values.

Given the broader chromatogram of the second block, it is possible that this shoulder is still present after chain extension, so it is not possible to conclude if backbiting is occurring after chain extension. Regardless, the dispersity remains low throughout all the polymerisations.

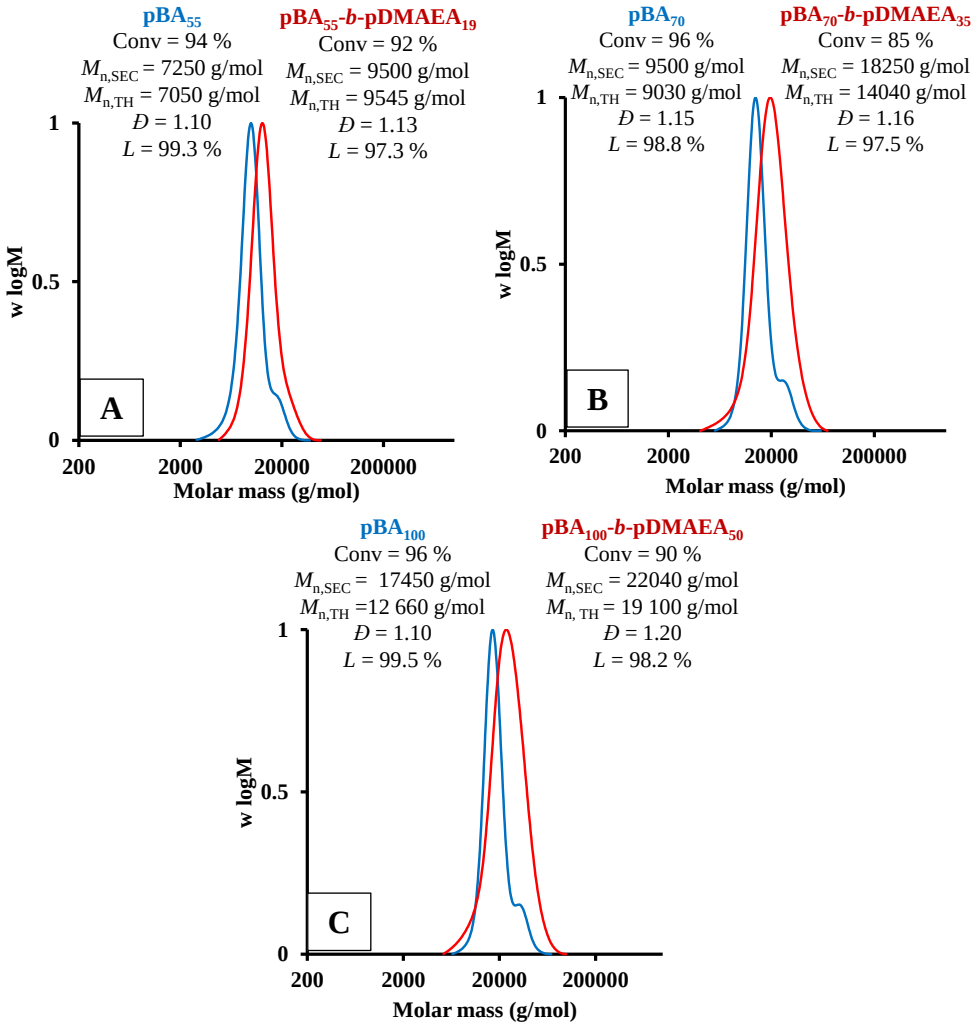

Figure 2.10: Comparison of SEC-THF chromatograms of block *n*-BA/DMAEA copolymers with DP of 55/19 (**A**); 70/35 (**B**) and 100/50 (**C**) respectively synthesised in presence of BMDPT RAFT agent with $[monomer]_0$ = 3 M, $[BMDPT]_0$ / $[V601]_0$ = 10 at 70 ˚C

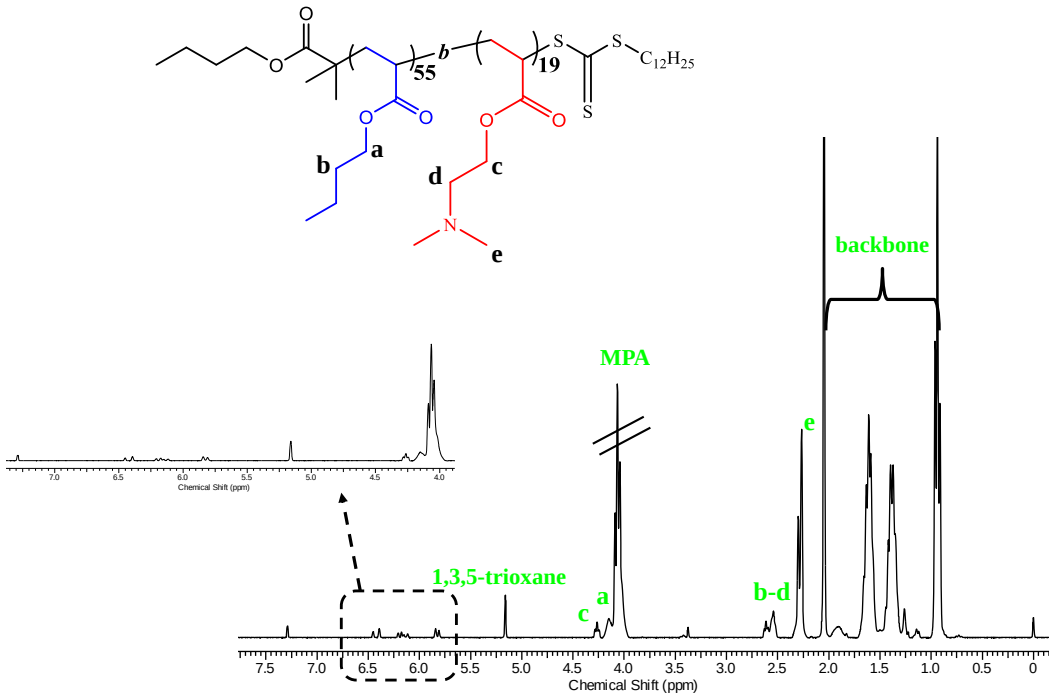

Figure 2.11: ^{1}H NMR analysis for block copolymer of poly(*n*BA)$_{55}$ macroinitiator and addition of DMAEA (19 equiv.) using BMDPT RAFT agent in MPA solvent. Initial conditions: [*n*BA] : [BMDPT]: [V601] = [55]: [1] : [10] in $CHCl_3$ and 1,3,5-trioxane as internal reference

All these amphiphilic acrylate diblock copolymers were used to disperse a carbon black pigment and to study the effect of polymer chain length on the dispersion process. DMAEA monomer is used in several applications due to the presence of the tertiary amine which can be easily quaternized, however, in the presence of water or more polar solvents, (poly)DMAEA can rapidly hydrolyse forming a carboxylic acid by-product.[25,28,25]

Therefore, in order prevent any side product formation, a methacrylate monomer bearing a tertiary amine, ensuring similar pigment surface affinity, was used.

Consequently, DMAEMA monomer was used to substitute DMAEA in the design of the amphiphilic diblock copolymer. All the details regarding methacrylate polymerisation with BMDPT are described in **Chapter 3**.

2.2.3.3. Poly(*n*-BA)-*block*-poly(DMAEMA) with BMDPT RAFT agent

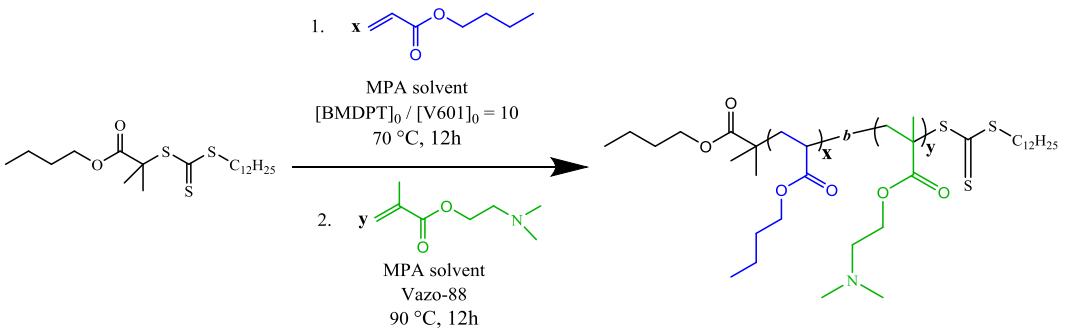

Scheme 2.6: General scheme of poly (*n*BA)-*block*-poly(DMAEMA) copolymer using BMDPT RAFT agent and V601 as azoinitator in MPA solvent at 70 ˚C for poly(*n*BA) macroCTA and 90 ˚C for the chain extension with DMAEMA using Vazo-88 initiator

Synthesis of the diblock copolymer was performed in MPA solvent at 70 ˚C, then chain extended by the DMAEMA monomer in a mixture with Vazo-88 as the initiator and heated to 90 ˚C (**Scheme 2.6)**. The poly(DMAEMA) propagating radical generated will add to poly(*n*butyl acrylate) macroRAFT agent. An intermediate radical is created and will fragment either towards the starting material or form a new propagating radical depending on the stability of the radical it will generate.

The presence of poly(*n*butyl acrylate) in a SEC chromatogram after the chain extension suggests that the macroCTA is not fully reinitiate. The small shift at high molar and the presence of the shoulder can be attributed to the formation of

poly(DMAEMA) homopolymer and poly(*n*BA)$_{55}$-*b*-poly(DMAEMA)$_{19}$ respectively (**Figure 2.12**).

Based on RAFT theory, the fragmentation would happen predominantly on the side that would leave a more stable radical. Under these conditions, predominantly a homopolymer of DMAEMA would be created and not the diblock copolymer expected.

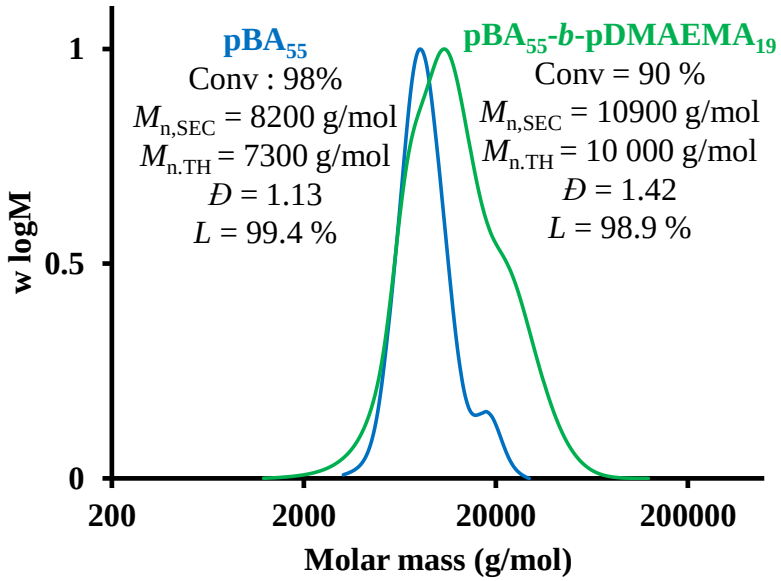

Figure 2.12: Comparison of SEC-THF chromatograms of block *n*BA/DMAEMA copolymers with DP of 55/19 synthesised in presence of BMDPT RAFT agent with $[monomer]_0$ = 3 M, $[BMDPT]_0$ / $[V601]_0$ = 10 at 70 ˚C and chain extension at 90 ˚C

In controlled radical polymerisation, the monomer bearing the most stable radical must be polymerised in the first step in order to prepare a well-defined diblock copolymer. Consequently based on this theory, the synthesis of the diblock was undertaken by polymerising DMAEMA first followed by the addition of *n*BA.

2.2.3.4. Poly(DMAEMA)-*block*-poly(*n*BA)with BMDPT RAFT agent

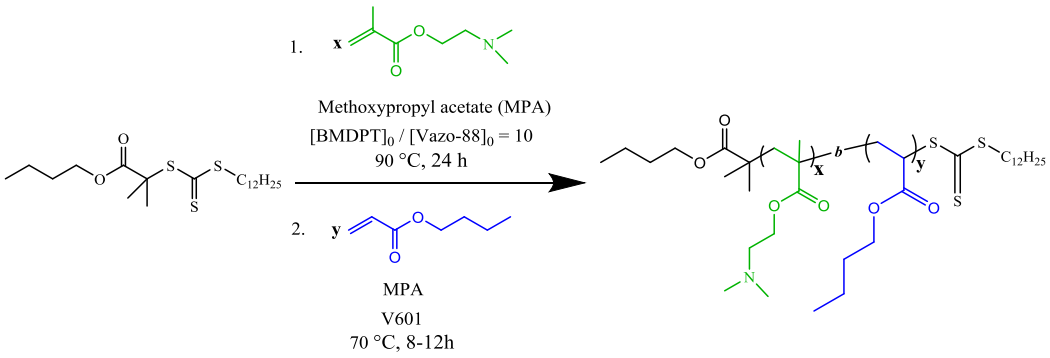

Scheme 2.7: General scheme of poly(DMAEMA)-*block*-poly(*n*BA) copolymer in MPA solvent using BMDPT RAFT agent and Vazo-88/V601 as azoinitators at 90 ˚C and 70 ˚C respectively

The design of the new amphiphilic block copolymer was performed in the exact same conditions as those previously established for DMAEMA and *n*BA polymerisation. The same degree of polymerisation was targeted for the acrylate block copolymer (see 2.2.4.2). As a starting point, the homopolymer DMAEMA was synthesised by targeting a DP of 19 and followed by the addition of *n*BA with a DP of 35. **Figure 2.13 A** shows the molecular weight distribution obtained by the refractive index (RI) and the ultraviolet-visible (UV/Vis, set up at λ = 309 nm since it is the trithiocarbonate wavelenght absorption) detectors (dashed line for the homopolymer and diblock copolymer).

The RI trace of $p(DMAEMA)_{19}$ shows a monomodal and symmetrical peak at 14 minutes and a presence of two small peaks at 18 and 19 minutes, respectively. Interestingly, the UV trace exhibit a broad peak with a presence of a tail for $p(DMAEMA)_{19}$, meaning that the first block is not well-defined, and lead to a poor control over polymerisation, which correlates with the significant difference between the theoretical and experimental molar mass.

It is worth noticing that the similar two small peaks observed at low molar masses by RI are also detected by UV/Vis suggesting that the BMDPT RAFT agent is not fully consumed despite the fact that a quantitative monomer conversion is reached (98 %). The chain extension with *n*BA was also attempted to prepare the block copolymer. A bimodal distribution is obtained for the diblock copolymer with one shoulder at 13 minutes suggesting the formation of the diblock copolymer and a second peak observed at 15 minutes corresponding to the formation of p(*n*BA) homopolymer after reaction of *n*BA with the free CTA. The small proportion of diblock copolymer suggests a poor reinition of the first block. At the end of the polymerisation the presence of unconsumed CTA is significant which indicates a weak addition of the propagating radical to the chain transfer agent ($C_{tr} < 1$). Finally, the values of theoretical, experimental molar mass and the large molar mass distribution ($Đ \approx 1.48$) confirm the poor control of methacrylate polymerisation in presence of BMDPT RAFT agent.

To remain consistent with the previous study and in order to compare these methacrylate/acrylate diblock copolymers with acrylate block copolymers for pigment dispersion, diblock copolymers of DMAEMA/BA (35/70 and 50/100) were also synthesised. Since the degree of polymerisation is related to the monomer and CTA concentration ($DP = [M]_0 / [CTA]_0$), it is interesting to investigate the effect of the CTA consumption when a high DP is targeted.

Figure 2.13 B and Figure 2.13 C show the SEC DRI and UV detector signals of p(DMAEMA)$_{35}$-*block*-p(*n*BA)$_{70}$ and p(DMAEMA)$_{50}$-*block*-p(*n*BA)$_{100}$, respectively. Increasing the DP of pDMAEMA does not seems to improve the consumption of the CTA

as the presence of the RAFT agent is clearly observable in both SEC chromatograms. In **Figure 2.13 B** the chromatogram of p(DMAEMA)$_{35}$ exhibits the same response with a broad signal around 14 minutes corresponding to the polymer bearing a trithiocarbonate and a sharp signal at 18 minutes belonging to non-consumed RAFT agent. No chain extension is observed after addition of *n*BA, but a peak corresponding to the formation of *n*BA homopolymer is observed eluting at 15 minutes.

Figure 2.13 C shows the exact results even if the CTA concentration is lower, the low consumption of this latter leads a poor control of the polymerisation over the molar mass distribution, a high dispersity ($Đ$ > 1.2) and only a few proportion of diblock copolymer formed.

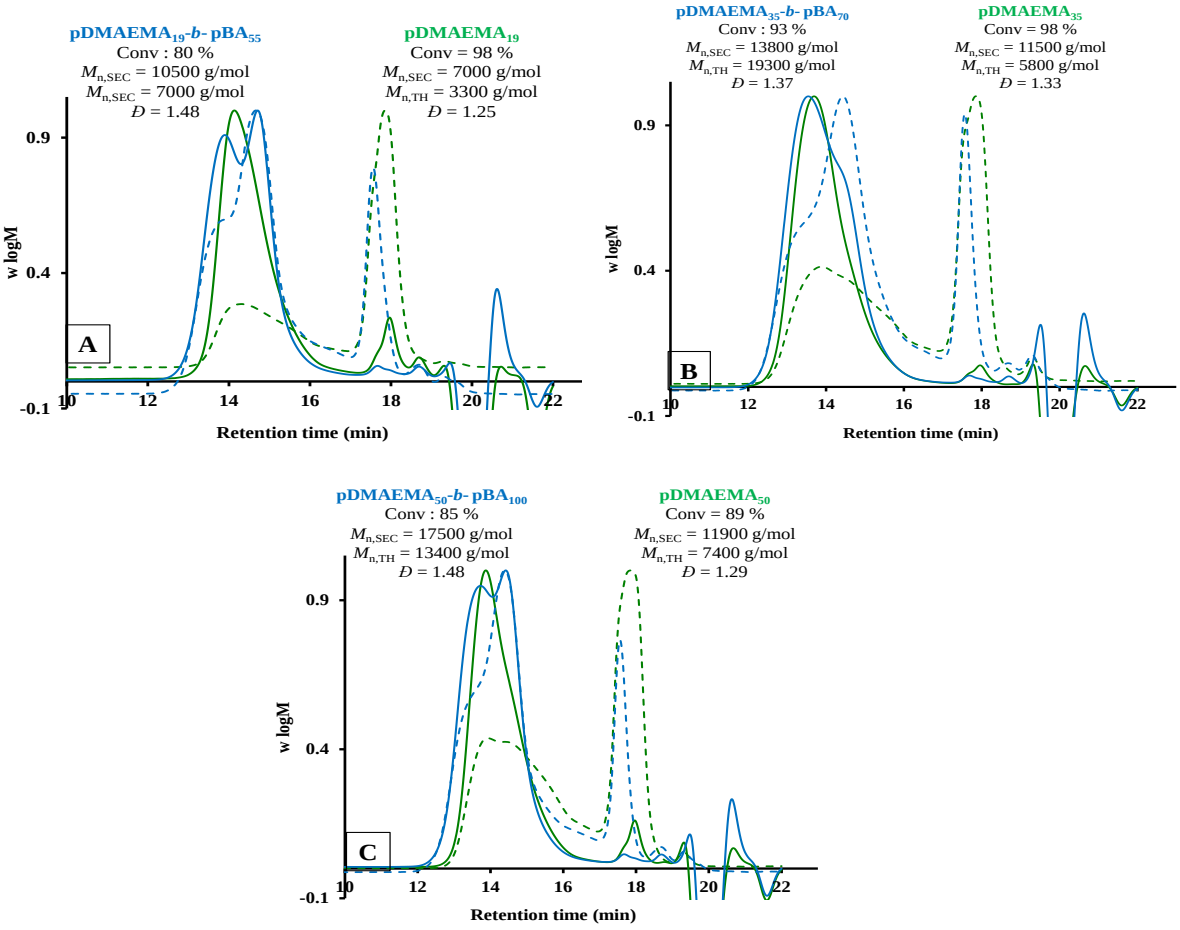

Figure 2.13: Comparison of RI (plain) and UV (λ = 309 nm in dash) SEC-THF chromatograms of block DMAEMA/*n*BA copolymers with DP of 55/19 (**A**); 70/35 (**B**) and 100/50 (**C**) respectively synthesised in presence of BMDPT RAFT agent with $[monomer]_0$ = 3 M, $[BMDPT]_0 / [V601]_0 = 10$ at 90 ˚C for the macroinitiator and 70 ˚C for the chain extension

As previously discussed, the reactivity of the RAFT agent, being strongly linked to the effect of the R and Z substituents, has been heavily studied in the literature.[29,30,31] This study shows that the methacrylate monomers are not compatible with BMDPT, as the trithiocarbonate is not activated enough to trigger methacrylic radical addition, and the R group (dimethyl) is not a good leaving group, leading to a poor control over the molecular weight.

An extensive investigation of methacrylate polymerisation with the Lubrizol RAFT agent (BMDPT) is reported in **Chapter 3**. As such, a second attempt to synthesis methacrylate and acrylate diblock copolymers was explored by using the RAFT agent MCTP bearing a –CN group, a better leaving group R, thus offering a better control over methacrylate polymerisation. Note that the Z group of MCTP ($C_{12}H_{25}$) is kept the same as that of BMDPT, thsu enabling to investigate the effect of the R group only.

2.2.3.5. Poly(DMAEMA)-*block*-poly(*n*BA) using MCTP RAFT agent

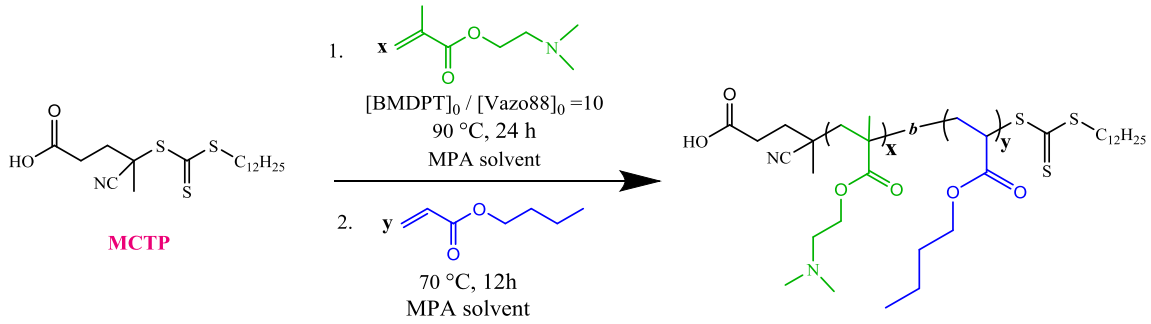

Scheme 2.8: General scheme of poly(DMAEMA)-*block*-poly(*n*BA) copolymer synthesised using MCTP RAFT agent and Vazo-88/V601 as azoinitators in MPA solvent

Methacrylates are a challenging family of monomers to polymerise *via* RAFT due to the steric hindrance of the tertiary propagating radicals. A relatively high transfer constant, dependant on the R group, is required to achieve a successful polymerisation. In an attempt to optimise the conditions, MCTP was used as RAFT agent for DMAEMA polymerisation. As described in the literature, the most efficient R groups for methacrylate polymerisations contain nitrile (-CN) and phenyl (-Ph) moieties, due to their bulkiness and capability to stabilize the radical.[32,33,34] Consequently, the synthesis of the diblock poly(DMAEMA) - *block*- poly(*n*BA) mediated by MCTP was performed under similar conditions as those used for BMDPT mediated polymerisations (**Scheme 2.8**) and the same DPs were targeted for each block. A SEC triple detection with a UV/Vis set at 309 nm was also used to study the polymerisation. In the **Figure 2.14 A**, a monomodale and symmetrical molar mass distribution with $M_{n,SEC}$ close to $M_{n,TH}$ and narrow MWD ($Đ \approx 1.12$) are obtained at high monomer conversion for p(DMAEMA)$_{19}$.

Despite the well-defined homopolymer, also confirmed by the UV/Vis trace, suggesting that a high percentage of polymeric chains are living, some unconsumed CTA remains. Subsequently, a chain extension was performed by adding *n*BA monomer to the polymeric mixture. The success of the chain extension was confirmed by the SEC trace which clearly shows a shift at low retention time for the diblock copolymer. However, a tail and small shoulder overlapping with p(DMAEMA)$_{19}$ were observed, and could be attributed the poor reinitiation of pDMAEMA.. The relative value obtained for the experimental and theoretical molar mass is overestimated for the second block as PMMA is used as calibration standard.

Two other diblock p(DMAEMA) - *block*- p(*n*BA) copolymers with DPs of 35/70 and 50/100 were synthesised following the same protocol. **Figure 2.14 B** and **Figure 2.14 C** exhibit a similarly shaped chromatogram with a well-controlled homopolymer DMAEMA with a narrow molar mass distribution but also an increase of the shoulder when the DP of *n*BA increased after the chain extension suggesting that pDMAEMA is not entirely chain extended.

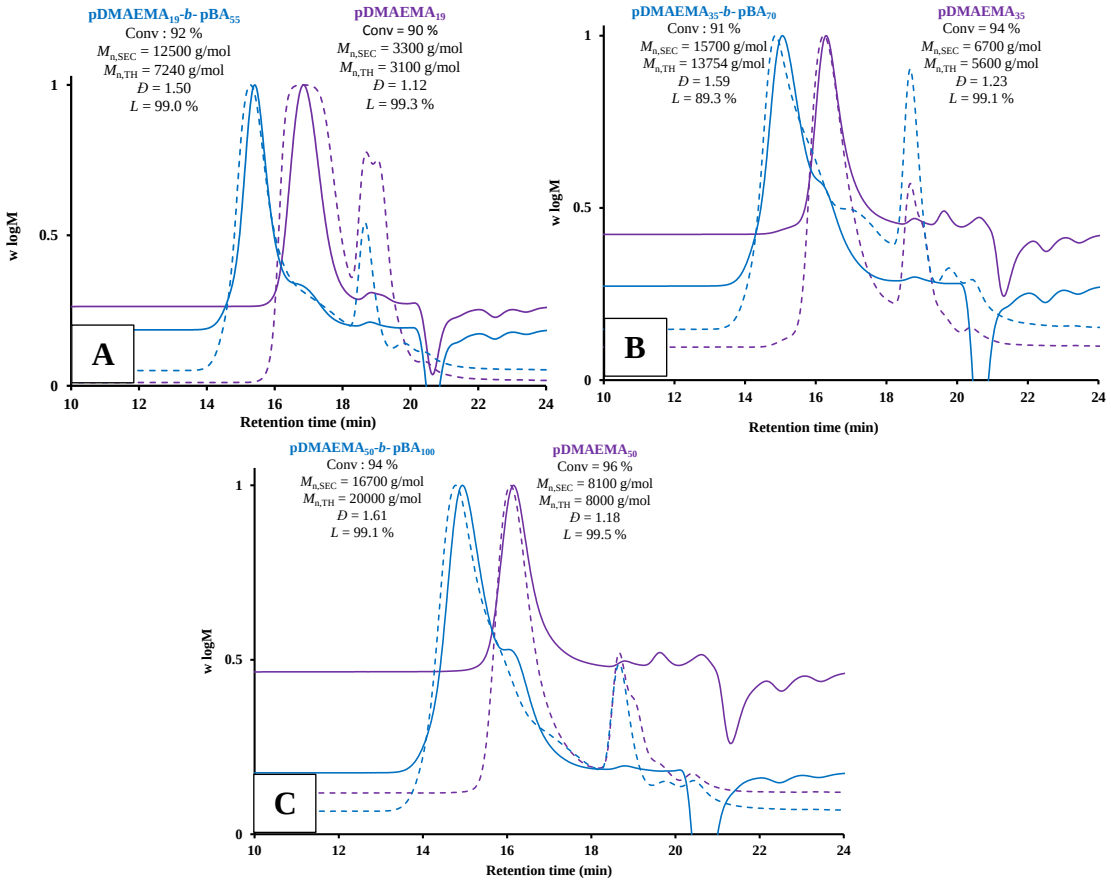

Figure 2.14: Comparison of SEC-THF chromatograms of block DMAEMA/*n*BA copolymers with DP of 55/19 (**A**); 70/35 (**B**) and 100/50 (**C**) respectively synthesised in presence of MCTP RAFT agent with $[monomer]_0$ = 3 M, $[MCTP]_0$ / $[I]_0$ = 10 at 90 ˚C for the macroinitiator and 70 ˚C for the chain extension prepared in MPA solvent

One of the parameter which can affect polymerisation is the choice of solvent. The nature of the solvent in RAFT polymerisation has been discussed in several studies.[35,36,37] Benaglia *et al*. have investigated the polymerisation of MMA in benzene, DMF and acetonitrile using 2-cyanopropyl-2-yl 4-pyridiniumdithiocarboxate 4-toluenesulfonate salt with AIBN as azoinitiator.[33] A good control is obtained in acetonitrile and DMF after 2 and 4 h of polymerisation. The SEC chromatograms are broad after 16 h suggesting that a potential transfer between the polymeric chain and the solvent occurs.

A poor control is obtained in benzene solvent explained by a low solubility of this CTA in the solvent and a low propagation rate constant (k_p). As such, the same diblock copolymer was synthesised using dioxane in order to prevent any chain transfer reaction between the solvent and polymer backbone. **Figure 2.15** shows the RI and UV SEC chromatograms of p(DMAEMA)-*block*-p(*n*BA) with DPs targeted of 19/55; 35/70; 50/100 respectively. **Figure 2.15 A**, a good control of $p(DMAEMA)_{19}$ in dioxane solvent is achieved with a narrow molar mass distribution ($Đ$ = 1.17) in a quantitative monomer conversion. The chain extension with *n*BA give a shift at a low retention time and a similar shoulder is present possibly corresponding to the poor reinitiation of pDMAEMA. In **Figure 2.15 B**, a comparable SEC traces are obtained with a good control over the molar mass for the homopolymer ($Đ$ < 1.2) and an increase of the dispersity after the chain extension with $p(nBA)_{70}$ is obtained due to the bimodality. **Figure 2.15 C** exhibit a similar control for the first block but a poor control for the second block as shown the RI and UV traces of the diblock copolymer. As noticed in **Figures 2.13** and **2.14**, some uncomsumed CTA remains after each block polymerisation.

Similarly to this work, Pietsch *et al.*[38] have polymerised a library of poly(DMAEMA)-*block*-poly(DEGMA) copolymers with the MCTP RAFT agent in DMF, using an automated parallel synthesizer. All the polymerisations were stopped at 10 hours to retain high RAFT end-group functionality, and the diblock copolymers were analysed in different SEC solvents, including DMF, DMAc (dimethyl acetamide) and $CHCl_3$ (chloroform). Interestingly, good control for most block copolymers was reported ($Đ$ < 1.23), however, a tail and shoulder can be observed in $CHCl_3$.

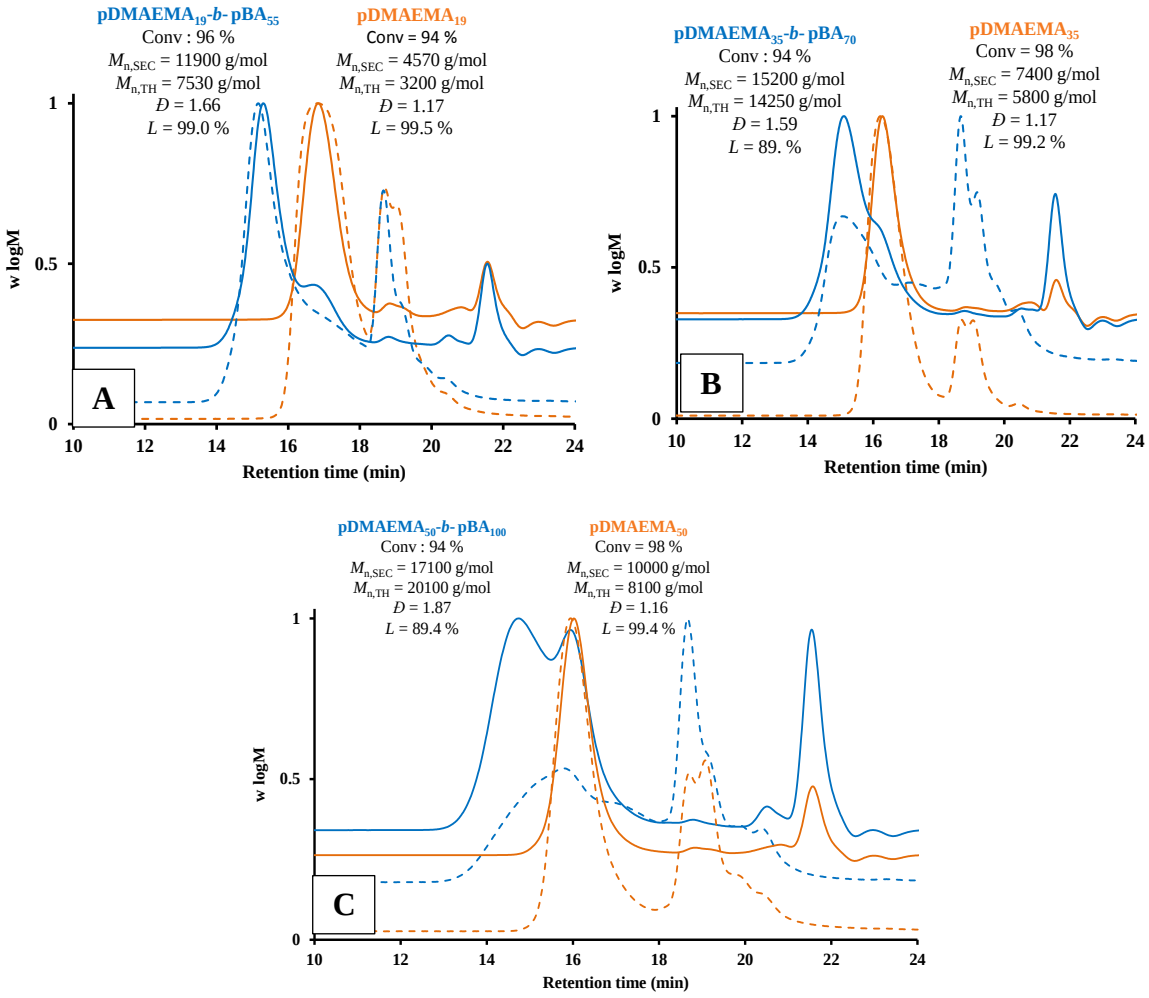

Figure 2.15: Comparison of SEC-THF chromatograms of block DMAEMA/*n*BA copolymers with DPs of 55/19 (**A**); 70/35 (**B**) and 100/50 (**C**) respectively synthesised in presence of MCTP RAFT agent with $[monomer]_0$ = 3 M, $[MCTP]_0$ / $[I]_0$ = 10 at 90 ˚C for the macroinitiator and 70 ˚C for the chain extension prepared dioxane solvent

2.3. Conclusion

In this chapter, the synthesis of acrylate poly(*n*-butyl acrylate)-*block*-poly(DMAEA) diblock copolymers *via* RAFT using the BMDPT RAFT agent is presented. Various polymer chain lengths (DP ~ 19/35; 35/70; 50/100) were successfully synthesised with a quantitative monomer conversion (> 90 %) and narrow molar distribution ($Đ$ < 1.25). The high probability of DMAEA to hydrolyse the polymer releasing a carboxylic acid can potentially affect carbon black dispersion. Consequently, DMAEMA was used as a substitute for DMAEA. Under the optimised conditions, a range of poly(DMAEMA)-*block*-poly(*n*BA) copolymers were synthesised, leading to a bimodal distribution after chain extension, explained by the poor leaving R group of the BMDPT RAFT agent. Alternatively, MCTP, bearing a better leaving R group, was used to obtain a well-defined diblock copolymers. As expected, a shift to high molar mass was recorded after the chain extension with *n*BA, however, some poly(DMAEMA) homopolymer was not chain extended. Finally, a potential interaction between the solvent and the polymer backbone was investigated by performing the same polymerisation in dioxane. However, no improvement was noticed suggesting that polymerisation in methoxypropyl acetate did not affect the RAFT mechanism.

2.4. Experimental

2.4.1. Materials

Butyl acrylate (BA, 99 %), 2-(Dimethylamino)ethyl acrylate (DMAEA, 98 %), and 2-(Dimethylamino)ethyl methacrylate (DMAEMA, 98 %) were purchased from

Sigma Aldrich. Butyl acetate (Chromasolv plus, 99.7 %), propylene glycol monoethyl ether acetate (Sigma-Aldrich, 99.5 %), Dimethyl2,2'-azobis(2-methylpropionate) (V601, Wako) Azobis(cyclohexanecarbonitrile) (Vazo-88, 98 %, Aldrich) were used as purchased. Butyl-2-methyl-2-[(dodecylsulfanylthiocarbonyl) sulfanyl] propionate (BMDPT, Lubrizol, 70 %) was provided by Lubrizol. 1,1'-Methyl-4-cyano-4-(dodecylthiocarbonothioylthio)pentanoate (MCTP, Boron molecular, > 99 %) was obtained from CSIRO and 2-(((butylthio)-carbonothioyl)propanoic acid (PABTC) as synthesised in the laboratory based on the Ferguson paper.[39] Bromo-propionic acid (> 99 %), 1-butanediol (99 %) and carbon disulfide (> 99%) were purchased from Sigma Aldrich .

2.4.2. Methods

- **Nuclear Magnetic Resonance**

NMR (^{1}H and ^{13}C) were recorded on a Bruker AV-300 and DPX-500 in deuterated chloroform ($CDCl_3$) or DMSO-d_6. Chemical shift values (δ) are reported in ppm.

The residual proton signal of the solvent is used as internal standard ($CDCl_3$, δ = 7.26 or δ = 2.5 for DMSO-d_6). The use of 1,3,5-trioxane is also used in a few ^{1}H NMR characterisation and mentioned in the spectra.

➢ Determination of $DP_{n,targeted}$ and monomer conversion

Monomer conversion (p) were calculated from ^{1}H NMR data using **equation 2.2:**

$$p = \frac{[M]_0 - [M]_t}{[M]_0} = 1 - \frac{[M]_t}{[M]_0} = 1 - \frac{\frac{\int I_{5.5-6.75\ ppm}}{\int I_a}}{DP_{n,targeted}}$$

Where $[M]_0$ and $[M]_t$ are the concentrations of the monomer at time 0 and at time t, respectively, $\frac{\int I_{5.5-6.75\ ppm}}{\int I_a}$ is the integral for the vinyl protons of the monomer, $DP_{n,targeted}$ is the number average degree of polymerisation targeted and $\int I_a$ is the integral of the two protons belonging to the CH_2 of the acrylate (-O-**CH_2**-CH_2).

➢ Determination of $M_{n,TH}$

The theoretical number-average molar mass ($M_{n,TH}$) is calculated using **equation 2.3**:

$$M_{n,TH} = \frac{[M]_0 p [M]_M}{[CTA]_0} + M_{CTA}$$

Where $[M]_0$ and $[CTA]_0$ correspond to the initial concentrations (in mol/L) of monomer and chain transfer agent respectively; p is the monomer conversion as determined by equation 1, M_M and M_{CTA} are the molar masses (g/mol) of the monomer and chain transfer agent.

➢ Example of determination of livingness (**eq 2.1**)

<u>Polymerisation of p(nBA)$_{55}$:</u>

-DP = 55, $[n\text{BA}]_0$ = 3M, $[CTA]_0$ / $[Initiator]_0$ = 10, time = 8 h, T = 70 ˚C.

-m_{BA} = 0.5 g, $[Initiator]_0$ = 0.005 M, $[CTA]_0$ = 0.055 M, f = 0.5, $k_{d(V601\ at\ 70\ ^\circ C)}$ = 3.30 x $10^{\wedge -5}$ s^{-1}, f_c = 1

$$L = \frac{[CTA]_0}{[CTA]_0 + 2.f.[I]_0.\left(1-e^{-kdt}\right).\left(1-\frac{fc}{2}\right)}$$

$$L = \frac{0.055}{0.055 + 2*0.5*0.005.\left(1-e^{-\left(3.30\ x\ 10^{-5}\right)*(8*60*60)}\right).\left(1-\frac{1}{2}\right)} = 97.2\ \%$$

- Size Exclusion Chromatography (SEC)

Number-average molar masses ($M_{n,SEC}$) and dispersity values ($Đ$) distributions were measured using size exclusion chromatography with THF as an eluent. The THF Agilent 390-LC MDS instrument was equipped with differential refractive index (DRI), viscometry (VS), dual angle light scatter (LS) and two wavelength UV detectors. The system was equipped with 2 x PolarGel Mixed C columns (300 x 7.5 mm) and a PLgel 5 µm guard column. The eluent is THF with 2 % TEA(triethyl amine) and 0.01 wt./ V% BHT (butylated hydroxytoluene) additives. Samples were run at 1 mL/min at 30 °C. Poly(methyl methacrylate) standards in rang of 2.0 x 10^2 g/mol to 2.0 x 10^6 g/mol was used to calibrate SEC system.. Analyte samples were filtered through a polytetrafluoethylene (PTFE) membrane with 0.22 μm pore size before injection. The calibration is setup by using a flow rate marker with a polynomial order of 3.

Respectively, experimental molar mass ($M_{n,SEC}$) and dispersity ($Đ$) values of synthesized polymers were determined by conventional calibration using Agilent GPC/SEC software.

2.4.3. General synthetic procedures

- Synthesis of (propanoic acid)yl butyl trithiocarbonate (PABTC)

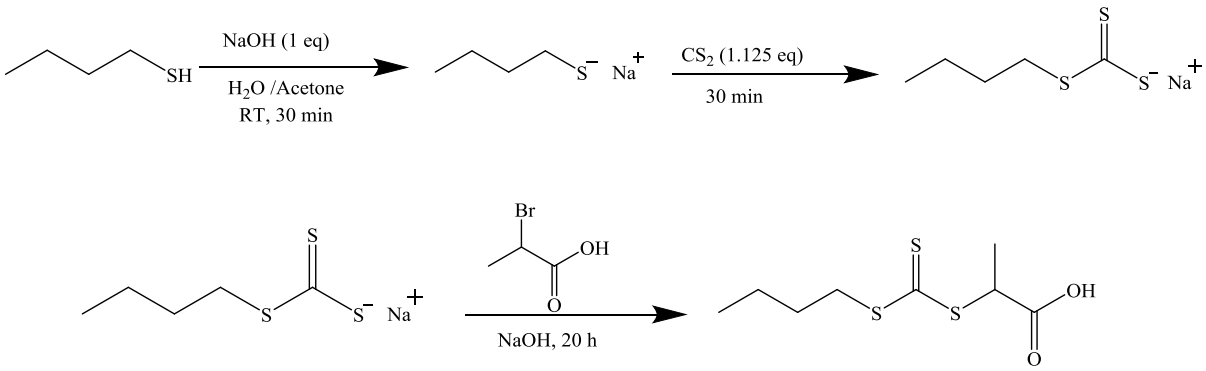

Scheme 2.9: Synthetic route of (propanoic acid)yl butyl trithiocarbonate PABTC RAFT agent

A solution of 50 w/w % of sodium hydroxide (3.9 g, 1.1 eq, 97.5 mmol) is mixed with butanethiol (8 g, 1.0 eq, 88.7 mmol) and water. Then, acetone (3.2 mL) is added and the clear solution is stirred for 30 minutes at room temperature. An orange solution is obtained after addition of carbon disulfide (6.92 g, 1.025 eq, 90.92 mmol). The mixture is stirred for 30 minutes and cooled by using dry ice bath. The following step is the slow addition of 2-bromopropionic acid (13.90 g, 1.025 eq, 90.92 mmol), keeping the temperature below 10 ˚C and a solution of NaOH (4.5 g of water, 2.25 g NaOH, and 57 mmol) is slowly added. A certain volume of water (23 mL) is mixed with the solution and the reaction is left to stir at room temperature for 20 hours.

Finally, cooled water is added and a solution of HCl (10 M) is added dropwise until a pH of 3 is reached. ^{1}H NMR($CDCl_3$, 300 MHz, pm): δ = 4.88 (q, 1H, C***H***(CH_3)), 3.39 (t, 2H , S-**CH_2**-CH_2), 1.70 (m, 2H, S-CH_2-CH_2-**CH_2**), 1.64 (d, 3H, CH(**CH_3**)), 1.44 (m, 2H, CH_2-**CH_2**-CH_3), 0.94 (t, 3H, CH_2-**CH_3**). ^{13}C-NMR ($CDCl_3$, 125 MHz, ppm): δ =221.5, 177.5, 47.5, 37.0, 29.8, 22.0, 16.5, 13.5. MS (ESI): *[M+H]+* calculated: 261.0, found: 260.9. *IR*: 2951, 2926, 28, 1701,1450,1420,1309 cm^{-1}.

The orange solid is collected and purified *via* recrystallization in hexane. Shiny yellow crystals are obtained with a yield of 49.1 % (11.2 g, 45.1 mmol). Melting point found: 52.4 ˚C

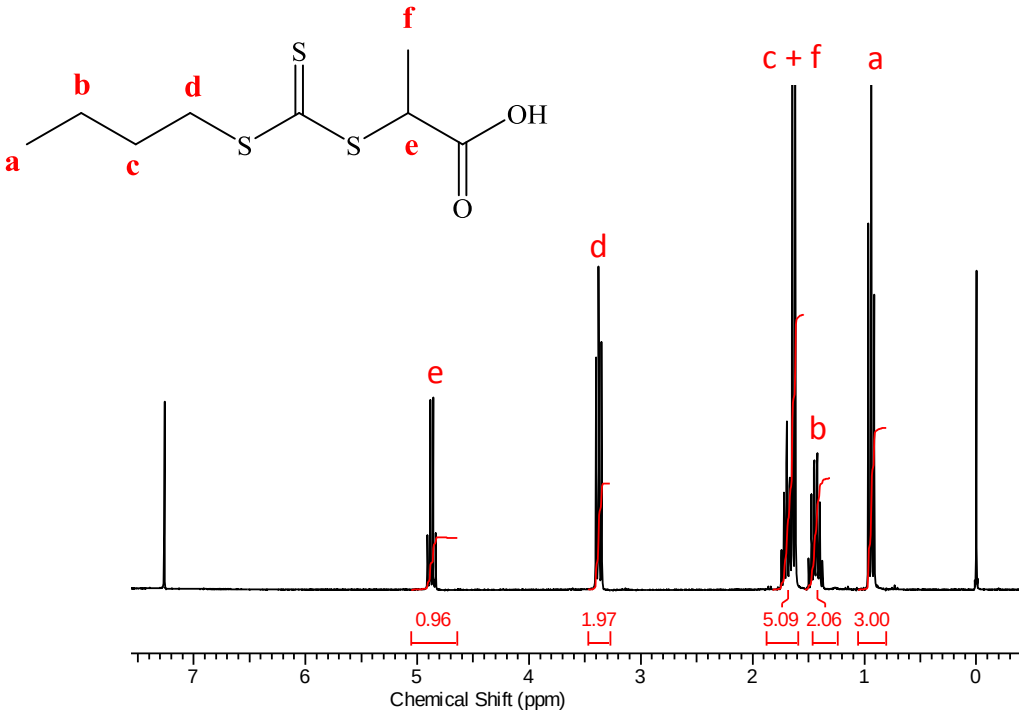

Figure 2.16: ^{1}H NMR analysis of PABTC after purification in hexane recorded on a Bruker DPX-300 in $CDCl_3$

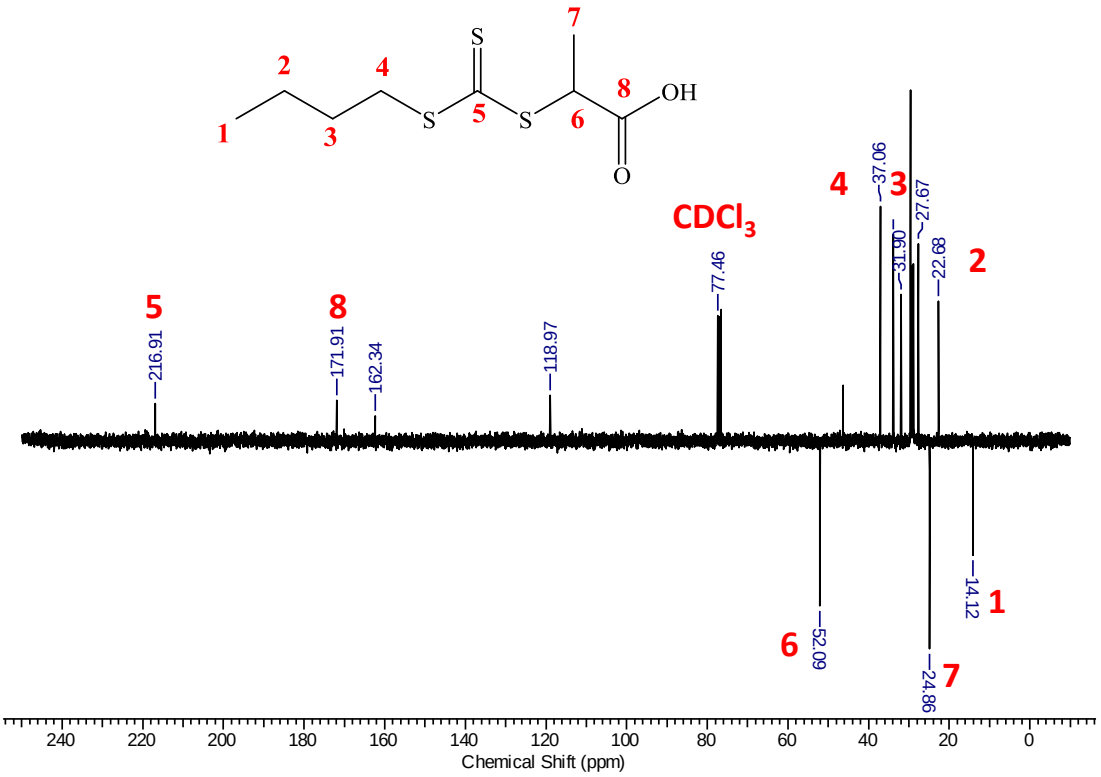

Figure 2.17: ^{13}C NMR analysis of PABTC after purification recorded on a Bruker DPX-400 in $CDCl_3$

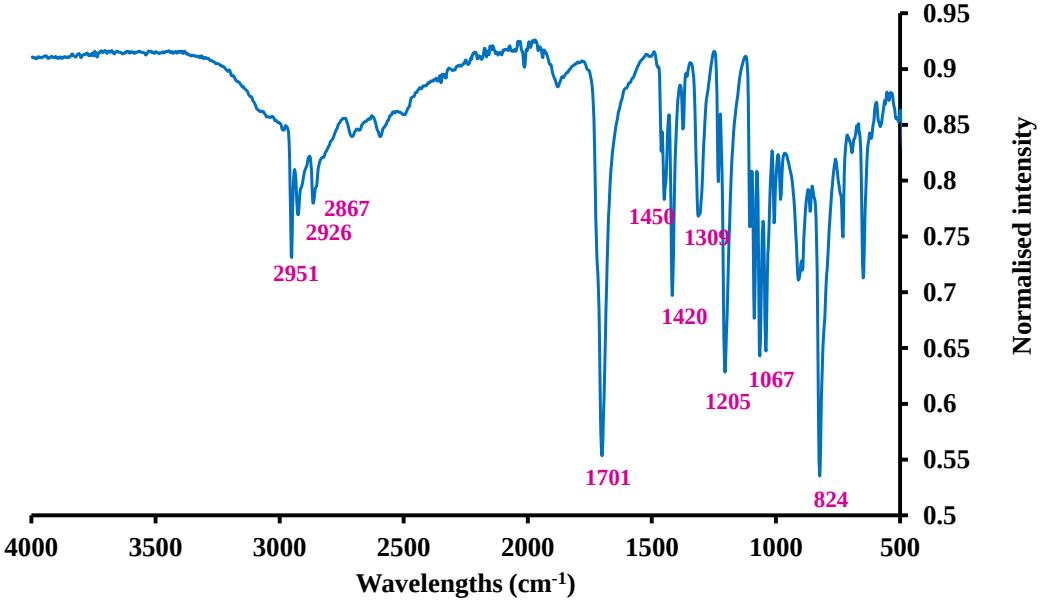

Figure 2.18: IR spectra of PABTC RAFT agent after purification in hexane

IR spectra shows some main characteristics peaks of PABTC RAFT agent. The finger print region (500 -1500 cm^{-1}) contains a series of absorptions which can makes the determination of the present peaks complicated. All the bands observed at 1420 – 1450 cm^{-1} and between 700 – 1000 cm^{-1} are attributed to the C-H of the methyl group. The stretched bond present at 1701 cm^{-1} belongs to the carbonyl group of the carboxylic group. The weak broad band observed between 2700 – 3200 cm-1 frequency region the O-H bond. The presence of the weak band in 2550 – 2620 cm^{-1} correspond to thiol (S-H) used as reactant to synthesised PABTC RAFT agent.

- General procedure for preparation of *n*-butyl acrylate homopolymer

  - **Synthesis of *n*butyl acrylate: p(*n*BA)**

For a typical polymerisation in which [nBA]: [BMDPT] : [I] = 55: 1: 0.1, *n*-BA (55 eq, 0.5 g, 3.9 mmol), BMDPT (1.0 eq, 0.0327 g, 7.8 x 10^{-2} mmol), V601 (3.9 x 10^{-3} mmol, 45 µL (stock solution of 20 mg/ml)) and methoxypropyl acetate (0.800 ml) are introduced into a vial equipped with a magnetic stirrer and sealed with a septum The reaction mixture is degassed using nitrogen for 10 min and then left in an oil bath at 70 ˚C (90 ˚C). The percentage of the impurities of BMDPT RAFT agent is not taking into account for the mass of CTA used. $M_{n,SEC}$ = 8430 g/mol , $Đ$ = 1.16 (THF-SEC, triple detection).

^{1}H NMR spectrum (300 MHz,DMSO-d_6, δ ppm): 4,21 (m, 2H,-C(O)O-C**H$_2$**-CH_2-CH_2-CH_3), 2.55 (m, 2H, -C(O)O-CH_2-C**H$_2$**-CH_2- CH_3), 1.92 (m, 2H, -C(O)O-CH_2-CH_2-C**H$_2$**-CH_3), 1.1 (m, 3H, -C(O)O-CH_2-CH_2-CH_2- **CH_3**), 2.0 - 0.95 (m, backbone).

➢ Synthesis of homopolymer DMAEA : pDMAEA

For a typical polymerisation in which [DMAEA]: [BMDPT] : [I] = 19: 1: 0.1, DMAEMA (19 eq, 0.5 g, 3.3 mmol), BMDPT (1.0 eq, 0.070 g, 0.17 mmol), V601 (1.77 x 10^{-3} mmol, 203 µL (stock solution of 20 mg/ml)) and methoxypropyl acetate (0.360 ml) are introduced into a vial equipped with a magnetic stirrer and sealed with a septum The reaction mixture is degassed using nitrogen for 10 min and then left in an oil bath at 90 ˚C. $M_{n,SEC}$ = 4700 g/mol , $Đ$ = 1.23 (THF-SEC, triple detection). ^{1}H NMR spectrum (300 MHz,DMSO-d_6, δ ppm): 4,17 (m, 2H,-C(O)O-C**H$_2$**-CH_2-NMe_2), 2.60 (m, 2H, -C(O)O-CH_2-C**H$_2$**-NMe_2), 2.27 (-CH_2-N**Me$_2$**).

➢ Synthesis of homopolymer methacrylate pDMAEMA

For a typical polymerisation in which [DMAEMA]: [BMDPT] : [I] = 19: 1: 0.1, DMAEMA (19 eq, 0.5 g, 3.1 mmol), BMDPT (1.0 eq, 0.070 g, 0.16 mmol), Vazo-88 (1.67 x 10^{-3} mmol, 204 µL (stock solution of 20 mg/ml)) and methoxypropyl acetate (0.300 ml) are introduced into a vial equipped with a magnetic stirrer and sealed with a septum The reaction mixture is degassed using nitrogen for 10 min and then left in an oil bath at 90 ˚C. $M_{n,SEC}$ = 7000 g/mol , $Đ$ = 1.25 (THF-SEC, triple detection). ^{1}H NMR spectrum (300 MHz,DMSO-d_6, δ/ppm): 4,07 (m, 2H,-C(O)O-C**H$_2$**-CH_2-NMe_2), 2.57 (m, 2H, -C(O)O-CH_2-C**H$_2$**-NMe_2), 2.29 (s, 6H,-CH_2-N(**Me)$_2$**)

Table 2.1: Characterisation data for the homopolymerisatrion of of *n*BA (targeted DP_n of 55). RAFT polymerisations were conducted over 10 h in butyl acetate (or MPA) at 70 ˚C using MCTP, PABTC and BMDPT RAFT agents with $[nBA]_0$ = 3 M and $[CTA]_0$ / $[V601]_0$ = 10

Entry	**RAFT agent**	**Conv** (%)	$M_{n,TH}$[a] (g/mol)	$M_{n,SEC}$[b] (g/mol)	$Đ$
1	MCTP	96	5770	8300	1.14
2	PABTC	97	6000	8400	1.22
3	BMDPT	93	7000	10000	1.16

[a] Determined using **equation 2.3** (experimental section)

[b] Determined using THF-SEC with PMMA narrow standards

Table 2.2: Characterisation data for the homopolymerisatrion of of *n*BA (targeted DP_n of 50). RAFT polymerisations were conducted over 10 h in acetate solvent at 70 ˚C with $[BMDPT]_0$ / $[V601]_0$ = 10

***n*BA**	**Conv (%)**	$M_{n,SEC}$[a] **(g/mol)**	$Đ$	**Solvent**
2	83	7800	1.19	Butyl acetate
3	96	8300	1.1	Butyl acetate
4	98	8700	1.13	Butyl acetate
2	92	9000	1.19	MPA
3	96	8700	1.1	MPA
4	95	8300	1.1	MPA

[a] Determined using THF-SEC with PMMA narrow standards

Table 2.3: Characterisation for the homopolymerisatrion of *n*BA (targeted DP_n of 55). RAFT polymerisations in butyl acetate solvent performed at 60 ˚C, 70 ˚C and 90 ˚C using $[BMDPT]_0$ / $[Initiator]_0$ = 10. V601 and Vazo-88 were used at initiator at 60 - 70 ˚C and 90 ˚C respectively.

Entry	**T** (˚C)	**Time** (hour)	**Conv** (%)	$M_{n,TH}$[a] (g/mol)	$M_{n,SEC}$[b] (g/mol)	$Đ$
1	60	20	83	7300	5800	1.05
2	70	10	95	7300	6700	1.06
3	90	10	97	7300	7000	1.31

[a] Determined using **equation 2.3** (experimental section)

[b] Determined using THF-SEC with PMMA narrow standards

➢ General procedure for preparation of statistical copolymer

➢ **Synthesis of statistical copolymer p(*n*BA_{55} – *stat*- DMAEA)$_{19}$**

For a typical synthesis of statistical copolymer in which [*n*BA]: [DMAEA]: [BMDPT]: [I] = 55: 19: 1: 0.1, *n*BA (55 eq, 0.5 g, 3.9 mmol), DMAEA (19 eq, 0.22 g, 14.8 mmol) was added to vial in presence of MPA (0.5 ml). Then, the vial is sealed with a septum and the reaction mixture was purged under nitrogen for 10 min and placed in thermostated an oil bath set at 70 ˚C. The quantitative monomer conversion is reached (> 99 %) was confirmed by ^{1}H NMR and the value of the experimental molecular weight was obtained by THF-SEC: $M_{n,SEC}$ = 11 750 g.mol^{-1} , $Đ$ = 1.23 (THF-SEC, triple detection). ^{1}H NMR spectrum (300 MHz,DMSO-d_6, δ/ppm): 4.49 (m, 2H,-C(O)O-C**H$_2$**-CH_2-NMe_2), 4.15 (m, 2H,-C(O)O-C**H$_2$**-CH_2-CH_2- CH_3), 2.57 (m, 2H, -C(O)O-CH_2-C**H$_2$**-NMe_2), 2.29 (s, 6H,-CH_2-N**Me$_2$**)

Due to the overlapping of the monomers peak and MPA solvent, the 1,3,5-trioxane is used at internal reference. After degassing the polymerisation, a sample is ran before and after the polymerisation. The monomer conversion is determined by using the integration of the vinyl peaks. For instance: % monomer : $(T_0 - T_{10}) / (T_0) = (5.50 - 0.67) / (5.50) = 0.87$ (87 %)

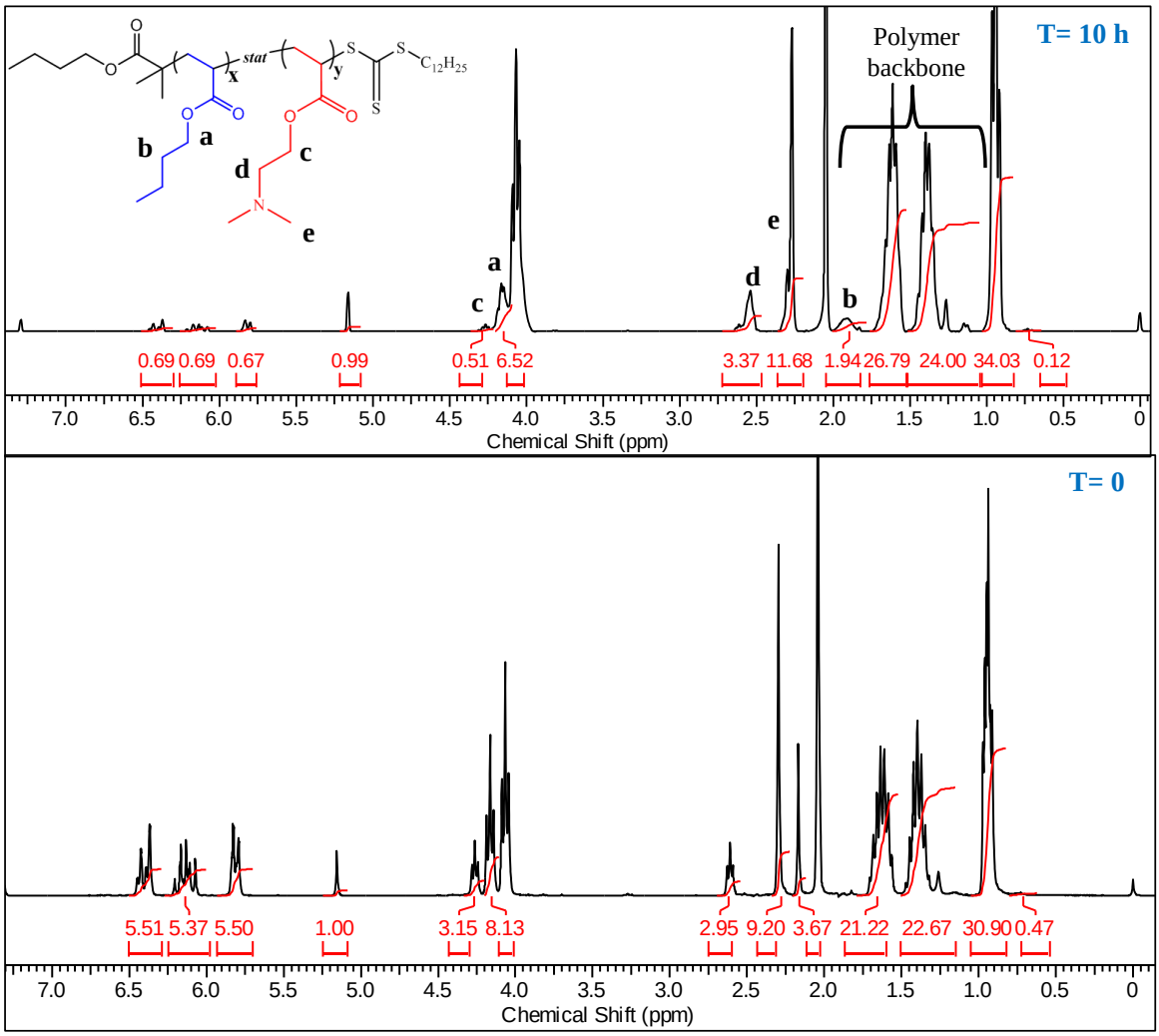

Figure 2.19: ^{1}H NMR analysis of p(DMAEMA)$_{19}$-*b*-p(*n*BA)$_{55}$ recorded on a Bruker DPX-300 in $CDCl_3$

- General procedure for preparation of subsequent block copolymers

  - **Synthesis of diblock copolymer p(DMAEMA)$_{19}$-*b*-p(*n*BA)$_{55}$**

For a typical synthesis of statistical copolymer in which [*n*BA]: [BMDPT]: [I] = 55: 19: 1: 0.1, *n*BA (55 eq, 0.5 g, 3.9 mmol), to vial in presence of MPA (0.5 ml). Then, the vial is sealed with a septum and the reaction mixture was purged under nitrogen for 10 min and placed in thermostated an oil bath set at 70 ˚C. After determination of the monomer conversion, DMAEA (19 eq, 0.22 g, 14.8 mmol) and 0.5 mL of MPA solvent are added to the macro-chain transfer agent (macro-CTA) into the polymerisation mixture. The quantitative monomer conversion is reached (> 99 %) was confirmed by ^{1}H NMR and the value of the experimental molecular weight was obtained by THF-SEC: $M_{n,SEC}$ = 10500 g.mol^{-1} , $Đ$ = 1.48 (THF-SEC, triple detection). ^{1}H NMR spectrum (300 MHz,DMSO-d_6, δ ppm): 4.49 (m, 2H,-C(O)O-C**H$_2$**-CH$_2$-NMe$_2$), 4.15 (m, 2H,-C(O)O-C**H$_2$**-CH$_2$-CH$_2$-CH$_3$), 2.57 (m, 2H, -C(O)O-CH$_2$-C**H$_2$**-NMe$_2$), 2.29 (s, 6H,-CH$_2$-N**Me$_2$**), 1.92 (m, 2H, -C(O)O-CH$_2$-CH$_2$-C**H$_2$**- CH$_3$)

2.5. References

1. Nabuurs, T.; Baijards, R. A.; German, A. L. *Progress in Organic Coatings* **1996,** *27* (1), 163-172.

2. Chiantore, O.; Trossarelli, L.; Lazzari, M. *Polymer* **2000,** *41* (5), 1657-1668.

3. Dube, M. A.; Rilling, K.; Penlidis, A. *Journal of Applied Polymer Science* **1991,** *43* (11), 2137-2145.

4. Chan-Seng, D.; Debuigne, A.; Georges, M. K. *European Polymer Journal* **2009,** *45* (1), 211-216.

5. Kohsaka, Y.; Ishihara, S.; Kitayama, T. *Macromolecular Chemistry and Physics* **2015,** *216* (14), 1534-1539.

6. Ishizone, T.; Yoshimura, K.; Hirao, A.; Nakahama, S. *Macromolecules* **1998,** *31* (25), 8706-8712.

7. Varshney, S. K.; Jacobs, C.; Hautekeer, J. P.; Bayard, P.; Jerome, R.; Fayt, R.; Teyssie, P. *Macromolecules* **1991,** *24* (18), 4997-5000.

8. Cameron, N. R.; Lagrille, O.; Lovell, P. A.; Thongnuanchan, B. *Polymer* **2014,** *55* (3), 772-781.

9. Becer, C. R.; Paulus, R. M.; Hoogenboom, R.; Schubert, U. S. *Journal of Polymer Science Part A: Polymer Chemistry* **2006,** *44* (21), 6202-6213.

10. Vargün, E.; Usanmaz, A. *Journal of Polymer Science Part A: Polymer Chemistry* **2005,** *43* (17), 3957-3965.

11. Chernikova, E.; Morozov, A.; Leonova, E.; Garina, E.; Golubev, V.; Bui, C.; Charleux, B. *Macromolecules* **2004,** *37* (17), 6329-6339.

12. Zhang, X.; Boisson, F.; Colombani, O.; Chassenieux, C.; Charleux, B. *Macromolecules* **2014,** *47* (1), 51-60.

13. Chong, Y. K.; Le, T. P. T.; Moad, G.; Rizzardo, E.; Thang, S. H. *Macromolecules* **1999,** *32* (6), 2071-2074.

14. Martin, L.; Gody, G.; Perrier, S. *Polymer Chemistry* **2015,** *6* (27), 4875-4886.

15. Gurnani, P.; Lunn, A. M.; Perrier, S. *Polymer* **2016,** *106*, 229-237.

16. Lai, J. T.; Filla, D.; Shea, R. *Macromolecules* **2002,** *35* (18), 6754-6756.

17. Plummer, R.; Goh, Y.-K.; Whittaker, A. K.; Monteiro, M. J. *Macromolecules* **2005,** *38* (12), 5352-5355.

18. Dossi, M.; Storti, G.; Moscatelli, D. *Macromolecular Symposia* **2010,** *289* (1), 119-123.

19. Rantow, F. S.; Soroush, M.; Grady, M. C.; Kalfas, G. A. *Polymer* **2006,** *47* (4), 1423-1435.

20. Junkers, T.; Barner-Kowollik, C. *Journal of Polymer Science Part A: Polymer Chemistry* **2008,** *46* (23), 7585-7605.

21. Peck, A. N. F.; Hutchinson, R. A. *Macromolecules* **2004,** *37* (16), 5944-5951.

22. Mayadunne, R. T. A.; Rizzardo, E.; Chiefari, J.; Moad, G.; Thang, S. H. *Macromolecules* **1999,** *32*, 6977.

23. Ahmad, N. M.; Heatley, F.; Lovell, P. A. *Macromolecules* **1998,** *31* (9), 2822-2827.

24. McCord, E. F.; Shaw, W. H.; Hutchinson, R. A. *Macromolecules* **1997,** *30* (2), 246-256.

25. McCool, M. B.; Senogles, E. *European Polymer Journal* **1989,** *25* (7), 857-860.

26. Li, G. Z.; Randev, R. K.; Soeriyadi, A. H.; Rees, G.; Boyer, C.; Tong, Z.; Davis, T. P.; Becer, C. R.; Haddleton, D. M. *Polym. Chem.* **2010,** *1* (8), 1196.

27. Gody, G.; Maschmeyer, T.; Zetterlund, P. B.; Perrier, S. *Nature Communications* **2013,** *4*, 2505.

28. Whitfield, R.; Anastasaki, A.; Truong, N. P.; Wilson, P.; Kempe, K.; Burns, J. A.; Davis, T. P.; Haddleton, D. M. *Macromolecules* **2016,** *49* (23), 8914-8924.

29. Destarac, M. *Polymer Reviews* **2011,** *51* (2), 163-187.

30. Keddie, D. J.; Moad, G.; Rizzardo, E.; Thang, S. H. *Macromolecules* **2012,** *45* (13), 5321-5342.

31. Chiefari, J.; Mayadunne, R. T. A.; Moad, C. L.; Moad, G.; Rizzardo, E.; Postma, A.; Thang, S. H. *Macromolecules* **2003,** *36* (7), 2273-2283.

32. Barner-Kowollik, C.; Blinco, J. P.; Perrier, S. In *Materials Science and Technology*, Wiley-VCH Verlag GmbH & Co. KGaA: 2006.

33. Lima, V.; Jiang, X.; Brokken-Zijp, J.; Schoenmakers, P. J.; Klumperman, B.; Van Der Linde, R. *Journal of Polymer Science Part A: Polymer Chemistry* **2005,** *43* (5), 959-973.

34. Perrier, S. *Macromolecules* **2017,** *50* (19), 7433-7447.

35. Benaglia, M.; Rizzardo, E.; Alberti, A.; Guerra, M. *Macromolecules* **2005,** *38* (8), 3129-3140.

36. Feldermann, A.; Ah Toy, A.; Phan, H.; Stenzel, M. H.; Davis, T. P.; Barner-Kowollik, C. *Polymer* **2004,** *45* (12), 3997-4007.

37. de Lambert, B.; Charreyre, M.-T.; Chaix, C.; Pichot, C. *Polymer* **2005,** *46* (3), 623-637.

38. Pietsch, C.; Mansfeld, U.; Guerrero-Sanchez, C.; Hoeppener, S.; Vollrath, A.; Wagner, M.; Hoogenboom, R.; Saubern, S.; Thang, S. H.; Becer, C. R.; Chiefari, J.; Schubert, U. S. *Macromolecules* **2012,** *45* (23), 9292-9302.

39. Ferguson, C. J.; Hughes, R. J.; Nguyen, D.; Pham, B. T. T.; Gilbert, R. G.; Serelis, A. K.; Such, C. H.; Hawkett, B. S. *Macromolecules* **2005,** *38* (6), 2191-2204.

Chapter 3: Polymerisation of sequential addition of methacrylate monomer *via* a semi-batch process

This Chapter reports the use of semi-batch reactors to optimise the control of methacrylate polymerisations using BMDPT, a RAFT agent bearing a poor leaving group. BMDPT is shown to exhibit a low chain transfer constant (0.23) via the Mayo plot method, and is not fully consumed during polymerisation. Higher consumption of RAFT agent was obtained by varying monomer-to-RAFT agent ratio and feeding monomers into the reaction. This approach was used to synthesise methacrylate diblock and multiblock copolymers by sequential monomer addition using a feeding approach, with a near quantitative monomer conversion targeted for each block and high ω- end chain retention. These amphiphlic block copolymers will be used as a polymeric surfactant to disperse carbon black pigment.

3.1. Introduction

Over the last decade new methods of living radical polymerisation (LRP) have been developed to overcome the poor control over molecular weight distribution obtained in conventional radical polymerisation methods. LRP techniques include NMP (nitroxide mediated polymerisation), ATRP (atom transfer radical polymerisation) and RAFT (Reversible Addition-Fragmentation chain Transfer) polymerisation techniques and are widely described in the literature.[1,2,3,4] A living polymerisation system is defined by the presence of a specific moiety, such as alkoxyamine in NMP, alkyl bromide in ATRP or thiocarbonylthio in RAFT, that permits a polymeric chain to be extended, thus leading to the preparation of more complex and controlled polymeric architectures such as diblock, star, comb or multiblock copolymers, insofar as the fraction of living chains remains high. Several options can be used to target a high number of living chains; for instance stopping the polymerisation at low monomer conversion, however this presents certain limitations in the range of structures that can be designed. Hence RAFT mediated polymerisation, being one of the most powerful and versatile Reversible-Deactivation Radical Polymerisation (RDRP) techniques suitable to polymerise a large range of monomers, was used to synthesis methacrylate multiblock copolymers. In a RAFT polymerisation, the choice of thiocarbonyl-thio moiety is crucial and is based on its reactivity to the monomer being polymerized.[5,6]

Control of the polymerisation is directly dependant on the choice of RAFT agent, which must have a high chain transfer constant (C_{tr} >1 based on the Mayo method). However, it is possible to circumvent this problem by using a low ratio of monomer to CTA concentration, thus increasing the chain transfer constant. Interestingly, the polymerisation of methacrylate monomers has received a lot of attraction due to their low cost and broad range in properties (good thermostability and high glass transition). For instance Moad *et al*. published a comparison of starve-feed and batch polymerisation methods for methacrylic monomers using a poor chain transfer agent.[7,8,9] Monteiro *et al*. also reported on the slow monomer addition in emulsion polymerisation using xanthate as RAFT agent.[10] The automatic sequence of DMAEMA and DEGMA monomer synthesis, with a RAFT agent using a trithiocarbonate leaving group, was first described by Krasia.[11] Following these previous studies, Klumperman *et al*. showed improvement over control of the polymerisation using semi-batch processing and a dithiobenzoate, dithiocarbamates or xanthate RAFT agents.[12, 13] The scalability of the semi-batch process was demonstrated by Wei-kang Yuan *et al,* by showing the kinetics of butyl acrylate in a starved feed reactor. Surprisingly, although the use of semi-batch processing has been investigated using a wide range of RAFT agents to improve the polymerisation control of the homopolymer by stopping the reaction at low monomer conversion (below 50 %), architectures such as diblock or multiblock copolymers have not been investigated.[14,15] In this chapter, a study of methacrylate monomers using the BMDPT RAFT agent is reported along with the determination of chain transfer constants. Optimisation of the methacrylate polymerisation is demonstrated using a feeding approach in order to synthesise multiblock copolymers.

The hydrophobic nature of the carbon black pigment required the use of functional (ionic or non-ionic) surfactant to let the adsorption between the pigment surface and the polymer occurs. Hence, the use of DMAEMA as hydrophilic segmemt will involves the interaction between the tertiary amine and the functional groups present on the carbon black surface. The steric repulsion preventing the formation of agglomerates will be induced by the long polymeric chain of BMA.

3.2. Results and Discussion

3.2.1. DMAEMA polymerisation in batch process

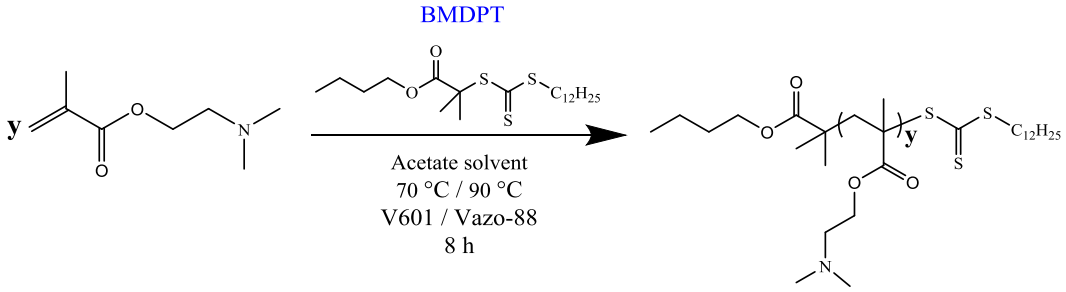

Scheme 3.1: General scheme of DMAEMA polymerisation in butyl acetate/MPA solvent using BMDPT RAFT agent with V601/Vazo-88 azoinitators at 70 ˚C and 90 ˚C in butyl acetate solvent

To identify the optimised conditions for the synthesis of well-defined methacrylate polymers, such as dimethylaminoethyl methacrylate (DMAEMA), in presence of the BMDPT RAFT agent, several factors were varied such as temperature, the initiator and monomer concentration and the nature of the solvent (**Scheme 3.1**).

3.2.1.1. Effect of temperature and initiator concentration

Initially, the polymerisation conditions were set-up based on previous studies demonstrating a good control over a wide range of methacrylate polymerisations using dithiobenzoate RAFT agents.[16,17] The temperature was set to 70 or 90 ˚C, optimal conditions for quantitative monomer conversion in a short period of time. Figure 3.1 shows the influence of the $[BMDPT]_0$ / $[Initiator]_0$ ratio on DMAEMA polymerisation. In order to keep the amount of the initiator generated through the polymerisation constant, V601 and Vazo-88 are used at 70 and 90 ˚C, respectively. The initial set of DMAEMA polymerisation with a ratio of $[BMDPT]_0$ / $[Initiator]_0$ of 5 is attempted. The SEC chromatograms show a monomodal and broad molar mass distribution at 90 ˚C suggesting poor control over the polymerisation at low temperature. The SEC chromatogram in **Figure 3.1** (left) exhibits a narrow and symmetrical molar mass distribution at high monomer conversion (93 %). Nevertheless, the values of the experimental and theoretical molar masses differ vastly, suggesting that the polymerisation is not well-controlled. The same polymerisation is performed at 70 ˚C giving a broader molar mass distribution with a dispersity of 1.4 and lower monomer conversion (83 %), sugesting a poor control of methacrylate polymerisation at low temperature, due to the low constant of propagation (k_p) of methacrylate monomer.[18,19] In order to improve the control of the polymerisation, the $[BMDPT]_0$ / $[Initiator]_0$ ratio is increased to 10 which decreased the the number of initiator-derived chains. However, increasing the ratio to 10 involves a slower polymerisation rate (due to a lower number of propgating chains) which consequently induces a lower monomer conversion.

In the **Figure 3.1** (right), a low monomer conversion and high dispersity are obtained for both temperatures with a narrower molar mass distribution at 90 ˚C suggesting an increase of the propagation rate constant and the chain-transfer constant. Based on this preliminary studies, the polymerisation of methacrylate monomers will be performed with a ratio of $[BMDPT]_0$ / $[Initiator]_0$ of 10 at 90 ˚C.

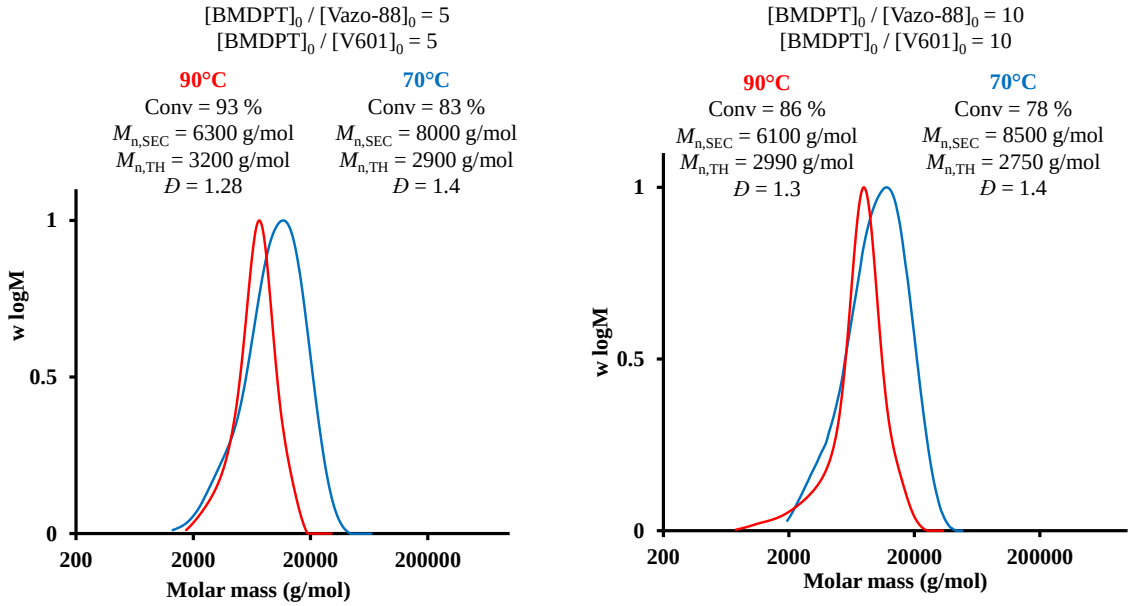

Figure 3.1: Comparison of SEC-THF chromatograms of DMAEMA homopolymerisation at 70 ˚C and 90 ˚C with $[DMAEMA]_0$ = 3 M, a ratio of $[BMDPT]_0$ / $[Initiator]_0$ 5 and 10 in butyl acetate

3.2.1.2. Effect of monomer concentration and solvent

The dispersion of carbon black pigment being performed either in butyl acetate or methoxypropyl acetate solvent, the polymerisation of DMAEMA is compared in both solvents. In addition, the monomer concentration, which can potentially affect the rate of polymerisation, is also investigated to determined the optimal conditions for methacrylate polymerisation using BMDPT RAFT agent.

Figure 3.2 shows a SEC chromatograms of pDMAEMA (DP = 19) synthesised in butyl acetate (left) at different monomer concentration. A high monomer conversion and dispersity ($Đ$ > 1.2) are reached for each polymerisation.The solvent does not affect the reactivity of the macroradical has demonstrated by Haehnel.[19,20] Regarding the polymerisation performed in MPA, a small shoulder at low molar mass is observed, as well as, an increase of the $M_{n,SEC}$ implying a possible transfer between the polymer chain and the solvent is occurring. From a general point of view, there is not a significant impact of the monomer concentration, even though, it should be noted that an increase of monomer concentration often leads to an increase in viscosity which can potentially affect the control of the polymerisation. The difference of the theoretical molar mass ($M_{n,TH}$ = 3400 g/mol) and experimental molar mass ($M_{n,SEC}$) obtained with the SEC-THF can be explained by the difference in hydrodynamic volume of the standard (calibration with PMMA) but also a poor control of the polymerisation.

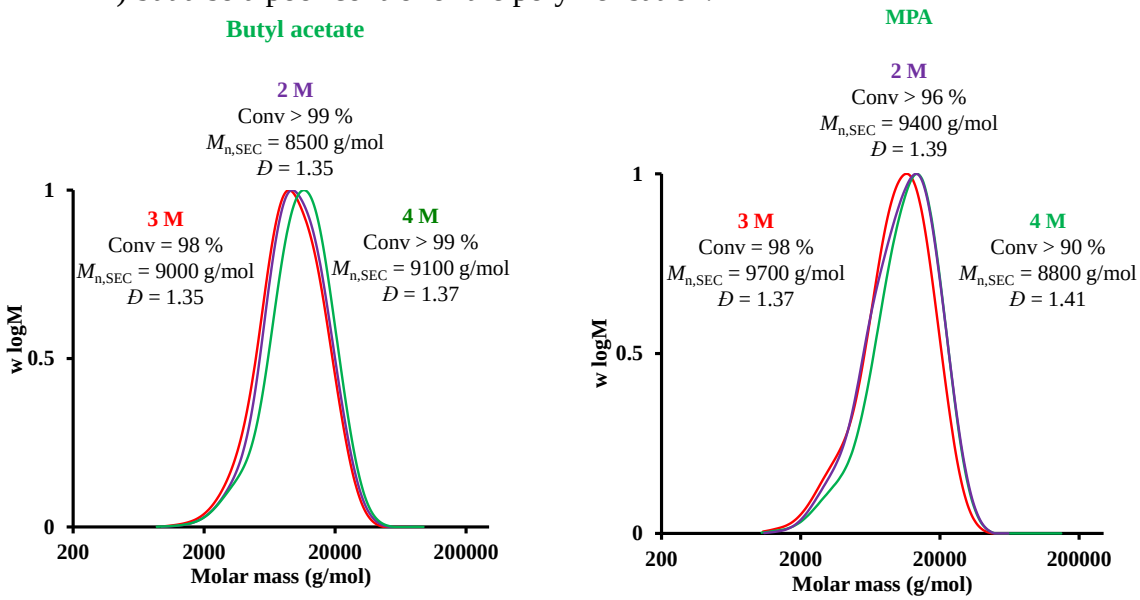

Figure 3.2: Comparison of SEC-THF chromatograms of $p(DMAEMA)_{19}$ at 90 ˚C with $[DMAEMA]_0$ = 2 M, 3 M and 4 M, a ratio of $[BMDPT]_0$ / $[Vazo\text{-}88]_0$ = 10 in butyl acetate and MPA solvents

The data of DMAEMA polymerisation at different concentrations and solvents obtained at 90 ˚C with a ratio $[BMDPT]_0$ / $[initiator]_0$ 10 are reported in **Table 3.1**.

Table 3.1: Characterisation data for the homopolymerisation of DMAEMA (targeted DP_n of 19). RAFT polymerisations were conducted over 10 -12 h in acetate solvent in batch mode at 90 ˚C using $[BMDPT]_0$ / $[Vazo\text{-}88]_0$ = 10

Entry	**$[DMAEMA]_0$ ($mol.L^{-1}$)**	**Solvent**	**Conv (%)**	**$M_{n,SEC}$[a] ($g.mol^{-1}$)**	**$M_{n,TH}$[b] ($g.mol^{-1}$)**	**$Đ$**
1	2	Butyl acetate	>99	8500	3400	1.35
2	3	Butyl acetate	97	9000	3300	1.37
3	4	Butyl acetate	>99	9100	3400	1.38
4	2	MPA	96	9400	3290	1.39
5	3	MPA	98	9700	3356	1.37
6	4	MPA	90	8800	3110	1.41

[a] Determined using **equation 3.5** (experimental section)

3.2.1.3. Kinetics of DMAEMA and BMA in batch polymerisation

A kinetic studies of DMAEMA and BMA polymerisation are performed using the optimal conditions established from the previous studies; 3 M monomer concentration, a $[BMDPT]_0$ / $[initiator]_0$ ratio of 10 at 90 ˚C in butyl acetate solvent. **Figure 3.3 A and C**, the plot of molecular weight *versus* conversion for DMAEMA and BMA polymerisation are linear but $M_{n,SEC}$ is not in good agreement with the theoretical molar mass, and the dispersity remains high throughout the polymerisation, suggesting that the polymerisation is not well-controlled.

However, the kinetic plot revealed that the polymerisation fulfils some criteria of a controlled radical polymerisation (CRP) with a first order dependence on both monomer with a linear increase of $\ln([M]_0/[M]_t)$, indicating a constant radical concentration during polymerisation (**Figure 3.3 B and D)**.

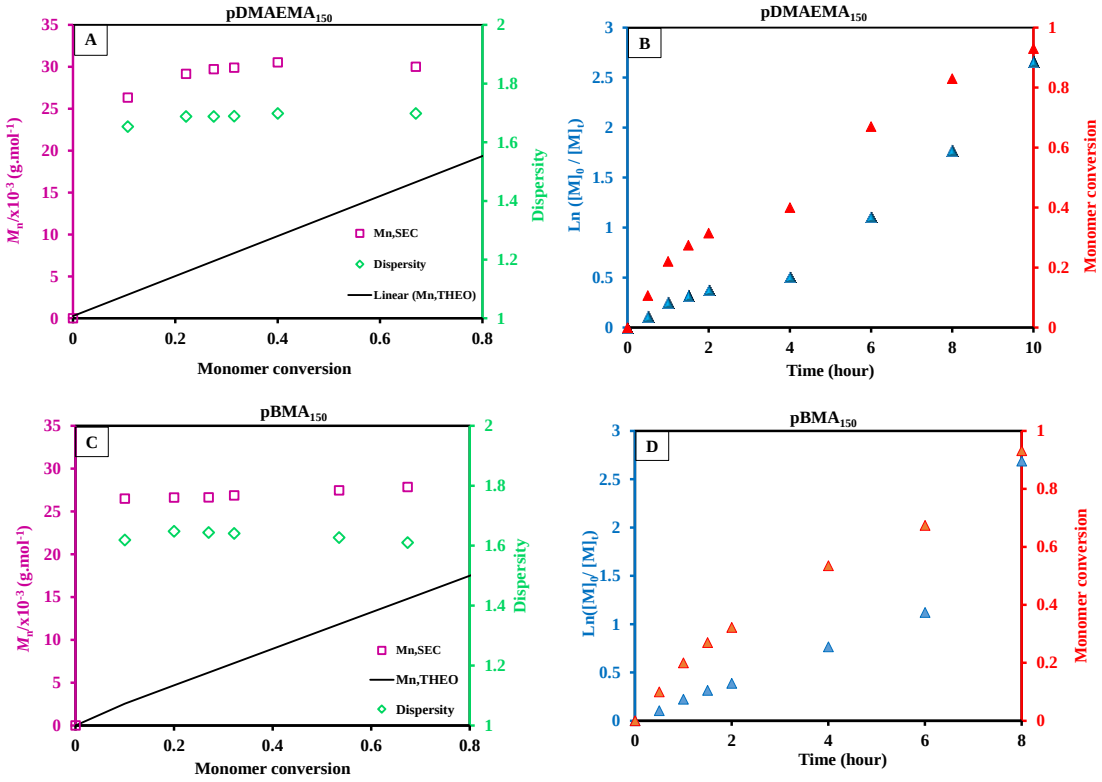

Figure 3.3: Molecular weight and dispersity evolution *versus* monomer conversion (**A**) and first order plot evolution *versus* time (**B**) of DMAEMA polymerisation in batch process. Molecular weight and dispersity evolution *versus* monomer conversion (**C**) and first order plot evolution *versus* time (**D**) of BMA polymerisation in batch process mediated by BMDPT RAFT agent in butyl acetate at 90 ˚C.

The poor control of the methacrylates polymerisation mediated by BMDPT RAFT agent shows clearly the incompatibility of the CTA with the monomer. As described in the literature, the reactivity of the CTA is directly affected by both the Z and R groups which will governs the reactivity of the C=S bond toward the radical addition and the efficiency of the reinitiate radical (R˙).

In this study, only the influence of the leaving group R is investigated by comparing R = -C-(**CH$_3$)$_2$**-C(O)O-C$_4$H$_9$ of BMDPT *versus* R = -(**CH$_3$**)-C-**CN**-(CH$_2$)$_2$-COOH of MCTP.

3.2.1.4. Influence of the chain transfer agents

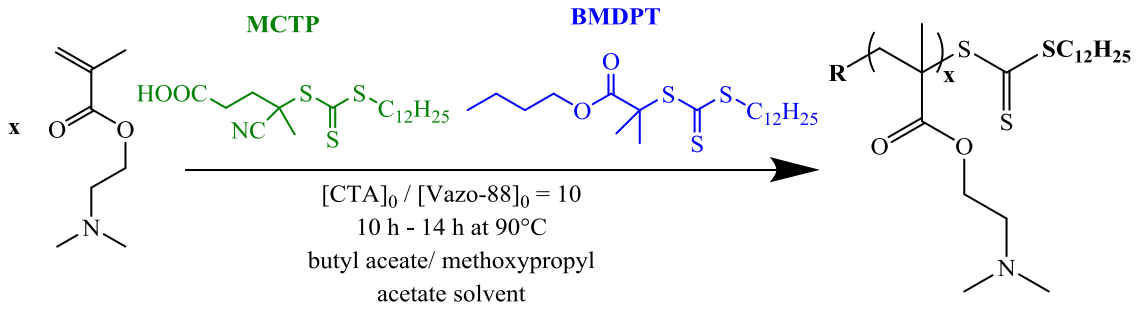

Scheme 3.2: General scheme of DMAEMA polymerisation using MCTP and BMDPT RAFT agents with V601 or Vazo-88 azoinitators at 70 ˚C and 90 ˚C in butyl acetate / MPA solvents

As shown previously, DMAEMA polymerisation using BMDPT RAFT agent leads to a broad dispersity and does not entirely fulfill the CRP requirement. Favier and Charreyre have published a review summarising the key parameters in a RAFT polymerisation reaction in order to generate efficient control over molecular weight distribution.[21] Of all these factors, the structure of the CTA is one of the most important as it strongly influences the addition fragmentation during the pre-equilibrium step.[6,22,23]

The main role of the "R" group is to increase the fragmentation and the re-initiation step, therefore a good leaving group is required to produce a radical R˙ fragment that allows the CTA to add another monomer unit as fast as possible.[24] Klumperman and coworkers have clearly shown the effect of semi-batch mode, comparing three dithiobenzoate CTAs bearing a poor leaving group to polymerise *N*-vinylpyrrolidone, styrene and methyl methacrylate at different temperatures.[25,12]

Indeed, the initialization process can be monitored by the nature of the leaving group radical (R•). In the present study the effect of the "R" group was investigated by comparing the polymerisation of DMAEMA using either MCTP or BMDPT as CTAs under similar conditions (**Scheme 3.2**). **Figure 3.4** shows the SEC chromatograms of p(DMAEMA)$_{19}$ using MCTP (green) and BMDPT (blue) RAFT agents. After 12 hours, a near quantitative monomer conversion is reached for both polymerisations with a narrow molar mass distribution and a lower dispersity ($Đ$ < 1.2) using MCTP RAFT agent while a broader molar mass distribution ($Đ$ ≥ 1.3) is obtained with BMDPT, suggesting a relatively low chain transfer constant due to a slow equilibration between active and dormant chains.[26,27,28]

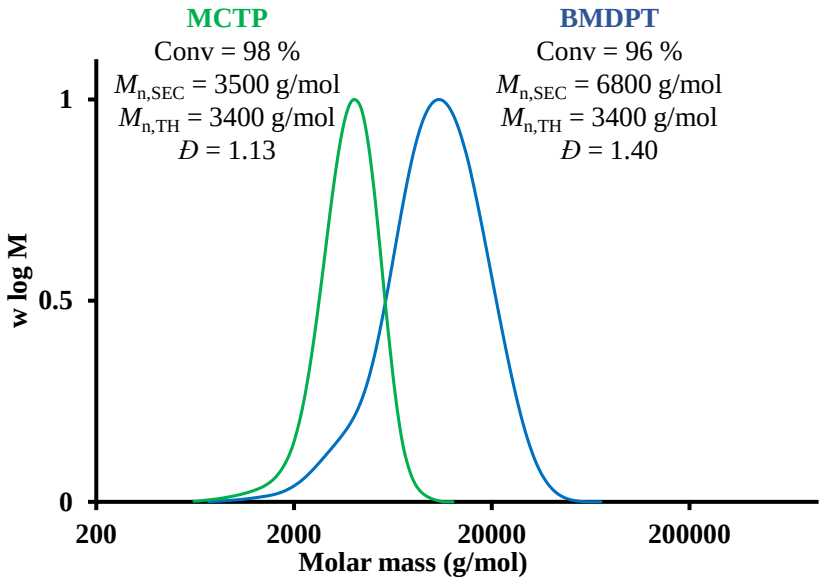

Figure 3.4: Comparison of SEC-THF chromatograms of DMAEMA polymerisation with BMDPT and MCTP RAFT agents with $[DMAEMA]_0$ = 3 M, ratio of $[RAFT\ agent]_0$ / $[Vazo\text{-}88]_0$ = 10 at 90 ˚C in butyl acetate solvent

This experiment illustrates clearly the influence of the nature of the leaving group on the polymerisation process, and is widely described in the literature.[6,22,29,30,31,31] The low control over the reaction efficiency can be explained by two main events.

First of all, the combination of a poor leaving group with a good "Z" group, allowing for efficient activation of the C=S double bond towards the reactivity of the propagating radical $P^{\bullet}_n$, leads to poor control over the polymerisation. Inversely, association between a good leaving group with an inefficient "Z" group gives poor control.[22] In the RAFT process, control of the polymerisation is based on the rapid fragmentation of the "R" group in the pre-equilibrium step.

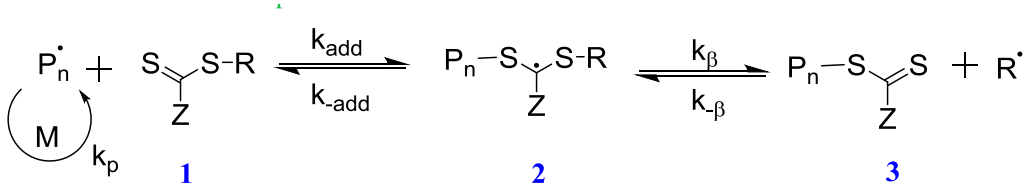

Scheme 3.3: Pre-equilibrium step of the RAFT polymerisation

The formation of the macroRAFT radical (**Scheme 3.3 species 2**) can either fragment towards the starting species (**Scheme 3.3 species 1**) if the R group substituent is not a good leaving group, or generate a polymeric RAFT agent (**Scheme 3.3 species 3**) and release the $R^{\bullet}$ species. Concerning the macroinitiator MCTP, the presence of the cyano group which an electron withdrawing group, will destabilise the C-S bond (**species 2**) *via* an inductive effect, and make the R side chain a better leaving group, thus allowing for the propagation of a new polymeric chain.

However, the R group of BMDPT RAFT agent yields a secondary radical while the [PDMAEMA•] forms a tertiary radical so the fragmentation pathway will be favoured toward the more stable leaving group, although a block copolymer can still be formed. Morover, the methyl group, being an electron donating group, will stabilise the radical of the BMDPT macroCTA intermediate, thus only a small amount of **species 3** will be produced.

3.2.1.5. Chain transfer constant determination

The evaluation of the chain transfer constant (C_{tr}) allows quantification of the reactivity of the R group towards the monomer. This value must be equal to or greater than that of the rate of propagation (k_p). All the parameters, such as the polarity/steric hindrance around the carbon-carbon bonds, have been reported by Fisher and Radom, and are used as a guide to select a suitable R group for a given monomer.[32] Similarly, the chain transfer constant can be determined for the "Z" substituent for a class of monomers in specific conditions.[33] Few methods have been developed for C_{tr} determination, including the Mayo method and chain length distribution (CLD).[34,35,36]

The rate constant for chain transfer can be evaluated based on **equation 3. 1**, where k_{add} is the rate constant for addition and ϕ the partition coefficient which determines the rate of partition from the adduct between products and starting materials; k_{tr} and k_{β} are the rate constant for chain transfer and rate of fragmentation respectively.[37]

$$k_{tr} = k_{add}\frac{k\beta}{k\beta + k - add} = k_{add}\phi \quad \textbf{(Equation 3.1)}$$

The rate of consumption of the CTA yields the molecular weight and molecular weight distribution, and also describes the reactivity of the expelled radical (R) and the

propagating radical towards the thiocarbonyl thio moieties, which can be defined by two transfer coefficients: C_{tr} (=k_{tr}/k_p) and C_{-tr} (=k_{-tr}/k_i). Several methods have been reported in the literature to determine the value of the transfer constants. For a high transfer constant, a kinetic model was developed by Walling-Müller.[38]

In parallel, another method suitable for a low chain transfer ($C_{tr} < 5$), determined by size-exclusion chromatography, is based on the Mayo plot method, in which DP is the number average degree of polymerization obtained in the presence of chain transfer agent. DP^0 is the number average degrees of polymerization obtained in absence of chain transfer agent (**Equation 3.2).**[22,39]

$$\frac{1}{DP} = \frac{1}{DP^0} + C_{tr}\frac{[CTA]}{[Monomer]} \quad \textbf{(Equation 3.2)}$$

From **equation 2**, the C_{tr} can be defined as:

$$C_{tr} = \frac{K_{tr}}{K_p} \quad \textbf{(Equation 3.3)}$$

Where k_{tr} is the chain transfer coefficient and k_p is the rate of propagation coefficient. Hence, the value of C_{tr} is obtained by plotting the inverse of the number average degree of polymerisation, DP_n, against the ratio of BMDPT (or MCTP) to DMAEMA at the beginning of the polymerisation.[40] In the current reaction, the value of chain transfer constant (C_{tr}) has been determined for both BMDPT and MCTP for DMAEMA polymerisations in acetate solvents using a Mayo plot **(Figure 3.5)**. Each polymerisation must be stopped at low monomer conversion in order to measure the exchange between the CTA and the growing chain in the pre-equilibrium step.

A range of degrees of polymerisation were targeted to polymerise DMAEMA with MCTP and BMDPT. The value of C_{tr}, obtained from the slope of the linear regression, shows a high chain transfer constant for MCTP (C_{tr} = 4.5) and a lower value for BMDPT (C_{tr} = 0.35). These data illustrate the previous hypothesis concerning the poor control of methacrylate monomers with BMDPT.

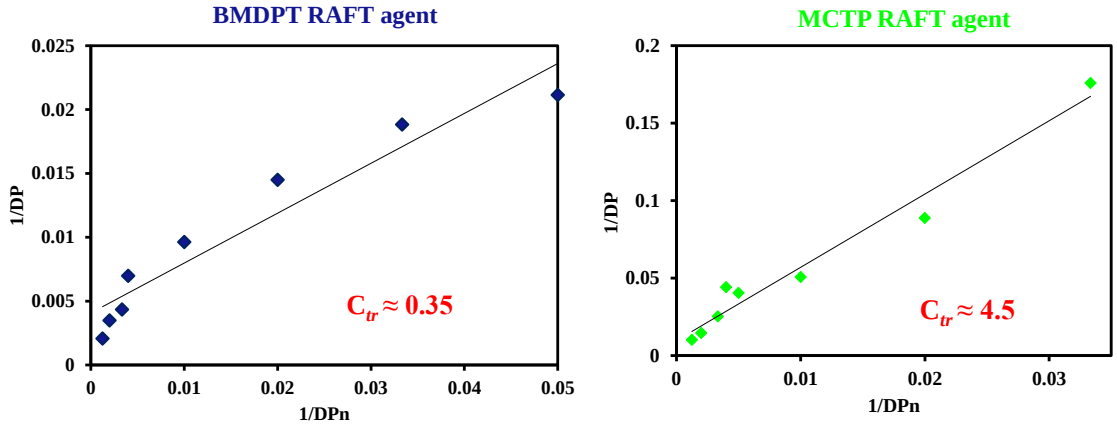

Figure 3.5: Determination of the chain transfer constant of DMAEMA (DP_n = 20, 30, 50, 100, 200, 300, 500, 800) polymerisation using BMDPT (**blue**) and MCTP (**green**) RAFT agents in butyl acetate solvent at 90 ˚C

3.2.2. DMAEME polymerisation in a semi-batch process

3.2.2.1. Rate of feeding determination

The preliminary study of DMAEMA in batch polymerisation revealed a hybrid mechanism during the RAFT pre-equilibrium where the RAFT agent remains (partially) intact instead of being converted into macroCTA. Davis *et al*. have reported the kinetic studies of the polymerisation of styrene and MMA using the cumyl phenyldithioacetate. The value of the chain transfer constant using Mayo plots increased at different temperatures (25 to 60 ˚C) and the kinetic information is similar to the conventional

radical polymerisation with and onset of the RAFT polymerisation.[41] For the less active RAFT agents (*i.e.* RAFT agents with low C_{tr} values), Moad *et al*. suggested the use of a semi-batch approach to improve the control of the polymerisation, which has been highlighted by Klumpermann.[12] As such, a starve-feed (semi-batch/feeding) system is set up to control the amount of monomer present in the system.

The monomer is degassed under nitrogen while the mixture of the RAFT agent, the initiatior and solvent are also degassed in a separat vessel. The concentration of RAFT agent being constant, the value of the propagation and chain transfer rates changed under monomer concentration. Hence, different rates of feeding of the DMAEMA are attempted. The reaction mixture was left for 4 hours until high monomer conversion was reached. An optimal rate of feeding of 4 hours with high monomer conversion and narrow dispersity ($Đ \leq 1.25$) was determined for DMAEMA with a degree of polymerisation of 19. In batch mode, the rate of propagation is higher than a chain transfer leading a high molecular weight polymer at the start of the polymerisation. At the beginning of the feeding process, any monomer is present in the vessel flask containing the CTA and initior. Assuming a constant concentration of the RAFT agent and a slow monomer addition in a polymerisation mixture, the control of the propagation rate over the chain transfer can be tune by increasing the consumption of the CTA in the pre-equilibrium step. Consequently, the dispersity decreased from 1.44 to 1.25 from the batch mode to the semi-batch, respectively illustrated by the THF-SEC chromatograms in the **Figure 3.6**.

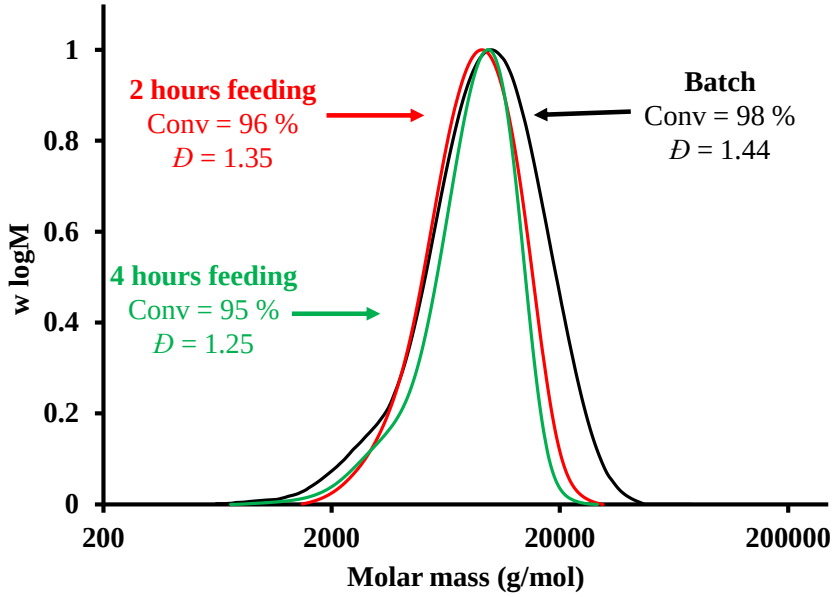

Figure 3.6: Comparison of SEC-THF chromatograms of DMAEMA polymerisation with BMDPT RAFT agent in batch mode (**black**) and rate of feeding of 2 h (**red**) and 4 h (**green**) with a ratio of $[BMDPT]_0$ / $[Vazo\text{-}88]_0$ = 10 at 90 ˚C in butyl acetate solvent

3.2.2.1. Kinetic study in semi-batch process

To establish the "living" characteristic of the DMAEMA (and BMA) polymerisation using the BMDPT RAFT agent in a semi-batch process, a kinetic study was undertaken with a targeted DP of 150. Monomer conversion was determined by ^{1}H NMR in $CDCl_3$ and the molar mass distribution by SEC in THF calibrated with PMMA. **Figure 3.7 A and 3.7 C** show a good agreement between the evolution of the $M_{n,SEC}$ and $M_{n,TH}$ of the DMAEMA/BMA homopolymers with the monomer conversion. The dispersity increase linearly ($Đ$ = 1.32) with the monomer conversion and remains lower than the dispersity value obtained in batch mode ($Đ$ = 1.5).

Figure 3.7 B and **3.7 D** exhibit a linear plot of $\ln([DMAEMA]_0 / [DMAEMA]_t)$ *versus* time indicates that the system is in a stationary state with respect to the ratio Rp / [M] = $k_p[P^\bullet]$ proving the "living" nature of this polymerisation.

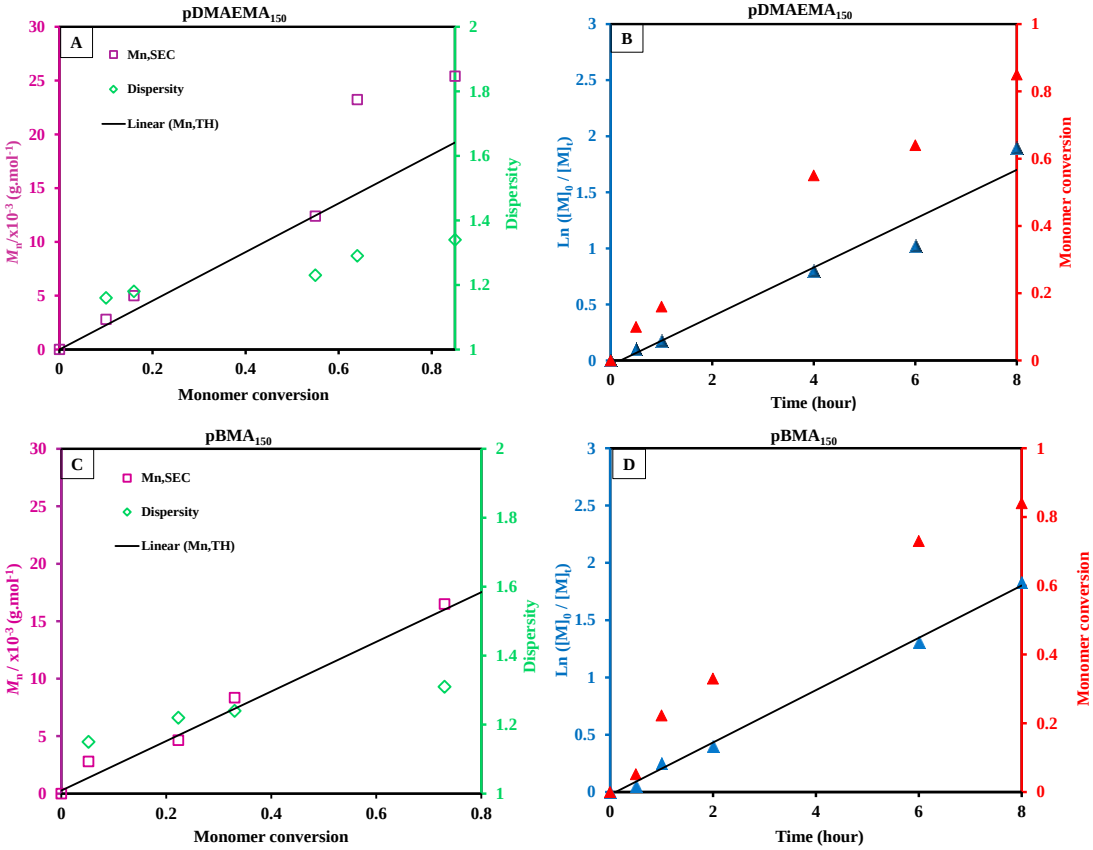

Figure 3.7: Molecular weight and dispersity evolution *versus* monomer conversion (**A**) and first order plot evolution *versus* time (**B**) of DMEAMA polymerisation in semi-batch process. Molecular weight and dispersity evolution *versus* monomer conversion (**C**) and first order plot evolution *versus* time (**D**) of BMA polymerisation in semi-batch process

3.2.3. Polymerisation of a range of methacrylate monomers in semi-batch process

Haehnel *et al*.have reported a study on the effect of the alkyl ester groups of acrylates and methacrylates monomers family by determining the rate of propagation coefficient (k_p) using the pulsed laser polymerisation technique (PLP). It has been observed that the k_p increases when the ester side chain length of methacrylate monomer increases going from MMA to Behenyl methacrylate (BeMA).[19] Similarly, a study on the ester chain length on methacrylate monomers (MMA, EMA, BMA and 2-EHMA) using CCTP (Catalytic Chain Transfer Polymerisation) technique in semi-batch process was studied by Haddleton.[42] A significant reduction of the chain transfer constant is observed ($Ctr_{(MMA)}$ = 1130 and $Ctr_{(BMA)}$ = 524). Here, the effect of the ester side and the presence of an aromatic group of methacrylate is investigated in RAFT polymerisation in presence of BMDPT RAFT agent. **Figure 3.8** (left) shows the SEC chromatograms of homopolymer targeted with a degree of polymerisation of 50. A monomodale and symetrical molar distribution for each homopolymer is observed with the presence of tail at low molar mass due to the low reinitiation step.The right picture shows the SEC chromatograms for a targeted degree of polymerisation of 150. A comparable molar mass distribution was observed for each homopolymer, with a shift at high molar mass for the bulky lauryl methacrylate monomer which can be attributed to the increase of the viscosity due to the long polymeric chains. Any significant effect of the ester chain length or molecular weight is noticed.

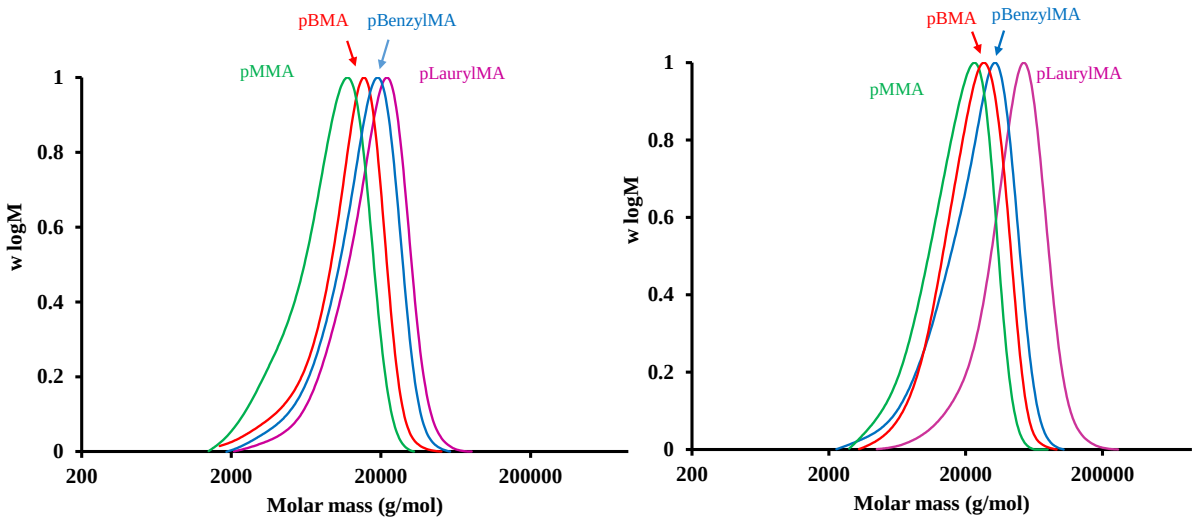

Figure 3.8: Comparison of SEC-THF chromatograms of methyl methacrylate (MMA), butyl methacrylate (BMA), benzyl methacrylate (BenzylMA), lauryl methacrylate (LaurylMA) polymerisation with BMDPT RAFT with a degree of polymerisation of 50 (left) and 150 (right) in semi-batch process 4 hours of feeding with a ratio of $[BMDPT]_0$ / $[Vazo\text{-}88]_0$ = 10 at 90 ˚C in butyl acetate solvent

Table 3.2 records a high monomer conversion for most of the homopolymers, with a constant dispersity ($Đ \approx 1.3$) indicating the versatility of the semi-batch mode for the methacrylate monomer using a RAFT agent bearing a poor leaving group.

Table 3.2: Conditions used for the methacrylates (DP_n targeted 50 and 150) homopolymerisation. RAFT polymerisations were conducted with $[monomer]_0$ = 3 M at 90 ˚C in butyl acetate solvent in semi-batch process

Entry	Monomer	Overall [M]:[CTA]:[Vazo88]	Monomer %	$M_{n,TH}$[a] g.mol^{-1}	$M_{n,SEC}$[b] g.mol^{-1}	$Đ$
1	BMA	50 : 1 : 0.1	>99	7500	10300	1.32
2	BMA	150 : 1 : 0.1	98	20900	21900	1.30
5	MMA	50 : 1 : 0.1	83	4600	7600	1.35
6	MMA	150 : 1 : 0.1	70	10900	14820	1.18
7	LaurylMA	50 : 1 : 0.1	98	12900	15200	1.29
8	LaurylMA	150 : 1 : 0.1	91	35150	38770	1.29
9	BenzylMA	50 : 1 : 0.1	96	8900	12800	1.32
10	BenzylMA	150 :1 : 0.1	97	26850	20300	1.35

[a] Determined using **equation 3.5** (experimental section)

[b] Determined using THF-SEC with PMMA narrow standards

3.2.4. Synthesis of statistical and block copolymer in semi-batch process

The efficient dispersity of carbon black in organic solvents depends strongly on several parameters; such as the composition of the anchoring block, the molecular weight of the polymer and finally the polymeric architecture. Having optimised the synthesis of the methacrylate monomers by a feeding approach, a range of statistical and diblock copolymers were designed in order to assess their impact on pigment dispersion.

The synthesis of methacrylate multiblock copolymers was performed as proof of the feeding concept. Their effectiveness as dispersing agents will be discussed in a later chapter (**Chapter 5**).

3.2.4.1. Statistical copolymer synthesis

The synthesis of homopolymer in starve-feeding approach being a success, the similar process is used to make statistical copolymers targeting several degrees of polymerisation (DP) for methacrylate block copolymers by keeping the ratio of the hydrophilic to hydrophobic block constant (1/3 and 2/3 respectively). Both monomers are mixed together in a same vial, degassed under nitrogen and fed into the second vial containg the CTA, Vazo-88 and butyl acetate. The monomer conversion is determined by ^{1}H NMR in $CDCl_3$ using 1,3,5-trioxane as internal reference and the dispersity was assessed by THF-SEC using PMMA as calibration. **Figure 3.9** shows the SEC chromatograms of each statistical copolymers. A monomodale molar mass distribution is obtained with a high monomer conversion for DMAEMA and BMA monomers. The dispersity remains low (in comparison to the batch mode), despite the fact that the difference of $M_{n,SEC}$ and $M_{n,TH}$ which firstly, can be attributed to the difference of the hydrodynamic volume of PMMA and secondly, suggesting that the polymerisations are not well-controlled, due to the fact that the RAFT agent is not fully consumed.

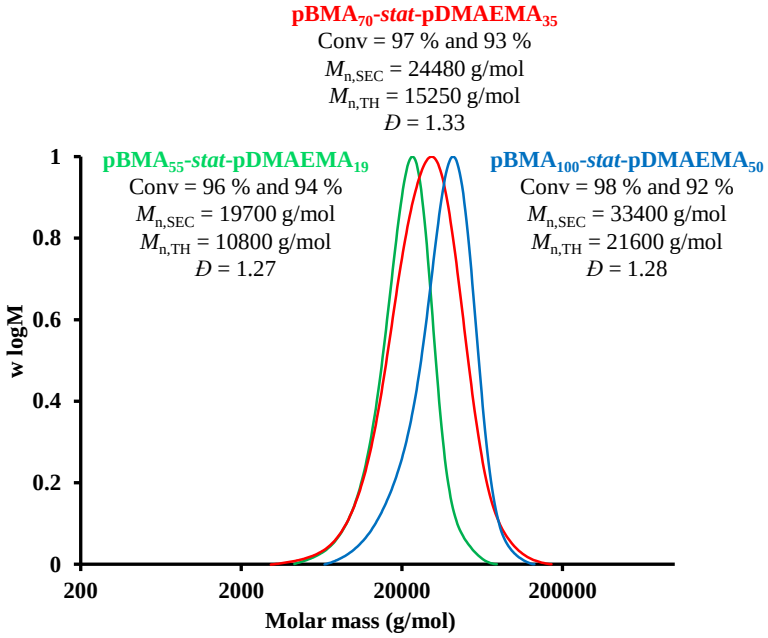

Figure 3.9*:* Comparison of SEC-THF chromatograms of p(BMA)-*statistical*-p(DMAEMA) performed in semi-batch process with a with a ratio of $[BMDPT]_0$ / $[Vazo\text{-}88]_0$ = 10 at 90 ˚C in butyl acetate solvent with a degree of polymerisation of 55/19 (**green**), 70/35 (**red**) and 100/50 (**blue**), respectively.

3.2.4.2. Diblock copolymer synthesis

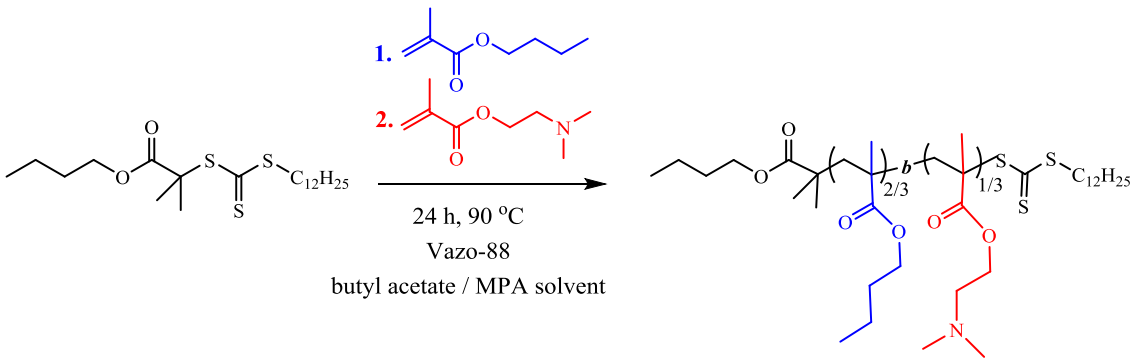

Scheme 3.4: General scheme of p(BMA)-*block*-p(DMAEMA) methacrylates copolymer synthesised by feeding process with BMDPT RAFT agent, $[BMDPT]_0$ / $[Vazo88]_0$ =10 at 90 ˚C in butyl acetate solvent.

With this synthetic approach, three diblock copolymers were synthesised by a sequential feeding of each monomer. A narrow molar mass distribution was obtained for each DP with a consistent dispersity ($Đ \leq 1.3$) for butyl methacrylate (BMA) homopolymers (**Table 3.3**). A shift to high molar mass was observed in all the SEC chromatograms after addition of DMAEMA monomer, demonstrating full consumption of the macroRAFT agent. The presence of a small shoulder can be attributed to the presence of non-reinitiated polymer chains and the tail suggests some dead chains (**Figure 3.10**). To reach full monomer conversion 24 hours was required, thus avoiding the precipitation step.

Table 3.3*:* Conditions used for the BMA homopolymerisation (targeted DP_n of 55,70 and 100) and chain extension with DMAEMA (targeted DP_n of 19,35 and 50) to make diblock copolymer. RAFT polymerisations were conducted in semi-batch process with 4 h of monomer feeding and 20 h of polymerisation at 90 ˚C with $[BMDPT]_0$ / $[Vazo88]_0$ = 10 in butyl acetate solvent

BMA (DP)	**Conv.** (%)	$M_{n,TH}$[a] (g/mol)	$M_{n,SEC}$[b] (g/mol)	$Đ$	**DMAEMA** (DP)	**Conv.** (%)	$M_{n,TH}$[a] (g/mol)	$M_{n,SEC}$[b] (g/mol)	$Đ$
55	95	7700	12400	1.24	19	98	10630	16000	1.38
70	94	9680	10500	1.25	35	93	14800	17500	1.34
100	96	13650	14600	1.29	50	90	20725	22100	1.38

[a] Determined using **equation 3.5** (experimental section)

[b] Determined using THF-SEC with PMMA narrow standards

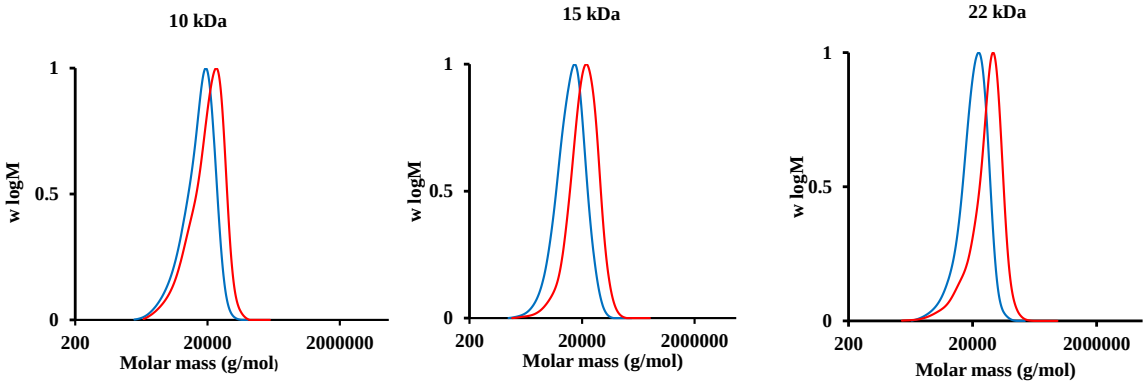

Figure 3.10: Comparison of SEC-THF chromatograms of p(BMA)-*block*-p(DMAEMA) copolymers performed in semi-batch process with a with a ratio of $[BMDPT]_0$ / $[Vazo\text{-}88]_0$ = 10 at 90 ˚C in butyl acetate solvent with a degree of polymerisation of 55/19, 70/35 and 100/50, respectively (left to right)

3.2.4.3. Scaling up the synthesis of diblock copolymers

To demonstrate the scalability of this process the reaction was performed using the exact same conditions as those used for the diblock copolymer to prepare one kilogram of polymer. A mass of 250 g of BMA was charged to a round bottom flask, sealed with a septum, and degassed with a nitrogen for 30 minutes. Separately, 14 g of BMDPT RAFT agent was mixed with 0.780 g of AIBN and 270 g of butyl acetate and degassed for 30 minutes under nitrogen. Then, the mixture containing the CTA and azoinitator was placed in oil bath thermostated at 90 ˚C and mechanically stirred, while the BMA monomer was slowly fed over 4 hours using an automatic syringe pump. The reaction was left for 20 h to allow the polymerisation to reach full monomer conversion. Finally, a mass of 96 g of DMAEMA was prepared in a similar manner to BMA, and added into the mixture containing the first block.

The quantities of each reactant used in small and large scale are reported in **Table 3.4** and the success of the scale up is illustrated by the SEC chromatogramwith the shift at high molar mass after the chain extension **Figure 3.11**.

Table 3.4: Conditions used to scale up p(BMA)$_{100}$-*block*-p(DMAEMA)$_{50}$ copolymer in 30 and 300 g using RAFT polymerisation in semi-batch process

BMA (L)	Vazo-88 (g)	BMDPT (g)	MPA (L)	Rate of feeding (mL.h^{-1})	DMAEMA (L)	Vazo-88 (g)	Rate of feeding (mL.h^{-1})
5.6 x10^{-3}	0.012	0.210	6 x10^{-3}	1.4 x10^{-3}	3 x10^{-3}	0.012	7.4 x10^{-4}
0.280	0.780	13.5	0.306	70	0.095	0.480	0.102

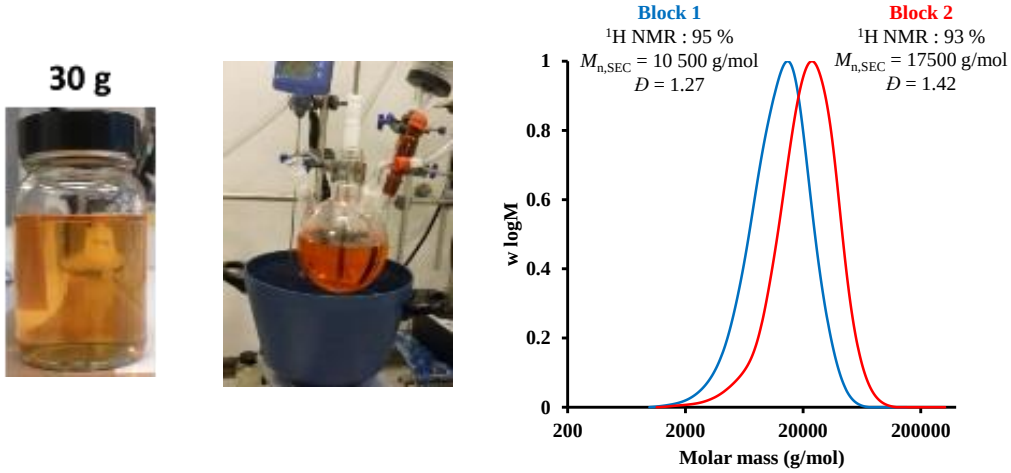

Figure 3.11: Pictures of 30 g and 300 g scale of diblock p(BMA)$_{100}$-*block*-p(DMAEMA)$_{50}$ and THF-SEC chromatogram of the 300 g diblock methacrylate copolymer synthesised in butyl acetate solvent at 90 ˚C in semi-batch process

3.2.4.4. Sequential addition of BMA monomer in semi-batch mode

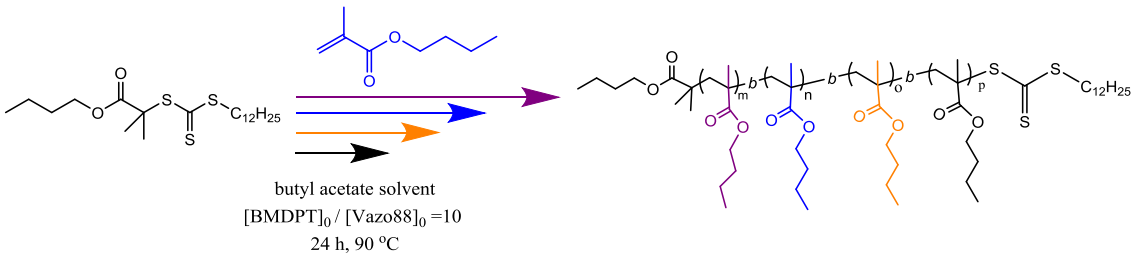

Scheme 3.5: General scheme of the sequential addition of BMA monomer using BMDPT RAFT agent with $[BMDPT]_0$ / $[Vazo\text{-}88]_0$ = 10 at 90 ˚C in MPA solvent

Several techniques allowing a precise control of the monomers sequence controlled were reported.[43,44,45,46,47] It is well-known that the methacrylates monomers exhibit a low rates of propagation (k_p) and chain transfer events which make the synthesis of BMA (or other methacrylate monomer) more challenging. In this attempts, the conditions previously established for the diblock copolymer are used to synthesise the sequential addition of BMA monomer using semi-batch processing without any purification steps by targeting a high monomer conversion. (**Scheme 3.5)**. The SEC traces of the sequential addition reported in the **Figure 3.12** show the molecular weight distributions of the iterative in situ chain extension cycles of BMA. A high initiator concentration ($[BMDPT]_0$ / $[Vazo\text{-}88]_0$ = 10) is needed to achieved high monomer conversion in a shorter time which, consequently will increased the number of dead chains. In order to keep the livingness as high as possible a small amount of initiator is added for the following blocks. This decreases of livingness is usually represented by the presence of the a shoulder at low molar mass which does not appaear in these chromatograms.

Additionally, the success of the chain extension is proved by the shift at high molar mass after each monomer addition.

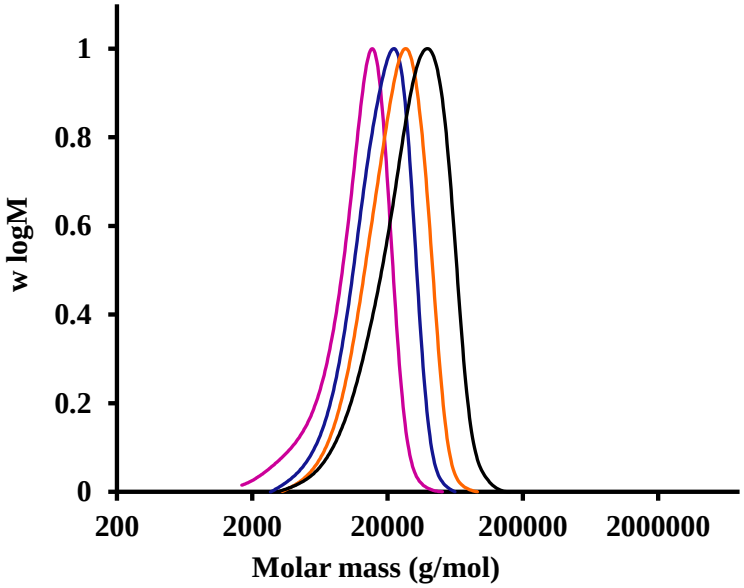

Figure 3.12: Comparison of SEC-THF chromatograms of sequential addition of BMA to synthesise p(**BMA**)$_{50}$-*b*-p(**BMA**)$_{50}$-*b*-p(**BMA**)$_{50}$-*b*-p(**BMA**)$_{50}$ with DP_n targeted 50 in semi-batch process. Initial conditions: $[BMA]_0$ = 3 M, $[BMDPT]_0$ / $[Vazo\text{-}88]_0$ = 10 at 90 ˚C in butyl acetate solvent.

A well-defined tetrablock copolymer was attained, as shown by the SEC molecular weight distributions (**Figure 3.12**). A small amount of initiator is added after each chain extension in order to maintain a high fraction of living chains (L > 90 %) and limit the accumulation of termination, however, the dispersity increased for the tetrablock copolymer due to a high viscosity of the polymerisation mixture (**Table 3.5**).

In the **Table 3.5**, the monomer conversion and the values of the experimental and theoretical molar mass and dispersity are reported. $M_{n,SEC}$ agrees with $M_{n,TH}$ in comparison to p(DMAEMA)$_{19}$. The structure of BMA and MMA being quite similar, the hydrodynamic volume of PMMA standard might not affect the $M_{n,SEC}$ value.

Table 3.5: Characterisation data for the symthesis of the sequential addition of BMA (DP_n = 50 per chain extension) obtained in semi-batch processvia RAFT polymerisation: [BMA] : [BMDPT] : [Vazo-88] = [50] : [1] : [10] in butyl acetate solvent at 90 ˚C

Entry	**Monomer**	$M_{n,TH}$ [a]	$M_{n,SEC}$ [b]	$Đ$	L
	% conv	g.mol^{-1}	g.mol^{-1}		%
1	94	7100	10300	1.30	98.5
2	92	13700	15400	1.26	97.9
3	93	20200	19350	1.28	95.5
4	97	27100	25200	1.40	94.2

[a] Determined using **equation 2.5** (experimental section)

[b] Determined using THF-SEC with PMMA narrow standards

The **Figure 3.15** shows the relation between the evolution of the experimental molecular weights and the dispersity in each sequential RAFT polymerisation. The ability of the chain extension indicates the presence of the ω-chain ends confirming the living character of this process.

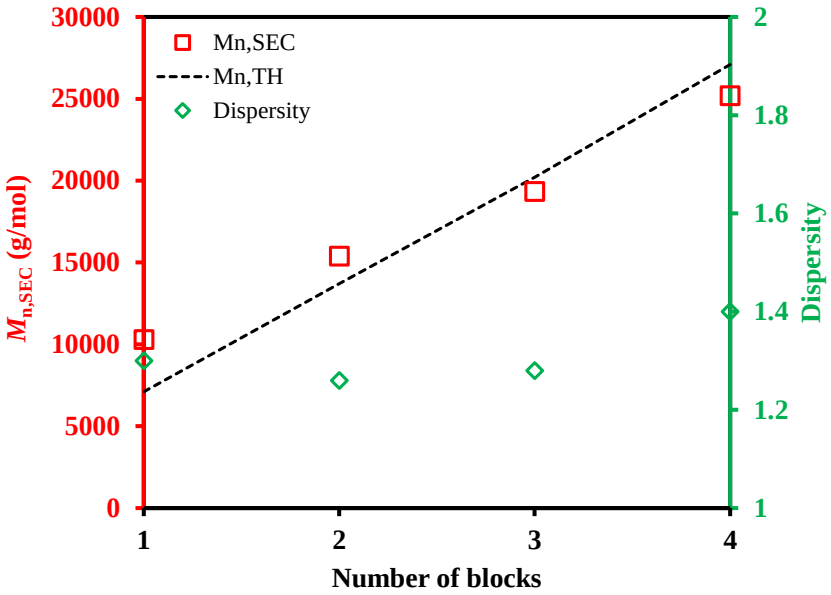

Figure 3.15: THF-SEC data for synthesis of sequential addition of BMA monomer. Evolution of experimental molar mass ($M_{n,SEC}$) and dispersity ($Đ$) *versus* the number of blocks for each successive block in the preparation p(**BMA**)$_{50}$-*b*-p(**BMA**)$_{50}$-*b*-p(**BMA**)$_{50}$-*b*-p(**BMA**)$_{50}$ mediated by BMDPT RAFT agent

3.3. Conclusions

A full kinetic study of methacrylate polymerisation *via* RAFT with BMDPT as chain transfer agent (CTA) is reported. Poor control of the methacrylate polymerisation ($Đ \geq 1.2$) using this CTA was supported by the determination of the chain transfer constant using a Mayo plot, obtaining a value of chain transfer constant below 1. Optimal control of the polymerisation was reached by employing a semi-batch process to yield well-defined multiblock copolymers, exhibiting narrow molecular weight distributions ($Đ \approx 1.28$) with different chain lengths and different methacrylate monomers. Subsequently, a tetrablock copolymer of BMA was easily synthesised maintaining excellent molar mass

control and narrow distributions. Proof of the feeding concept was finally established by scaling the methacrylate diblock copolymer to large scale, whereby 300 g in 50 % w/w of polymer was produced.

3.4. Experimental

3.4.1. Materials

DMAEMA (hydroquinone stabilizer, ≥ 99.0%, Merck), lauryl methacrylate (Sigma-Aldrich, ≥ 98%), benzyl methacrylate (Sigma-Aldrich, ≥ 96%), methyl methacrylate (Sigma-Aldrich, ≥ 98%), 2-(Dimethylamino) ethyl methacrylate (Sigma-Aldrich, ≥ 98%), Butyl acetate (Chromasolv plus, 99.7 %), propylene glycol monoethyl ether acetate (Sigma-Aldrich, 99.5%), Dimethyl2,2'-azobis(2-methylpropionate) (V601,Wako) Azobis(cyclohexanecarbonitrile) (Vazo-88, 98%, Aldrich) were used as purchased. Butyl-2-methyl-2-[(dodecylsulfanylthiocarbonyl) sulfanyl] propionate (BMDPT, Lubrizol, 70 %). 1,1'-Methyl-4-cyano-4-(dodecylthiocarbonothioylthio)pentanoate (MCTP, Boron molecular, > 99%) were used as received.

3.4.2. Methods

- **Proton Nuclear Magnetic Resonance (^{1}H NMR) spectroscopy**

NMR (^{1}H and ^{13}C) were recorded on a Bruker AV-300 and DPX-500 in deuterated chloroform ($CDCl_3$) or DMSO-d_6. Chemical shift values (δ) are reported in ppm. The residual proton signal of the solvent is used as internal standard ($CDCl_3$, δ = 7.26 or δ = 2.5 for DMSO-d_6).

- **Determination of $DP_{n,targeted}$ and monomer conversion**

Monomer conversion (p) were calculated from ^{1}H NMR data using **equation 3.4:**

$$p = \frac{[M]_0 - [M]_t}{[M]_0} = 1 - \frac{[M]_t}{[M]_0} = 1 - \frac{\frac{\int I_{5.5-6.75\ ppm}}{\int I_a}}{DP_{n,targeted}}$$

Where $[M]_0$ and $[M]_t$ are the concentrations of the monomer at time 0 and at time t, respectively, $\frac{\int I_{5.5-6.75\ ppm}}{\int I_a}$ is the integral for the vinyl protons of the monomer, $DP_{n,targeted}$ is the number average degree of polymerisation targeted and $\int I_a$ is the integral of the two protons belonging to the CH_2 of the acrylate (-O-**CH_2**-CH_2).

- **Determination of $M_{n,TH}$**

The theoretical number-average molar mass ($M_{n,TH}$) is calculated using **equation 3.5**:

$$M_{n,TH} = \frac{[M]_0 p [M]_M}{[CTA]_0} + M_{CTA}$$

Where $[M]_0$ and $[CTA]_0$ correspond to the initial concentrations (in mol/L) of monomer and chain transfer agent respectively; p is the monomer conversion as determined by equation 1, M_M and M_{CTA} are the molar masses (g/mol) of the monomer and chain transfer agent.

➢ Size Exclusion Chromatography (SEC)

Number-average molar masses ($M_{n,SEC}$) and dispersity values ($Đ$) distributions were measured using size exclusion chromatography with THF as an eluent. The THF Agilent 390-LC MDS instrument was equipped with differential refractive index (DRI), viscometry (VS), dual angle light scatter (LS) and two wavelength UV detectors. The system was equipped with 2 x PolarGel Mixed C columns (300 x 7.5 mm) and a PLgel 5 µm guard column. The eluent is THF with 2 % TEA(triethyl amine) and 0.01 wt./ V% BHT (butylated hydroxytoluene) additives. Samples were run at 1 mL/min at 30 °C. Poly(methyl methacrylate) standards in rang of 2.0 x 10^2 g/mol to 2.0 x 10^6 g/mol was used to calibrate SEC system.. Analyte samples were filtered through a polytetrafluoethylene (PTFE) membrane with 0.22 μm pore size before injection. The calibration is setup by using a flow rate marker with a third-order polynomial in the elution volume. Respectively, experimental molar mass ($M_{n,SEC}$) and dispersity ($Đ$) values of synthesized polymers were determined by conventional calibration using Agilent GPC/SEC software.

➢ Calculation of the Theoretical Number Fraction of Living Chains (*L*)

The number fraction of living chains was determined by the following **Equation 6:**

$$L\ (\%) = \frac{[\mathrm{CTA}]_0}{[\mathrm{CTA}]_0 + 2.f.[\mathrm{I}]_0.\left(1-e^{-kdt}\right).\left(1-\frac{fc}{2}\right)} \qquad \textbf{(3.6)}$$

For the system butyl acetate/Vazo-88 / 90 ˚C, we considered: $k_{d(\text{Vazo-88,90 }^{\circ}\text{C})}$ = 1.9254 x $10^{-5}s^{-1}$ with Ea = 154.1 KJ/mol.K. For the system butyl acetate/ V-601 / 70 ˚C the constant of dissociation (k_d) is similar to Vazo-88 at 90 ˚C with Ea = 131.2 KJ/mol.K.

3.4.3. General synthetic procedures

- **Diblock copolymer synthesis**

Batch polymerisation of pDMAEMA$_{50}$: For a typical polymerisation in which [DMAEMA]: [BMDPT]: [I] = 50: 1: 0.1 , DMAEMA (50 eq, 1g, 6.3 mmol), BMDPT (1.0 eq, 0.054 g, 0.12 mmol), Vazo-88 (0.00311 g, 0.013 mmol, 63 µL (50 mg/mL)) and 1 mL of butyl acetate solvent are charged with a magnetic stirring bar into a vial and degassed for 10 min under nitrogen. Then, the vial is placed in oil bath at 90 ˚C and stirred overnight. $M_{n,SEC}$ = 8200 g/mol , $Đ$ = 1.31 (THF-SEC, triple detection). ^{1}H-NMR ($CDCl_3$, 400 MHz, ppm): 4,21 (m, 2H,-C(O)O-C**H$_2$**-CH_2-NMe_2), 2.65 (m, 2H, ,-C(O)O-CH_2-C**H$_2$**-NMe_2), 2.3 (s, 6H, -C(O)O-CH_2-CH_2-N**Me$_2$**), 2.1 – 0.9 (m, backbone).

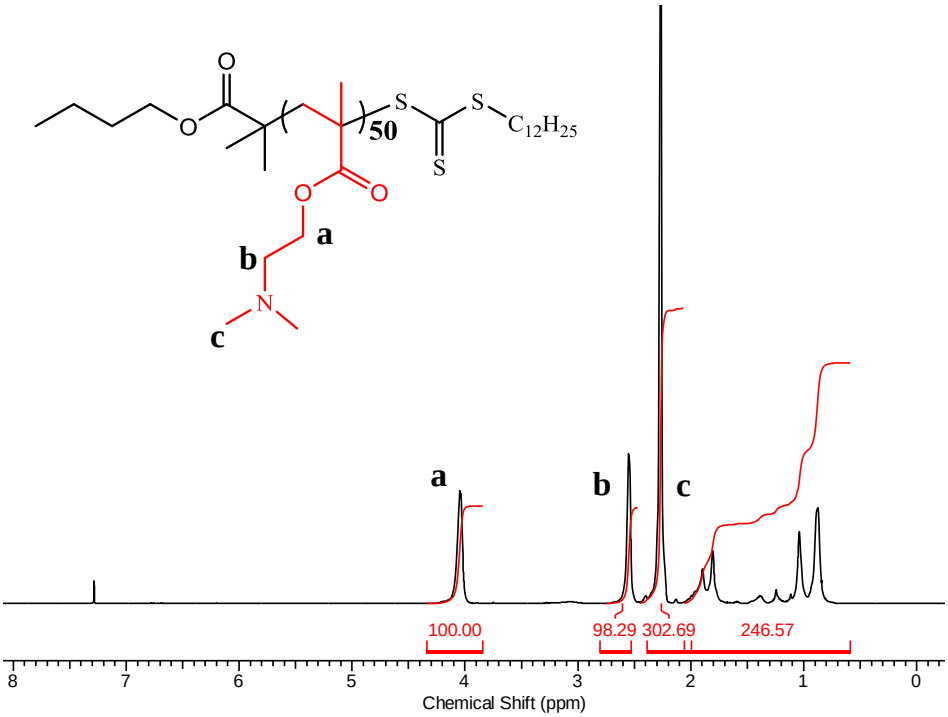

Figure 3.16: ^{1}H NMR of p(DMAEMA)$_{50}$ synthesised with BMDPT RAFT agent in butyl acetate solvent at 90˚C with [DMAEMA]$_0$ = 3 M and [BMDPT]$_0$ / [Vazo88]$_0$ = 10.Spectrum run in $CDCl_3$.

- **Semi-batch polymerisation of poly(BMA$_{100}$)-*block*-poly(DMAEMA$_{50}$):**

For a typical polymerisation in which [BMA]: [DMAEMA]: [BMDPT]: [I] = 100: 50: 1: 0.1, BMA (100 eq, 0.5 g, 3.4 mmol), BMDPT RAFT agent (1.0 eq, 0.015 g, and 0.035 mmol), Vazo-88 (0.0008 g, 0.0035 mmol, 57 µL (20 mg/mL) and 0.580 mL of butyl acetate are charged into a flask with a magnetic stirring bar and degassed for 10 min. In parallel, BMA (50 eq, 0.275 g) is added in a separate vial, sealed with a septum and bubbled under nitrogen for 10 min. Then, BMA is introduced *via* an automatic syringe pump for 4 hours using a Hamilton gas-tight glass syringe with a rate of 0.25 ml/h. The reaction mixture is placed in a thermostated oil bath set at the desired temperature for 24 hours. $M_{n,SEC}$ = 22100 g/mol , $Đ$ = 1.38 (THF-SEC, triple detection).

^{1}H-NMR ($CDCl_3$, 400 MHz, δ/ppm): δ = 4.3 (m, 2H,-C(O)O-C**H$_2$**-CH_2-NMe_2), 4.1 (m, 2H,-C(O)O-C**H$_2$**-CH_2-CH_2-CH_3), 2.53 (m, 2H, ,-C(O)O-CH_2-C**H$_2$**-NMe_2), 2.3 (s, 6H, -C(O)O-CH_2-CH_2-N**Me$_2$**), 1.9 – 0.9 ppm (m, backbone)

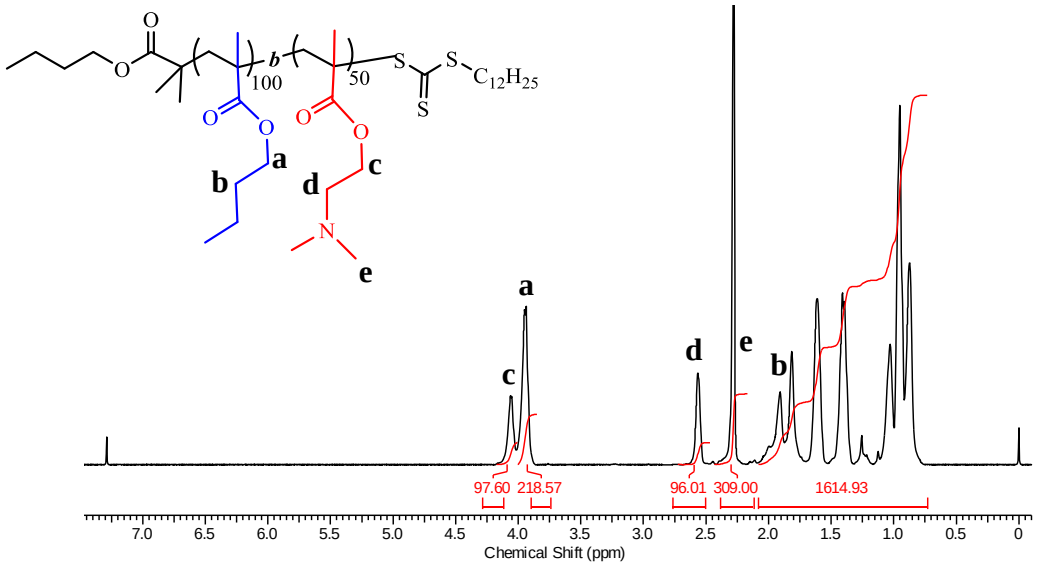

Figure 3.17: ^{1}H NMR of p(BMA)$_{100}$-*b*-p(DMAEMA)$_{50}$ synthesised with BMDPT RAFT agent in butyl acetate solvent at 90˚C with $[DMAEMA]_0$ = 3 M and $[BMDPT]_0$ / $[Vazo88]_0$ = 10. Spectrum run in $CDCl_3$.

- Synthesis of a sequential methacrylate addition

The synthesis of sequential addition of BMA block copolymer in a semi-batch mode is performed in the similar condition previously established. BMA (50 eq, 1.0 g, 7.0 mmol) is added in a vial and degassed under nitrogen. BMDPT RAFT agent (1.0 eq, 0.059 g, and 0.140 mmol), Vazo-88 (0.0034 g, 0.0140 mmol, 69 µL (50 mg/mL) and 1.2 mL of butyl acetate are charged into a flask with a magnetic stirring bar and degassed for 10 min.

Then, the vial is placed in an oil bath set up at 90 ˚C while BMA is added to the vial by using the automatic syringe pump. The vial is removed from the oil bath and cooled to room temperature. A high monomer conversion (> 95 %) is confirmed by ^{1}H NMR in $CDCl_3$ and dispersity ($Đ$ = 1.21) are determined by SEC in THF. The chain extension of the homopolymer is immediately conducted with an addition by feeding of BMA (50 eq, 1.0 g, 7.0 mmol) prior degassed. A constant volume of 2 ml of butyl acetate and a volume of 35 µL (50 mg/mL) of Vazo-88 are added between each block. $M_{n,SEC}$ = 25200 g/mol , $Đ$ = 1.40 (THF-SEC, triple detection). ^{1}H-NMR ($CDCl_3$, 400 MHz, δ/ppm): δ = 4.1 (m, 2H,-C(O)O-C**H$_2$**-CH_2-CH_2-CH_3), 2.05 (m, 2H,-C(O)O-CH_2-C**H$_2$**- CH_2-CH_3), 1.8 (m, 2H, C(O)O-CH_2-CH_2- **CH$_2$**-CH_3), 1.85 – 0.9 ppm (m, backbone)

3.5. References

1. Braunecker, W. A.; Matyjaszewski, K. *Progress in Polymer Science* **2007,** *32* (1), 93-146.

2. Barner-Kowollik, C.; Vana, P.; Davis, T. P.; Matyjaszewski, K.; Davis, T. P. 2002; p 187.

3. Zetterlund, P. B.; Kagawa, Y.; Okubo, M. *Chemical Reviews* **2008,** *108* (9), 3747-3794.

4. Odian, G. In *Principles of Polymerization*, John Wiley & Sons, Inc.: 2004; pp 198-349.

5. Chiefari, J.; Mayadunne, R. T. A.; Moad, C. L.; Moad, G.; Rizzardo, E.; Postma, A.; Thang, S. H. *Macromolecules* **2003,** *36* (7), 2273-2283.

6. Chong, Y. K.; Krstina, J.; Le, T. P. T.; Moad, G.; Postma, A.; Rizzardo, E.; Thang, S. H. *Macromolecules* **2003,** *36* (7), 2256-2272.

7. Krstina, J.; Moad, C. L.; Moad, G.; Rizzardo, E.; Berge, C. T. *Macromol. Symp.* **1996,** *111*, 13.

8. Moad, G.; Chiefari, J.; Chong, Y. K.; Krstina, J.; Mayadunne, R. T. A.; Postma, A.; Rizzardo, E.; Thang, S. H. *Polym. Int.* **2000,** *49*, 993.

9. Krstina, J.; Moad, G.; Rizzardo, E.; Winzor, C. L.; Berge, C. T.; Fryd, M. *Macromolecules* **1995,** *28*, 5381.

10. Monteiro, M. J.; de Barbeyrac, J. *Macromolecules* **2001,** *34*, 4416.

11. Krasia, T. C.; Patrickios, C. S. *Macromolecules* **2006,** *39*, 2467.

12. Ilchev, A.; Pfukwa, R.; Hlalele, L.; Smit, M.; Klumperman, B. *Polymer Chemistry* **2015,** *6* (46), 7945-7948.

13. Cao, G.-P.; Zhu, Z.-N.; Zhang, M.-H.; Yuan, W.-K. *Journal of Applied Polymer Science* **2004,** *93* (4), 1519-1525.

14. Gody, G.; Maschmeyer, T.; Zetterlund, P. B.; Perrier, S. *Nature Communications* **2013,** *4*, 2505.

15. Gody, G.; Maschmeyer, T.; Zetterlund, P. B.; Perrier, S. *Macromolecules* **2014,** *47* (2), 639-649.

16. Fournier, D.; Hoogenboom, R.; Thijs, H. M. L.; Paulus, R. M.; Schubert, U. S. *Macromolecules* **2007,** *40* (4), 915-920.

17. Sordi, M. L. T.; Riegel, I. C.; Ceschi, M. A.; Müller, A. H. E.; Petzhold, C. L. *European Polymer Journal* **2010,** *46* (2), 336-344.

18. Barner-Kowollik, C.; Beuermann, S.; Buback, M.; Castignolles, P.; Charleux, B.; Coote, M. L.; Hutchinson, R. A.; Junkers, T.; Lacik, I.; Russell, G. T.; Stach, M.; van Herk, A. M. *Polymer Chemistry* **2014,** *5* (1), 204-212.

19. Haehnel, A. P.; Schneider-Baumann, M.; Hiltebrandt, K. U.; Misske, A. M.; Barner-Kowollik, C. *Macromolecules* **2013,** *46* (1), 15-28.

20. Malavašič, T.; Osredkar, U.; Anžur, I.; Vizovišek, I. *Journal of Macromolecular Science: Part A - Chemistry* **1988,** *25* (1), 55-64.

21. Favier, A.; Charreyre, M. T. *Macromol. Rapid Commun.* **2006,** *27*, 653.

22. Chiefari, J.; Mayadunne, R. T. A.; Moad, C. L.; Moad, G.; Postma, A.; Rizzardo, E.; Postma, A.; Skidmore, M. A.; Thang, S. H. *Macromolecules* **2003,** *36*, 2273.

23. Benaglia, M.; Rizzardo, E.; Alberti, A.; Guerra, M. *Macromolecules* **2005,** *38* (8), 3129-3140.

24. Moad, G.; Chiefari, J.; Mayadunne, R. T. A.; Moad, C. L.; Postma, A.; Rizzardo, E.; Thang, S. H. *Macromolecular Symposia* **2002,** *182* (1), 65-80.

25. Moad, G.; Rizzardo, E.; Thang, S. H. *Australian Journal of Chemistry* **2009,** *62* (11), 1402-1472.

26. Chiefari, J.; Chong, Y. K.; Ercole, F.; Krstina, J.; Jeffery, J.; Le, T. P.; Mayadunne, R. T. A.; Meijs, G. F.; Moad, C. L.; Moad, G.; Rizzardo, E.; Thang, S. H. *Macromolecules* **1998,** *31*, 5559.

27. Mueller, A. H. E.; Zhuang, R.; Yan, D.; Litvinenko, G. *Macromolecules* **1995,** *28* (12), 4326-4333.

28. Moad, G.; Rizzardo, E.; Thang, S. H. *Accounts of Chemical Research* **2008,** *41* (9), 1133-1142.

29. Monteiro, M. J.; Adamy, M. M.; Leeuwen, B. J.; van Herk, A. M.; Destarac, M. *Macromolecules* **2005,** *38* (5), 1538-1541.

30. Destarac, M.; Charmot, D.; Franck, X.; Zard, S. Z. *Macromolecular Rapid Communications* **2000,** *21* (15), 1035-1039.

31. Destarac, M.; Brochon, C.; Catala, J.-M.; Wilczewska, A.; Zard, S. Z. *Macromolecular Chemistry and Physics* **2002,** *203* (16), 2281-2289.

32. Fischer, H. In *Free Radicals in Biology and Environment*, Minisci, F., Ed. Springer Netherlands: Dordrecht, 1997; pp 63-78.

33. Adamy, M.; van Herk, A. M.; Destarac, M.; Monteiro, M. J. *Macromolecules* **2003,** *36* (7), 2293-2301.

34. Mayo, F. R. *Journal of the American Chemical Society* **1968,** *90* (5), 1289-1295.

35. Clay, P. A.; Gilbert, R. G. *Macromolecules* **1995,** *28* (2), 552-569.

36. Beuermann, S.; Buback, M.; Davis, T. P.; Gilbert, R. G.; Hutchinson, R. A.; Olaj, O. F.; Russell, G. T.; Schweer, J.; van Herk, A. M. *Macromolecular Chemistry and Physics* **1997,** *198* (5), 1545-1560.

37. Moad, G.; Rizzardo, E.; Thang, S. H. *Polymer* **2008,** *49* (5), 1079-1131.

38. Litvinenko, G.; Müller, A. H. E. *Macromolecules* **1997,** *30* (5), 1253-1266.

39. Goto, A.; Fukuda, T. *Macromolecules* **1997,** *30*, 4272.

40. Mayo, F. R. *Journal of the American Chemical Society* **1943,** *65* (12), 2324-2329.

41. Barner-Kowollik, C.; Quinn, J. F.; Nguyen, T. L. U.; Heuts, J. P. A.; Davis, T. P. *Macromolecules* **2001,** *34*, 7849.

42. Haddleton, D. M.; Morsley, D. R.; O'Donnell, J. P.; Richards, S. N. *Journal of Polymer Science Part A: Polymer Chemistry* **1999,** *37* (18), 3549-3557.

43. Zamfir, M.; Lutz, J.-F. *Nature Communications* **2012,** *3*, 1138.

44. Vandenbergh, J.; Reekmans, G.; Adriaensens, P.; Junkers, T. *Chemical Communications* **2013,** *49* (88), 10358-10360.

45. Badi, N.; Lutz, J.-F. *Chemical Society Reviews* **2009,** *38* (12), 3383-3390.

46. Boyer, C.; Soeriyadi, A. H.; Zetterlund, P. B.; Whittaker, M. R. *Macromolecules* **2011,** *44* (20), 8028-8033.

47. Anastasaki, A.; Waldron, C.; Wilson, P.; Boyer, C.; Zetterlund, P. B.; Whittaker, M. R.; Haddleton, D. *ACS Macro Letters* **2013,** *2* (10), 896-900.

Chapter 4: Synthesis of SMA and subsequent modification of the polymer backbone

In this chapter, Reversible Addition-Fragmentation Chain transfer (RAFT) polymerisation has been employed to synthesise amphiphilic diblock and multiblock copolymers using poly(nbutyl acrylate) as the hydrophobic block and styrene-alternating-maleic anhydride (SMA) as the hydrophilic block in acetate solvent. Under optimised conditions, a well-defined diblock and tetrablock copolymer were obtained (Đ = 1.23) with a high monomer conversion (> 95 %) achieved throughout all the iterative monomer additions. The hydrophilic character of the diblock copolymer is brought after modification of SMA copolymer into SMI (styrene-alternating-maleimide) using the small organic molecule di(methylaminopropyl)amine. The use of a primary amine leads the formation of an amide compound (poly(nBA)-block-poly(SMAD)) followed by an imide product (poly(nBA)-block-poly(SMI)) after dehydration. The alternating character of maleic anhydride (MA) copolymerised with styrene is determined by ^{1}H and ^{13}C NMR, and the further modification of the polymer backbone using amines is characterised by infra-red (IR), proton NMR (^{1}H NMR) and elemental analysis (EI). The data of efficiency of both amphiphilic diblock copolymers on carbon black dispersion are reported in Chapter 5.

4.1. Introduction

The copolymer styrene-maleic anhydride (SMA) is produced on an industrial scale since many years for diverse applications.[1] Homopolymerisation of maleic anhydride (MA) is not possible due to the high steric hindrance of the radical.[2,3] The copolymerisation of styrene (S) and maleic anhydride (MA) has been established since 1940, however, the mechanism concerning the alternating behaviour between these two monomers is relatively unknown, and many theories have been explored.[4] Several controlled radical polymerisation techniques (such as ATRP, nitroxide-mediated polymerisation, and RAFT) have emerged in the past decade, allowing for better control and more sophisticated polymer architectures. The copolymerisation of styrene-*alternating*-maleic anhydride (SMA) using Atom Transfer Radical Polymerisation (ATRP) is not straightforward due to highly reactive monomers which preferentially interact with the copper complex, however, using nitroxide-mediated polymerisation at high temperature, the synthesis can be successfully achieved.[5,] However, the final composition of SMA is directly depend on the temperature of the polymersisation. NMP technique required a high temperature reaction (80 – 120 ˚C) which leads a formation of mixture of poly(SMA) and poly(styrene).[6] A lower temperature can be used in Reversible Addition-Fragmentation chain Transfer (RAFT) polymerisation which makes this polymerisation technique more appropriate choice to polymerise SMA in different solvents under mild conditions.[7,6,8,9] The process of RAFT polymerisation involves insertion of the monomer into the C-S bond of a tri-thiocarbonyl moiety (known as the Chain Transfer Agent). This gives a yellow-red colour to the polymer and allows it to behave as a chromophore with a wavelength maxima at 309 nm.

The presence of this tri-thiocarbonyl in the polymer chain at the end of the polymerisation means the reaction can be halted or restarted readily, and gives the living characteristic to this technique. This allows for the synthesis of complex architectures (for example multiblock, star and comb). Alternating copolymers provide a wide range of applications and are used in industry for their diverse range of properties.

Indeed, the high thermal stability of maleic anhydride (MA) copolymerised with alkyl vinyl ether (AVE)[10] or styrenic polymers allows them to find application as polymer blend compatibilisers and adhesion promoters.[11,12,13,14] The high sensitivity of maleic anhydride towards nucleophilic reagents (amines, thiol, alcohols, and water) allows for the synthesis of functional SMA. This modification process has been reported in the literature[15,16,17] and expands applications towards anti-viral agents and drug nanocarriers.[18,19,20,21,22] As a pigment stabiliser, the polymer backbone is required to have a specific functional moiety for good surface affinity, such as a tertiary amine. Maleic anhydride can be easily reacted with an amine compound, yielding the required tertiary amine in the ring as described in **Scheme 4.1**. This method was first developed by Dupont[23] in the 1950's and is currently the main route used to prepare polyimides in polar aprotic solvents.

Scheme 4.1 illustrates the general mechanism of the reversible ring opening and closing using an amine for maleimide formation. Maleimide formation requires a two step procedure involving the use of an amine or alcohol (Mitsunobu reaction). The poly(maleic amido acid) is formed *via* nucleophilic attack by the amine group on the carbon of the anhydride group. This step is exothermic and is carried out at low temperature.[24, 25]

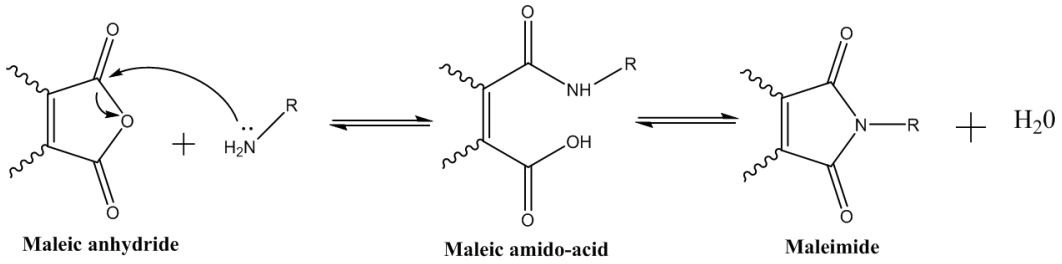

Scheme 4.1: Mechanism of maleic anhydride ring opening using a primary amine to form an maleimide

The process of maleic anhydride modification was used after polymerisation of poly(SMA). It is necessary to point out the high sensitivity of the trithiocarbonate. Indeed, the C–S bond can be cleaved in the presence of nucleophilic compounds, ionic reducing agents and UV radiation/thermolysis, causing it to degrade. Consequently, the primary and secondary amines, being good nucleophiles, can react by aminolysis with the CTA, halting the polymerisation. Few methods regarding the cleavage of the thiocarbonylthio group were developed (**Scheme 4.2**).[26, 27, 28]

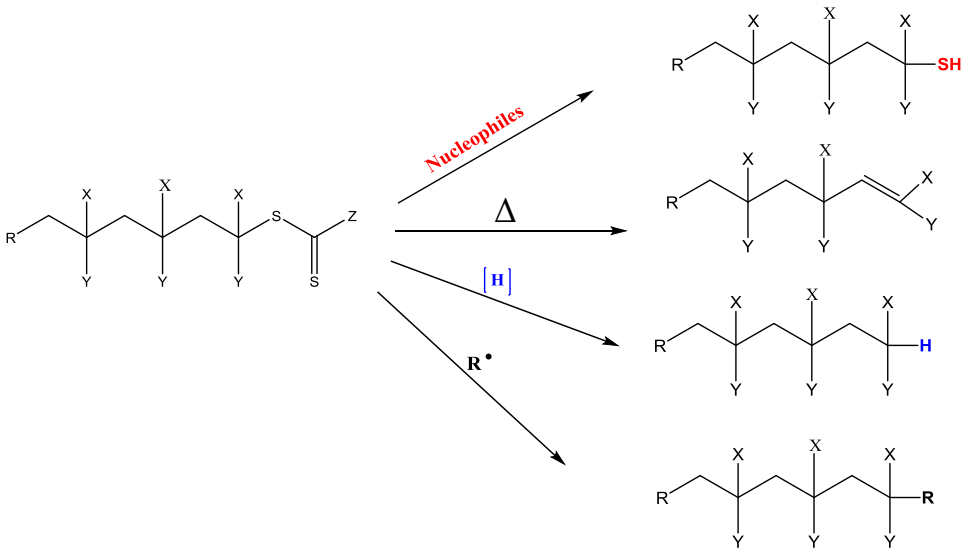

Scheme 4.2: Several processes of RAFT end-group removal using nucleophiles compound, temperature, reducing agent or radical.[26]

This chapter describes the use of RAFT polymerisation to polymerise a range of well-defined diblock and multiblock copolymers of poly(styrene-*alternating*-maleic anhydride) block *n*-butyl acrylate in a one pot synthesis. For the Carbon black dispersion, the acrylate block will dissolve in organic media, while the pSMA, after functionalisation, will interact with the pigment surface. Different molecular weights of acrylate were synthesised to study the effect of polymer chain length on pigment interaction. The thermal properties of the homopolymer and multiblock copolymers before and after modification are also reported.

4.2. **Results and Discussion**

4.2.1. Synthesis of p(SMA) copolymer *via* RAFT polymerisation

An alternating sequence of styrene and maleic anhydride is observed when a 1:1 monomer ratio is used. The reaction is fast and exothermic (ΔH = -81 KJ/mol) and therefore does not require high temperatures, however, it should be noted that a high concentration of maleic anhydride (MA) induces the formation of a gel, explained by a high rate of polymerisation of styrene/maleic anhydride. Belkhira *et al*.[29] determined the kinetics of this copolymerisation by DSC, and established that a molar fraction of MA ($f_{2,0}$ = 0.3) was required to prevent the gel effect. To overcome the viscosity challenges, in industry this reaction is performed above 160 ˚C in a reactor. The kinetics studies of SMA copolymerisation using RAFT polymerisation was reported by Chernikova.[30] It has been shown that the rate of the polymerisation decreased dramatically when the proportion of styrene is increased.

For instance, 1.5 hours are required to achieved 40 % of monomer conversion in presence of 50 mol% of styrene while 9 h are needed with 90 mol% of styrene in the initial composition. Thus, the propagation rate is strongly affected by the monomer composition but also by the self-initiation of the styrene monomer.[31]

In the current study, polymerisations were initially carried out in an acetate solvent to determine the optimal conditions. Given that a concentration of MA above 1.75 M induces gel formation, all the following polymerisations were performed at 1 M (**Scheme 4.3**). The kinetic study and the alternating behaviour of SMA were studied in MPA solvent and reported.

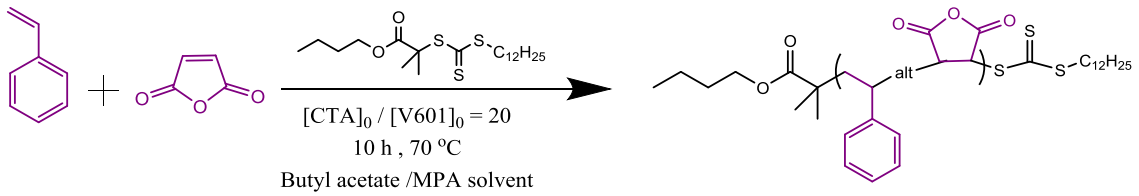

Scheme 4.3: General scheme of styrene and maleic anhydride homopolymerisation using BMDPT RAFT agent in presence of V601 as azoinitiator at 70 ˚C in acetate solvent

The kinetic studies displayed in a **Figure 4.1 A** revealed a linear behaviour of the $\ln([M]_0/[M]_t)$ *versus* time plot, indicating a first order reaction with respect to monomer concentration. Moreover, a good agreement between the theoretical and experimental molar mass distribution with a low dispersity ($Đ$ < 1.2) throughout the polymerisation (**Figure 4.1 B**).

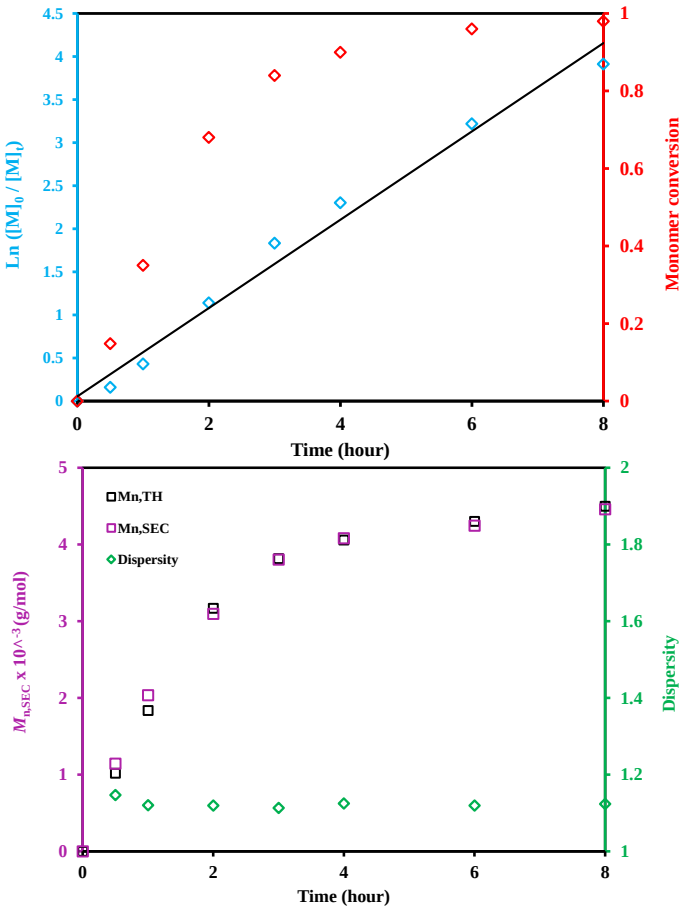

Figure 4.1: Polymerisation kinetics for SMA using BMDPT RAFT agent in MPA solvent at 70 ˚C. Pseudo-first order kinetics (**A**) and evolution of molar mass and molar mass distribution monomer (*Đ*) *versus* time (**B**).

The conversion of styrene and maleic anhydride polymerised is determined by ^{1}H NMR in DMSO-d_6 using 1,3,5-trioxane as internal reference due to the overlapping of the styrenenic aromatic protons (δ = 7.25 -7.3 ppm) and the single peak of maleic anhydride (δ = 7.5 ppm) as shown in **Figure 4.2**.

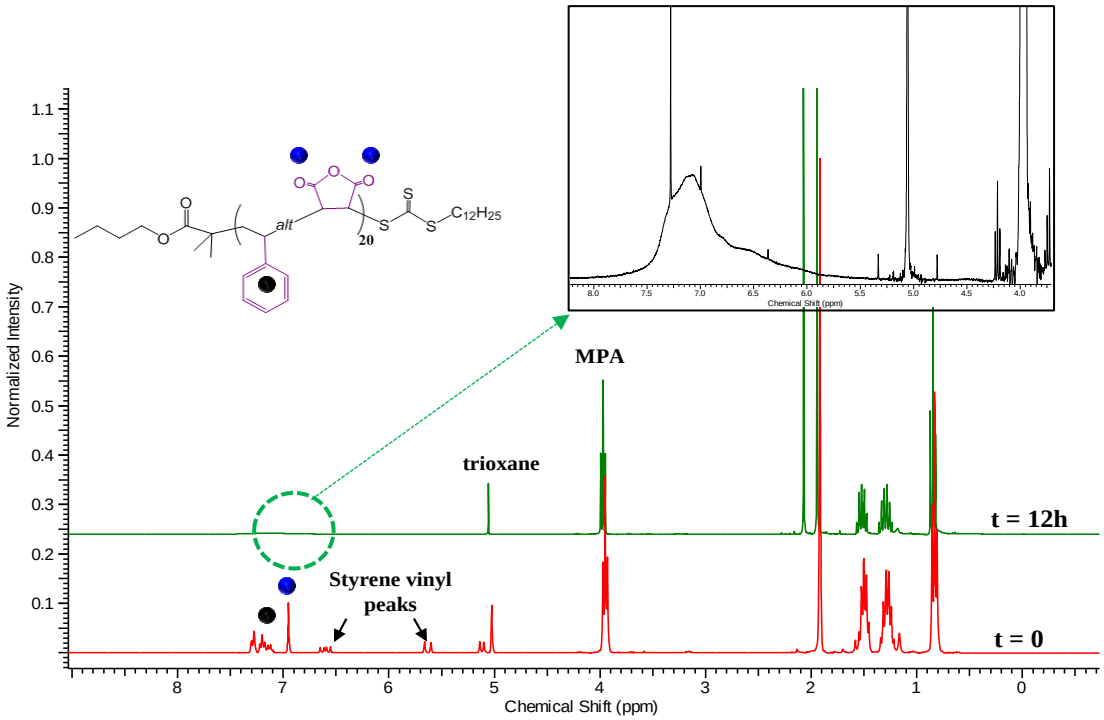

Figure 4.2: Comparison of ^{1}H NMR analysis in DMSO-d_6 for $p(SMA)_{20}$ copolymerisation obtained in MPA solvent using trioxane as internal reference before and after polymerisation

In addition to ^{1}H NMR, ^{13}C NMR can also be used to characterise the structure of the polymer. Characterising alternating blocks of SMA by using ^{13}C NMR has been demonstrated several times in the literature.[6,32,33,34] The determination of the triad sequence distribution between the maleic anhydride and its donor monomers derivatives (styrene, *trans*-stilbene, *α*-methylstyrene) using ^{13}C NMR spectroscopy has been investigated by Ha.[32] In this work, the author compared the position of the chemical shifts of the poly(styrene) homopolymer with diverse copolymer bearing functionalities. The presence of the bulky group ($-CH_3$) or the high electronegativity of the halogens groups have a deshielding effect on the quarternary carbon of the styrene (C7). Different triads have been determined as a marker to characterise the non-alternating (SSS), semi-alternating (SSM) and alternating (SMS) behaviour.

For an alternating sequence, the CH_2 group (**Figure 4.3**, **C1**) on the styrene backbone is expected at δ = 33 - 37 ppm and the aromatic group (**Figure 4.3**, **C7**) peak at δ = 137 - 140 ppm, while for SSM and SSM sequences they appear at δ = 42 - 47 ppm and δ = 145 - 148 ppm respectively. Moreover, the alternating behaviour of the maleic anhydride is demonstrated by the determination of the reactivity ratio.[6]

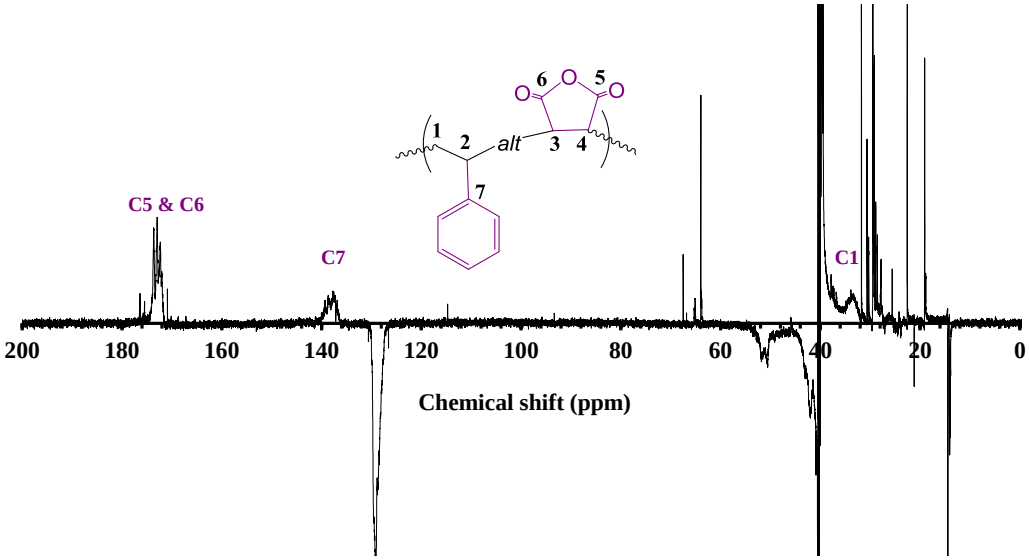

Figure 4.3: ^{13}C NMR analysis of $p(SMA)_{20}$ copolymer in DMSO-d_6 recorded on a Brucker Avance (400 MHz)

Furthermore, MALDI- ToF MS has been used to confirm ther alternating behaviour of SMA copolymers. Matrix-assisted laser desorption ionization (MALDI) is a soft ionization technique producing intact molecular ions. The process of the ionization starts when the matrix in the analyte absorbs a pulsed laser beam. Then, when the matrix is entirely dried, the plate is inserted into a high vaccum which will prevent collision between ions. The energy of the laser absorbed by the matrix is transferred to the analyte molecules which ionized the molecules.

Finally, the ions are accelerated when reached the mass analyser (Time-of-Flight : ToF) *via* an electric field. An overview of the spectrum of $p(SMA)_{20}$ synthesised *via* RAFT polymerisation using BMDPT trithiocarbonate in methoxypropyl acetate solvent is given in **Figure 4.4**. The m/z region between 2000 and 4000 shows a perfect interval of m/z values of 98.06 and 104.14, corresponding to mass units of monomeric styrene and maleic anhydride respectively, thus confirming the alternating composition of $p(SMA)_{20}$ homopolymer. The alternating mass units confirm the alternating structure of SMA. However, a zoom of the m/z region between 2000 and 2750 indicates the presence of three type of populations including a majority of of $p(SMA)_{20}$ at 2464.94 g/mol but also, some defects such as $p(SMA)_9$-*b*-$p(Styrene)_3$ at 2579.9 g/mol or with two styrene on a row like $p(SMA)_{18}$-*b*-$p(Styrene)_2$ at 2469.01 g/mol.

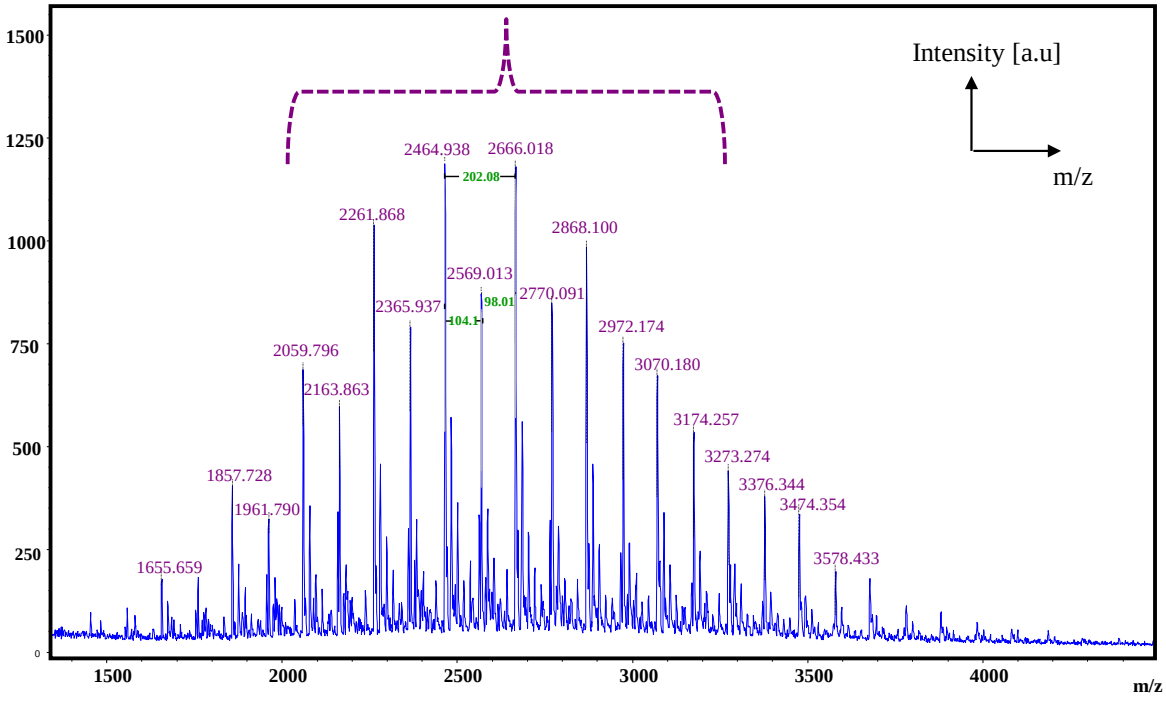

Figure 4.4: MALDI-ToF spectrum of poly $(SMA)_{20}$ is performed using Bruker Daltonic Autoflex Speed with $PEG_{1,500}$ and PEG_{5000} as external calibration

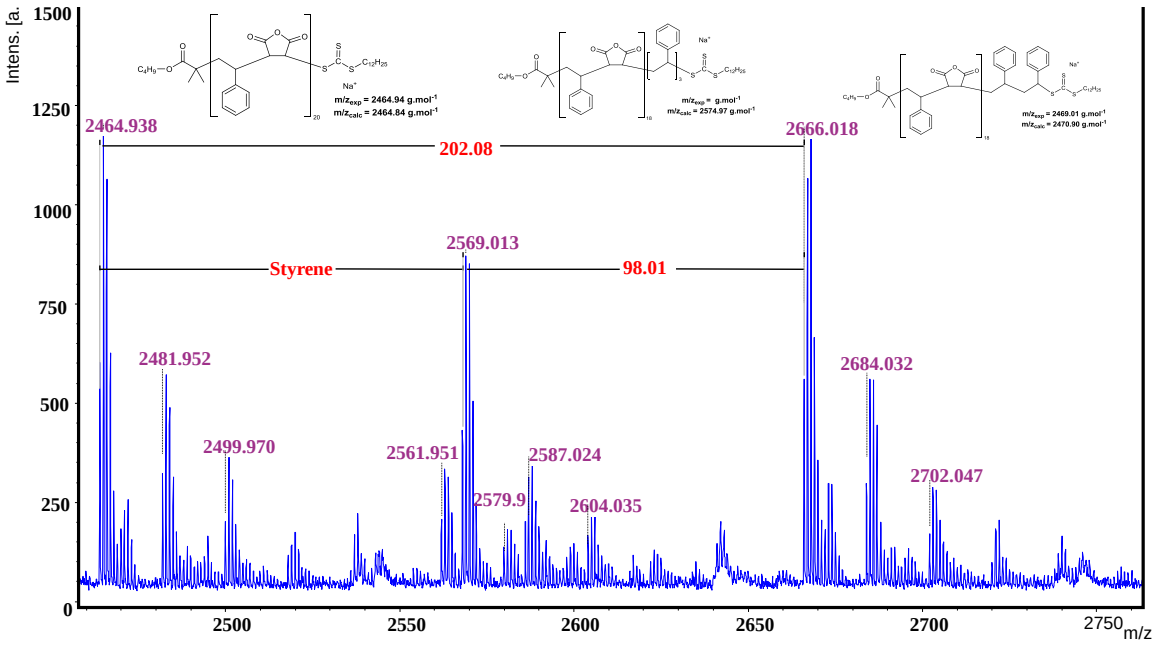

Figure 4.5: MALDI-ToF spectrum of poly $(SMA)_{20}$ between m/z = 2000 and 2750

4.2.2. Synthesis of SMA and *n*-butyl acrylate block copolymer *via* RAFT polymerisation

Sequence controlled multiblock copolymer synthesis in one pot with high conversions and using a wide range of monomers has recently been developed.[35,36,37,33,38,39] Here, this technique was used to prepare diblock and multiblock copolymers of poly (*n*-butyl acrylate)-*block*-poly(SMA).[40,41,42] Interestingly, this work is the first report of a multiblock structure of SMA. The living characteristic of the RAFT process makes it easy to chain extend one block with another. Here, the poly (*n*-butyl acrylate) block was synthesised first and, after reaching full conversion, a mixture of 1:1 SMA was added.

The insertion of a hydrophobic block is directly linked to the dispersion of pigment in organic media.

Indeed, the acrylate block is fully soluble in acetate, thus allowing the styrene-alternating-maleic anhydride block to interact with the pigment surface.

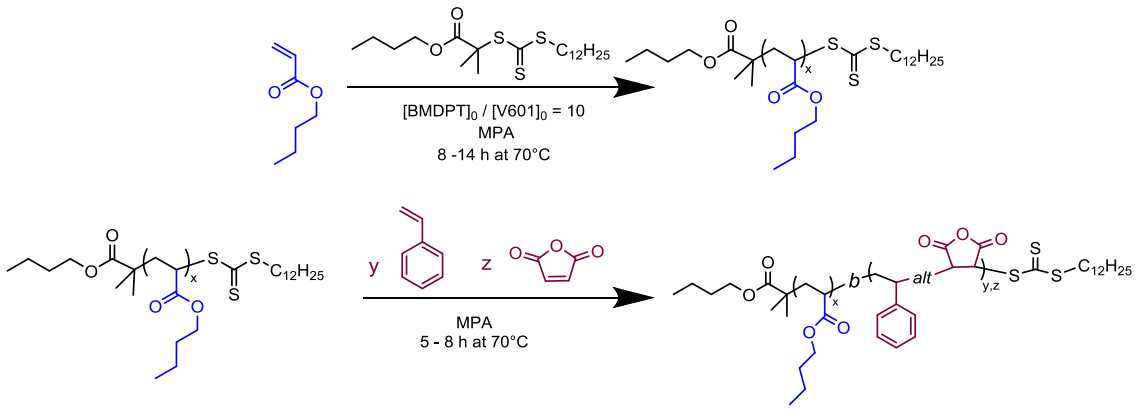

Scheme 4.4: General scheme of p(*n*BA) macroinitiator synthesis and chain extension with SMA mixture in presence of BMDPT RAFT agent using V601 as azoinitiator at 70 ˚C in MPA solvent

The block copolymer synthesis was performed using conditions established previously for acrylate copolymerisation (**Chapter 2**).

A poly (*n*-butyl acrylate) macroCTA was synthesised in the first step, then chain extended with a mixture of styrene and maleic anhydride monomers. The monomer conversion was determined by ^{1}H NMR in $CDCl_3$ for the first block and DMSO-d_6 for the second block. Trioxane was used as an internal reference to determine the conversion for the last block. A near quantitative conversion was reach for each block, with a narrow dispersity and molar mass distribution, as determined by THF-SEC (**Scheme 4.5**).

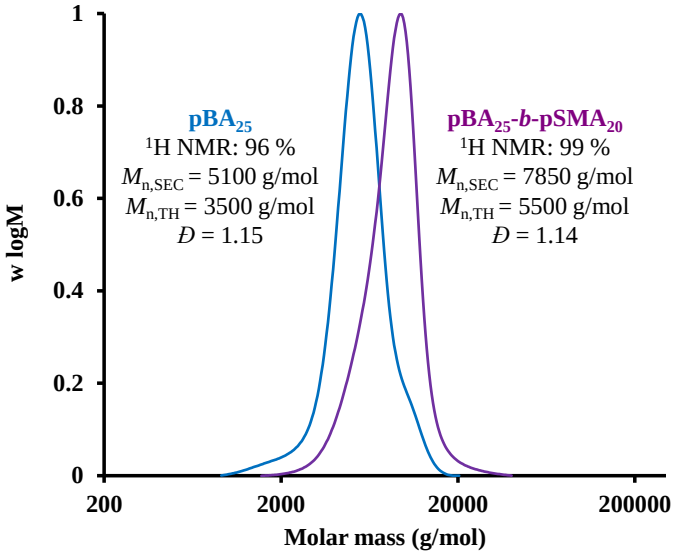

Figure 4.6: Comparison of SEC-THF chromatograms of diblock p(*n*BA)$_{25}$-*block*-p(SMA)$_{20}$. Initial conditions: [*n*BA] : [BMDPT] : [V601] = [25] : [1] : [10] in MPA solvent at 70 ˚C

A monomodal molar mass distribution was observed for both blocks, however, the presence of a small shoulder at high molecular weight suggests the presence of mid-chain branching for butyl acrylate.

The SEC trace shows the success of the chain extension of poly (SMA), suggesting full macroCTA consumption, and displays narrow dispersity ($Đ$ < 1.2).

In order to study the effect of the molecular weight of poly (*n*BA) - *block* - poly (SMA) in a carbon black dispersion, a range of diblock copolymers were synthesised under similar conditions (**Table 4.1**).

Table 4.1: Characterisation data for the poly(*n*BA)-*block*-poly(SMA) copolymer obtained *via* RAFT polymerisation in butyl acetate at 70 ˚C with $[BMDPT]_0$ / $[V601]_0$ = 10

p(SMA)$_x$-*b*-p(*n*BA)$_y$	$M_{n,TH}$[a] (g/mol)	$M_{n,SEC}$ [b] (g/mol)	$Đ$
40-50	10800	13900	1.15
40-80	14640	17700	1.14
40-100	17200	19500	1.2

[a] Determined using **equation 4.4** (experimental section)

[b] Determined using THF-SEC with PMMA narrow standards

After, the success of the diblock copolymer synthesis, we investigated the one pot synthesis of a multiblock copolymer, without purification steps.

4.2.3. Synthesis of p(SMA) and p(*n*BA*)* multiblock copolymer

Applying the conditions established previously (**Chapter 2**) for butyl acrylate ($[BA]_0$ = 3 M, DP = 20, $[BMDPT]_0$ / $[V601]_0$ = 20) and styrene maleic anhydride ($[SMA]_0$ = 1.3 M, DP = 20) in acetate (40 % v/v), a multiblock copolymer of pBA-*block*-pSMA was prepared, achieving high monomer conversion (≥ 95 %) within 14 hours (**Scheme 4.6**).

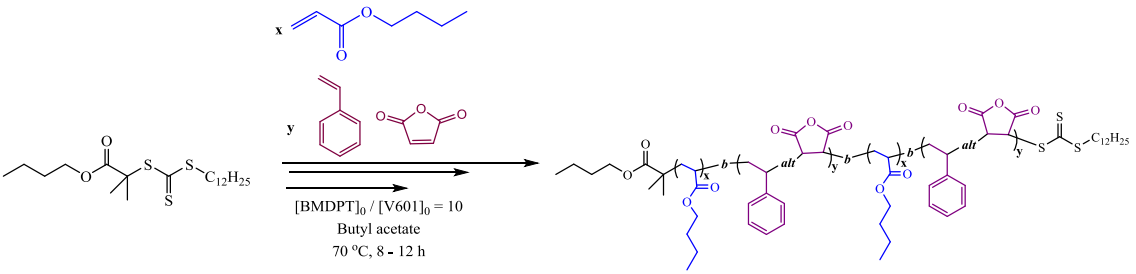

Scheme 4.5: Generalised approaches for preparing multiblock copolymers *via* a sequential addition of *n*BA and SMA in presence of V601 at 70 ˚C in butyl acetate or methoxypropyl acetate.

The SEC molecular weight distribution (**Figure 4.6**) shows successful chain extension for each block, with a low dispersity, however, a small shoulder appears after the chain extension with *n*-butyl acrylate. As explained previously (**Chapter 2**), it is common to observe this shoulder for an acrylate monomer, possibly due to chain transfer to polymer or termination reactions, however, it could also be due to poor reinitation of pSMA with an acrylate.

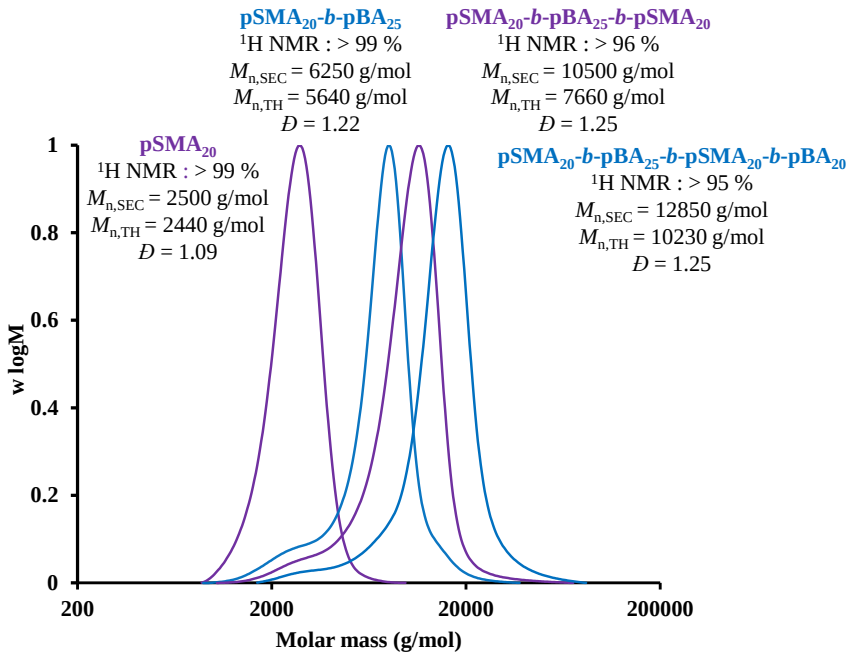

Figure 4.7: SEC-THF chromatograms analysis for p(SMA)$_{20}$ macroinitiator and sequential addition of *n*BA$_{25}$ and SMA$_{20}$ prepared *via* RAFT polymerisation in presence of BMDPT RAFT agent in MPA solvent

The **Figure 4.7** shows a linear evolution of $M_{n,SEC}$ with the number of blocks and a low dispersity ($Đ \approx 1.25$ for the tetrablock) after each chain extension confirming the controlled/living characteristic of the multiblock copolymer polymerisation.

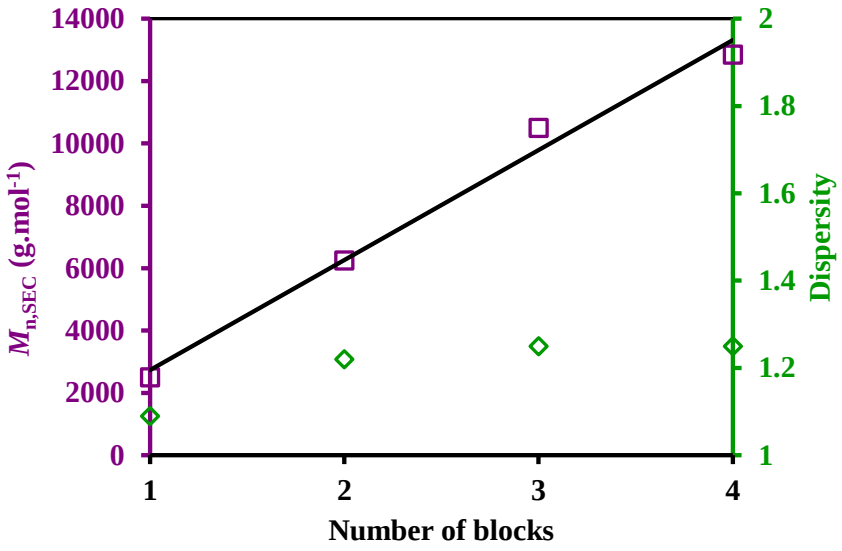

Figure 4.8: THF-SEC data for synthesis of sequential addition of *n*BA_{25} and SMA_{20} monomers. Evolution of experimental molar mass ($M_{n,SEC}$) and dispersity ($Đ$) *versus* the number of blocks for each successive block addition

The low $Đ$ values during each chain extension confirm the polymerisation control (**Figure 4.7**). By using a non-covalent process to coat the surface of a pigment, it is compulsory to have a specific functionality in the polymer, allowing for interaction between the CB surface and the polymer, hence the modification of maleic anhydride in the polymer backbone was performed using a highly reactive amine.

4.2.4. Modification of poly(SMA) into poly (SMAD) in polymer backbone

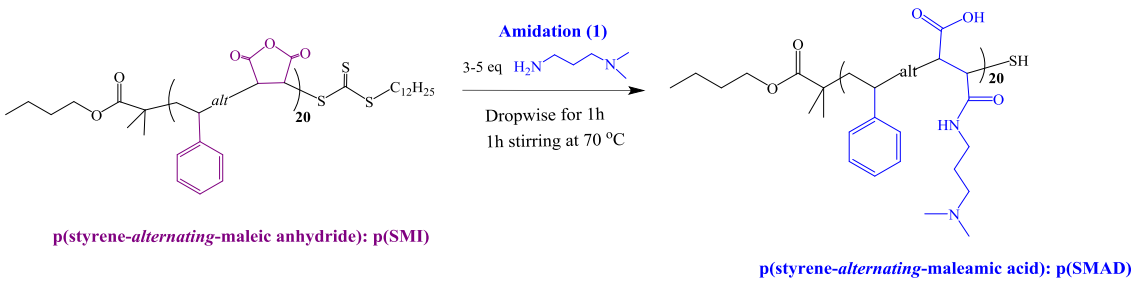

p(styrene-*alternating*-maleic anhydride): p(SMI)

p(styrene-*alternating*-maleamic acid): p(SMAD)

Scheme 4.6*:* First step of pSMA backbone using 3-5 eq of (dimethyl)aminopropylamine at 70 ˚C.

He-Yang Liu *et al*. have studied the mechanism and kinetics of pSMA in presence of aniline in order to prepare a maleimide derivative. They showed the two steps procedures with formation of an acido-amide group after ring opening, and the formation of the corresponding imide after ring closing.[43] The analytical composition of each products is obtained by titration and confirmed by FT-IR measurements. In another paper published by He and coworkers, the equilibrium constant of the ring opening of the MA in presence of the amine in THF is determined at different temperatures (0-200 ˚C) and proved the potential reverse reaction can occurs at high temperature ($k_{(200\ ^\circ C)}$ = 11 L/mol/s). Also, increasing the temperature increased the ring-opening reaction rate.[44] In this chapter, ring opening is performed at mild-temperature reaction (70 ˚C) in MPA solvent to allow the stirring of the polymerisation mixture as a strong gel is formed as soon as the amine is added. Performing this reaction as such low temperature, the reversible reaction can be neglected (**Scheme 4.7**).

The poly(imide) is obtained by heating the reaction mixture at a high temperature, after water removal by Dean Stark apparatus, to yield a yellow powder.

The starting material (pSMA) is slightly yellow due to the presence of the trithiocarbonate. The use of a primary amine induced the cleavage of the end group in the polymer chain yields a white compound. The ^{1}H NMR in DMSO-d_6 in the **Figure 4.9** shows clearly the disappearance of the alkyne chain ($C_{12}H_{25}$) from the RAFT agent present between δ = 1.0 - 2.5 ppm (blue trace) disappears after addition of DMAPAA to form the pSMAD homopolymer, however, the formation of the maleimide after the ring closure exhibits a strong yellow colour which is also observed for the diblock copolymer.

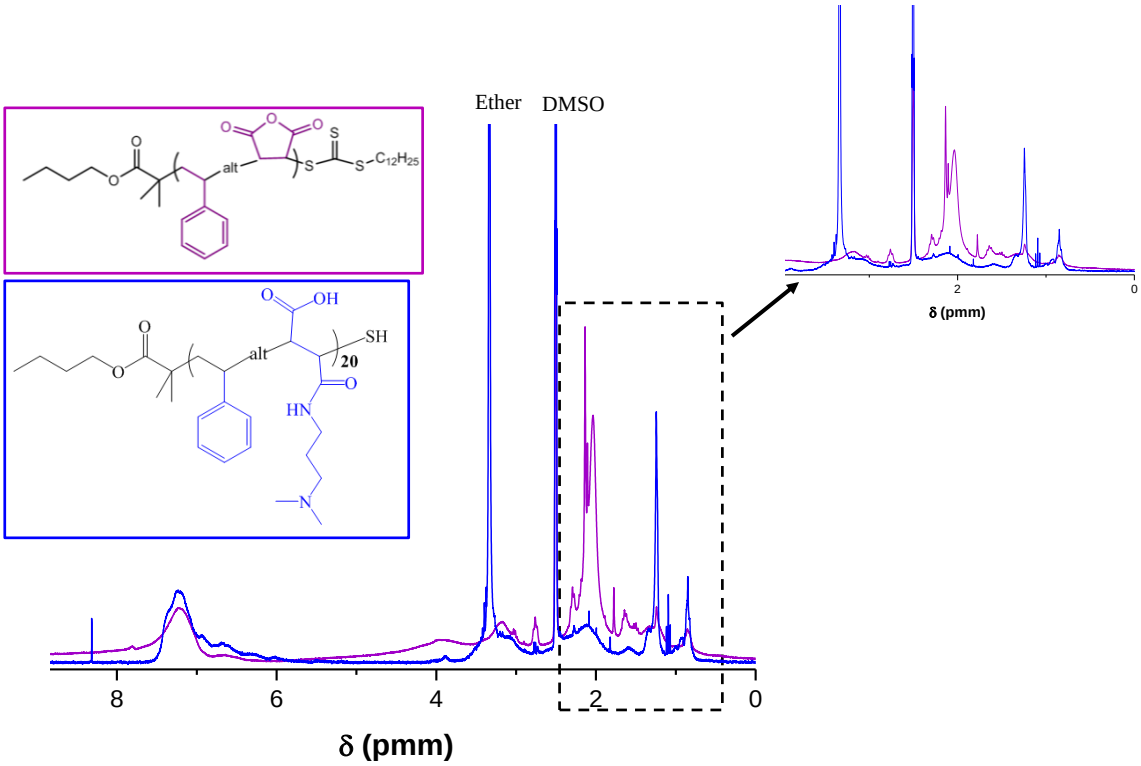

Figure 4.9: ^{1}H NMR analysis of $p(SMA)_{20}$ before and after ring opening using dimethylaminopropyl amine (3-5 eq equiv.) run in a Brucker Avance (400 MHz) in DMSO-d_6

Additionally, a concentrated samples (60 mg of purified polymer in 0.7 mL of DMSO-d_6 solvent) are run in ^{13}C NMR to confirm the ring opening of maleic anhydride.

Figure 4.10, both ^{13}C NMR spectra of $p(SMA)_{20}$ (purple trace) and $p(SMAD)_{20}$ (blue trace) are overlapped. The success of the modification of the polymer backbone is proved by the disappearance of the peak characteristic of the maleic anhydride between 170 – 180 ppm. However, a small shoulder seems to be present and can be attributed to a few units of unreacted maleic anhydride. Interestingly, the peak of the quarternary carbon of the styrene (δ = 140 ppm) is not anymore visible after addition of the amine. In Ha's paper, the ^{13}C NMR of pSMA (synthesised *via* free radical polymerisation in DMF with $[SMA]_0$ = 4 M) shows two broad peaks. One peak between 141.5 – 147.5 ppm (styrene) and the second peak between 136.5 -140.5 ppm (maleic anhydride). The author compared several ^{13}C NMR and showed that using a small bulky group such as CH_3 (present on a citraconic (α-methylmaleic) deshield or overlaped with the C7 of the styrene. A similar hypothesis can be used by considering a potential affect from the carboxylic acid group, the amine or the amide present in the homopolymer.[32]

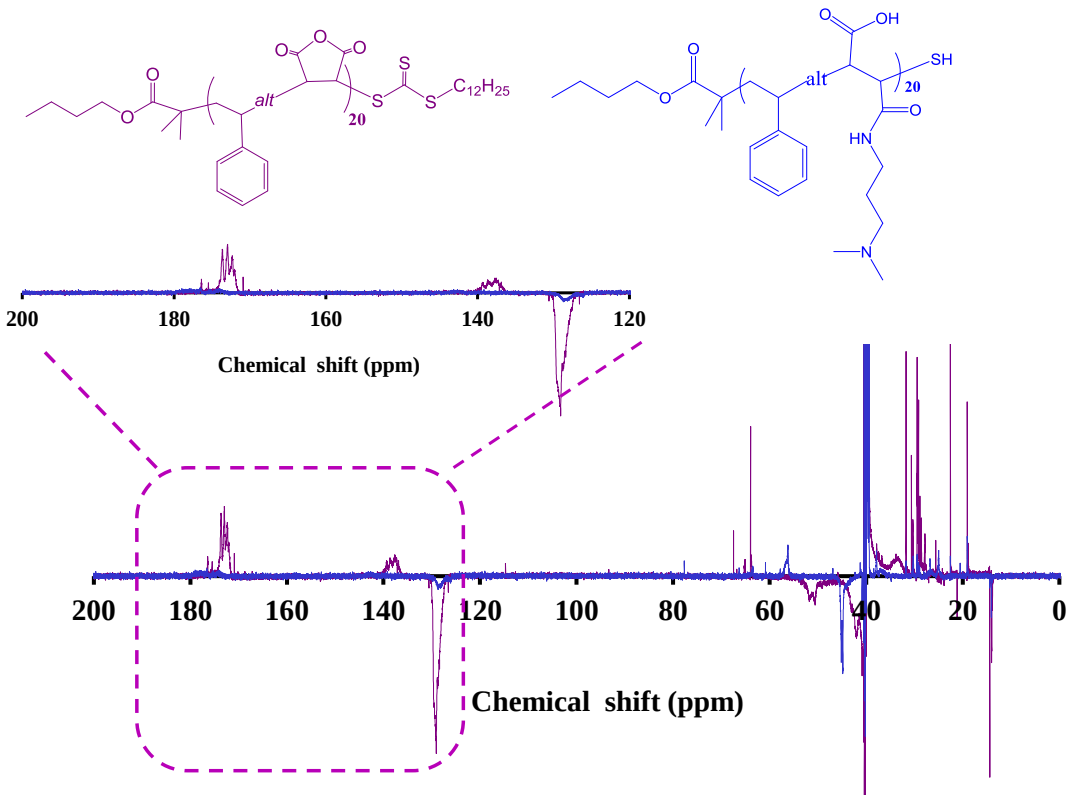

Figure 4.10: Comparison of ^{13}C NMR spectra analysis of $p(SMA)_{20}$ (**purple trace**) and $p(SMAD)_{20}$ (**blue trace**) obtained after a slow addition of DMAPA (3-5 equiv.) at 70 ˚C in MPA and precipitated in cold Et_2O Spectrum recorded on a Brucker Avance (400 MHz) in DMSO-d_6

The FT-IR spectrum of p(Styrene-*alternating*-MA) is given in **Figure 4.11** the sharp peaks at 1770 and 1850 cm^{-1} are attributed to the symmetric and antisymmetric stretching vibration absorption peak of the carbonyl group (C=O) present in a maleic anhydride units, respectively.

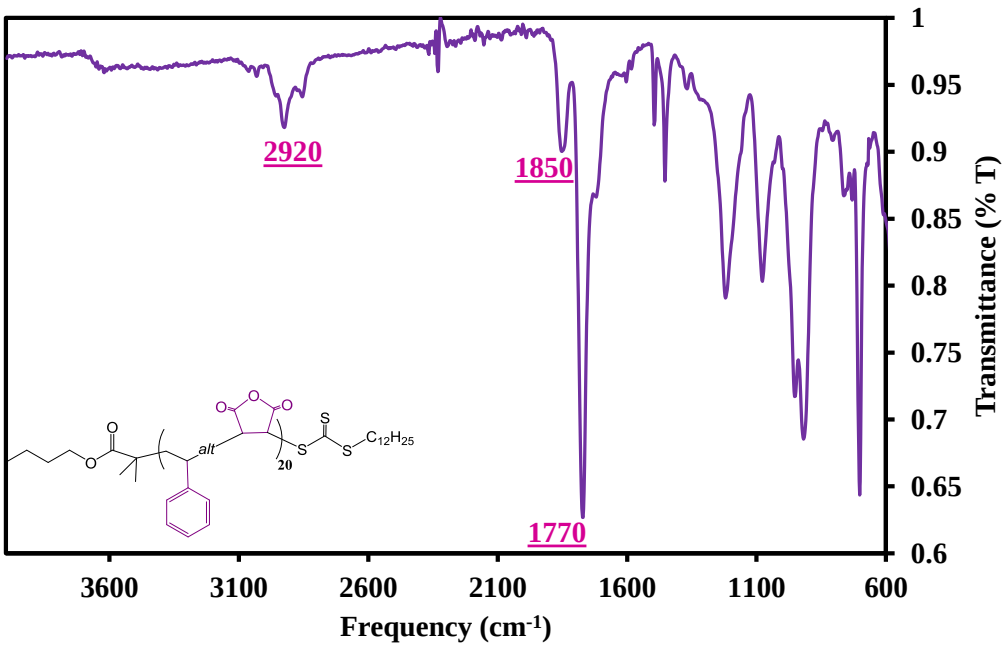

Figure 4.11: FT-IR spectrum of $p(SMA)_{20}$ recorded after precipitation in cold hexane using Bruker Vector instrument

The modified pSMAD homopolymer FT-IR spectrum in the **Figure 4.12** is also reported in order to assess the presence or absence of functional groups. The emergence of the asymmetric carbonyl group (C=O) at 1780 cm^{-1} and the disappearance of the symmetric carbonyl group (-C-O-C) peak at 1860 cm^{-1} confirm the success of the maleic anhydride ring opening. Additionally, the presence of the 3100 cm^{-1} (C-NH-) band attests the successful completion of the reaction.

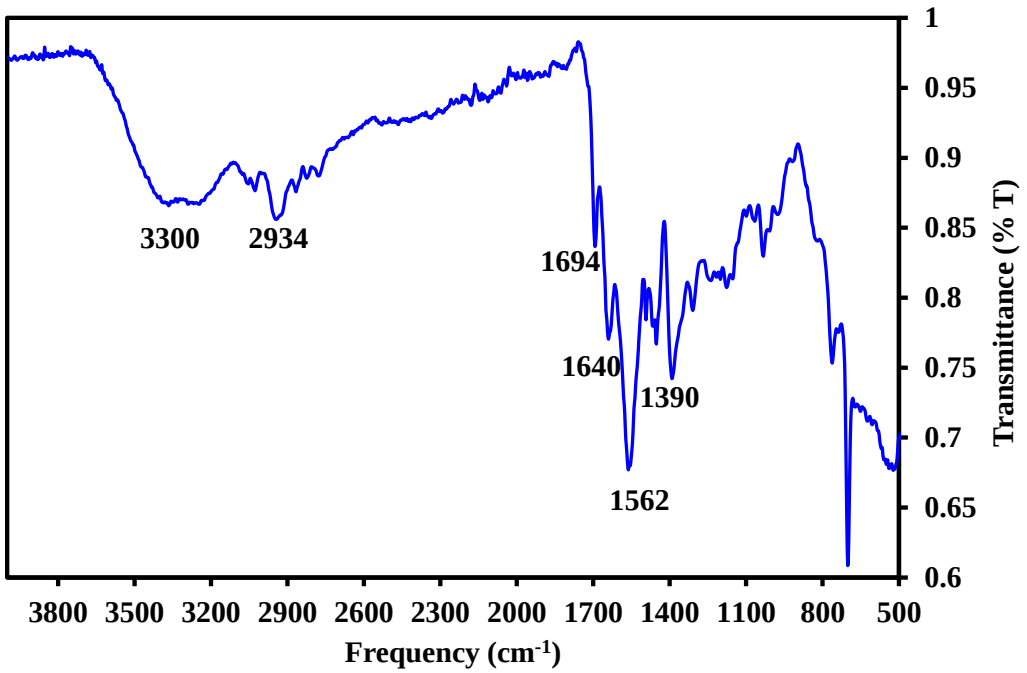

Figure 4.12: FT-IR spectrum of $p(SMAD)_{20}$ recorded after precipitation in cold Et_2O using Bruker Vector instrument

4.2.5. Modification of poly(SMAD) into poly (SMI) in polymer backbone

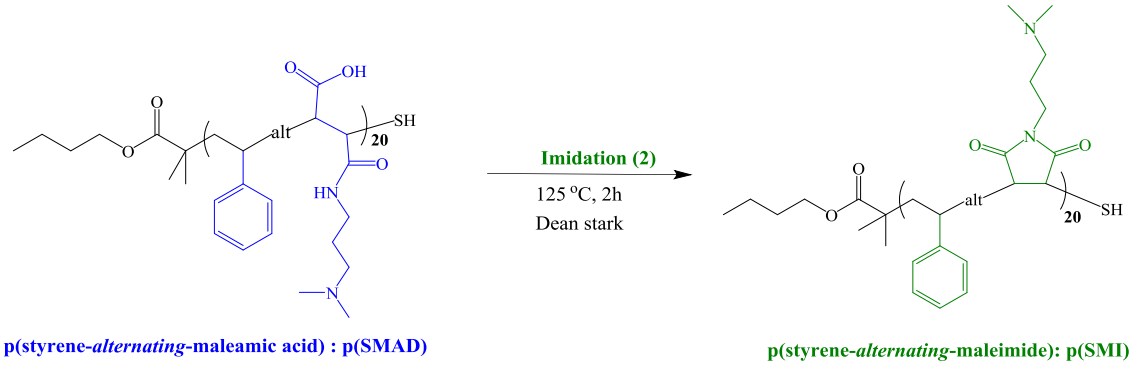

Scheme 4.8: Formation of maleimide formation after dehydration of p(SMAD) intermediate at 125 ˚C.

The imide formation occurs *via* a cyclization process which increased according to the SMA concentration or reaction temperature.[43] Due to the gel formation on the previous step, an excess of solvent is added to the transparent viscous-gel solution and heated up at 125 ˚C to remove the water. After 2 hours, the excess of solvent is removed and the polymer is purified by precipitation in cold hexane. The ring closing of p(SMAD) leading the p(styrene-*alternating*-maleimide) product is confirmed by ^{13}C NMR analysis with the presence of the both symmetrical and asymmetrical bonds at 180 ppm. Surprinsingly, the peak at 140 ppm corresponding to the quartenary carbon of the styrene (C7) appears confirming the hypothesis of the potential overlapping peaks induced by a steric hindred intermediate pSMAD (**Figure 4.13**).

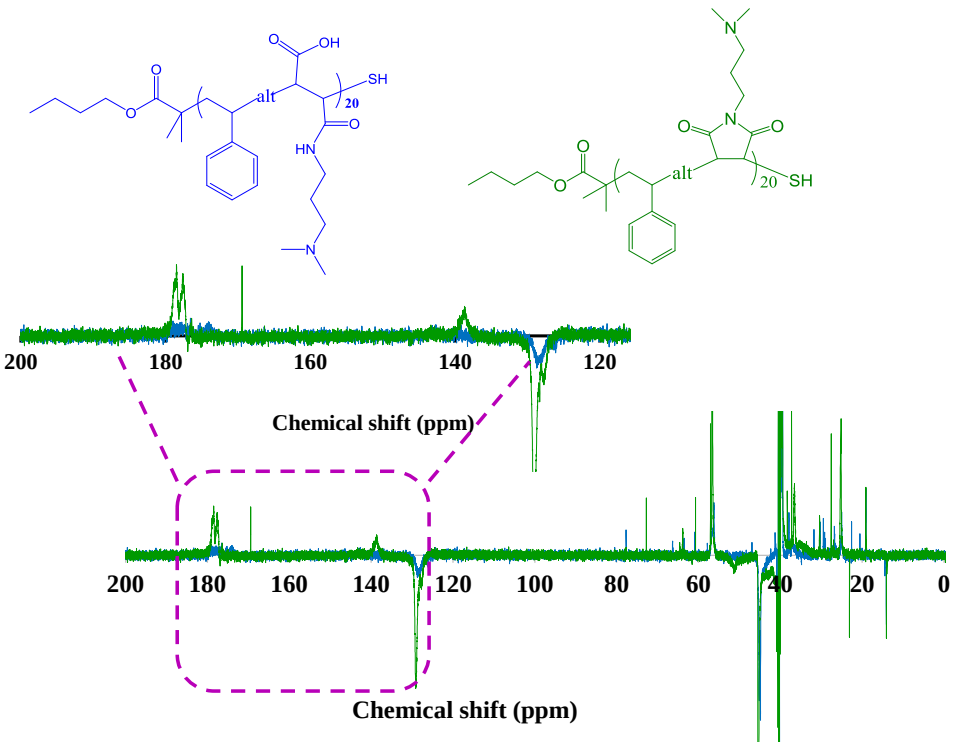

Figure 4.13: Comparison of ^{13}C NMR spectra analysis of p(SMAD)$_{20}$ (**blue trace**) and p(SMI)$_{20}$ (**green trace**) obtained after water removal at 125 ˚C in MPA and precipitated in cold hexane recorded on a Brucker Avance (400 MHz) in DMSO-d$_6$

Figure 4.14 of the FT-IR spectrum of the $p(SMI)_{20}$ shows a strong imide peak appeared at 1683 and 1770 cm^{-1}. No peaks characteristics of maleic anhydride (1780 -1850 cm^{-1}) are observed and consequently, confirmed the full conversion of p(SMA) into p(SMI).[45]

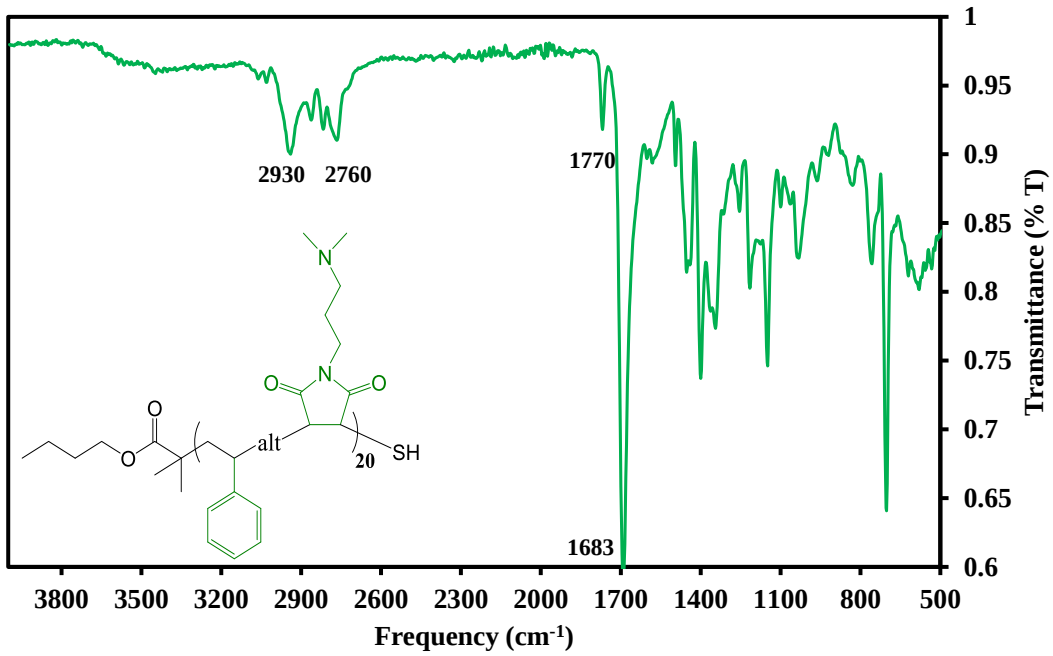

Figure 4.14: FT-IR spectrum of $p(SMI)_{20}$ recorded after precipitation in cold hexane using Bruker Vector instrument

The modification of the polymer backbone can also be assessed visually with the white color of the polymer after the cleavage of the RAFT agent in **Figure 4.15 B** and the strong yellow color suggesting the formation of the maleimide **Figure 4.15 C**. Several authors report the colouration of systems involving a maleimide homopolymer. Coleman *et al*. suggest the colouration is due to unsaturation of the maleimide.[46] Tawney[47] reported the anionic homopolymerisation of maleimide which yielded a red polymer. Finally, Kojima *et al*.[48] have demonstrated a potential hydrogen transfer polymerisation procedure when a base-catalyst is used to polymerise maleimide.

Different organic bases have been tested to form a maleimide, where it was found that the intensity of the colour increases significantly with increasing organic base strength.[49,50]

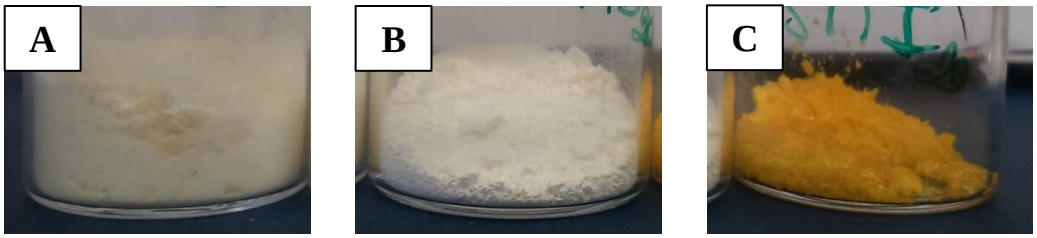

Figure 4.15: Pictures of $p(SMA)_{20}$ (**A**), $p(SMAD)_{20}$ (**B**) and $p(SMI)_{20}$ (**C**) showing the color modification after each steps.

A complementary quantitative analysis method is used to compare the theoretical and experimental percentage of carbon, nitrogen and hydrogen before and after each modification step of the polymer backbone. In **Table 4.2**, a good agreement between the experimental and theoretical percentage of C,H,N for $p(SMA)_{20}$. The increase in composition of nitrogen and oxygen confirms the successful functionalisation with DMAPAA in the polymer backbone, however, a difference of 10 and 2 % of carbon and nitrogen is noticed for $p(SMAD)_{20}$ homopolymer indicating that some (dimethyl)aminopropyl amine is remaining after precipitation step. The $C_{12}H_{25}$ removal from the RAFT agent is also evidenced by the decreased carbon percentage (% C) of pSMA compared to pSMAD. An increase of % C from pSMAD into pSMI is observed and may be attributed to the presence of hexane used for polymer precipitation or one of the combustion products releasing either the nitric oxide, carbon dioxide or water.

Table 4.2: Elemental analysis of $p(SMA)_{20}$, $p(SMAD)_{20}$ and $p(SMI)_{20}$ of theoretical and experimental carbon (% C), nitrogen (% N), and hydrogen (% H) after purification

Sample	$\%C_{exp}$	$\%C_{TH}$	$\%H_{exp}$	$\%H_{TH}$	$\%N_{exp}$	$\%N_{TH}$
$p(SMA)_{20}$	68.8	69.3	5.6	5.8	0.06	-
$p(SMAD)_{20}$	59.3	66.6	8.03	8.8	8.1	6.2
$p(SMI)_{20}$	69.09	70.3	9.03	7.8	7.80	9.2

4.2.5 Modification of p(*n*BA)-*b*-pSMA backbone copolymer

Similar maleic anhydride modifications and analyses were conducted for the diblock and multiblock copolymers. Here, FT-IR and elemental analysis techniques are the most efficient methods.

In the **Figure 4.16** the FT-IR spectra of $p(nBA)_{25}$-*b*-$p(SMAD)_{20}$ and $p(nBA)_{25}$-*b*-$p(SMI)_{20}$ are compared. The peak at 1560 cm^{-1} (C-NH-) and the disappearance of the MA peaks (1780 -1850 cm^{-1}) confirmed the ring-opening of the MA present in the diblock copolymers. Moreover, the peaks at 1729 and 1769 cm^{-1} proved the maleimide formation.

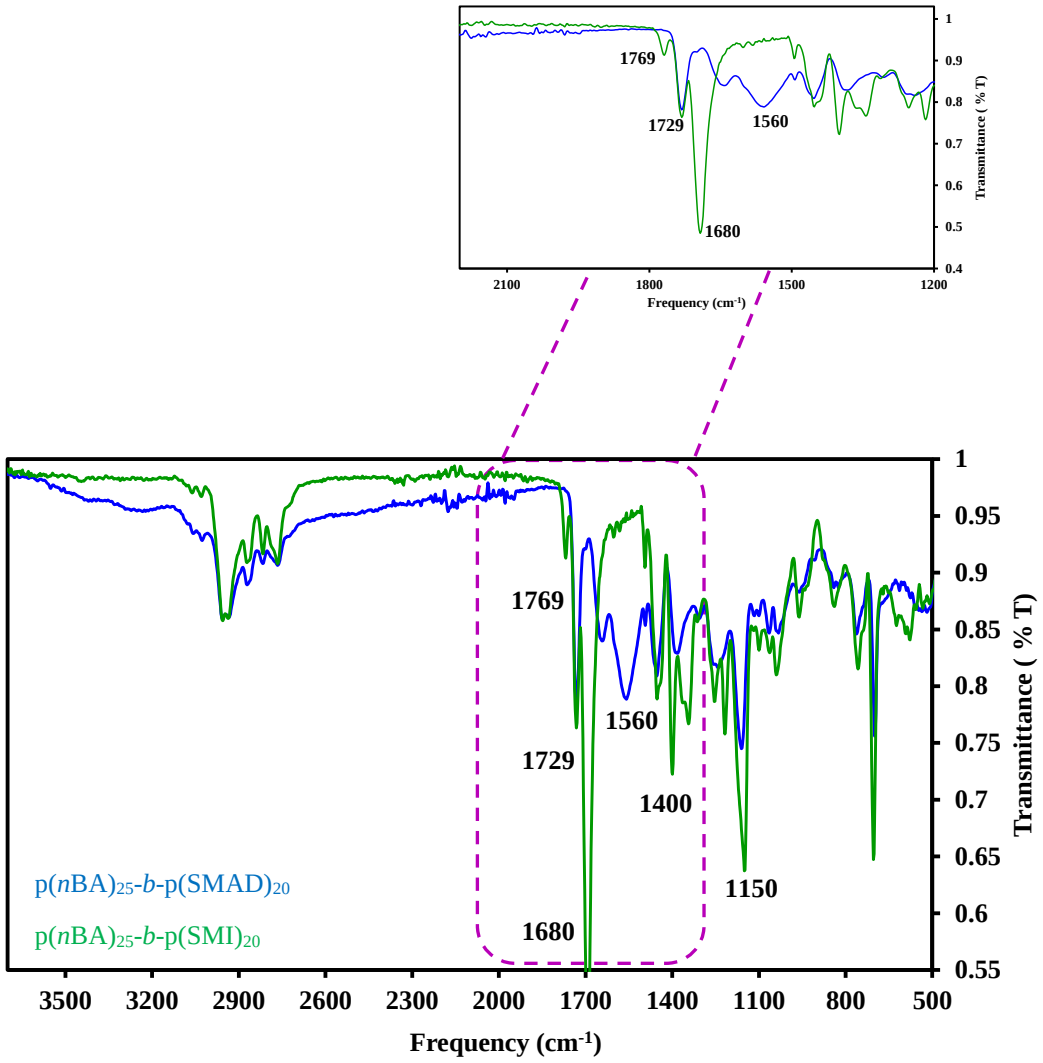

Figure 4.16: FT-IR spectrum of p(*n*BA)$_{25}$-*b*-p(SMAD)$_{20}$ in blue trace and p(*n*BA)$_{25}$-*b*-p(SMI)$_{20}$ in green trace are recorded after precipitation in cold hexane using Bruker Vector instrument

Table 4.3 records the theoretical and experimental percentage of C,H,N before and after starting modification of the MA. There is a good aggrement for the hydrogen percentage (% H) while the experimental percentage of carbon and nitrogen is slightly higher suggesting a presence of some residual reactant (DMAPAA) or the production of gas during the compound combustion.

Table 4.3 Elemental analysis of p(nBA)$_{20}$-*b*-p(SMA)$_{25}$, p(nBA)$_{20}$-*b*-p(SMAD)$_{25}$ and p(nBA)$_{20}$-*b*-p(SMI)$_{25}$ after purification in cold hexane

Sample	%C$_{exp}$	%C$_{TH}$	%H$_{exp}$	%H$_{TH}$	%N$_{exp}$	%N$_{TH}$
p(nBA)$_{20}$-*b*-p(SMA)$_{25}$	69.8	67.2	6.8	7.9	-	-
p(nBA)$_{20}$-*b*-p(SMAD)$_{25}$	67.1	66.0	8.5	8.7	6.5	4.4
p(nBA)$_{20}$-*b*-p(SMI)$_{25}$	70.08	67.9	8.42	8.7	6.83	4.5

The Infra-red and elemental analysis data are similar for all the diblock co-polymer (8 kDa, 10 kDa, and 15 kDa) synthesised, as well as the multiblock copolymer. Interestingly, we observe poly(nBA)$_{20}$-*b*-poly(SMAD)$_{25}$ to be a sticky, white powder while the diblock p(nBA)$_{20}$-*b*-p(SMI)$_{25}$ is a yellow, viscous solution.

4.2.6. Characterisations of homopolymer, diblock and multiblock copolymer

- **Size Exclusion Chromatography & Viscosity by Mark-Houwink-Sakurada**

The physical, rheological and mechanical properties of a polymer depend strongly on the molecular weight distribution. Several techniques can be used to determine this information, such as ^{1}H NMR, DOSY NMR, static light scattering (SLS) or size exclusion chromatography (SEC).

Conventional SEC, whereby the refractive index (RI) is used to measure the molar mass distribution based on the elution time of the polymer, is usually not accurate as the elution time is related to the calibration of the column using polymers (such as poly(methyl methacrylate) or poly(styrene) with a narrow dispersity.

Hence, the molar mass obtained can be underestimated or overestimated, depending on the relative hydrodynamic volume compared to the standards used and also on the solubility of the polymer in the eluent. However, by combining a refractometer with a light scattering (LS) detector in the size exclusion chromatography (SEC) instrument it is possible to determine a more accurate molar mass distributions, M_n, and weight average molar masses, M_w. Another method to calculate the molar mass distribution is to use the intrinsic viscosity (IV), which is related to the hydrodynamic volume using Equation 1, where η is the intrinsic viscosity, V is the hydrodynamic volume, M is the molecular weight, and K is the constant.

$$[\eta] = K \frac{V}{M} \qquad \textbf{Equation 4.1}$$

The presence of a viscosity detector allows for the determination of the IV and the molecular weight distribution of the polymer based on the Mark-Houwink equation (**Equation 4.2**).

$$M = K\,[\eta]^{\alpha}$$

Equation 4.2: M is the molecular weight, [η] is intrinsic viscosity, K and α are constants

Few studies have been undertaken to understand the effect of short chain of maleic anhydride on a molar mass distribution using size exclusion chromatography and dilute solution viscosity.[51,52]

Here, triple detection SEC (a combination of DRi, LS and VS detectors) was used to determine an accurate molecular weight distribution of all the poly(*n*BA)-*block*-poly(SMA) diblock copolymers before and after maleic anhydride modification, using

SEC in DMF eluent, with a UV detector set to 309 nm (absorbance of the RAFT agent). This was then compared with the molar mass defined by conventional size exclusion chromatography (**Table 4.4**).

Table 4.4: Molar mass distribution of diblock copolymer of p(*n*BA)-*b*-p(SMA) after modification determined by RI and triple detection (UV : λ = 309 nm) by SEC-DMF

Sample	Solubility	$M_{n.RI}$	$M_{w,RI}$	$M_{n.TRI}$	M_{wTRI}
pBA_{50}-*b*-$pSMAD_{40}$		-	-	-	-
pBA_{80}-*b*-$pSMAD_{40}$	partially	21700	25000	72690	78500
pBA_{100}-*b*-$pSMAD_{40}$	✓	28800	34600	73700	74300
pBA_{50}-*b*-$pSMI_{40}$	✓	28650	33700	63570	70000
pBA_{80}-*b*-$pSMI_{40}$	✓	32800	36650	27502	31500
pBA_{100}-*b*-$pSMI_{40}$	✓	32720	39400	18500	21900

The molar mass distribution, M_n, and the weight average molar mass, M_w, obtained by triple detection was three time higher than the result obtain using the refractive index (RI), suggesting a self-assembly behaviour of the amphiphilic block copolymer in DMF. The Mark-Houwink exponent, α, which assesses the conformation of the polymer in solution, was also defined by viscometry. For the intermediate polymer, α was close to 0.20 suggesting the formation of a branched polymer, while for the maleimide equivalent, the exponent α is close 0.55 indicating a more linear conformation. The triple detection analysis highlights the formation of branching or aggregate formation of the poly(maleic amido acid) in solution.

➢ Thermogravimetric analysis

Thermogravimetric analysis (TGA) was used to study the thermal stability of the homopolymers and diblock copolymers before and after polymer backbone modifications. This analysis records the weight loss or gain throughout the heating profile (from 25 ˚C to 600 ˚C in this investigation) under nitrogen, or other, gaseous environment, at a given rate. Increasing the temperature causes the covalent bonds to break, and the polymer begins combusting. Therefore, changing in the chemical structure of the polymer backbone will likely influence the profile of decomposition. In order to maintain consistence of results, a similar sample weight (from 5 mg to 8 mg) was required. The normalized thermal degradation was analysed to determine the percentage of mass remaining (**Figure 4.17**). The three traces reveal a considerable difference between the precursor polymer and the two amine derivatives. A single decomposition temperature (T_d) for pSMI and pSMA at 375 ˚C and 230 ˚C, respectively, can be observed, while pSMAD exhibits three distinct decomposition temperatures at 100, 150 and 350 ˚C. The decomposition temperature at 100 ˚C is attributed to the water evaporation then, the degradation at 150 ˚C can be related to the elimination of the carboxylic acid side chain, and the main decomposition at 350 ˚C results from polymer backbone degradation.

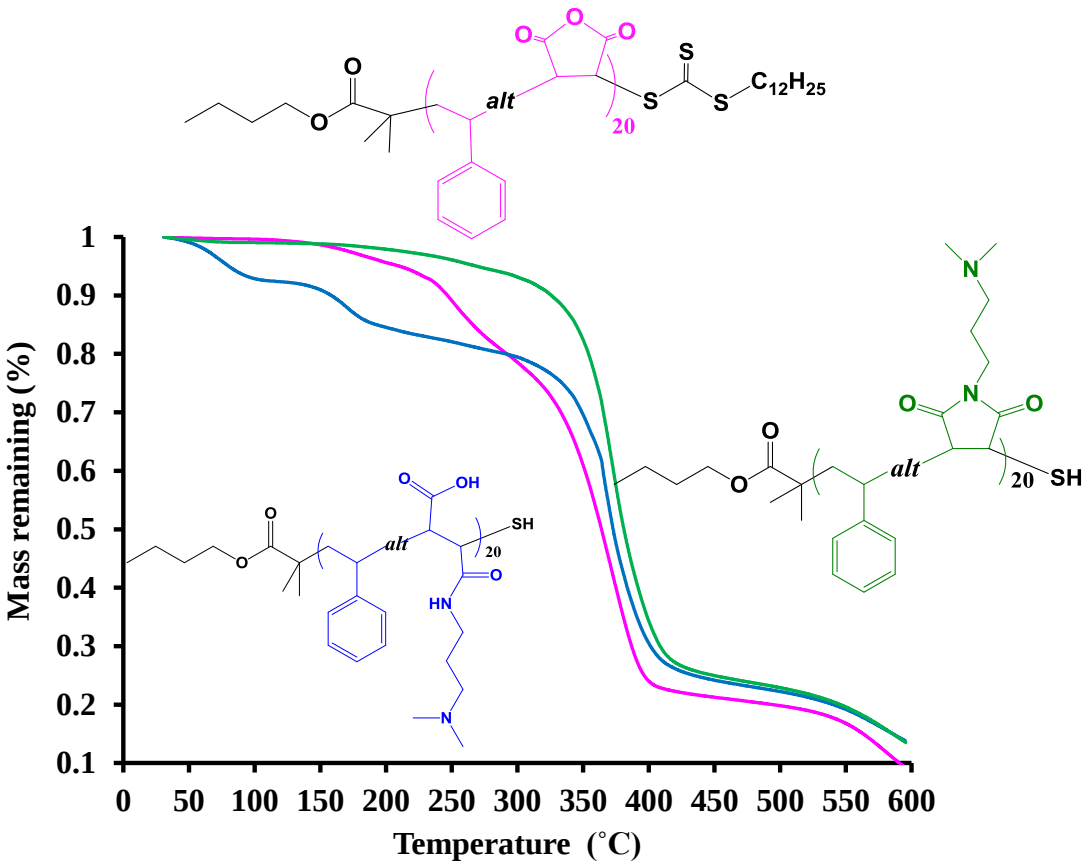

Figure 4.17: TGA chromatograms of pSMA, pSMAD and pSMI homopolymers degradation submitted under nitrogen with a heating rate of 10 ˚C/min from 25 ˚C to 600 ˚C recorded with Mettler Toledo instrument

Overall, the thermal stability increases in the following order pSMAD > pSMA > pSMI.

Following on, the diblock copolymer and its derivatives were analysed by TGA under similar conditions. The presence of the poly (*n*-butyl acrylate) with different degrees of polymerisation did not seem to affect significantly the profile of decomposition in comparison to the homopolymers previously described (**Figure 4.18**).

Here degradation temperatures at 100, 150 and 350 °C were found for poly(*n*-BA)-*block*-poly(SMAD). An additional degradation is observed at 280 °C for poly(*n*-BA)-*block*-poly(SMA) while only the degradation at 350 °C is present for the homopolymer.

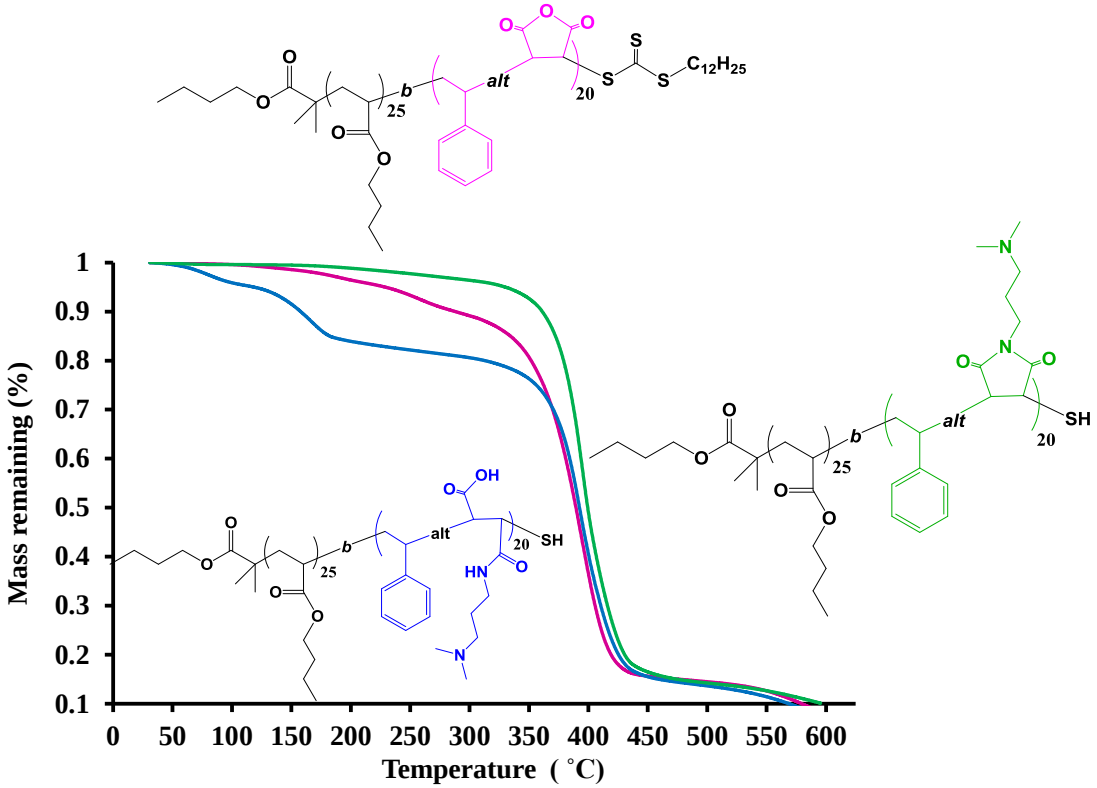

Figure 4.18: TGA chromatograms of p(*n*BA)$_{25}$-*b*-p(SMA)$_{20}$, p(*n*BA)$_{25}$-*b*-p(SMAD)$_{20}$, and p(*n*BA)$_{25}$-*b*-p(SMI)$_{20}$, diblock copolymers degradation submitted under nitrogen with a heating rate of 10 ˚C/min from 25 ˚C to 600 ˚C recorded with Mettler Toledo instrument

Similar data were obtained for the tetrablock copolymer poly(BA)$_{25}$-*block*-poly (SMA)$_{20}$-*block*-poly(BA)$_{25}$-block-poly(SMA)$_{20}$, and its derivatives (**Figure 4.19**). The molar mass of the multiblock, being similar to the diblock copolymer, would suggest the same rate of degradation would be expected.

Moreover, the polymer architecture does not affect the profile of degradation as the polymer backbone and the side chain are similar to the homopolymers and diblock copolymers.

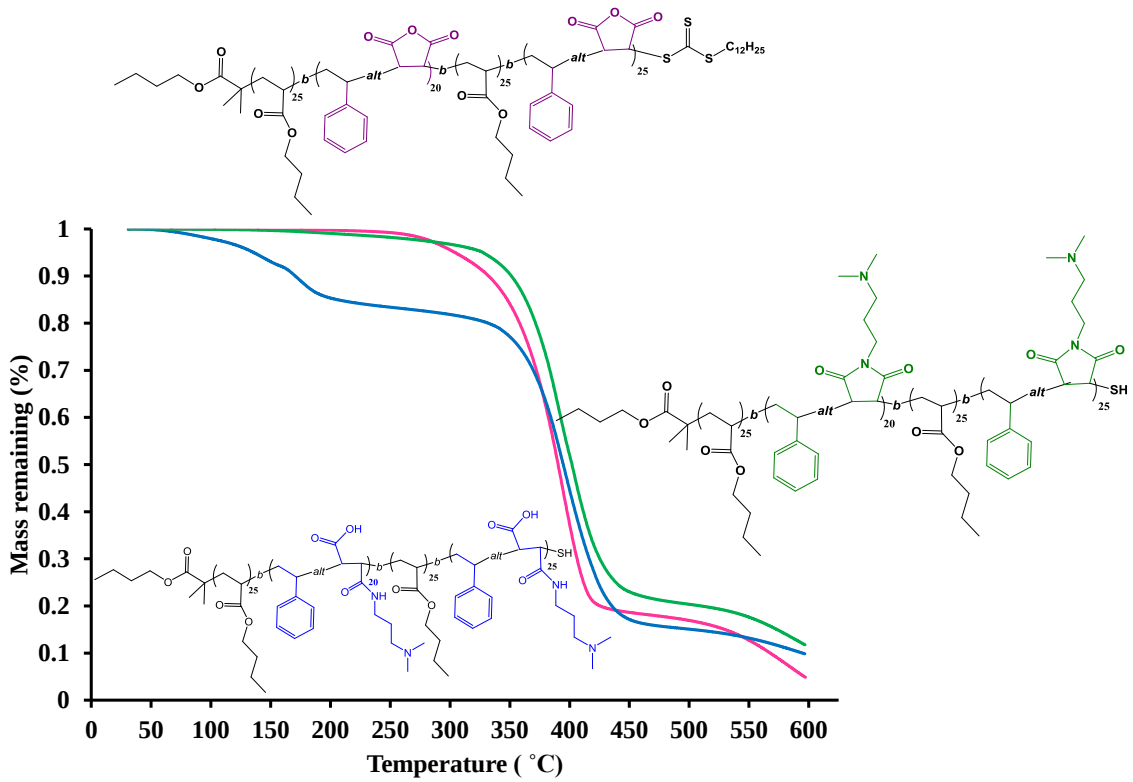

Figure 4.19: TGA chromatograms of p(nBA)$_{25}$-*b*-p(SMA)$_{20}$-*b*-p(nBA)$_{25}$-*b*-p(SMA)$_{20}$-, p(nBA)$_{25}$-*b*-p(SMAD)$_{20}$-*b*-p(nBA)$_{25}$-*b*-p(SMAD)$_{20}$ and p(nBA)$_{25}$-*b*-p(SMI)$_{20}$-*b*-p(nBA)$_{25}$-*b*-p(SMI)$_{20}$, tetablock copolymers degradation submitted under nitrogen with a heating rate of 10 ˚C/min from 25 ˚C to 600 ˚C recorded with Mettler Toledo instrument.

Thermogravimetric analysis allows the study of the degradation of polymer structures over a wide range of temperatures. The presence of some functionalities gives rise to an earlier degradation of the polymer backbone. Moreover, a symmetrical architecture does not impact the profile of degradation as shown the TGA mass loss curves of the homopolymer (**Figure 4.17**), diblock copolymer (**Figure 4.18**) and tetrablock copolymer

(**Figure 4.19**). This powerful technique is also used in a **Chapter 5** to quantify the percentage of carbon black pigment coated onto the polymer.

4.3. **Conclusion**

In summary, a series of diblock copolymers with varied molecular weights (10 - 17 kDa) containing *n*-butyl acrylate and styrene-maleic anhydride with an overall dispersity of 1.24, without purification steps, was synthesised using BMDPT RAFT agent. The versatility of SMA in nucleophilic substitutions allowing the establishment of a diverse library of functional polymers is reported. Then, the functionalisation of the polymer backbone was undertaken *via* a multistep process by using a functional primary amine. Spectroscopic techniques such as ^{1}H NMR and FT-IR were used to confirm the presence of the functional moieties. In addition, the effect of these moieties on the polymer degradation is recorded by TGA for each polymeric architecture. Interestingly, the presence of the carboxylic acid impacts the behaviour of the polymer in the solvent and the rate of degradation of the polymer.

The synthesis and modification of diblock poly(*n*-BA)-*block*-poly(SMA) *via* RAFT polymerisation was reported, for the first time in literature, and the materials were used as dispersant for carbon in a solvent born system.

4.4. **Experimental**

4.4.1. Materials.

Styrene (Aldrich, 99 %), maleic anhydride (Aldrich, 99%), 3-dimethylamino-1-propylamine(DMAPAA) (Aldrich, 98%), *n*-butyl acrylate (Sigma, 98%), butyl acetate (Chromasolv plus, 99.7 %), propylene glycol monoethyl ether acetate (Sigma-Aldrich, 99.5%), dimethyl2,2'-azobis(2-methylpropionate) (V601,Wako) azobis(cyclohexanecarbonitrile), butyl-2-methyl-2-[(dodecylsulfanylthiocarbonyl) sulfanyl] propionate (BMDPT, Lubrizol, 70 %). All chemicals were used without further purification.

4.4.2. Method

- Synthesis of poly(styrene-*alternating*-maleic anhydride) copolymer

For a synthesis of SMA_{20} an equimolar amounts of styrene (10 eq, 0.5 g, 4.8 mmol) and maleic anhydride (10 eq, 0.47 g, 4.8 mmol) are mixed in a round-bottom flask with the initiator, BMDPT (1 eq, 0.20 g, 0.48 mmol) and 3 mL of MPA solvent. After 10 min of degassing with nitrogen, the reaction mixture is placed in an oil bath at 70 ˚C for 12 h. It has been extensively described in the literature that the copolymerisation of styrene and maleic anhydride are perfectly alternating, so we predict that the conversion of the maleic anhydride is similar to that of styrene. $M_{n,SEC}$ = 7850 g/mol , $Đ$ = 1.14 (THF-SEC, triple detection). ^{1}H-NMR (400 MHz, DMSO-d_6, δ /ppm): 7.5 (s, 2H, -C(O)-**HC=HC**-C(O)-O-), 7.25- 7.3 (m, 2H, Ar-**CH=CH**-), 5(s, 6H, trioxane),

1.9 – 0.9 (m, backbone). The vinyl peaks are compared at t = 0 and t =12 h. ^{13}C-NMR: (400 MHz, DMSO-d_6, δ /ppm): 19.1 (s), 22.5 (s), 28.5 (m), 30.2 (m), 65 – 63 (m), 67.5 (s), 140 (m), 180- 170 (m). FT-IR: (cm^{-1}) 2920 (m), 1850 (w), 1770 (s), 1454 (s), 1275 (s), 1077 (s), 950 (s),916 (m), 700 (s).

- Ring-opening of maleic-anhydride in $p(SMA)_{20}$

For a typical amidation process: $p(SMA)_{20}$ (1 eq, 0.5g, 2442 g/mol, 2.0 x 10^-4 mol) is placed into a two neck round-bottom flask with a magnetic stirrer with 3 mL of MPA. The solvent was added in excess to avoid any gelation during the amidisation. Then, (dimethyl)aminopropyl amine reagent (3 eq, 0.613g, 6.0 x 10^-3 mol) is added slowly for 30 min under strong mechanical stirring at 70 ˚C. The mixture was left to stir for 2 hours to form the poly(styrene-*alternating*-maleic acid) (pSMAD). The yellow viscous solution of pSMA became a white viscous mixture. The colourless nature of the system arises from the cleavage of the trithiocarbonate RAFT agent, and was confirmed by ^{1}H NMR. Then, the solvent is removed and the polymer is precipitated in cold ether, and then dried overnight in vacuum oven. ^{1}H-NMR (400 MHz, DMSO-d_6, δ /ppm): 7.3 (m, 6H, Ar-CH_2-), 6.9 (broad, 1H, R-C(O)**NH**-$(CH_2)_2$-$N(CH_3)_2$), 4.0 (m, 2H, R-C(O)O-(**CH_2**)$_4$-), 2.3 – 2.0 (m, 4H, R-C(O)NH-**$(CH_2)_2$**-$N(CH_3)_2$), 2.07 (s, 6H, R-C(O)NH-$(CH_2)_2$-N(**$CH_3)_2$**), 1.9 – 0.9 (m,backbone). ^{13}C-NMR: (400 MHz, DMSO-d_6, δ /ppm): 19.07 (s), 20.54 (s), 22.57 (s), 24.90 (m), 29.41 (m), 30.92 (m), 37.90 (s), 44.86 (s), 45.17 (s), 56.22 (br,m), 60.86 (s), 63.50 (s), 77.68 (s), 143.13 (m), 179.0 (m). FT-IR: (cm^{-1}) 3300 (br,w), 2934 (w), 1694 (w), 1640 (m),1562 (s), 1390 (m).

- Synthesis of maleimide p(SMI)$_{20}$

The imidisation process was performed using Dean-Stark apparatus. An excess of solvent was added in order to dissolve the gel. Then the mixture was heated-up at 125 ˚C for 2 hours in order to get rid off of the water and form the poly(styrene-*alternating*-maleimide). The amide intermediate product was solubilised in methanol and precipitated in hexane. ^{1}H-NMR (400 MHz, DMSO-d$_{6,}$ δ /ppm): 7.2 (m, 6H, **Ar**-CH$_2$-), 3.9 – 3.2 (4.0 (m, 2H, R-C(O)O-(**CH$_2$**)$_4$- & R-CO-CH-CH-CO-N(**CH$_2$**)$_3$-N(CH$_3$)$_2$), 2.0 (s, 6H, R-C(O)NH-(CH$_2$)$_2$-N(**CH$_3$)$_2$**), 1.9 – 0.9 (m,backbone). ^{13}C-NMR: (400 MHz, DMSO-d$_6$, δ /ppm): 19.10 (s), 23.09 (s), 25.15 (s), 27.55 (s), 30.09 (s), 36.54 (s), 38.29 (s), 45.38 (s), 56.60 (s), 57.07 (s), 60.72 (s), 63.83 (s), 72.74 (s), 129.09 (m), 138.68 (m), 177.70 (m). FT-IR: (cm^{-1}) 2930 (w), 2760 (w), 1770 (w), 1683 (s), 1440 (w), 1400 (m), 1346 (m), 1150 (m), 1030 (w), 704 (s).

- Synthesis of poly(SMA)-*block*-poly(*n*BA) copolymer

For a typical synthesis of p(SMA)$_{20}$-*b*-p(BA)$_{25}$: In the same flask set-up for the synthesis of pSMA$_{20}$ as mentioned in 4.4.2.1, *n*-butyl acrylate (25 eq, 1.54 g, 12 mmol) and 2 mL of MPA are added to the macroinitiator. The mixture is bubbled with nitrogen for 10 min before being heated to 70 ˚C. To synthesise a multiblock copolymer, the sequential addition of SMA and butyl acrylate are added alternatively. ^{1}H-NMR (400 MHz, DMSO-d$_{6,}$ δ /ppm): 7.2 (m, 6H, **Ar**-CH$_2$-), 4,21 (m, 2H,-C(O)O-C**H$_2$**-CH$_2$-CH$_2$-CH$_3$), 2.55 (m, 2H, -C(O)O-CH$_2$-C**H$_2$**-CH$_2$-CH$_3$), 1.9 – 0.91 (m,backbone, C$_{12}$H$_{25}$). FT-

IR: (cm^{-1}) 2930 (w), 2760 (w), 1850 (w), 1770 (w), 1683 (s), 1440 (w), 1400 (m), 1346 (m), 1150 (s), 1030 (w), 750 (s).

- **Nuclear Magnetic Resonance (NMR) spectroscopy**

NMR (^{1}H and ^{13}C) were recorded on a Bruker AV-300 and DPX-500 in deuterated chloroform ($CDCl_3$) or DMSO-d_6. Chemical shift values (δ) are reported in ppm. The residual proton signal of the solvent is used as internal standard ($CDCl_3$, δ = 7.26 or δ = 2.5 for DMSO-d_6). The use of 1,3,5-trioxane is also used in a ^{1}H NMR characterisation and mentioned in the spectra.

- **Determination of $DP_{n,targeted}$ and monomer conversion**

Monomer conversion (*p*) were calculated from ^{1}H NMR data using **equation 4.3:**

$$p = \frac{[M]_0 - [M]_t}{[M]_0} = 1 - \frac{[M]_t}{[M]_0} = 1 - \frac{\frac{\int I_{5.5-6.75\ ppm}}{\int I_a}}{DP_{n,targeted}}$$

Where $[M]_0$ and $[M]_t$ are the concentrations of the monomer at time 0 and at time *t*, respectively, $\frac{\int I_{5.5-6.75\ ppm}}{\int I_a}$ is the integral for the vinyl protons of the monomer, $DP_{n,targeted}$ is the number average degree of polymerisation targeted and $\int I_a$ is the integral of the two protons belonging to the CH_2 of the acrylate (-O-**CH_2**-CH_2).

- **Determination of $M_{n,TH}$**

The theoretical number-average molar mass ($M_{n,TH}$) is calculated using **equation 4.4**:

$$M_{n,TH} = \frac{[M]_0 p [M]_M}{[CTA]_0} + M_{CTA}$$

Where $[M]_0$ and $[CTA]_0$ correspond to the initial concentrations (in mol/L) of monomer and chain transfer agent respectively; p is the monomer conversion as determined by equation 1, M_M and M_{CTA} are the molar masses (g/mol) of the monomer and chain transfer agent.

- **Size exclusion chromatography (SEC)**

Number-average molar masses ($M_{n,SEC}$) and dispersity values ($Đ$) distributions were measured using size exclusion chromatography with THF as an eluent. The THF Agilent 390-LC MDS instrument was equipped with differential refractive index (DRI), viscometry (VS), dual angle light scatter (LS) and two wavelength UV detectors. The system was equipped with 2 x PolarGel Mixed C columns (300 x 7.5 mm) and a PLgel 5 µm guard column. The eluent is THF with 2 % TEA(triethyl amine) and 0.01 wt./ V% BHT (butylated hydroxytoluene) additives. Samples were run at 1 mL/min at 30 °C. Poly(styrene) standards in rang of 2.0 x 10^2 g/mol to 2.0 x 10^6 g/mol was used to calibrate SEC system.. Analyte samples were filtered through a polytetrafluoethylene (PTFE) membrane with 0.22 μm pore size before injection. The calibration is setup by using a flow rate marker with a polynomial order of 3. Respectively, experimental molar mass ($M_{n,SEC}$) and dispersity ($Đ$) values of synthesized polymers were determined by conventional calibration using Agilent GPC/SEC software. DMF-SEC -Agilent 390-LC

MDS instrument equipped with differential refractive index (DRI), viscometry (VS), dual angle light scatter (LS) and UV detectors. The system was equipped with 2 x PLgel Mixed D columns (300 x 7.5 mm) and a PLgel 5 µm guard column. The eluent is DMF with 5 mmol NH_4BF_4 additive. Samples were run at 1ml/min at 50 ˚C. Poly(methyl methacrylate) standards (Agilent EasyVials) were used for calibration between 500 – 955,00 $gmol^{-1}$. Analyte samples were filtered through a nylon membrane with 0.22 μm pore size before injection. Respectively, experimental molar mass ($M_{n,SEC}$) and dispersity ($Đ$) values of synthesized polymers were determined by conventional calibration and universal calibration using Agilent GPC/SEC software. The Kuhn-Mark-Houwink-Sakurada parameter α, relating to polymer conformation in solution is determined from the plot of intrinsic viscosity as a function of the molecular weight, using Agilent software.

- **MALDI-ToF-MS analysis**

Matrix assisted laser desorption-ionization time of flight mass spectrometry is performed on a Brucker Daltonics Ultraflex in the positive ion and reflection mode using external calibration (PEG1500 and PEG5000). DCTB (trans-2-[3-(4-tert-Butylphenyl)-2-methyl-2-propenylidene]malonitrile is used as a matrix (300 mg/mL in THF) and used as purchased (Sigma-Aldrich). NaTFA salt is used as ionization agents (10 mg/mL in THF). Matric, salt and polymer solution (10 mg/mL in THF) are mixed in a 1:1:1 ratio and then, 2 µL of the mixture is applied to the target plate.

➢ Thermogravimetric analysis (TGA)

Experiments were performed to determine the thermal degradation of the copolymers and to quantify the amount coated on the carbon black surface. TGA measurements used a Mettler Toledo StareE TGA which was run in aluminium pan (40 µL) with a sample mass between 4 and 12 mg. All the samples were submitted under nitrogen with a heating rate of 10 ºC/min from 25 °C to 600 °C for the polymer and from 25 °C to 1000 °C for the carbon black.

➢ Fourier transform infrared (FTIR)

FTIR analysis was used to monitor the reaction and find the optimum condition for imidisation of the maleic anhydride. Data were recorded on a Bruker Vector instrument using ATR mode (attenuated total reflection). The pSMAD and pSMI were precipitated and dried overnight in the vacuum oven before analysis. Each spectrum was obtained from 50 scans at room temperature with a resolution of 1 cm^{-1} in absorption mode.

➢ Determination of the number fraction of living chains L

The number fraction of living chains is determined by the following **equation 4.5**:

$$L\ (\%) = \frac{[\mathrm{CTA}]_0}{[\mathrm{CTA}]_0 + 2.f.[I]_0.\left(1-e^{-kdt}\right).\left(1-\frac{fc}{2}\right)} \quad \textbf{(Eq 4.5)}$$

For the butyl acetate/Vazo-88/90 ˚C system, we considered: $k_{d(\text{Vazo-89,90 }^{\circ}\text{C})}$ = 1.9254 x $10^{-5}s^{-1}$ with E_a = 154.1 KJ/mol.K. For the butyl acetate/V601/70 ˚C system, the constant of dissociation (k_d) is similar to V-40 at 90 ˚C with Ea = 131.2 KJ/mol.K.

4.5 References

1. Moore, E. R. *Industrial & Engineering Chemistry Product Research and Development* **1986,** *25* (2), 315-321.

2. Klumperman, B. *Polymer Chemistry* **2010,** *1* (5), 558-562.

3. Fordyce, R. G.; Ham, G. E. *Journal of the American Chemical Society* **1951,** *73* (3), 1186-1189.

4. Tsuchida, E.; Tomono, T. *Die Makromolekulare Chemie* **1971,** *141* (1), 265-298.

5. Benoit, D.; Hawker, C. J.; Huang, E. E.; Lin, Z.; Russell, T. P. *Macromolecules* **2000,** *33* (5), 1505-1507.

6. Lessard, B.; Marić, M. *Macromolecules* **2010,** *43* (2), 879-885.

7. Chiefari, J.; Chong, Y. K.; Ercole, F.; Krstina, J.; Jeffery, J.; Le, T. P.; Mayadunne, R. T. A.; Meijs, G. F.; Moad, C. L.; Moad, G.; Rizzardo, E.; Thang, S. H. *Macromolecules* **1998,** *31*, 5559.

8. Sanders, G. C.; Duchateau, R.; Lin, C. Y.; Coote, M. L.; Heuts, J. P. A. *Macromolecules* **2012,** *45* (15), 5923-5933.

9. Davies, M. C.; Dawkins, J. V.; Hourston, D. J. *Polymer* **2005,** *46* (6), 1739-1753.

10. Zhu, Y.; Geng, B.; Xu, A.; Zhang, L.; Zhang, S. *Designed Monomers and Polymers* **2013,** *16* (3), 283-290.

11. Jeon, H. K.; Feist, B. J.; Koh, S. B.; Chang, K.; Macosko, C. W.; Dion, R. P. *Polymer* **2004,** *45* (1), 197-206.

12. Khaydarov, A. A.; Kazlauciunas, A.; Mounterey, P. E.; Perrier, S. *Polymer Bulletin* **2011,** *66* (8), 1089-1098.

13. Kalambur, S.; Rizvi, S. S. H. *Journal of Plastic Film & Sheeting* **2006,** *22* (1), 39-58.

14. Jiao, J.; Kramer, E. J.; de Vos, S.; Möller, M.; Koning, C. *Macromolecules* **1999,** *32* (19), 6261-6269.

15. Lee, S.-S.; Ahn, T. O. *Journal of Applied Polymer Science* **1999,** *71* (7), 1187-1196.

16. Bezděk, M.; Hrabák, F. *Journal of Polymer Science: Polymer Chemistry Edition* **1979,** *17* (9), 2857-2864.

17. Wan, D.; Shi, L.; Huang, J. *Journal of Polymer Science Part A: Polymer Chemistry* **1998,** *36* (16), 2927-2931.

18. Larson, N.; Greish, K.; Bauer, H.; Maeda, H.; Ghandehari, H. *International Journal of Pharmaceutics* **2011,** *420* (1), 111-117.

19. Donati, I.; Gamini, A.; Vetere, A.; Campa, C.; Paoletti, S. *Biomacromolecules* **2002,** *3* (4), 805-812.

20. Davaa, E.; Lee, J.; Jenjob, R.; Yang, S.-G. *ACS Applied Materials & Interfaces* **2017,** *9* (1), 71-79.

21. Pompe, T.; Zschoche, S.; Herold, N.; Salchert, K.; Gouzy, M. F.; Sperling, C.; Werner, C. *Biomacromolecules* **2003,** *4* (4), 1072.

22. Henry, S. M.; El-Sayed, M. E. H.; Pirie, C. M.; Hoffman, A. S.; Stayton, P. S. *Biomacromolecules* **2006,** *7* (8), 2407.

23. Sroog, C. E. *Journal of Polymer Science: Macromolecular Reviews* **1976,** *11* (1), 161-208.

24. Harris, F. W. In *Polyimides*, Wilson, D.; Stenzenberger, H. D.; Hergenrother, P. M., Eds. Springer Netherlands: Dordrecht, 1990; pp 1-37.

25. Davis, P. D.; Bit, R. A. *Tetrahedron Letters* **1990,** *31* (36), 5201-5204.

26. Willcock, H.; O'Reilly, R. K. *Polymer Chemistry* **2010,** *1* (2), 149-157.

27. Lewis, R. W.; Evans, R. A.; Malic, N.; Saito, K.; Cameron, N. R. *Polymer Chemistry* **2017,** *8* (24), 3702-3711.

28. Chong, Y. K.; Moad, G.; Rizzardo, E.; Thang, S. H. *Macromolecules* **2007,** *40* (13), 4446-4455.

29. Belkhiria, S.; Meyer, T.; Renken, A. *Chemical Engineering Science* **1994,** *49* (24B), 4981-90.

30. Chernikova, E.; Terpugova, P.; Bui, C.; Charleux, B. *Polymer* **2003,** *44* (15), 4101-4107.

31. Khuong, K. S.; Jones, W. H.; Pryor, W. A.; Houk, K. N. *Journal of the American Chemical Society* **2005,** *127* (4), 1265-1277.

32. Ha, N. T. H. *Polymer* **1999,** *40* (4), 1081-1086.

33. Moriceau, G.; Gody, G.; Hartlieb, M.; Winn, J.; Kim, H.; Mastrangelo, A.; Smith, T.; Perrier, S. *Polymer Chemistry* **2017,** *8* (28), 4152-4161.

34. Barron, P. F.; Hill, D. J. T.; O'Donnell, J. H.; O'Sullivan, P. W. *Macromolecules* **1984,** *17* (10), 1967-1972.

35. Perrier, S.; Takolpuckdee, P.; Westwood, J.; Lewis, D. M. *Macromolecules* **2004,** *37*, 2709.

36. Gody, G.; Maschmeyer, T.; Zetterlund, P. B.; Perrier, S. *Nature Communications* **2013,** *4*, 2505.

37. Lutz, J.-F.; Ouchi, M.; Liu, D. R.; Sawamoto, M. *Science* **2013,** *341* (6146).

38. You, Y.-Z.; Zhou, Q.-H.; Manickam, D. S.; Wan, L.; Mao, G.-Z.; Oupický, D. *Macromolecules* **2007,** *40* (24), 8617-8624.

39. Gody, G.; Maschmeyer, T.; Zetterlund, P. B.; Perrier, S. *Macromolecules* **2014,** *47* (2), 639-649.

40. Harrisson, S.; Wooley, K. L. *Chemical Communications* **2005,** (26), 3259-3261.

41. Feng, X.-S.; Pan, C.-Y. *Macromolecules* **2002,** *35* (13), 4888-4893.

42. Baranello, M. P.; Bauer, L.; Benoit, D. S. W. *Biomacromolecules* **2014,** *15* (7), 2629.

43. Liu, H.-Y.; Cao, K.; Huang, Y.; Yao, Z.; Li, B.-G.; Hu, G.-H. *Journal of Applied Polymer Science* **2006,** *100* (4), 2744-2749.

44. Liu, H.-Y.; Yao, Z.; Cao, K.; Li, B.-G. *Journal of Applied Polymer Science* **2010,** *116* (5), 2951-2957.

45. Ahokas, M.; Wilén, C.-E. *Progress in Organic Coatings* **2009,** *66* (4), 377-381.

46. Coleman, L. E.; Conrady, J. A. *Journal of Polymer Science* **1959,** *38* (133), 241-245.

47. Tawney, P. O.; Snyder, R. H.; Conger, R. P.; Leibbrand, K. A.; Stiteler, C. H.; Williams, A. R. *The Journal of Organic Chemistry* **1961,** *26* (1), 15-21.

48. Kojima, K.; Yoda, N.; Marvel, C. S. *Journal of Polymer Science Part A-1: Polymer Chemistry* **1966,** *4* (5), 1121-1134.

49. Haas, H. C.; MacDonald, R. L. *Journal of Polymer Science: Polymer Chemistry Edition* **1973,** *11* (2), 327-343.

50. Haas, H. C. Colored image formation from maleimide copolymers.1973-06-29, 1979.

51. Davis, F.; Hodge, P.; Towns, C. R.; Ali-Adib, Z. *Macromolecules* **1991,** *24* (20), 5695-5703.

52. Davies, M. C.; Dawkins, J. V.; Hourston, D. J.; Meehan, E. *Polymer* **2002,** *43* (15), 4311-4314.

Chapter 5: Carbon Black dispersion using amphiphilic block copolymers

This chapter compares the properties of a range of dispersing agents. In addition, the specific physico-chemical properties required for block copolymers to act as dispersants are discussed. The block copolymer contained a binding moiety compatible block, providing steric stabilisation and allowing an anchor point, allowing for enhanced pigment surface affinity increasing the adsorption mechanism on the pigment surface. Based on this, the block copolymers described in Chapters 2, 3 and 4 were tested in their ability to enhance dispersion of carbon black FW200 (CB FW200) in solvent borne media. Dynamic light scattering (DLS) and Nanotrac Analysis were used to study the potential self-assembly of the amphiphilic block copolymer in organic media and to characterise the particle size distribution of the carbon black coated by the polymer, which is supported by TEM images. Also, the quantification of the polymer coated was determined by thermogravimetric analysis to determine the polymer architecture most suited to dispersing carbon black effectively.

Chapter 5: Carbon Black dispersion using amphiphilic diblock copolymers

5.1. Introduction

- Carbon Black pigment

Carbon black (CB) manufacturing leads to small and fine porous carbon particles obtained after pyrolysis of hydrocarbons from a petroleum-based feedstock. Most of the carbon pigments are supplied either as powders, which can be easily dispersed, or as granules, which are more challenging to disperse as the dense and compact granules require the use of a source of shear stress, such as grinding or milling, to break the agglomerates. There are numerous different forms of carbon black well suited to different applications. A summary of CB have been reported in this following table (**Table 5.1**):

Table 5.1: Size of Carbon Black particles, aggregates and agglomerates

Carbon black	Primary particle (nm)	Aggregate (nm)	Chemical process
Thermal	120-500	400-600	Thermal-oxidative
Oil-furnace	10-400	50-400	Thermal-oxidative
Channel	10-30	50-200	Thermal-oxidative
Lampblack	60-200	300-600	Thermal
Acetylene Black	30-50	350-400	Thermal

- Manufacturing processes

The *thermal* black pigment is predominantly used as filler elastomer and is obtained by the decomposition of hydrocarbon gases in the absence of oxygen, producing a very coarse particle.

Furnace black is the most commonly used carbon black pigment, and corresponds to roughly 90 % of the world production. It is obtained from aromatic hydrocarbons (oil or gas), and has a heterogeneous particle size distribution with a neutral pH surface. The oil is injected into a heated chamber and decomposed to form carbon black particles. The reaction is quenched with water which allows the separation of the gas and product.

Channel type carbon black has the smallest particle size. The manufacturing process involves the contact of a natural gas flame with a steel channel in the presence of atmospheric oxygen, resulting in a particle with a high concentration of oxygen on the surface and low pH. This process is not environmentally friendly and gives a low yield. Moreover, other types of carbon black can be easily oxidised to give similar surface properties as channel black; a process which is more cost effective.

Lampblack pigment is the result of burned petroleum products and is composed of large particle sizes. This technique is not suitable for a mass production.

Acetylene black is obtained from the thermal decomposition of acetylene gas forming a carbon black pigment with a high crystallinity and is widely used for electric devices.[1]

All these manufacturing processes directly impact the physical and chemical properties, allowing targeting towards a wide range of applications, such as a reinforcing filler, for the long-term weathering performance, UV stability and coating.[2,3]

Properties such as structure, surface chemistry[4,5] porosity[6,7] and particle size of carbon black can directly influence its performance for different applications. Some carbon black pigments have thermal and conductivity properties[8] and therefore can be used in thermal pastes.[9,10,11] Alternatively, adding dispersing additives to the pigment in solution can improve the conductivity, and thus expand the potential applications.[12]

- Fundamental properties

As previously discussed, the manufacturing process can result in very different physico-chemical properties, which can ultimately affect their desired application. The structure and morphology (shape, size and distribution) are other criteria which strongly influence the colour and resulting application properties. The most important parameters to consider when coating carbon black is the jetness (or opacity of the colour), (consequently the optical density, viscosity and the tinting strength), which is related to the particle size. The term "structure" is usually referred to as the formation of particles such as agglomerates or aggregates, which vary from an individual particle to cluster (**Figure 5.1**).[13]

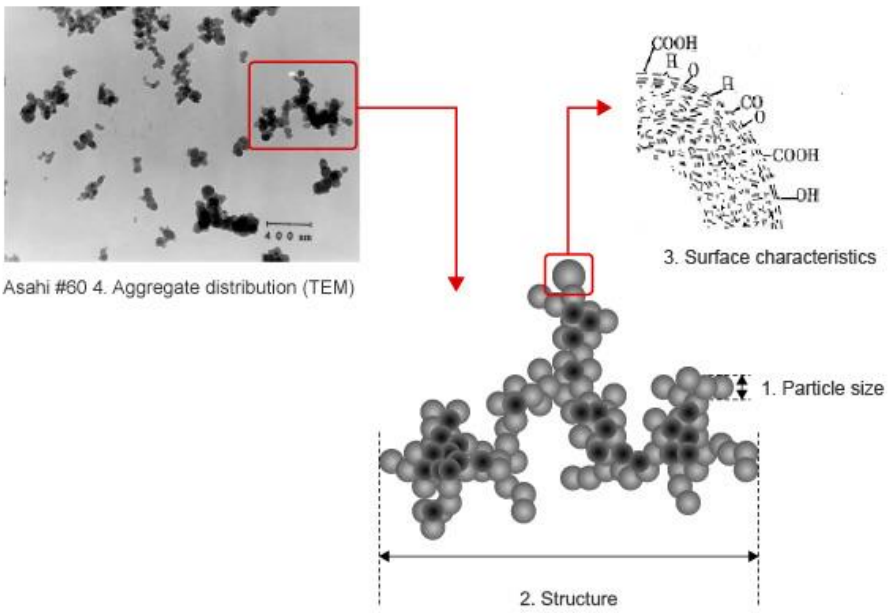

Figure 5.1: Structure and surface characteristics of CB[13]

Porosity and surface area are also considered in industrial application. Indeed, the surface activity highlights all the potential interactions with the material surface. Many chemical and physical reactions can been performed to modify the surface activity. For instance, an oxidation processes will increase the ratio of oxygen on the surface, while induction at high temperature in an inert atmosphere will cap all the functional groups present on the pigment, resulting in an inert particle.[8,14,15,16] The oxidised carbon black having the capability to alter the pH of carbon pigment is by far the most abundant and can be the result of one of the three types of surfaces; neutral, basic or acidic. A neutral surface is obtained by the irreversible adsorption of oxygen at the unsaturated sites present at the surface. Treatment of the carbon surface above 1000 ˚C in the presence of oxygen forms some heterocyclic oxygen-containing rings, leading to basic conditions.

Lastly, the formation of phenolic, quinone, or carboxylic groups, provides a polar character to the carbon black and is obtained either at a high temperature (up to 400 ˚C) in presence of oxygen or by using an oxidising solution at room temperature. Some other heteroatoms can be utilised, such as nitrogen, sulphur and chlorine, to modify the CB surface.[17] Other bonds are also present at the surface, such as carbon-hydrogen bonds, located at the edges and corners of the graphitic crystallites due to the chemisorption of water, allowing the formation of hydroxyl, hydroquinone or phenolic groups. A complex of carbon-nitrogen bonds, at a concentration below 1 % depending on the manufacturing conditions, can also be found and are formed at a temperatures above 900 ˚C. Different structures of carbon-sulphur moieties (such as organo-sulphur and inorganic sulphate) can be detected in some black pigments. The presence of hydrogen at high temperature will release hydrogen sulphide, which is a very poisonous and corrosive gas, which is an important safety consideration during surface modification. Finally carbon-halogen bonds can be present on the surface depending on the chemical process used during manufacture and the nature of the carbon surface.

As mentioned previously, the high specific area requiring a high dispersant loading, the poor polarity and the good affinity for oil absorption, highlight the challenges in dispersing the carbon black pigment in water or organic media. Also, due to the fine nature of the material, it can be difficult to obtain a stable dispersion after the grinding process. To face this problem and to reduce the production cost, industrial processes use additives[18,19] including amine[20] and imide.[21]

As such, this chapter describes the efficiency of different classes of polymers (statistical and diblock), polymerised *via* reversible addition-fragmentation chain transfer, used as dispersants. One specific grade of carbon black pigment (CB FW200) is characterised by; BET, TGA, Raman spectroscopy, infra-red, pH, TEM and dynamic light scattering (DLS) to evaluate the structure and functionalities present on the pigment surface and to determine the interactions with the dispersant. Then, the polymeric dispersants were milled in presence of CB FW200 and the particle size distribution analysed using Nanotrac analysis and TEM. The quantitative study of the polymer coated on the carbon black surface was performed by thermogravimetric analysis.

5.2. **Results and Discussion**

5.2.1. Carbon Black characterisation

- BET

One of the most important criteria for a good pigment wetting is the shape and the surface of the pigment. The Langmuir model was developed by Irvin Langmuir in 1916, it describes the surface coverage of an adsorbed gas above a single layer surface and is commonly used to determine the surface area.[22] An extension of this model was developed by Stephen Brunauer, Paul Hugh Emmet and Edward Teller, known as the "BET" model.[23] Contrary to the Langmuir model, they consider the formation of multiple layers of gas molecules adsorbed physically onto the solid surface (**Figure 5.2)**.

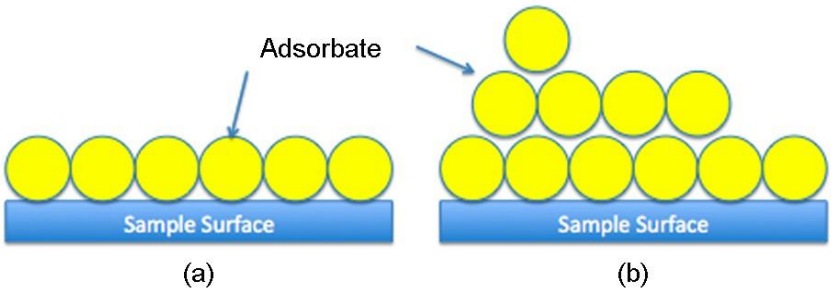

Figure 5.2: Langmuir model (**a**) and BET (Stephen Brunauer, Paul Hugh Emmet and Edward Teller) measurement mechanism (**b**)

To determine the adsorption mechanism and properties of carbon black used in this study, the BET model was considered. The amount of adsorbed nitrogen is used to evaluate the total and external surface areas at several pressures of nitrogen. The adsorption and desorption isotherms for CB FW200 under nitrogen are shown in **Figure 5.3**. A hysteresis loop is observed indicating Type IV isotherms, which suggests that the surface of the carbon black particles are mesoporous *i.e.* there is multilayer formation occurring, suggesting a weak interaction between the adsorbate molecules.

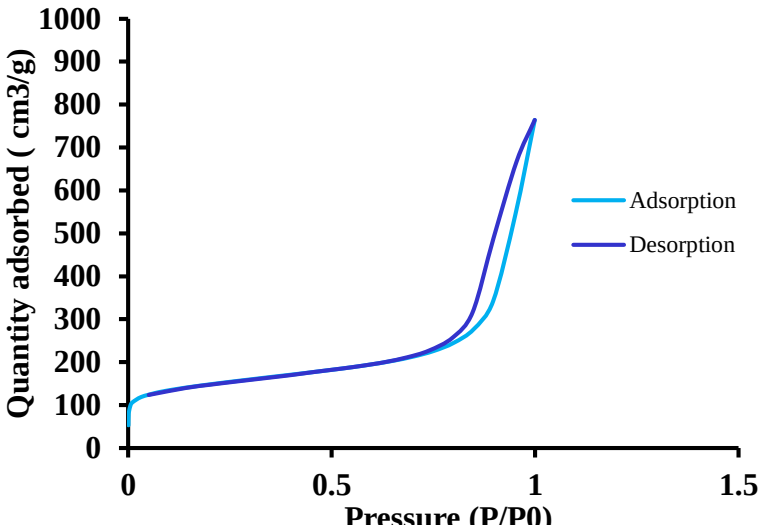

Figure 5.3: Adsorption and desorption measurement of CB FW200

The BET equation was then used to determine the surface area of CB FW200 and the particle diameter (**Table 5.2**), which correlate with the data reporter by Pawlyta.[24]

Table 5.2: Carbon content, surface area and particle diameter of CB FW200

	Carbon Black FW200
Carbon content (%)	99.1
Particle surface area (m^2/g)	539.1
Particle diameter (nm)	18

This preliminary data is required in order to optimise the subsequent milling steps. A higher surface area will improve the penetration of the solvent into the pigment particle (wetting step) and so reduce the viscosity of the polymer and carbon black mixture (milling).

- Determination of functional group by Raman and Infra-Red spectroscopy

Carbon black is well-known to be a mixture of graphitic and amorphous like particles, giving specific properties. Here, the structure was analysed by different techniques such as Raman spectroscopy and microscopy (HRTEM). HRTEM images provide few options for quantitative analysis and need to be combined with powder X-ray diffraction (XRD) and Raman spectroscopy.[25,26] Raman, XPS and Infra-Red (IR) are a complementary techniques giving different information about the carbon composition and functional groups present within a system.

Pawlyta *et al*. have described the carbonisation and graphitisation of five grades of carbon black including the CB FW200 used here.[24] Raman spectra were collected in the 500 – 3000 cm^{-1} range using a 20 mW laser at 532 nm and spectral resolution at 4.5 cm^{-1}. A video microscope system coupled to the spectrometer was used to facilitate the laser on the sample surface. Using the microscope objective, non-uniform spherical particles were observed. The spectra were collected at different places with objectives at x20, 50 and 100, at room temperature in 120 seconds to avoid any sample degradation. The decomposition of the spectra was carried out using instrument specific software following Sadezky's method.[27] The spectrum reveals the presence distinctive Raman peaks suggesting different structure of carbon materials (**Figure 5.4**). The D-band peak at 1340 cm^{-1} represents the level of disorder of the crystal structure while the G-band peak at 1580 cm^{-1} is associated with the graphite structure.

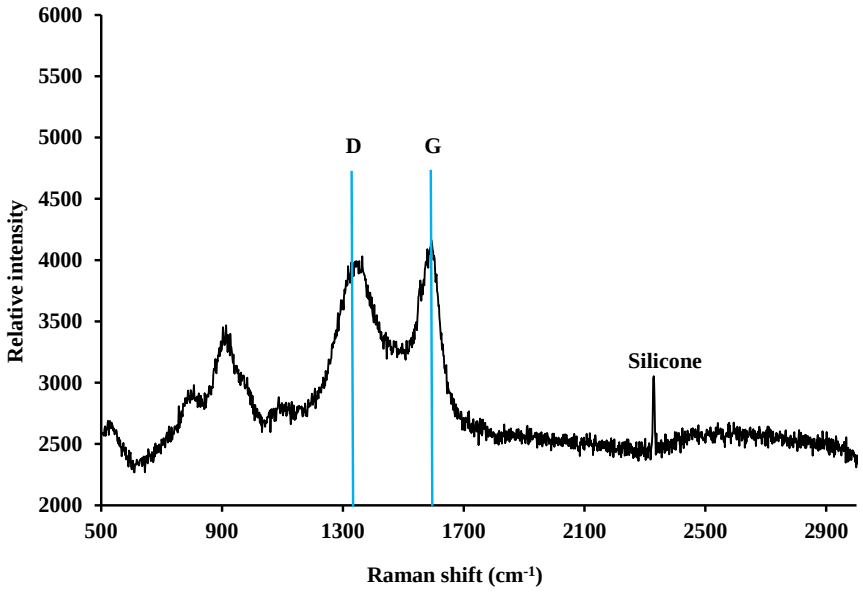

Figure 5.4: Raman spectrum of CB FW200

The infra-red (IR) spectrum of carbon black pigment was also recorded but it was not possible to assess the different functional groups due to poor resolution due to the strong opacity (**Figure 5.5**). Despite this, carbonyl groups are observed which can suggest the presence of carboxylic acid and ester moieties on the surface.

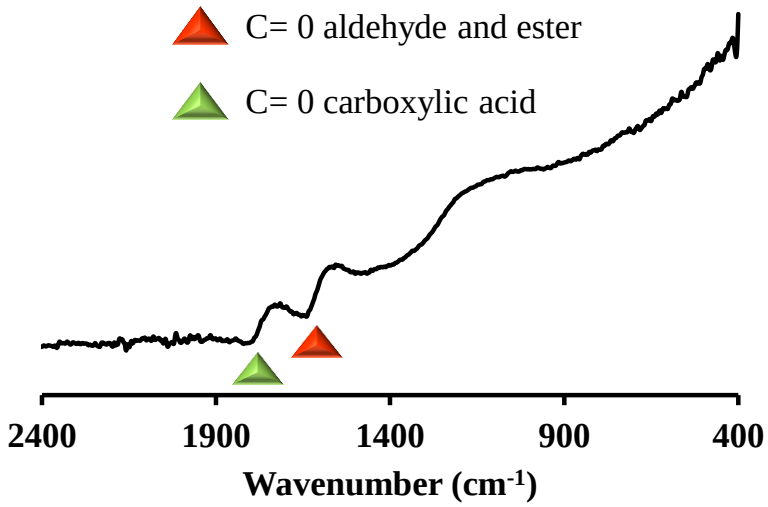

Figure 5.5: Infra-red of Carbon black FW200

- X-ray Photoelectron Spectroscopy analysis

Deconvolution of XPS signals gives the energy of the (C1 s) peak for CB FW200, presented in **Table 5.3**. The percentage of carbon (85.73 %), oxygen (14.0 %) and sulphur (0.27 %) is obtained by XPS analysis and performed with a monochromatic Al kα x-ray source (hν 1486.6 eV).

Table 5.3: XPS data of Carbon Black FW200

Binding energy (eV)	Bonding environment	% of region
284.48	Carbon Sp^2	82.45
286.42	C-O	5.06
288.52	C = O	7.8
290.5	π-π*	4.70

- TEM analysis

The carbonisation and partial graphitization of carbon black pigment (CB FW200) predominantly used for this thesis was also analysed by HRTEM as a raw sample (untreated) at 2600 ˚C by Pawlyta *et al.*[24] (**Figure 5.6**).

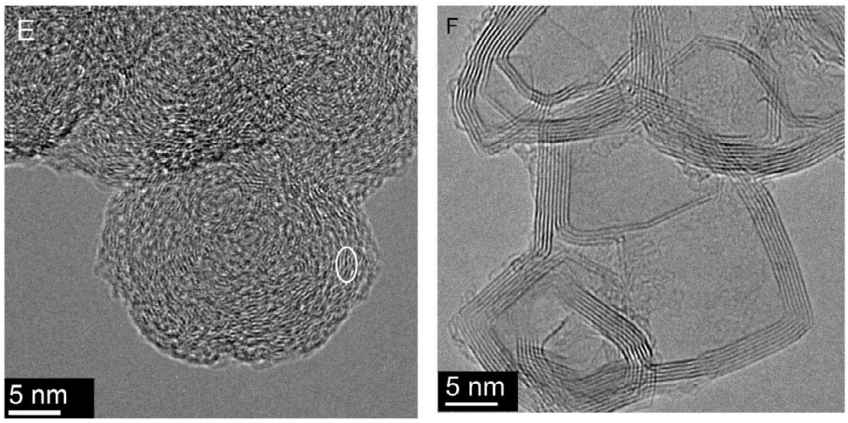

Figure 5.6: HRTEM of Carbon black FW200 [24]

The formation of distorted and disoriented concentric layers are clearly detected. The temperature appears to affect the shape of the layer, giving polyhedral planar forms also observed in previous studies.[28]

Only small stacks of planar layers are present in CB FW200 *via* HRTEM which is typical for a nongraphic carbon. The diameter and morphology of the materials were recorded by transmission electron microscopy (TEM) at different magnifications. This is a powerful technique to measure the particle size distribution using imaging software (ImageJ). The images (**Figure 5.7**) reveal that carbon black is partially dispersed, however, the majority of the sample is composed of aggregates.

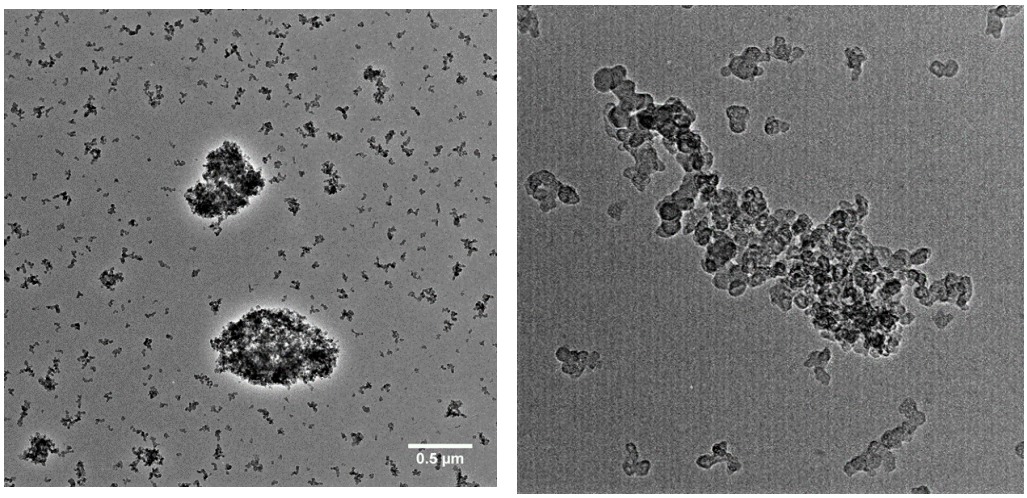

Figure 5.7: TEM images of Carbon black FW200 pigment dispersed in acetate solvent (0.1 % w/w). Scale: 500 nm (left) and 0.1 nm (right)

These primary aggregates (clusters) are usually formed by a fusion of primary particles, while the agglomerates contained a large number of aggregates physically linked together.

- Thermogravimetric Analyses of Carbon Black FW200

The thermal decomposition of the carbon black (FW200) was fully studied by Jakab *et al*.[29] They studied the effect of the thermal decomposition of carbon black in presence of broad range of polymers, such as polypropylene (PP), polyethylene (PE), polystyrene (PS), polyacrylonitrile (PAN) and polymethyl methacrylate (PMMA), using thermogravimetric analysis coupled with mass spectrometry (TGA/MS) and pyrolysis-gas chromatography coupled with mass spectrometry (Py-GC/MS). The presence of the carbon in the polymerisation mixture modified the decomposition rate of PAN, PE, PS and PP due to the interactions (hydrogenation, intermolecular reactions or steric hindrance) between the polymer backbone and the pigment.

Here, the thermal degradation of the carbon black pigment was studied by thermogravimetric analysis from 25 - 800 ˚C. A first rate of degradation is observed before 150 ˚C, which may be attributed is related to the degradation of small molecules such as solvents (including water an carbon dioxide) or residual reactants (**Figure 5.8**). The mass spectrometry data reported by Jakab confirm the release of carbon dioxide and water.[29] They also found 93 % of residual carbon between 200 – 550 ˚C, which is in good agreement with our data, in which the full degradation of the pigment begins above 550 ˚C.

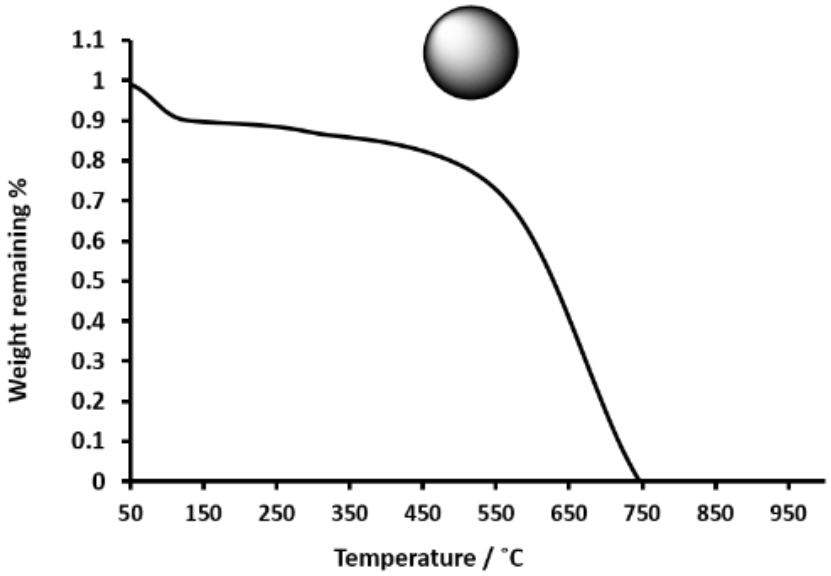

Figure 5.8: TGA chromatogram of Carbon black FW200 heated to 1000 ˚C with an heating rate of 10 ˚C /min in nitrogen.

- Solution acidity

For the carbon material, Boehm titration has been used in order to determine the different functional groups present in three different carbon surfaces.[30] Jakab *et al.* found that for CB FW200, any basic group could be present, but predominantly carbonyl, phenolic, carboxyl and lactone groups were found, which suggests that the pigment is highly acidic.

To confirm this, 700 mg of pigment was mixed in 10 mL of water and sonicated for 10 min. The mixture was left for 10 more minutes to allow the carbon to settle. A pH-meter was used to determine the pH of this slurry. After calibration, a pH of 1.95 was recorded which confirms the acidic nature of this sample.

- Measure of particle size of Carbon black pigment in organic solvent by DLS

Several grades (furnace, channel, lamp, acetylene or thermal blacks) of carbon black are commercially available and are different in their aggregate shapes, sizes and distributions. Moreover, some chemical or thermal treatments can also potentially change their properties. The formation of spherical primary particles of carbon black are due to the rearrangement of carbon radicals and fragments. The average surface area is around 1500 m^2 for fine particles and 25 m^2 for coarse (aggregates). It is crucial to consider the particle size distribution as it is related to the pigment properties, such as wetting, rheology and thermal degradation caused by temperature. The size of the particles is generally determined by using dynamic light scattering in aqueous or organic solutions. In a solvent, the particles move randomly due to Brownian motion. As the laser is fired through the suspension, it interacts with and scatters from the moving particles. By measuring the change in scattering over time (due to particle movement), it is possible to calculate a diffusion coefficient, from which a particle size distribution can be determined. For reliable data, the solution must be non-turbid and the component should not absorb the light, as is the case for some forms of carbon black. Additionally, the refractive index of both solvent and sample must be known for reliable DLS data. In the present study, a solution of 1 mg/mL carbon black in butyl acetate was sonicated for 10 mins to break any agglomerates, and then filtrated. The particle size was determined by DLS using Malvern Zetasizer NanoZS instrument in a quartz cuvette. The intensity of scattered light from the suspension gives an overview of different sized particles present in suspension.

It is important to note that DLS gives preference to larger particles due to an increased intensity of scattered light from larger particles.

The broad and bimodal distribution recorded in methoxypropyl acetate (refractive index 1.402) indicates the presence of the large aggregates with an average size of 190 nm and a Pdi of 0.37 (**Figure 5.9**).

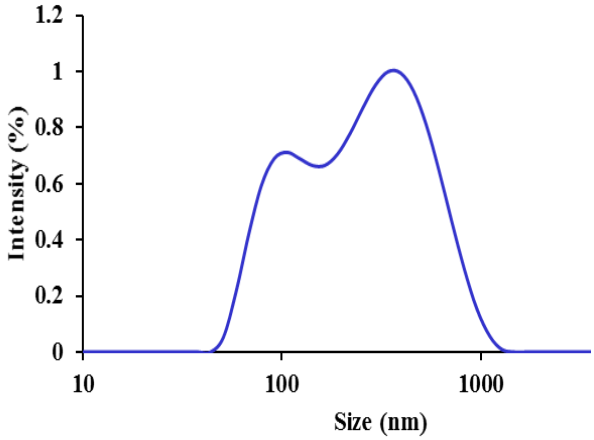

Figure 5.9: Particle size distribution of CB FW200 in acetate solvent

5.2.2. Dispersion of Carbon Black using block copolymer

The dispersion of pigment using polymers is guided by the affinity of the non-covalent interactions from the anchor group of the polymer with the surface of the material, however, many other parameters must be considered for a strong pigment affinity. All the range of diblock copolymers using a several classes of monomers (acrylate, methacrylate and styrene-alternating-maleimide) synthesised and reported in **Chapters 2, 3 and 4** were milled with a loading of 60 % in the presence of carbon black and glass beads in similar conditions. The effect of the molecular weights of 10 kDa, 15 kDa and 22 kDa were tested in order to assess effectiveness as dispersion agents.

Dynamic light scattering and Nanotrac analysis were also used to evaluate the amphiphilic block after milling and to measure the particle size distribution. An average particle size of between 200 nm and 400 nm is targeted to reach the optimal physical properties for the coating application. Transmission electronic microscopy was performed on all samples to confirm the data obtained by DLS. Finally, thermogravimetric analysis is inescapable to quantify the amount of polymer coated on the carbon black pigment surface.

5.2.2.1. Dispersion using p(DMAEMA)$_x$-*b*-p(*n*BA)$_y$ block copolymers

The first diblock copolymer attempted, composed of DMAEMA and *n*BA, was tested on dispersion. As stated in **Chapter 2**, a poor control of methacrylate homopolymer using BMDPT leads to a bimodal distribution after addition of *n*BA ($Đ \approx 1.5$). Only the presence if homopolymers (DMAEMA and *n*BA) are observed. As a control, MCTP RAFT agent was used in order prepare a well-defined copolymer. Using MCTP CTA gives a high proportion of block copolymer but some non-reinitiated pDMAEMA remains after the chain extension. Nevertheless, the dispersion studies of these blocks were performed in order to assess the importance of the polymeric structure on pigment dispersion. The particle size distribution was analysed by DLS and Nanotrac in butyl acetate after 16 hours of milling of each diblock copolymer of poly(DMAEMA)-*block*-poly(*n*BA) with a degree of polymerisation of 55/19, 70/35 and 100/50 respectively. Particle size distribution of carbon black obtained by using poly(DMAEMA)-*block*-poly(*n*BA) as a surfactant shows a constant value of D50 (50 % of the particles have a size below D50) with an average value between 300 and 400 nm.

However, a broad distribution of D90 (90 % of the particles have a size below D90) indicates the presence of aggregates (**Figure 5.10**). The non-controlled particle size distribution shows the poor efficiency of the diblock copolymer. The bimodal molar mass distribution observed in the SEC molecular weight distribution suggests the presence of free poly(DMAEMA) and diblock copolymer in the polymerisation mixture. However, the homopolymer DMEAMA can easily cover the carbon black surface *via* Van der Waals interactions, thus competing with the diblock copolymer in solution and decreasing the steric stabilisation effect brought by the *n*-BA block to act as a stabiliser. Also, the highly acidic surface of the pigment allows the protonation of the tertiary amine and forms a strong hydrogen bound. In comparison, using a well-defined diblock copolymer obtained with MCTP RAFT agent allows better control over the particle size distribution with the value of D50 and D90 expected (**Figure 5.11**). Hence, this control proves the importance of the polymer structure on pigment dispersion. The only effect of the diblock copolymer in solution is to induce a perfect interaction of DMAEMA block with the pigment surface, and allows the *n*-BA block to repulse the other pigment in solution *via* a steric mechanism.

Interestingly, the degree of polymerisation does not affect the size of the particle, giving the opportunity to design a wide range of macromolecules.

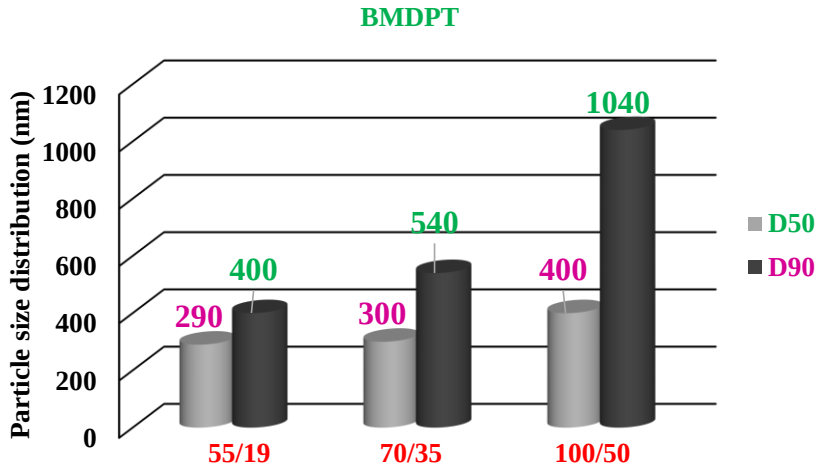

Figure 5.10: Particle size distribution of p(DMAEMA)-*b*-p(BA) copolymer synthesised with BMDPT RAFT agent (DP_n = 55/19, 70/35, 100/50) at 25 ˚C using in butyl acetate solvent analysed by Nanotrac instrument

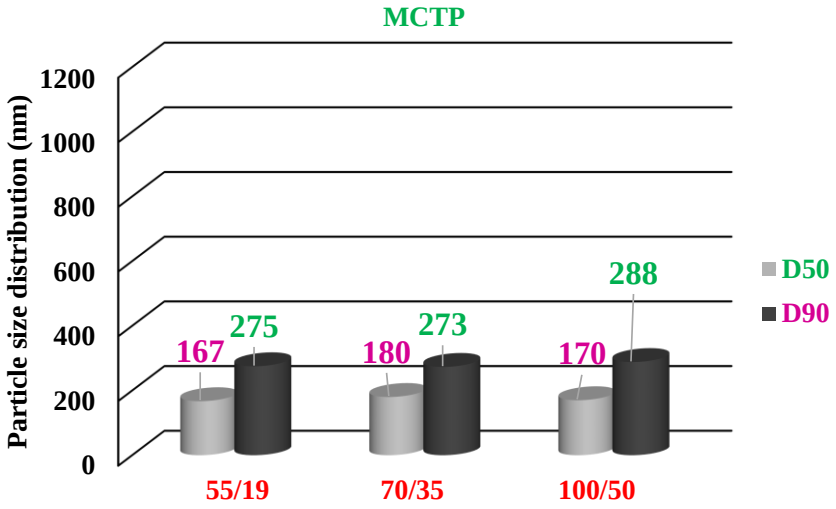

Figure 5.11: Particle size distribution of p(DMAEMA)-*b*-p(nBA) copolymer synthesised with MCTP RAFT agent (DP_n = 55/19, 70/35, 100/50) at 25 ˚C using in butyl acetate solvent analysed by Nanotrac instrument

As such, in order to use the BMDPT RAFT agent to prepare diblock copolymers, an alternative synthetic strategy was investigated to design a well-defined diblock copolymer. To this end, polymerisation of acrylates using BMDPT is relatively well-controlled, and therefore a pure acrylate diblock copolymer was made by batch polymerisation.

5.2.2.2. Dispersion using acrylate block copolymer

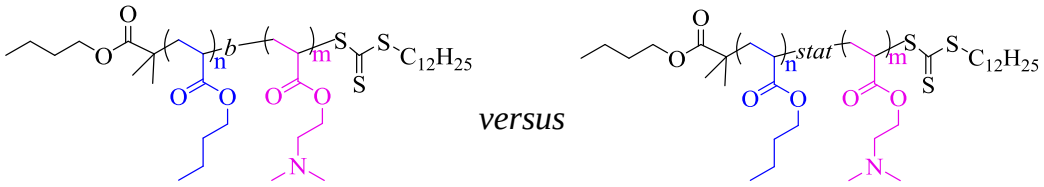

Figure 5.12: Polymeric structure of p(*n*BA)$_n$-*b*-p(DMAEA)$_m$ *versus* p(*n*BA)$_n$-*stat*-p(DMAEA)$_m$ copolymers

The acrylic monomers are widely used due to their large commercial availability and good compatibility with coating systems. Auschra *et al.* have reported the synthesis of p(*n*BA)-*block*-p(DMAEA) *via* NMP and ATRP methods and used to disperse red pigments with different surface area in butyl acetate solvent. The variation of the anchoring block (pDMAEA) and stabilizer block p(*n*BA) molecular weight was studied and found that increasing the length of the anchoring group leads a better stabilisation while a the effect of the p(nBA) length can significantly change the block copolymer efficiency.[31] Here, the structure of the both block and statistical p(*n*BA)$_n$-p(DMAEA)$_m$ copolymer synthesied in presence of BMDPT RAFT agent via RAFT polymerisation technique is reported in the **Figure 5.12**. The statistical copolymer is used to assess the importance of the polymer configuration on the pigment dispersion efficiency.

Figure 5.13 gathered the physical, thermogravimetric and microscopic characterisations of the carbon black dispersion in presence of the polymer. The nanotrac data (**Figure 5.13 A**) gives a consitant particle size distribution for the block copolymers for a targeted molecular weight of 10 kDa and 15 kDa while an increase of the D50 and D90 is observed when a higher molecular weight is targeted (22 kDa) which can be attributed to the interpenetration of long hydrophobic polymer chains leading to the formation of aggregates. In parallele, the particle size distribution is also investigated in dynamic light scattering (DLS) by analysing an accurate solution with a concentration of 2 mg/ml prepared from the milling (pigment + polymer + solvent + glass beads) mixture (**Figure 5.13 B**). The particle size obtained by DLS is lower in comparison to nanotrac analysis. The DLS measurement is limited to a range of size comprise between 1 nm and 1000 nm suggesting that the sample is compatible with DLS technique. It is worth mentioning that there are many parameters which should potentially affect the data such as the concentration of the sample, the solubility of the polymer in the solvent, the wavelength used…Also is the system is polydisperse, the larger particles could hide the scsttering from the smaller one which gives an erroneous results. Additionally, the measure of the dispersity is giving by the value of the PDI. Lower is the PDI (close to 0) more the system is monodispersed. The PDI of the block copolymers obtained being below 0.2, the system can be considered monodispersed. **Figure 5.13 C**, thermogravimetric analysis was used to quantify the amount of polymer coated onto the surface of the carbon black. Purified polymers were initially analysed to determine the thermal degradation points. As stated previously, the carbon black FW 200 begins to degrade around 550 ˚C, which is higher than polymeric materials (250 -350 ˚C).

Milled samples were loaded with 60 % w/w of polymer and the analysis was run under nitrogen at a heating rate of 10 ˚C/min from 25 to 600 ˚C. Additionally, a certain volume (between 0.5 mL and 1.5 mL) of the loaded mixture was centrifuged, to remove any non-coated polymer, and left to allow the carbon black coated material to settle. The supernatant was removed and the sediment was washed with acetate. The thermograms representing the mass loss curves of carbon black coated with the well-defined diblock copolymers show two temperatures degradation. The first degradation was around 150 ˚C, which can be attributed to the evaporation of acetate (117 ˚C for butyl acetate and 143 ˚C for methoxypropyl acetate). Then, a full pyrolysis of the diblock copolymer is observed from 250 ˚C to 450 ˚C. **Figure 5.13 D**, an overview of the samples recorded by TEM at low magnification (x 12000) where a few dispersed pigments can be observed. It should be noted, however, that the drying process can lead to the formation of aggregates. Despite this, the sizes obtained correlate with the particle size distribution obtained by Nanotrac. As a general statement, the different polymer chain length targeted for the anchoring and stabiliser group did not affect the dispersion efficiency.

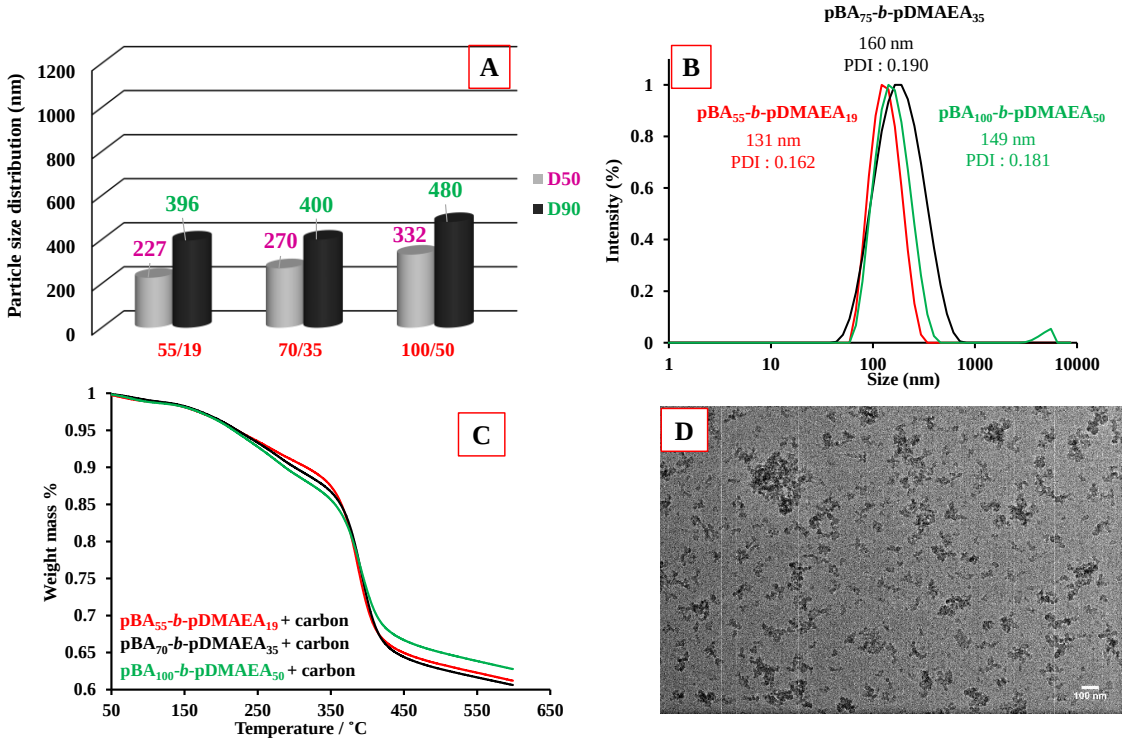

Figure 5.13: Block p(*n*BA)-*b*-p(DMAEA) copolymer synthesised with BMDPT RAFT agent (DP_n = 55/19, 70/35, 100/50) characterisations. Particle size distribution analysed by Nanotrac instrument (**A**) and DLS (**B**). TGA graphs of CB FW200 coated with p(*n*BA)$_n$-*block*-p(DMAEA)$_m$ copolymer heated up to 600 ˚C (**C**). TEM images conducted using a JEOL 2100 operating with a 200 kV prepared by drying a drop of dilute sample (0.01 wt.%) on a 300 Mesh carbon coated grid: **Scale :** 100 nm (**D**)

In contrast, the statistical copolymer used to disperse carbon black generates only aggregates and agglomerates species with high D50 (~ 500 nm) and D90 (~ 700 nm), indicating poor adsorption of the anchor group to the pigment surface (**Figure 5.14 A**). It is likely that the alternating structure of DMAEA and *n*BA does not exhibit sufficient interaction points, meaning that the tertiary amine is not available to interact with a carbon surface. The particle size distributions obtained by DLS are bimodal and the PDI is above 0.2.

The broader particle size distribution with a shoulder around 100 nm suggestes a presence of the primary particles and aggregates mixture. The main peak is around 350 nm which is smaller in comparison to Nanotrac data (460 nm) which can be explained by the low concentration of the solution or the biggest particles are settled and not detected. The TGA profiles remain identique to the TGA recorder for the block copolymer (**Figure 5.14 C)**, however, the percentage of polymer coated is 43 % for the statistical while is 65 % for the block copolymer which prove that the efficiency of the pigment dispersion is strongly related to the polymer configuration (*i.e.* diblock *versus* statistical). To be consistant, the TEM sample was prepared (0.01 w %) and analysied (x 12 000) by using the same condition. **Figure 5.14 D**, shows clearly the formation of aggregate which correlates with the scattering data.

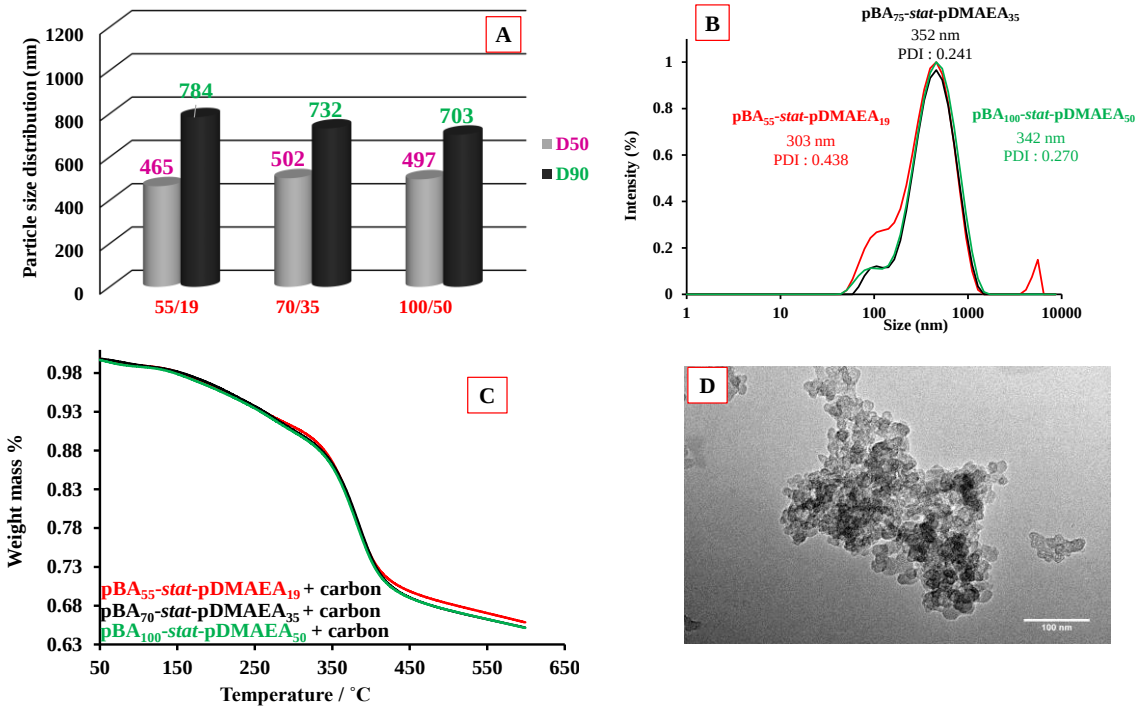

Figure 5.14. p(*n*BA)-*stat*-p(DMAEA) copolymer synthesised with BMDPT RAFT agent (DP_n = 55/19, 70/35, 100/50) characterisations. Particle size distribution analysed by Nanotrac instrument (**A**) and DLS (**B**). TGA graphs of CB FW200 coated with $p(nBA)_n$-*stat*-$p(DMAEA)_m$ copolymer heated up to 600 ˚C (**C**). TEM images conducted using a JEOL 2100 operating with a 200 kV prepared by drying a drop of dilute sample (0.01 wt.%) on a 300 Mesh carbon coated grid: **Scale :** 100 nm (**D**)

5.2.2.3. Dispersion using methacrylate block copolymer

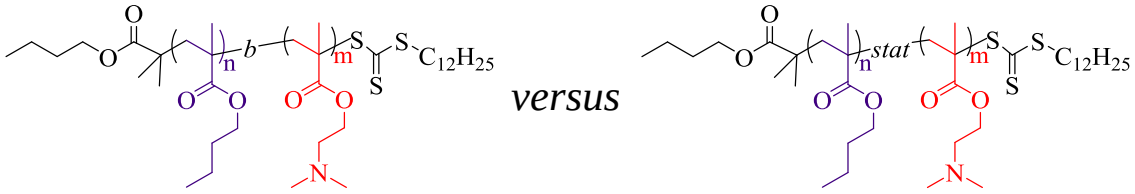

Figure 5.15: Polymeric structure of methacrylate block *versus* methacrylate statistical copolymers

A third class of copolymer was studied and compared to the previous systems with respect to CB dispersion (**Figure 5.15)**. The success of the methacrylate block copolymers prepared by a semi-batch process allowed the targeting of a large selection of molecular weights. Similarly to the acrylate block copolymers, a well-dispersed and a narrow particle size distribution is observed for block copolymers with an average size of 170 nm and 290 nm for D50 and D90 respectively (**Figure 5.16 A**). A few drops of milling solution were charged to a vial with a certain volume of MPA solvent to determine the size distribution of the carbon black dispersions. An identical size of particles (130 -160 nm) is recorded for the acrylate and methacrylate block copolymers by DLS measurements (**Figure 5.16 B**). The quantification of polymer coating is determined by TGA after purification *via* a centrifugation process. A mass between 3 and 6 mg were introduced in an aluminium pan and heated from 25 to 600 ˚C under nitrogen with a heating rate of 10 ˚C/min. A degradation of 35 % is observed for block copolymers and a percentage of 62 % is determined after pyrolysis (**Figure 5.16 C**). The TEM of methacrylate block copolymer is recorder in **Figure 5.16 D** and shows a great dispersion of the pigment. Moreover, a dispersion with a narrower particle size distribution is achieved for methacrylate diblock copolymers in comparison to the acrylate diblock.

It is possible that there is residual homopolymer, butyl acrylate, in the mixture with the diblock copolymer after purification *via* precipitation process. The purification was challenging due to the low glass transition of acrylates, which requires the precipitation at very low temperatures or at room temperature, depending on the molecular weight.

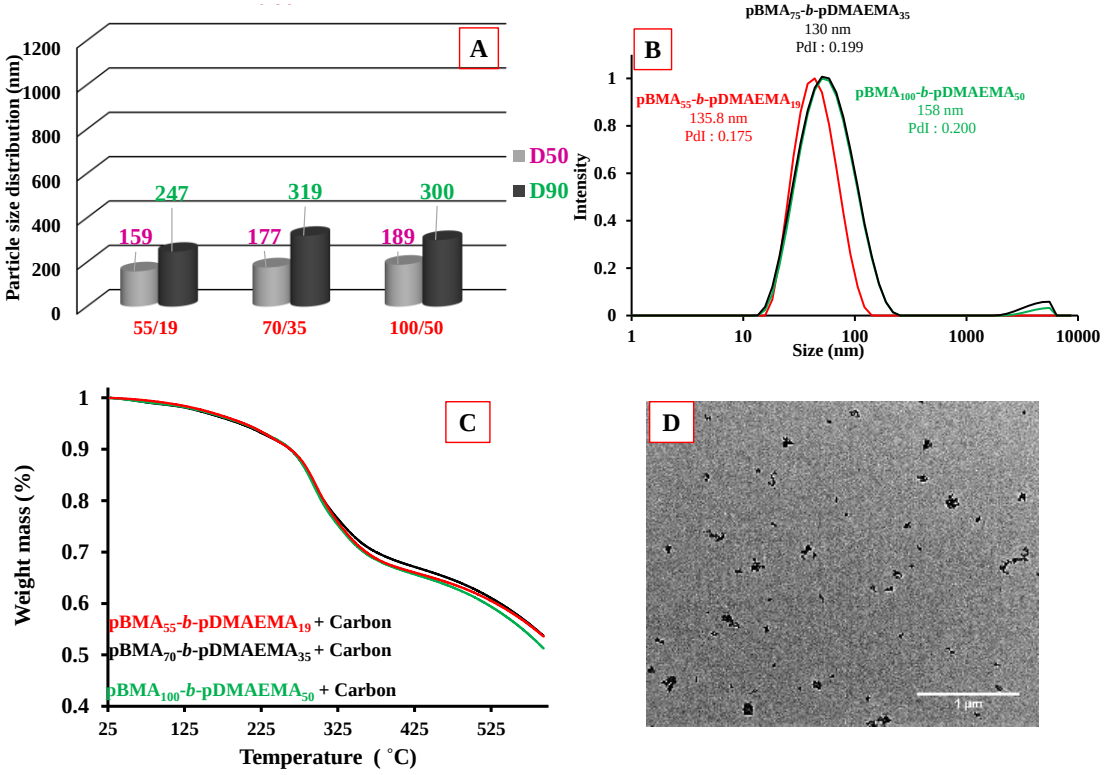

Figure 5.16: Block p(BMA)-*b*-p(DMAEMA) copolymer synthesised with BMDPT RAFT agent (DP_n = 55/19, 70/35, 100/50) characterisations. Particle size distribution analysed by Nanotrac instrument (**A**) and DLS (**B**). TGA graphs of CB FW200 coated with $p(BMA)_n$-*block*-$p(DMAEMA)_m$ copolymer heated up to 600 ˚C (**C**). TEM images conducted using a JEOL 2100 operating with a 200 kV prepared by drying a drop of dilute sample (0.01 wt.%) on a 300 Mesh carbon coated grid: **Scale :** 100 nm (**D**)

In a similar way, the dispersion of the statistical copolymers obtained by feeding process was used a surfactant and compared to the block copolymers. As expected, the nanotrac and DLS data of the statistical copolymer (**Figure 5.17 A and B**) proved the poor efficiency of the statistical polymer configuration by exhibiting a heterogeneous dispersion with D50 - D90 (300 - 850 nm) and a high PDI (> 0.2). The thermolysis of the statistical copolymers shows a similar trend as the previous copolymers (**Figure 5.17 C**). All the thermograms overlapped but and early degradation is observed for the copolymer with the highest molecular weight (pBMA$_{100}$-*stat*-pDMAEMA$_{50}$). The percentage of the copolymers coated on the pigment surface is 51 %. **Figure 5.17 D** illustrates the aggregate formation recorded by TEM.

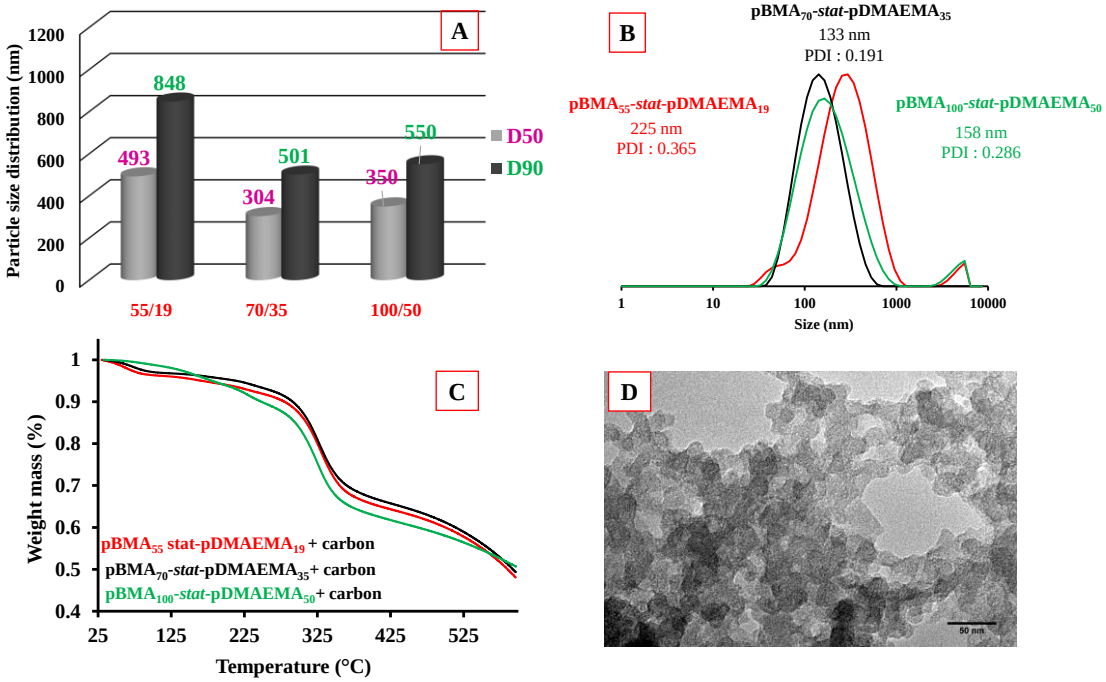

Figure 5.17: p(BMA)-*stat*-p(DMAEMA) copolymer synthesised with BMDPT RAFT agent (DP_n = 55/19, 70/35, 100/50) characterisations. Particle size distribution analysed by Nanotrac instrument (**A**) and DLS (**B**). TGA graphs of CB FW200 coated with $p(BMA)_n$-*stat*-$p(DMAEMA)_m$ copolymer heated up to 600 ˚C (**C**). TEM images conducted using a JEOL 2100 operating with a 200 kV prepared by drying a drop of dilute sample (0.01 wt.%) on a 300 Mesh carbon coated grid: **Scale :** 50 nm (**D**)

5.2.2.4. Dispersion using p(SMAD) block copolymer

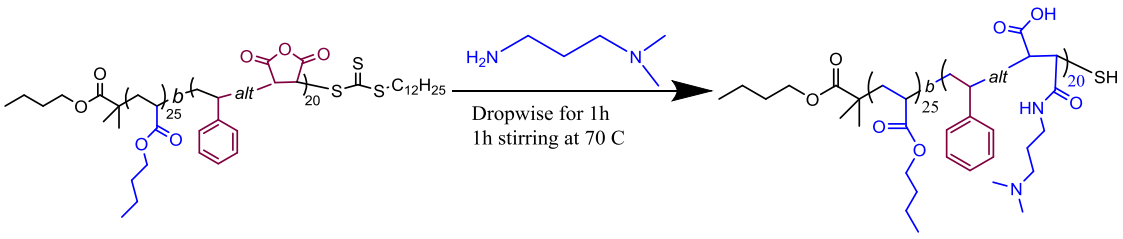

Scheme 5.1: Ring-opening of maleic anhydride with DMAPAA to form poly(styrene-alternating maleic acid)

The design of the block copolymer containing styrene-*alternating*-maleic anhydride permits an easy route to modify the polymer backbone due to the highly reactive maleic anhydride (**Scheme 5.1**). Few studies using poly(SMA) as anionic, cationic or nonionic surfactants in pigment dispersion were reported.[32,33] Hence, the use of a small equivalent of di(methylamino)propyl amine (DMAPAA) involves the maleic anhydride ring opening mechanism, leading the formation of a difunctional polymer, poly(styrene-*alternating*-maleic acid) (pSMAD). In comparison to the previous amphiphilic copolymers bearing only a tertiary amine, this new diblock provides multi anchor groups, including an aromatic functionality, introducing some steric hindrance, therefore improving the

stabilisation process, and also a tertiary amine and carboxylic acid as a pendant group for pigment affinity. One of the crucial condition to reach an effective dispersion of the pigment is the full solvability of the polymer in a giving solvent. When, the preparation of the milling was started, it has been noted the strong turbitity of the polymer solution and the partial solubility of the final block (17 kDa). As shown in **Figure 5.18**, the 10 kDa polymer give rise to a partially cloudy solution while the 15 kDa is observed to be entirely cloudy and viscous. It was not possible to filter these samples due to the presence of the aggregates. Finally, the 17 kDa sample is clear, however, the polymer was nearly insoluble after 30 minutes of sonication and two hours of strong stirring. Dynamic light scattering measurement was attempted before milling reveals a monomodal and narrow particle size distribution for the 10 kDa and 15 kDa, whereas a broad distribution with a small distribution is obtained for the last block (**Figure 5.18**). DLS seems not to be the ideal technique to measure the particle size distribution. However, this preliminary test shows already important interaction between the solvent and the polymer which suggest some additional interactions when the pigment will be added.

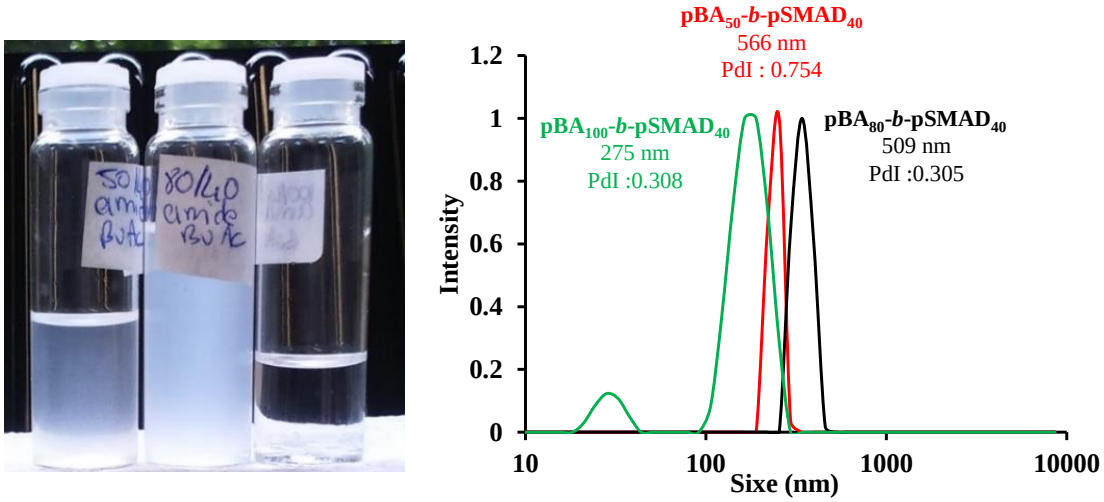

Figure 5.18: Images of p(*n*BA)-*block*-p(SMAD) copolymers in acetate solution: 10 kDa (left), 15 kDa (middle), 17 kDa (right) and particle size distribution recorded by DLS at 25 ˚C with a concentration of 2 mg/mL.

In order assess the impact of the p(*n*BA)$_{50}$-*b*-p(SMAD)$_{40}$, a blank sample containing CB FW200 and solvent is compared to CB FW 200 mixed with the block copolymer in butyl acetate (**Figure 5.19**). After 10 minutes, the pigment is settled when mixed with polymer, meaning that the polymer does not interact with the pigment. The poor solubility of these diblock copolymers can be explained by the presence of the carboxylic acid which can form of strong hydrogen bonding with tertiary amines. Nsib *et al.* reported a similar work using the same carbon black pigment with homopolymer and diblock copolymers bearing carboxylic acid groups as a dispersant.[34]

Figure 5.19: Pictures of carbon black (FW 200) dispersed in butyl acetate solvent in left (blank) and carbon black dispersed in presence of block copolymer and butyl acetate with a samples concentration of 2 mg/mL and 10 min of sonication (right).

Figure 5.20 A shows a broad particle size distribution recorded for the diblock 15 kDa and 17 kDa. The D50 and D90 increased as the molecular weight increased, while a low degree of polymerisation of p(*n*BA)-*block*-p(SMAD) leads to better control over the dispersion.

The milled samples were prepared under similar conditions as the acrylate and methacrylates samples, with 60 % w/w of polymer. A good solubility of the polymer in acetate offers a good wetting, and therefore a better dispersion. The first observation made when the samples were prepared for the milling tests was an increase of viscosity (for the 10 kDa diblock copolymer in solution) while the 15 kDa and 17 kDa yield a more viscous solution and a soft gel respectively. Such an observation explained the broad particle size distribution obtained by light scattering, and suggests that the polymer forms a strong network in solution and, therefore, does not fully interact with the pigment surface. All the samples were analysed after milling, however, this data cannot be compared with the previous DLS data as the concentration of the polymer in milling sample is extremely high (71.5 mg/mL) compared to the concentration used for DLS measurements (2 mg/mL). **Figure 5.20 B** shows a monomodal distribution and the broad distributions of the DP 80/40 and 100/40 indicates an accumulation of agglomerates.

Carbon black coated with polymer was pyrolysed under nitrogen to avoid any oxidation of the pigment surface. The TGA graphs reported in **Figure 5.20 C** clearly show an early degradation around 100 ˚C corresponding to water and solvent evaporation, then a second degradation beginning at 180 ˚C which could be attributed to the carboxylic group degradation, and finally a degradation from 250 ˚C to 400 ˚C which belongs to the polymer backbone of the diblock copolymers. With respect to surface coating, 42 % of polymer pyrolysis is found for the copolymer with a degree of polymerisation of 50/40 and only 36 % of copolymer with a DP of 80/40 and 100/40. The TEM images recorded for poly(*n*BA)-*block*-poly(SMAD) show only the formation of aggregates for each copolymer and confirm the data obtained by Nanotrac and DLS (**Figure 5.20 D**).

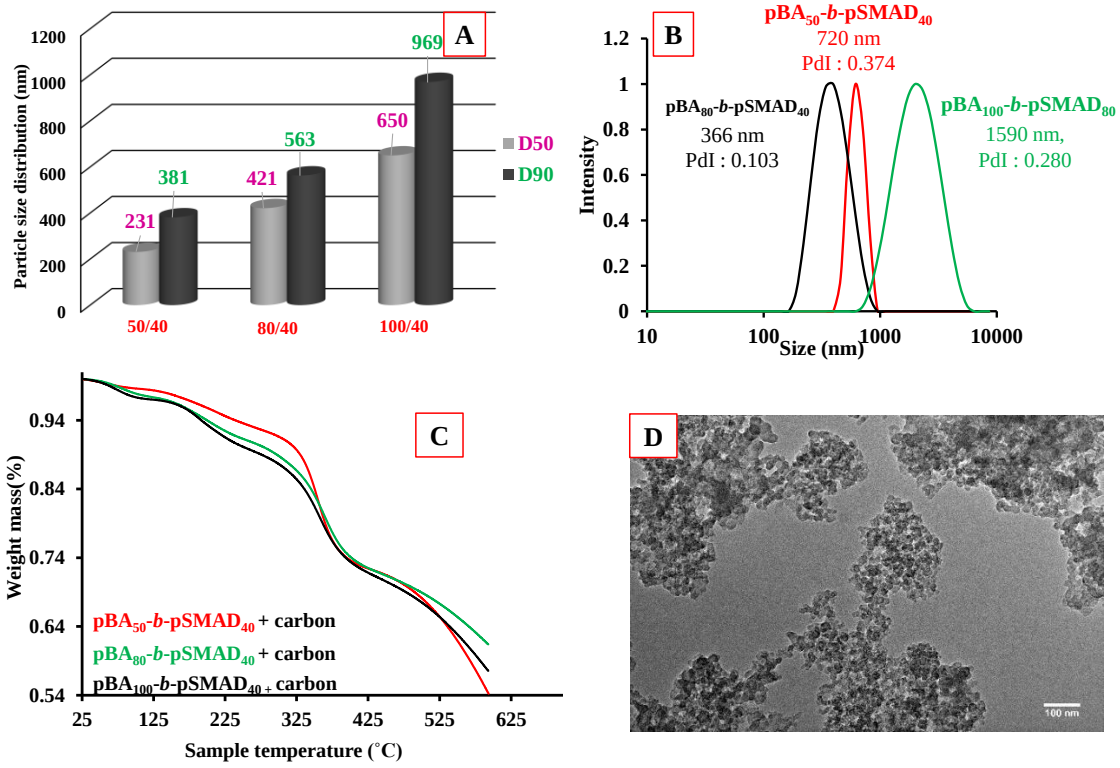

Figure 5.20: p(*n*BA)-*block*-p(SMAD) copolymer synthesised with BMDPT RAFT agent (DP_n = 55/19, 70/35, 100/50) characterisations. Particle size distribution analysed by Nanotrac instrument (**A**) and DLS (**B**). TGA graphs of CB FW200 coated with p(*n*BA)$_n$-*block*-p(SMAD)$_m$ copolymer heated up to 600 ˚C (**C**). TEM images conducted using a JEOL 2100 operating with a 200 kV prepared by drying a drop of dilute sample (0.01 wt.%) on a 300 Mesh carbon coated grid: **Scale :** 100 nm (**D**)

5.2.2.5. Dispersion using p(SMI) block copolymer

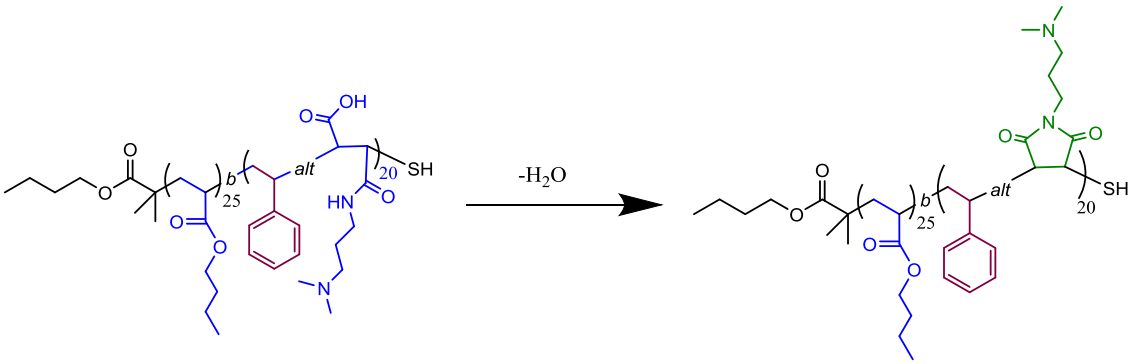

Scheme 5.2: Ring-closing of poly(SMAD) to form poly(SMI)

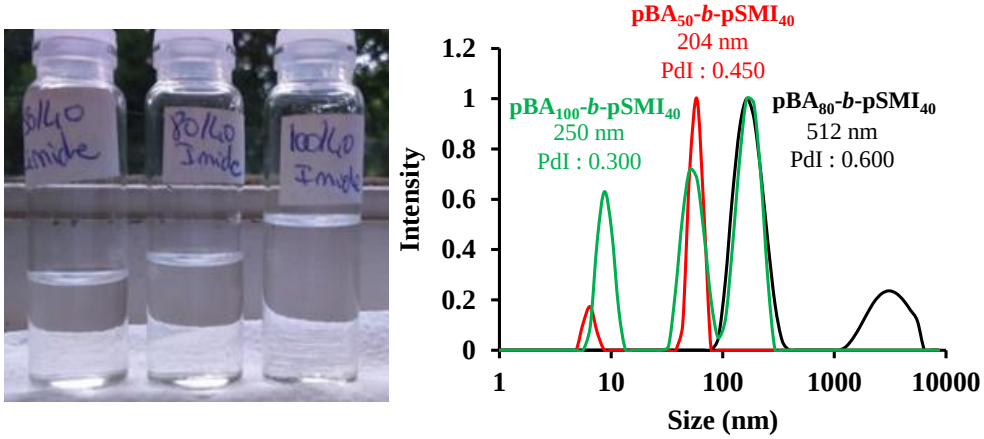

Figure 5.21: Images of p(*n*BA)-*block*-p(SMI) copolymers in acetate solution: 10 kDa (left), 15 kDa (middle), 17 kDa (right) and particle size distribution recorded by DLS at 25 ˚C with a concentration of 2 mg/mL.

Figure 5.22: Pictures of carbon black (FW 200) dispersed in butyl acetate solvent (blank) and carbon black dispersed in presence of block copolymer and butyl acetate with a samples concentration of 2 mg/mL and 10 min of sonication.

The solubility challenge of the previous diblock copolymer poly(*n*BA)-*block*-poly(SMAD) was overcome by decreasing the polarity of the polymer chains. For that, the synthesis of the amphiphilic block copolymer containing a functional maleimide was investigated. The intermediate poly(*n*BA)-*block*-poly(SMAD) copolymer was charged to a conical flask in the presence of a certain volume of MPA solvent and heated to 125 ˚C using Dean-stark apparatus, in order to close the maleic acid ring, leading to the formation of the maleimide p(*n*BA)-*block*-pS(MI) (**Scheme 5.2**). Conversely to the intermediate copolymer, a homogeneous and optimal particle size distribution for all sizes of diblock copolymer are observed. In comparison to the previous diblock copolymers (acrylates, methacrylates and amido acid), the maleimide copolymer has the most homogeneous particle size (**Figure 5.23 A**). The presence of the benzyl group can enhance the stabilization *via* π-π stacking with the quinone and other aromatic groups present on the CB FW200 surface. The particle size distribution of the maleimide diblock copolymers before and after milling is presented in **Figure 5.23 B**. A bimodal distribution is observed before milling, indicating the formation of aggregates for all the diblock copolymers in organic solvent, which, then, are broken into a smaller particles under the shear stress applied during the milling process. The TGA thermograms show only one main degradation, beginning at 200˚ C, with 65 % of dispersant coated on the surface of the pigment and an additional degradation at 325 ˚C can be attributed to the polymer backbone degradation (**Figure 5.23 C**). The percentage of polymer coated between the maleimide and maleic acid in the diblock copolymer demonstrates the influence of the functional groups present on the polymer backbone.

Finally, the successful dispersion of CB FW200 using p(*n*BA)-*block*-pSMI diblock copolymers is observed in the TEM image in **Figure 5.23 D**, despite the presence of some aggregates, almost full dispersion is achieved.

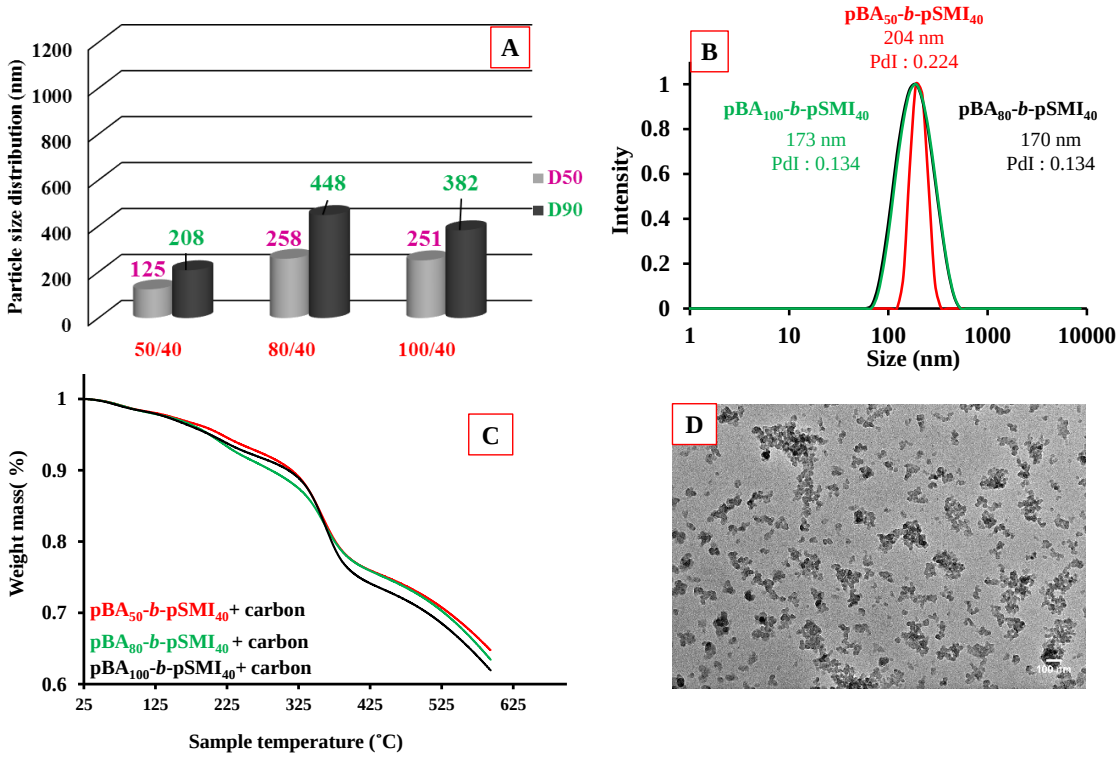

Figure 5.23: p(*n*BA)-*block*-p(SMI) copolymer synthesised with BMDPT RAFT agent (DP_n = 55/19, 70/35, 100/50) characterisations. Particle size distribution analysed by Nanotrac instrument (**A**) and DLS (**B**). TGA graphs of CB FW200 coated with $p(nBA)_n$-*block*-$p(SMI)_m$ copolymer heated up to 600 ˚C (**C**). TEM images conducted using a JEOL 2100 operating with a 200 kV prepared by drying a drop of dilute sample (0.01 wt.%) on a 300 Mesh carbon coated grid: **Scale :** 100 nm (**D**)

5.3. Conclusion

In this work, a library of copolymers synthesised *via* RAFT polymerisation, were used from the polymerisation mixture to disperse CB FW200 in organic solvent. The importance of the carbon black surface characterisation to understand the mechanism between the polymeric dispersant and the pigment was assessed. Moreover, a strong link between the dispersion efficiency and the polymeric architecture was reported by comparing a poorly controlled and well-controlled diblock copolymer.

A good dispersion is strongly dependant on the polymeric chain's conformation in a solvent, which in the optimal case, should stabilise the primary pigment particles through a steric repulsion mechanism. The main advantage of working in organic solvent *versus* aqueous is to avoid solubility challenges of dispersants with a high molecular weight (> 10 kDa), and also some potential charge interaction between the solvent and the polymer backbone. The versatility and a high tolerance towards the presence of impurities of the RAFT polymerisation allows the polymerisation of different classes of monomers (acrylate, methacrylate and styrene) using an industrial RAFT agent with a low purity; hence, the impact of several functionalities present on the polymer backbone on the dispersion. The tertiary amine appears to be a suitable anchoring group with a strongly acidic surface, whilst the carboxylic acid involves a strong electrostatic repulsion. To this end, a broad range of molecular weights targeted in this work does not show any major difference with respect to particle size distribution and the amount of polymer coated. It is worth noting that the particle size of pigment obtained is strongly dependant on the milling process used. Indeed, smaller the particle, the higher the surface area will be and a higher dispersant loading will be required. Consequently, depending on the size of the

glass bead, the milling time must be clearly defined for an optimal dispersion. In order to keep a monomodal particle size distribution, a glass beads with 3 mm of diameter are added in a slurry and mixed over 18 hours. An average particle size between 250 and 400 nm is determined by Nanotrac analysis while an amount of 55 % of polymer adsorbed onto the pigment surface is determined by TGA for each diblock copolymer synthesis.

5.4. Experimental section

5.4.1. Materials and methods

Carbon black FW200 (Degussa, > 90 %), butyl acetate (Chromasolv plus, 99.7 %), propylene glycol monoethyl ether acetate (Sigma-Aldrich, 99.5%) were purchased.

pH measurements: 700 mg of Carbon black was dissolved in 10 mL of deionised water and sonicated for 10 minutes. The pH-meter was calibrated with buffers of pH 4 and 10 before measurement.

DLS measurements: A solution of 2 mg/mL of milling mixture in MPA solvent was prepared for all the samples and the measurements were performed at 25 ˚C, with a refractive index of 1.394 and viscosity of 1.0020 cP, using Malvern zetasizer software.

Preparation of milling sample: The milling mixture contained 60 % wt. of copolymer in the presence of acetate solvent, CB FW200 and glass beads.

For instance: 0.6 g of copolymer is firstly solubilise in a solvent, then, introduced into a vial with 1 g of carbon black, 8.4 g of solvent and a certain amount of glass beads. The vial is sealed with a cap and tape a milled for 18 h in a cold room (**Figure 5.24**).

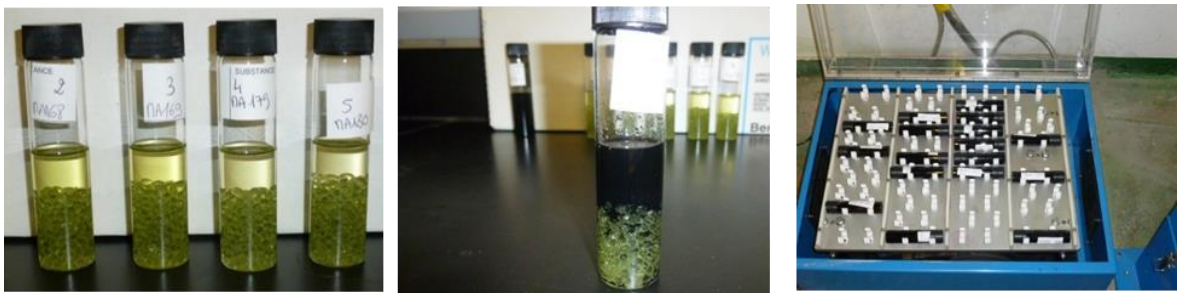

Figure 5.24: Picture of milling sample preparation where glass beads of 3 mm of diameter, carbon black, polymer and solvent are mixed and milled for 18 h.

Copolymers synthesis: All the syntheses are reported in **Chapter 2, 3, 4** for acrylate, methacrylate and SMA contained copolymer.

5.4.2. Characterisations

- XPS analysis

X-ray photoelectron spectroscopy (XPS) data were collected at the Warwick Photoemission Facility, University of Warwick [1]. The samples investigated in this study were attached to electrically-conductive carbon tape, mounted on to a sample bar and loaded in to a Kratos Axis Ultra DLD spectrometer, which possesses a base pressure of 2 10^{-10}mbar. XPS measurements were performed in the main analysis chamber, with the sample being illuminated using a monochromated Al kα x-ray source. The measurements were conducted at room temperature and at a take-off angle of 90° with respect to the surface parallel.

The core level spectra were recorded using a pass energy of 20 eV (resolution approx. 0.4 eV), from an analysis area of 300 x 700 μm.

The spectrometer work function and binding energy scale were calibrated using the Fermi edge and $3d^{35}$ peak recorded from a polycrystalline Ag sample prior to the commencement of the experiments. The data were analysed in the CasaXPS package, using Shirley backgrounds and mixed Gaussian-Lorentzian (Voigt) lineshapes and asymmetry parameters where appropriate. For compositional analysis, the analyser transmission function has been determined using clean metallic foils to determine the detection efficiency across the full binding energy range.

- BET analysis

The Brunauer–Emmett–Teller (BET) specific surface area, pore volume, and average pore diameter were measured under nitrogen at 77 K on a Micromeritics TriStar II. A mass of 50 mg for CB FW200 was previously degassed under nitrogen at 150 °C overnight before using Micromeritics FlowPrep.

- Raman spectroscopy

Raman spectra were collected in the 400 – 2300 cm^{-1} range with a Raman spectrometer using a 20 mW laser at 532 nm and a Leica (50x) magnification objective. Spectra were obtained with an exposure time of 60 s. Any visual degradation was visible after measurement. The microscope showed that the carbon black used is mainly composed of spherical aggregates with an average diameter of40 -100 nm. For this sample, six Raman spectra were collected at different areas.

- Thermogravimetric analysis

The experiments were performed to determine the thermal degradation of the diblock copolymer and to quantify the amount of polymer coated on the carbon black surface using a Mettler Toledo TGA. All the samples were run under nitrogen with a scan rate of 10 K/min from 25 °C to 600 °C for the polymer and from 25 °C to 1000 °C for the carbon black.

- Nanotrac analysis

Particle size distribution was measured by using NANO-flex analyser (Microtrac, USA) at room temperature. A few drops of the milling sample were diluted in a certain volume of solvent and an external electrode was inserted for the measurement.

- TEM analysis

Studies were conducted using a JEOL 2100 operating with a 200 kV accelerating voltage on unstained samples, prepared by drying a drop of dilute sample (0.01 wt. %) on a 300 Mesh carbon coated grid.

5.5. References

1. Zhang, B.; Lai, C.; Zhou, Z.; Gao, X. P. *Electrochimica Acta* **2009,** *54* (14), 3708-3713.

2. Bradley, R. S. *Journal of Colloid Science* **1956,** *11* (3), 237-239.

3. Rattanasom, N.; Saowapark, T.; Deeprasertkul, C. *Polymer Testing* **2007,** *26* (3), 369-377.

4. Pantea, D.; Darmstadt, H.; Kaliaguine, S.; Roy, C. *Applied Surface Science* **2003,** *217* (1), 181-193.

5. Nagornaya, M. N.; Razdyakonova, G. I.; Khodakova, S. Y. *Procedia Engineering* **2016,** *152* (Supplement C), 563-569.

6. Atkins, J. H. *Carbon* **1965,** *3* (3), 299-303.

7. Bradley, R. H.; Sutherland, I.; Sheng, E. *Journal of Colloid and Interface Science* **1996,** *179* (2), 561-569.

8. Pantea, D.; Darmstadt, H.; Kaliaguine, S.; Sümmchen, L.; Roy, C. *Carbon* **2001,** *39* (8), 1147-1158.

9. Leong, C.-K.; Aoyagi, Y.; Chung, D. D. L. *Carbon* **2006,** *44* (3), 435-440.

10. Hauptman, N.; Vesel, A.; Ivanovski, V.; Gunde, M. K. *Dyes and Pigments* **2012,** *95* (1), 1-7.

11. Ciobanu, M.; Lepadatu, A.-M.; Asaftei, S. *Materials Today: Proceedings* **2016,** *3* (Supplement 2), S252-S257.

12. Hauptman, N.; Gunde, M. K.; Kunaver, M.; Bester-Rogac, M. *Journal of Coatings Technology and Research* **2011,** *8* (5), 553-561.

13. Asahi carbon CO., L. http://www.asahicarbon.co.jp/global_site/product/cb/characteristic.html.

14. Sosa, R. C.; Parton, R. F.; Neys, P. E.; Lardinois, O.; Jacobs, P. A.; Rouxhet, P. G. *Journal of Molecular Catalysis A: Chemical* **1996,** *110* (2), 141-151.

15. E, D. A.; R, P. W., Google Patents: 1966.

16. Kamegawa, K.; Nishikubo, K.; Kodama, M.; Adachi, Y.; Yoshida, H. *Carbon* **2002,** *40* (9), 1447-1455.

17. Papirer, E.; Lacroix, R.; Donnet, J. B. *Carbon* **1996,** *34* (12), 1521-1529.

18. Nagai, K.; Igarashi, Y.; Taniguchi, T. *Colloids and Surfaces A: Physicochemical and Engineering Aspects* **1999,** *153* (1), 161-163.

19. Fujitani, T. *Progress in Organic Coatings* **1996,** *29* (1), 97-105.

20. Ma, S. H.; Hertler, W. R.; Spineli, H. J.; Shor, A. C., Google Patents: 1993.

21. Romyen, N.; Thongyai, S.; Praserthdam, P. *Journal of Applied Polymer Science* **2010,** *115* (3), 1622-1629.

22. Barbieri, O.; Hahn, M.; Herzog, A.; Kötz, R. *Carbon* **2005,** *43* (6), 1303-1310.

23. D1799-03a, A. *ASTM international* **2012**.

24. Pawlyta, M.; Rouzaud, J.-N.; Duber, S. *Carbon* **2015,** *84* (Supplement C), 479-490.

25. Toth, P.; Palotas, A. B.; Eddings, E. G.; Whitaker, R. T.; Lighty, J. S. *Combustion and Flame* **2013,** *160* (5), 909-919.

26. Oberlin, A. *Carbon* **1984,** *22* (6), 521-541.

27. Sadezky, A.; Muckenhuber, H.; Grothe, H.; Niessner, R.; Pöschl, U. *Carbon* **2005,** *43* (8), 1731-1742.

28. Kaye, G. *Carbon* **1965,** *2* (4), 413-419.

29. Jakab, E.; Blazsó, M. *Journal of Analytical and Applied Pyrolysis* **2002,** *64* (2), 263-277.

30. Oickle, A. M.; Goertzen, S. L.; Hopper, K. R.; Abdalla, Y. O.; Andreas, H. A. *Carbon* **2010,** *48* (12), 3313-3322.

31. Auschra, C.; Eckstein, E.; Mühlebach, A.; Zink, M.-O.; Rime, F. *Progress in Organic Coatings* **2002,** *45* (2), 83-93.

32. Rasmusen, H.; Thorsson, J. R.; Moore, J. E.; Perry, C. W.; LaBazzo, J. P., Google Patents: 2007.

33. Braun, D.; Sauerwein, R.; Hellmann, G. P. *Macromolecular Symposia* **2001,** *163* (1), 59-66.

34. Nsib, F.; Ayed, N.; Chevalier, Y. *Progress in Organic Coatings* **2006,** *55* (4), 303-310.

35. Ju, S.-Y.; Utz, M.; Papadimitrakopoulos, F. *Journal of the American Chemical Society* **2009,** *131* (19), 6775-6784.

Chapter 6: Conclusions and Outlook

The aims of this thesis were to design a library of amphiphilic block copolymers based on hydrophobic blocks, acting as a steric stabiliser, and hydrophilic blocks, bearing one or more functionalities having a specific pigment surface affinity that can be used to disperse carbon black (CB FW200) in organic media. RAFT polymerisation, being a powerful technique, was explored to synthesise all the diblock and multiblock copolymers using the BMDPT RAFT agent at industrial grade (~ 70 - 80 % of purity). Different classes of monomers were used to synthesise the amphiphilic diblock copolymers in a solution.

The Chapter 2 describes the synthesis of acrylate diblock copolymers in both butyl acetate and MPA solvents. Kinetic studies were undertaken using the conditions established based on the temperature, ratio of $[BMDPT]_0$ / $[V601]_0$, and solvent optimisation conditions. Highly controlled polymerisations with different degrees of polymerisation were obtained with a quantitative monomer conversion (> 95 %), narrow molar distribution ($Đ \leq 1.25$) and high livingness ($L > 97$ %). However, after many optimisations the presence of β-scission remained at low temperatures and at very low initiator concentrations for each acrylate homopolymerisation. In paralleled, the synthesis of acrylate copolymers were investigated in order to compare the efficiency of these dispersants on a carbon black pigment.

The DMAEA monomer was then substituted by DMAEMA to enhance the robustness of the polymers. Unfortunately, using the BMDPT RAFT agent was challenging to polymerise methacrylate monomers, and no controlled diblock copolymers were made. As such, the polymerisation of acrylate / methacrylates were performed with the MCTP RAFT agent, designed for methacrylate monomers. Better control over the polymerisation was observed, however, few homopolymer chains were reinitiated.

The challenge of polymerising methacrylate with BMDPT in acetate solvents was investigated in Chapter 3. For this, the MCTP RAFT agent, bearing a better leaving R group provided better control over the methacrylate polymerisation and was used to understand the mechanism between the consumption of RAFT agent and the control of the polymerisation. Also, the chain transfer constant was determined for both BMDPT and MCTP using Mayo plots. The values of the chain transfer constant obtained, 0.25 and 4 for BMDPT and MCTP respectively, confirmed the poor control over methacrylate polymerisation for BMDPT. The optimisation of the methacrylate polymerisation was assumed by using a semi-batch process, and the potential of this technique was demonstrated by synthesising a well-defined diblock and multiblock copolymers at large scale.

Chapter 6: Conclusions and Outlook

In a Chapter 4, a new class of polymeric dispersant was investigated, combining the use of styrene and maleic anhydride monomers to design an amphiphilic dispersant. Similarly to the previous chapters (2 and 3), variation of the polymer backbone was tuned by varying the degree of polymerisation. Interestingly, the high reactivity of maleic anhydride enhanced the possibility to modify the polymer backbone. Additionally, zwitterionic maleic amido acid and maleimide compounds were obtained after two modification steps. The success of the synthesis of this novel dispersant was proved by the industrial scale up of the process using the exact same conditions established in lab scale.

Finally, Chapter 5 describes the dispersion Carbon Black FW200 which, having a high specific area, required a high loading of dispersant to achieve an acceptable dispersion. Also, the efficiency of dispersion using 60 % w/w of diblock copolymer, described in a Chapter 5 showed a well-dispersed pigment with a monomodal particle size distribution and D50/D90 values between 180 and 400 nm. Finally, an average value of 55 % w/w polymer coated on the pigment surface was determined *via* thermal analysis.

This thesis describes the performance of diblock copolymers as a dispersant for carbon black. The use of the BMDPT RAFT agent allows for control of the polymer architecture, and the monomers selected allowed for understanding of the interaction between the pigment surface and the polymer. To further this work, understanding of RAFT mechanism for BMDPT can be expand to more complex polymeric architectures such as

stars, combs or graft copolymers, and then compare the efficiency on pigment dispersion. Interestingly, the insertion of new functionalities or a combination of different structures can also be envisaged to enhance the adhesion between the pigment surface and the polymeric dispersant.

In summary, the synthesis of diblock copolymers at a large scale utilising different classes of monomer in the presence of BMDPT was reported in this thesis. The success of dispersing challenging pigments using these polymeric dispersants was demonstrated and can easily be extended towards any other pigment, or further investigated to look at different polymeric architectures/functionalities.

Appendix: Chapter 2

Lubrizol Chain Transfer Agent

BMDPT synthesis

The Lubrizol Corporation is one of the rare of the few industrial companies which produced in tonnes scale the chain transfer agent (CTA) allowing the synthesis of complexes architectures *via* Reversible Addition-Fragmentation chain transfer (RAFT) and used for several applications such as lubricating fluids or coating.[1,2] The synthesis of the "Butyl-2-methyl-2-[(dodecylsulfanylthiocarbonyl) sulfanyl] propionate" (BMDPT RAFT agent) is obtained after esterification of S-1- dodecyl-S'-(α, α'-dimethyl-α'-acetic acid) trithiocarbonate[3,4] as shown in **Scheme A.1**.

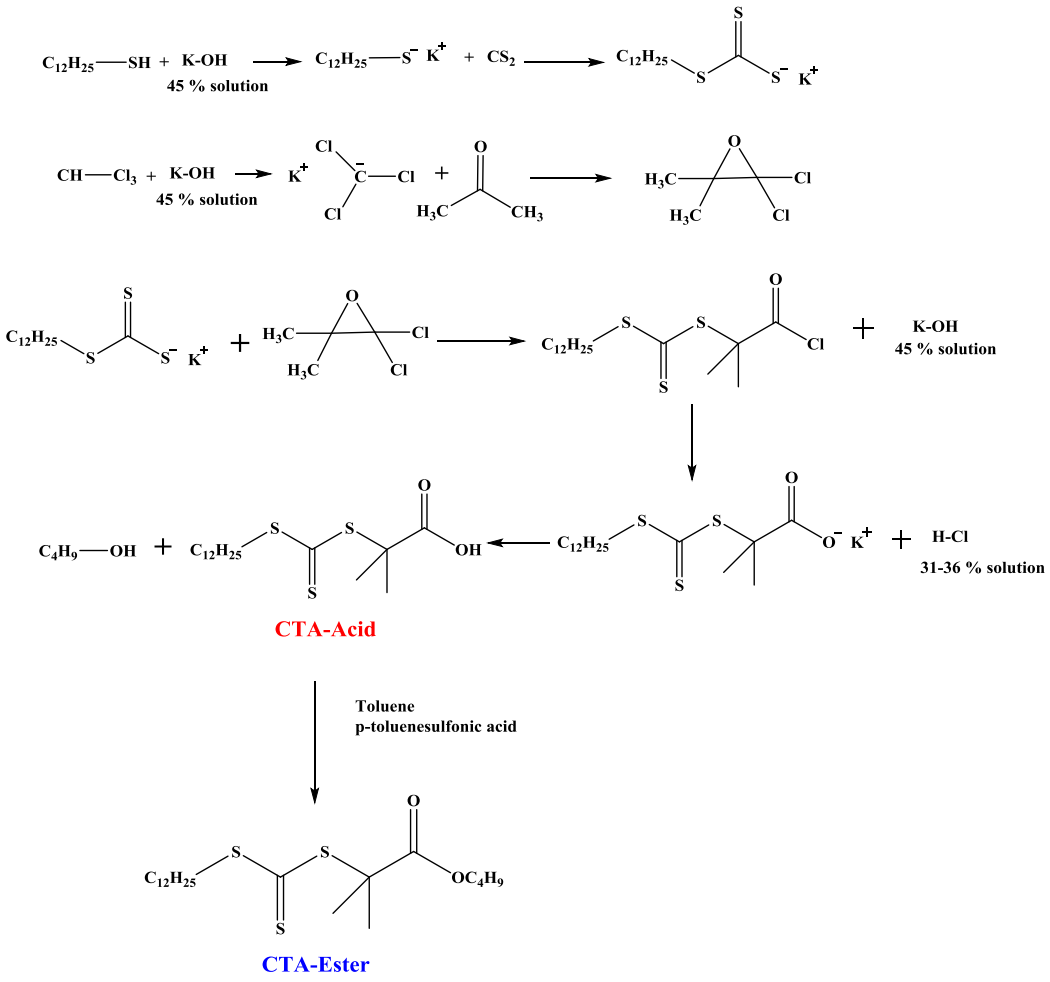

Scheme A.1: General scheme of Lubrizol RAFT agent synthesis

BMDPT characterisations

- ^{1}H Nuclear Magnetic Resonance

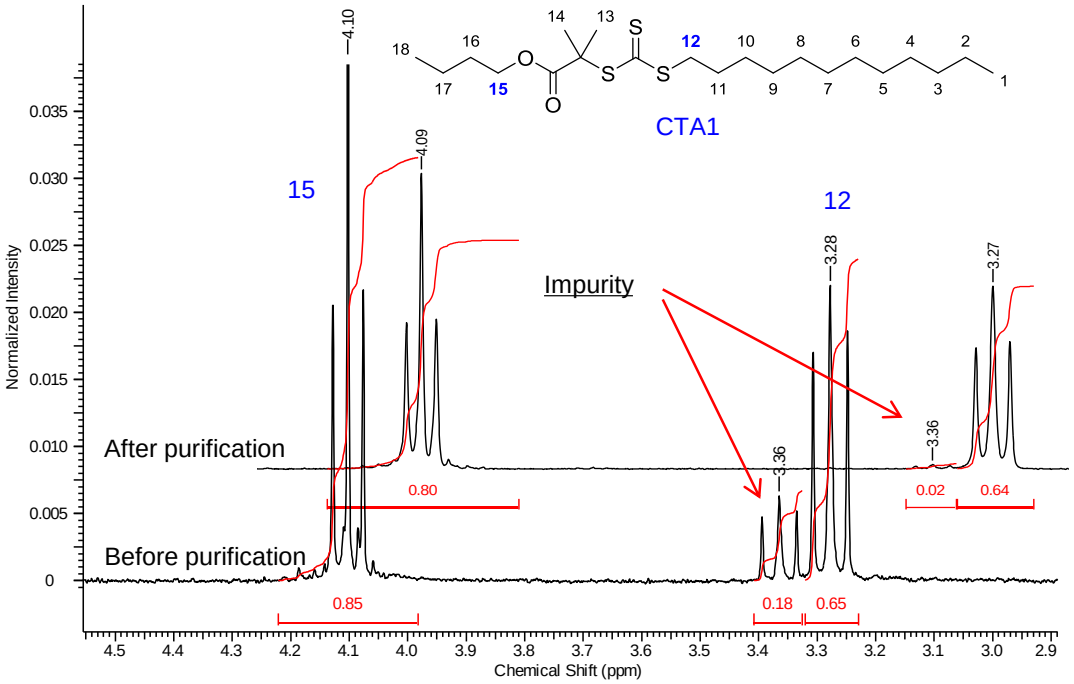

Figure A.1: ^{1}H NMR spectrum of BMDPT industrial grade before and after purification in ethanol

Mass spectroscopy

The composition of the RAFT agent is studied by using mass spectroscopy. Several peaks were determined with the main peak 4 (**Figure A.2**) corresponding the pure BMDPT RAFT agent. However, few peaks remained undetermined and can be attributed to the impurities left over.

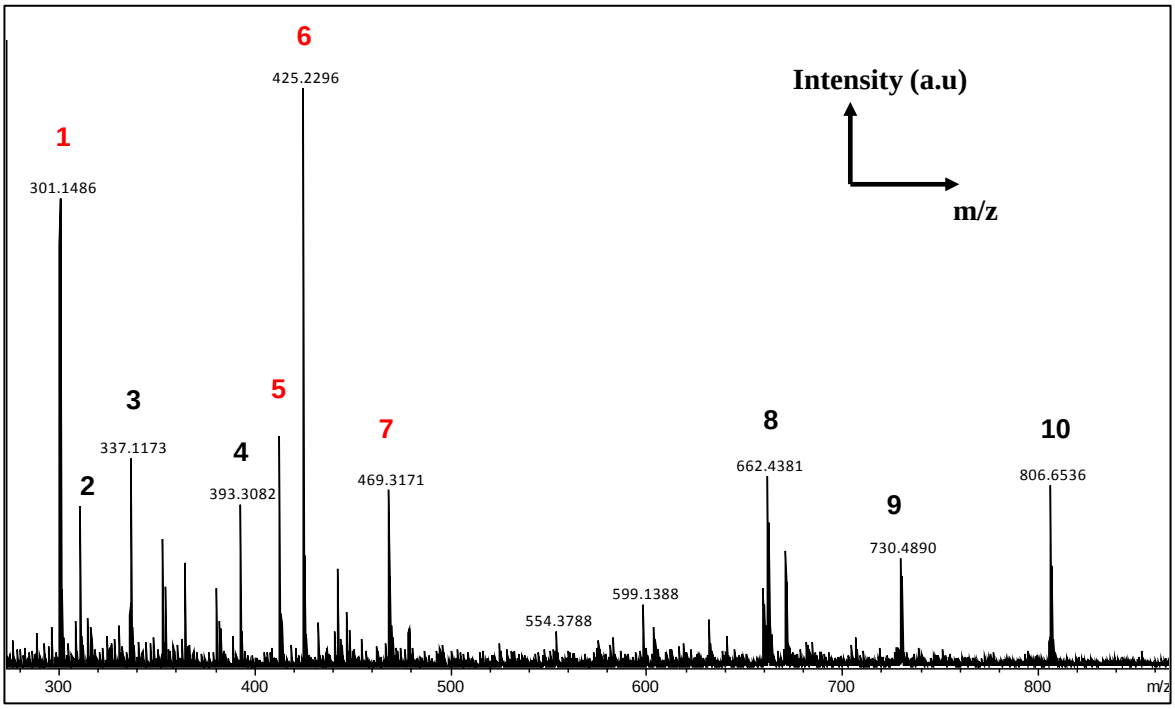

Figure A.2: MALDI-ToF-MS analysis of the industrial BMDPT RAFT agent

Table A.1: Experimental and theoretical monoisotopic mass of industrial BMDPT RAFT agent obtained by MALDI-ToF

Peak	Monoisotopic mass (**Experimental**)	Monoisotopic mass (**Theoretical**)	Counter-ion salt
1	301.14	301.11	Na^+ , K^+
2	311.26	**NA**	**NA**
3	337.11	337	Na^+
4	393.3	**NA**	**NA**
5	413.28	413.22	Na^+
6	425.23	425.32	Na^+
7	469.32	469.32	Na^+
8	662.32	663.25	Na^+
9	730.49	733.29	Na^+
10	806.69	803.33	Na^+

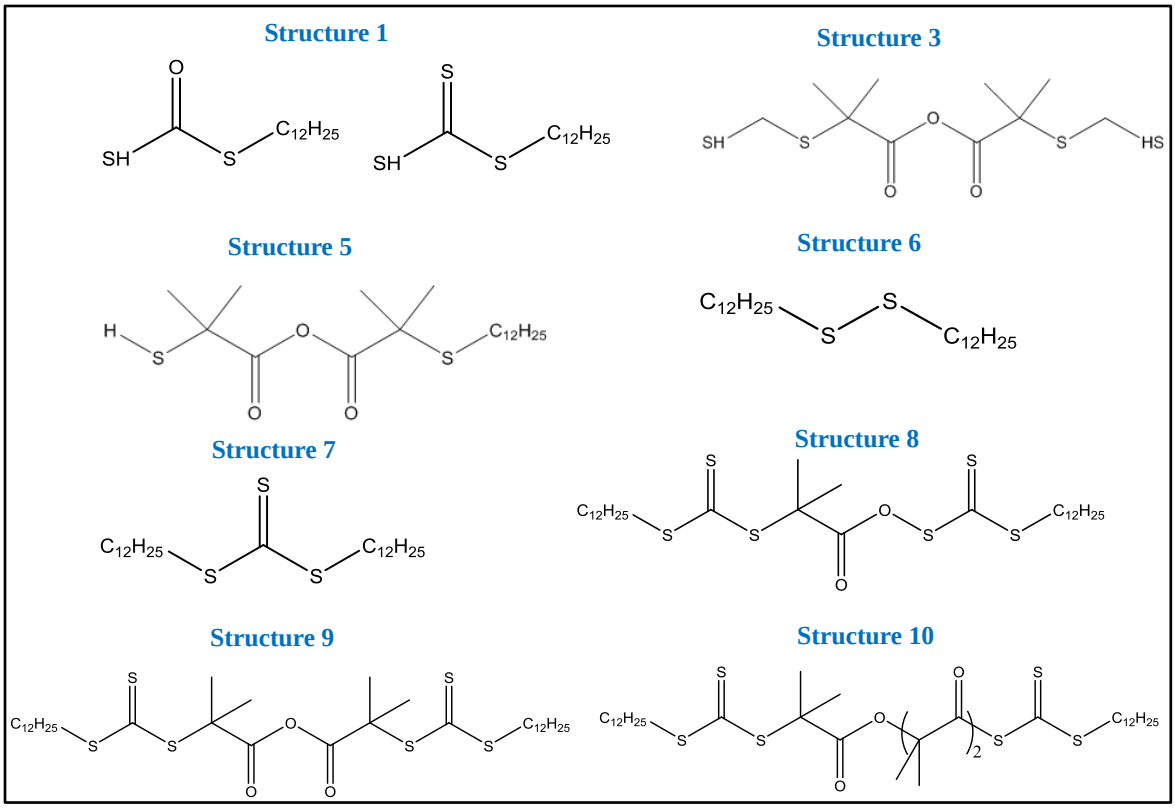

Figure A.3: Stuctures of impurities present in industrial BMDPT RAFT agent based on the MALDI-ToF spectrum

Thermogravimetric Analysis (TGA)

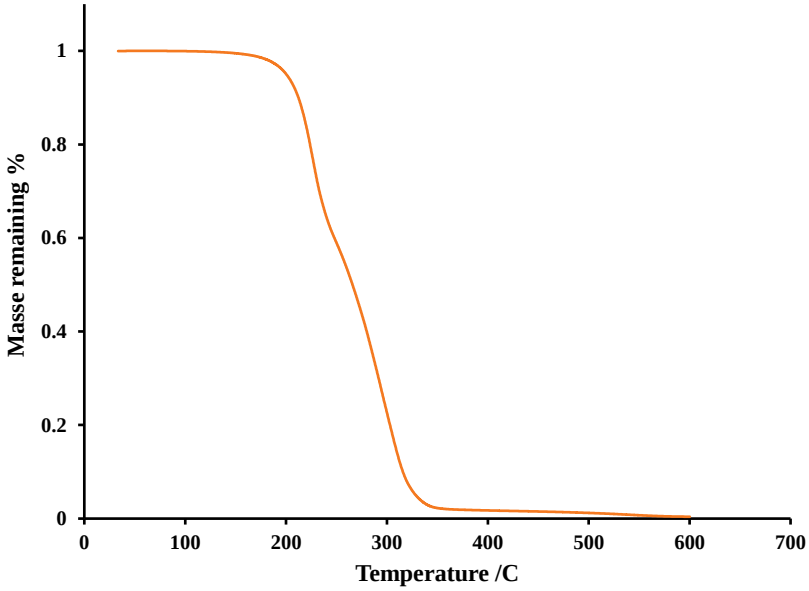

Figure A.4: TGA chromatogram of BMDPT RAFT degradation submitted under nitrogen with a heating rate of 10 °C/min from 25 °C to 1000 °C

1. Shooter, A. J.; Thetford, D.; Richards, S. N.; Jennings, R. A., Google Patents: 2017.

2. Shooter, A. J.; Thetford, D.; Jennings, R.; Richards, S. N., Google Patents: 2015.

3. Lai, J. T.; Filla, D.; Shea, R. *Macromolecules* **2002,** *35* (18), 6754-6756.

4. Keddie, D. J.; Moad, G.; Rizzardo, E.; Thang, S. H. *Macromolecules* **2012,** *45* (13), 5321-5342.